EXPLORING THE ROLE OF FGFR2C MISREGULATION IN SYNDROMIC CRANIOSYNOSTOSIS

A THESIS SUBMITTED IN FULFILMENT OF THE DOCTOR OF PHILOSOPHY DEGREE AT
UNIVERSITY COLLEGE LONDON

2018

KING LAM LEE

DEVELOPMENTAL BIOLOGY & CANCER PROGRAMME

UCL GREAT ORMOND STREET INSTITUTE OF CHILD HEALTH
UNIVERSITY COLLEGE LONDON

I-Declaration

I, King Lam Lee, confirm that the work presented here is my own.

King Lam Lee performed the majority of experiments and conceived the project. Contributions from others are stated in this section otherwise. Emma Peskett (Pauws lab c.2013) performed RT-qPCR analysis on E12.5 $R26R^{Fgfr2cV5/+}$; $\beta actin^{CRE/+}$, and immunohistochemistry on paraffin sections for the V5 epitope prior to the start of this project (Chapter 2). I was assisted by Charlotte Quinn (MSc 2017, Pauws lab) for quantitative analysis in Chapter 5A, and Sherine Pranata (BSc 2017, Pauws lab) for cartilage analysis in the Crouzon mouse model (Chapter 5B). RNAseq was performed in collaboration with UCL Genomics and genes ranked in 'R' console by John Apps (J.P Martinez-Barbera lab) prior to Gene Set Enrichment Analysis. RT-qPCR of candidate genes was performed by Somaya Taha (MSc 2017, Pauws lab) and reanalysed by King Lam Lee.

_____

II-Acknowledgements

This PhD took almost 4 years. I sit here on a chilly February afternoon contemplating on the people who made this endeavour possible. Looking back, it has been an incredible journey, a rollercoaster ride both on and off the pitch. I have met wonderful colleagues turning into friends along the way, and all of you have contributed immensely to my overall growth in one respect or another. Firstly, I would like to express my deepest gratitude to my supervisors Erwin Pauws and Philip Stanier for their continued support over the past few years. Both of you have watched me mature as a scientist and grown out of my natural milieu to drive this project. In addition, I want to thank Peter Munro and Matt Hayes at UCL IOO for laser captured microdissection, Mike Hubank, Tony Brooks and Mark Kristiansen at UCL Genomics for RNAseq, and Dale Moulding for microscopy assistance. Special credit also goes to my sponsors UCL and GOSHCC for making this research possible.

It is not uncommon to experience a stalemate of scientific inspirations throughout this journey. This doctorate would not have been possible without the sustained support of friends and colleagues in the BDRC and GGM, who were always approachable in times of adversity. I want to specially thank Chloe Santos, who has been patient with me comes rain or shine. Phil and Gudrun's lab (informally known as 'Lunch Mob'): Emma Peskett, Dale Bryant, William Baird, Pambos Demetriou, Miho Ishida, Rimante Seselgyte, Melissa Riachi, Constance Maurer, Nita Solanky, Jess Buxton, Cristina Aleman-Charlet; and past members Lucas Alvizi, Susanne Stalman and Lydia Leon. All of you have given me incredible memories in and outside the lab, and I look forward to many more to come. I also had the pleasure to mentor nine students throughout my PhD, and I am very pleased to have witnessed all of you to excel in your own rights, and am grateful for your contributions to my project in one way or another-special credits to Rosanna Aiello, Charlotte Quinn, Sherine Pranata and Somaya Taha for your inconceivable efforts. Scott Haston and 'Captain' Leonidas Panousopoulos-you've managed to make life at ICH and beyond hilarious. I also owe my debt to my wonderful friends outside the lab and my undergraduate supervisor Clemens Kiecker, without your inspiration I wouldn't

have pursued a PhD. Last but not least, the greatest debt is owed to my family for their continued support through the many walks of life.

I sit here concluding my thoughts as another chapter in my book draws to a close. I suppose this chapter was written to its full potential and is a memorable one. It is doubtless there will be challenges and fine performances along the way, and pursuing a PhD has certainly accomplished in strengthening my character and resilience. Finally, I would like to dedicate this thesis to those individuals who taught me, with specific regards to my mentors in academia and the teachers at school. To this end, I shall conclude with a principle from a great wartime Prime Minister:

'Success is not final, failure is not fatal:
it is the courage to continue that counts.'-Sir Winston Churchill.

Until we meet again,
Kevin K.L Lee.
Sunday 11th February 2018.
London, United Kingdom.

III-Table of Contents

Chapter 2

Chapter 3 Results (Part I)

IV-List of Figures

V-List of Appendices

VI-List of Abbreviations

VI.a-General abbreviations

AER	Apical epidermal ridge
ALP	Alkaline phoshatase
ATP	Adenosine triphosphate
BCIP	5-bromo-4-chloro-3-indolyl phosphate
BSA	Bovine serum albumin
cNCCs	Cranial neural crest cells
DAPI	4',6-diamidino-2-phenylindole
DIG	Digoxygenin
ECL	Enzymatic chemiluminescence
ECM	Extracellular matrix
Eks	Elbow-knee synostoses
ELISA	Enzyme-linked immunosorbent assay
EMT	Epithelial mesenchymal transition
ES	Enrichment score
EtOH	Ethanol
FACS	Fluorescence activated cell sorting
FDR	False discovery rate
FRET	Forster resonance energy transfer
GCP	Greig cephalopolyndactyly
GOF	Gain of function
HCMV	Human cytomegalovirus
HISS	Heat inactivated sheep serum
HRP	Horse radish peroxidase
HSCs	Hemapoetic stem cells
HZ	Hypertrophic zone
IFN	Interferon
IgI	Immunoglobulin like
IHC	Immunohistochemistry
ISH	In situ hybridisation
LADD	Lacrimo-auriculo-dento-digital
LOF	Loss of function
MeOH	Methanol
MPs	Mesenchymal progenitors
MSCs	Mesenchymal stem cells
MSS	Multiple synostoses syndrome
NaOH	Sodium hydroxide
NBT	Nitro blue tetrazolium chloride
NCC	Neural crest cells
NTMT	Nacl; tris-hcl (hydrochloric acid); $mgcl_2$ (magnesium chloride); 0.1% tween-20
PBS	Phosphate buffered saline
PCA	Principal component analysis
PFA	Paraformaldehyde
PTW	Phosphate buffered saline-0.1% tween
PZ	Proliferation zone
ROI	Region of interest
RT	Room temperature
RT-qPCR	Real time quantitative polymerase chain reaction
RZ	Resting zone
SADDAN	Severe achondroplasia with developmental delay and acanthosis nigricans
SSC	Saline sodium citrate
TBST	Tris buffered saline-tween-20
TK	Tyrosine kinase
TSA	Tyramide signal amplification
WT	Wild type
ZPA	Zone of polarising activity

VI.b-Genes and protein abbreviations

ADAM	A disintegrin and metalloproteinase
ADAMTS1	A Disintegrin And Metalloproteinase with Thrombospondin Type 1 motifs
ASK1	Apoptosis signalling regulating kinase 1
ASK2	Apoptosis signalling regulating kinase 2
Atf4	Activating transcription factor 4
bHLH	Basic helix loop helix
BMP	Bone morphogenetic protein
CCT	CTP: phosphocholine cytidydyltransferase
CDK	Cyclin dependent kinase
Col	Collagen
CRKL	CRK-Like protein
Dusp6	Dual specificity phosphatase 6
Dusp6	Dual specificity phosphatase 6
EGFR	Epidermal growth factor receptor
En-1	Engrailed1
ERF	Ets domain-containing transcription factor
ESRP	Epithelial spicing regulatory protein
ETS	E-twenty six
FBN	Fibrillin
FGF	Fibroblast growth factors
FGFR	Fibroblast growth factors receptor
FoxA	Forkhead box A
FOXO	Forkhead box O
FOXO1	Forkhead box protein 1
Frem1	Fras1 related extracellular related gene 1
FRS2α	Fibroblast growth factor substrate alpha
GAPDH	Glyceraldehyde-3-phosphate dehydrogenase
Gdf6	Growth differentiation factor 6
Grb2	Grwoth factor receptor bound2
HDAC	Histone acetylase
HSPG	Heparin sulphate proteoglycans
Id	Inhibitor of DNA binding protein
Ihh	Indian hedgehog
Jag1	Jagged1
Map3k6	Mitogen activated protein kinase kinase kinase 6
Mef2c	Myocyte enhancer factor 2c
Mesp1	Mesoderm posterior 1
Msx2	Msh homeobox 2
mV5	Mouse V5
Nell1	Nel-like type 1 molecule
NGF	Nerve growth factor
Papln	Papilin
Pcty1b	Phosphate cytidylyltransferase 1, choline, beta
Pdgf	Platelet derived growth factor
Pdgfr	Platelet derived growth factor receptor
PPR	Pthrp Receptor
Ptch	Patched
PTHrP	Parathyroid hormone related peptide
Rab23	Ras-related protein Rab23
Rsad2	Radical SAM domain containing 2
Rsk2	Ribosomal times Kinase
RTK	Receptor tyrosine kinase
Runx2	Runt related transcriptor factor 2
Shp2	Src homology region 2 domain containing phosphatase
SKI	SKI proto-oncogene
Sos	Son of sevenless
Sox9	Sry hmg box 9
Spry	Sprouty
STAT	Signal Transducer and Activator of Transcription
Tcf12	Transcription factor 12
TGF	Transforming growth factor
TGFBR	Transforming growth factor beta receptor
TNFα	Tumour Necrosis Factor α

VII-Abstract

Craniosynostosis is a common feature of craniofacial birth defects, and is characterised by premature fusion of the cranial sutures in the developing calvarium. Pathogenic FGFR2 signalling is a major cause of syndromic craniosynostosis and is caused by activating mutations within the *FGFR2* gene. In particular, mutations affecting the IIIc isoform (i.e. FGFR2c-C342Y) contribute to coronal synostosis, a common phenotype in human Crouzon syndrome. This study aims to address the downstream effects of misregulated FGFR2c signalling *in vivo*. Conditional overexpression of *Fgfr2c* ($R26R^{Fgfr2cV5/+}$; $\beta actin^{CRE/+}$) results in craniofacial hypoplasia without coronal synostosis, which is in contrast to $Fgfr2c^{C342Y/+}$, a well-studied mouse model for human Crouzon syndrome. Assessment of the coronal suture reveals that $R26R^{Fgfr2cV5/+}$; $\beta actin^{CRE/+}$ and $Fgfr2c^{C342Y/+}$ have opposing phenotypes, where the former display insufficient osteoblast activity. However, biochemical examination of RAS-MAPK activity in embryonic sutures of $Fgfr2c^{C342Y/+}$ and $R26R^{Fgfr2cV5/+}$; $\beta actin^{CRE/+}$ demonstrates upregulated pERK expression. The opposing phenotypes seen between $Fgfr2c^{C342Y/+}$ and $R26R^{Fgfr2cV5/+}$; $\beta actin^{CRE/+}$ mice suggested the possibility that *Fgfr2c* overexpression on the $Fgfr2c^{C342Y/+}$ ($R26R^{Fgfr2cV5/+};\beta actin^{CRE/+};Fgfr2c^{C342Y/+}$) genotype may serve to ameliorate the Crouzon phenotype. This study reports that the Crouzon phenotype was only partly spared in $R26R^{Fgfr2cV5/+};\beta actin^{CRE/+};Fgfr2c^{C342Y/+}$ mice, together with a partial rescue of the coronal suture. The latter was due to delayed calvarial ossification as well as reduced osteoblast activity. Therefore, this study demonstrated that an intricate balance would be required for FGF signalling in order to correct calvarial bone and suture morphogenesis, and that increasing the expression of the wild-type FGFR2c isoform may be a viable method to prevent or delay craniosynostosis progression. In addition, this study has uncovered a novel role for cartilage in craniosynostosis development and has performed comparative expression-profiling (RNAseq) on the E16.5 coronal suture of $Fgfr2c^{C342Y/+}$ and WTs to uncover novel genes potentially involved in syndromic craniosynostosis. Further elucidation of the highly complex FGFR2c signalling pathway remains to be deciphered in order to improve our understanding of normal craniofacial development and its related pathologies, while providing a framework for the innovation of novel therapeutic strategies.

Chapter 1

General Introduction

1.1-An overview of the mammalian skull

The mammalian skull is a complex anatomical structure comprising of the neurocranium and viscerocranium. The framework of the skull offers protection and support as well as forming the basis for the face. The neurocranium ensheathes the brain whilst the viscerocranium supports functions such as those related to eating, breathing and hearing. The major bones of the neurocranium in the human include the frontal, parietal, occipital, sphenoid and temporal bones (Wilkie and Morriss-Kay, 2001) (Figure 1 A). In the mouse, there is an additional interparietal bone located posterior to the parietal bone (Figure 1 B). In order to accommodate brain growth, the calvarium (skull vault) expands throughout infancy along the cranial sutures, which are channels of undifferentiated mesenchyme located between individual bones (Johnson and Wilkie, 2011). Figure 2 illustrates the sutures of the human calvaria.

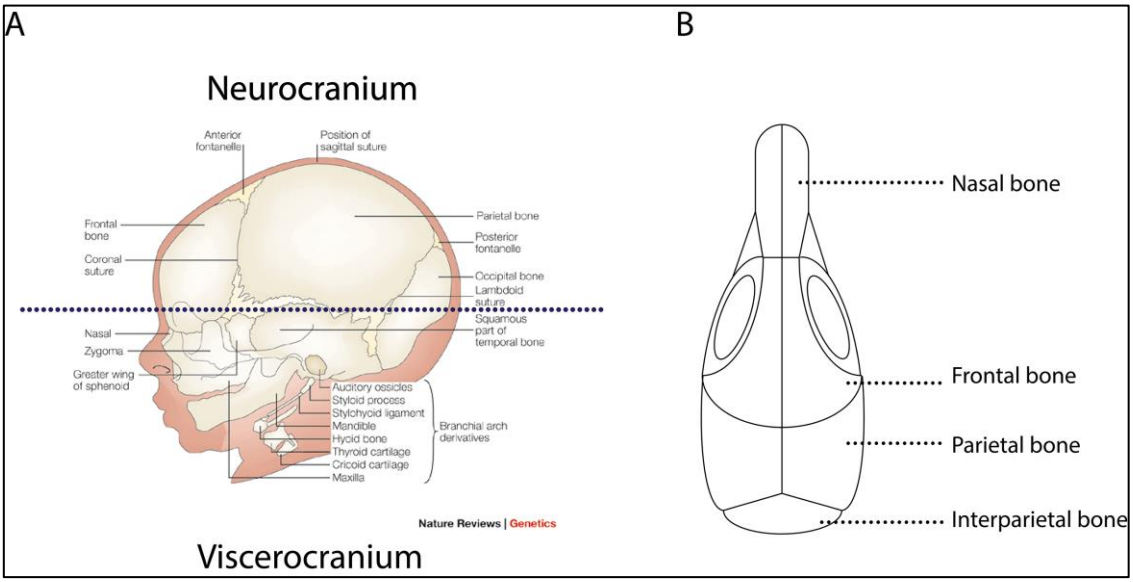

Figure 1: Anatomy of the mammalian skull.

(A) Illustration showing the major bones in the human; (B) and in murine animal. (A) is modified from Wilkie and Morris-Kay 2001.

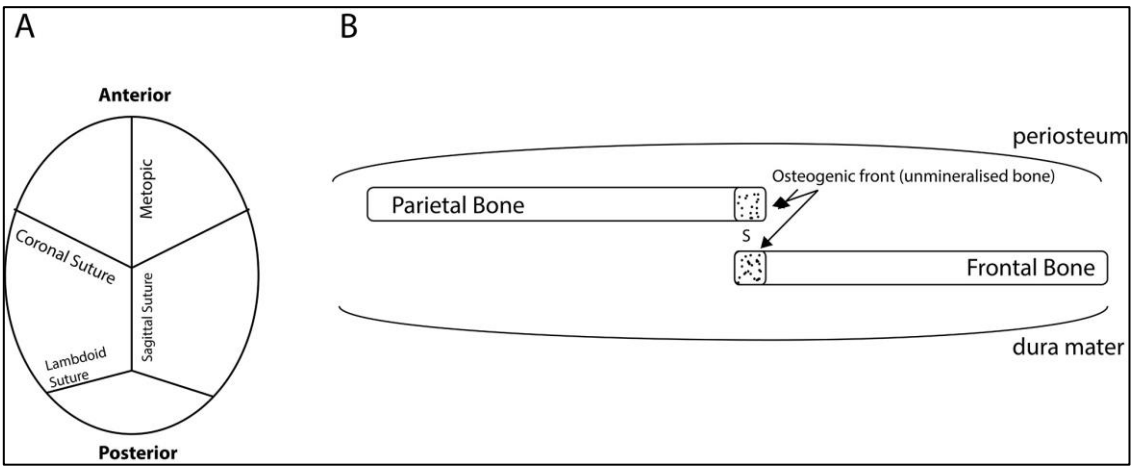

Figure 2: Sutures of the calvaria.

(A) Diagram indicating the sutures of the calvarium; (B) Cross section illustration of a cranial suture.

1.2-Embryonic origins of the head and coronal suture morphogenesis

Significant progress has been made to fate map the embryonic origins of the vertebrate head using a combination of classical embryology techniques (i.e. Carbocyanine Dye labelling) and mouse reporter lines (eg. *Rosa26-LacZ*) (Jiang et al., 2002, McBratney-Owen et al., 2008, Chai et al., 2000, Yoshida et al., 2008, Jiang et al., 2000, Serbedzija et al., 1992, Lumsden et al., 1991). In particular, the availability of mouse reporters enabled lineage tracing of specific groups of cells at a spatial-temporal resolution that were previously limited with classical embryology techniques. The vertebrate skull is derived from two distinct germ layers with skeletogenic potential: the mesoderm and neural crest cells (NCC). Specifically, NCCs located in cranial regions (cranial NCCs; cNCCs) contribute to a large majority of derivatives in the head- forming the basis for the orofacial, frontal-nasal prominence in the calvarium and the viscerocranium ('chondrocranium') (Chai et al., 2000, McBratney-Owen et al., 2008, Yoshida et al., 2008). In addition to this, cNCCs contribute towards cartilaginous elements of the skull: Transplantation of cNCCs into host mesoderm tissue is sufficient to ectopically induce cartilage in the avian embryo (Schneider, 1999, McBratney-Owen et al., 2008). cNCCs are organised into three migratory streams known as the trigeminal, hyoid and post-otic (Figure 3). The latter two streams are beyond the scope of this section (for a comprehensive review, see (Graham et al., 2004)) but the trigeminal stream, arising from the midbrain and rhombomeres 1 and 2, is of significance as it gives rise to the viscerocranium and the orofacial prominence (Serbedzija et al., 1992, Lumsden et al., 1991, McBratney-Owen et al., 2008).

Additionally, cNCCs rostral to the hindbrain-such as the mesencephalic and diencephalic NCCs, are also involved in neurocranium morphogenesis and frontonasal prominence (Lumsden et al., 1991, Yoshida et al., 2008). In combination with reporter lines in higher vertebrates, cell labelling using $Wnt1^{CRE/+}$ specific for NCCs and $Mesp1^{CRE/+}$ for the mesoderm, reveal that the calvaria is derived from two embryonic lineages (Yoshida et al., 2008). NCCs contribute to the frontal bone whilst the parietal bone is solely mesodermal (Figure 4). However, the interparietal bone is of dual embryonic origin. The frontal and parietal

bones are bisected by the coronal suture, juxtaposed at the neural crest-mesoderm interface. Due to the distinct embryonic origins of the calvaria, it can be perceived as an embryonic compartment whereby distinct cell populations are segregated and separated by a cell lineage restricted boundary (Kiecker and Lumsden, 2005). There is a suggestion that the coronal suture is derived from the mesoderm, since these cells appear to be derived from the paraxial mesoderm at E7.5 and are specified by Hedgehog signalling (Yoshida et al., 2008, Deckelbaum et al., 2012, Deckelbaum et al., 2005). Deckelbaum and colleagues (2012) demonstrated that cells forming the coronal suture express the homeodomain factor Engrailed-1 (*En-1*), a transcription factor involved in anterior-posterior patterning, and is responsible for the correct positioning of the coronal suture. These *En-1* precursor cells migrate from the supraorbital region in a rostral-dorsal manner between E11.0-E17.5, forming a boundary with the cNCCs and mesodermal precursors (Figure 5) (Deckelbaum et al., 2012). As the coronal suture mesenchyme is flanked by the osteogenic fronts of the intramembranous bones, maintaining suture patency will therefore require tightly co-ordinated cross-talk between the osteogenic fronts and the suture mesenchyme to sustain cellular proliferation and differentiation.

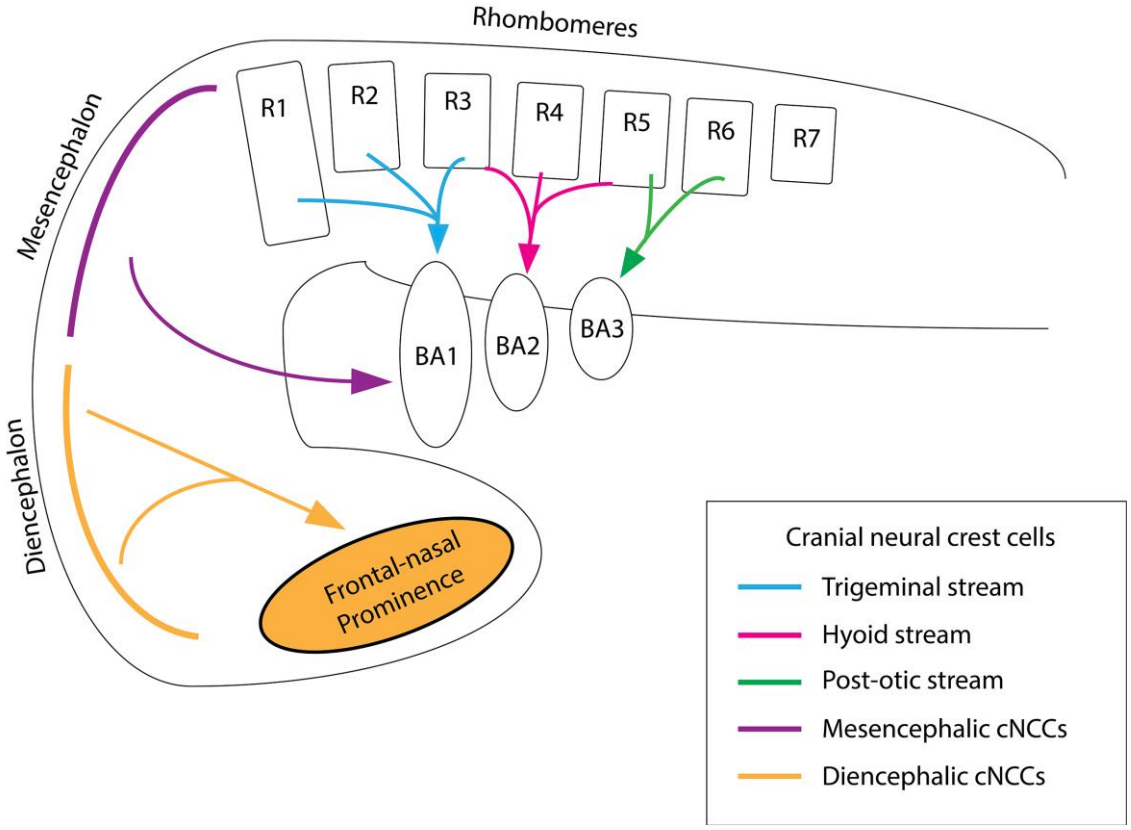

Figure 3: Schematic showing cNCCs in the developing embryo.

Rostral cNCCs include diencephalic and mesencephalic cNCCs (Yellow and purple respectively). Major cNCCs migratory streams of the rhombomeres include the Trigeminal (Blue), Hyoid (Pink), Post-Otic (Green) streams.

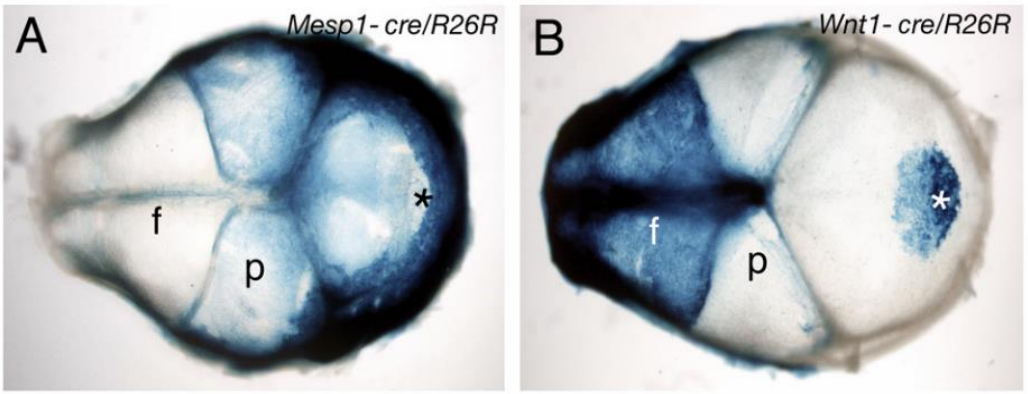

Figure 4: The embryonic derivatives of the calvaria.

The frontal bone (F) is derived from the NCCs while the parietal bone (P) is from the mesoderm. Adapted from Yoshida et al., 2008.

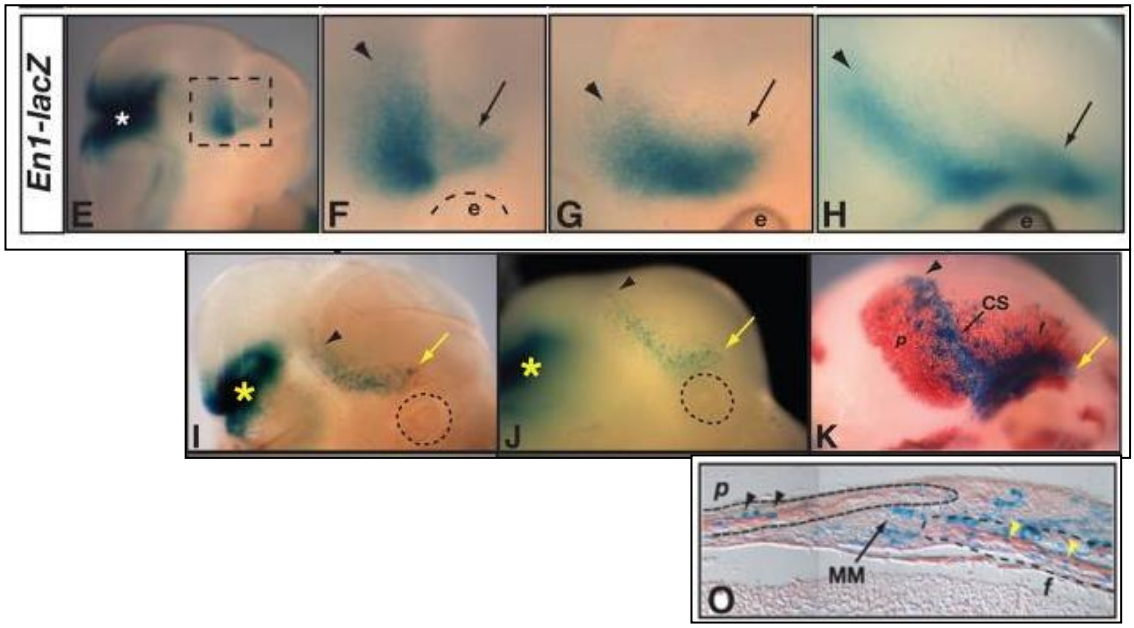

Figure 5: Embryonic derivative of the coronal suture.

Coronal suture precursors (En^+ cells) are Hedgehog responsive and are derived from the paraxial mesoderm at E7.5 as indicated by *En1-R26-LacZ* lineage tracing. These cells halt at the supraorbital region before migrating dorsally and apically to form the suture. Adapted from Deckelbaum et al., 2012.

1.4-Molecular basis of FGF signalling

There are 23 distinct Fibroblast Growth Factors (FGF) which interact with 4 families of FGF receptors (FGFR) (FGFR1, FGFR2, FGFR3, FGFR4) (Ornitz and Itoh, 2015). FGFs are grouped by sequence homology and are structurally similar, where they have a conserved sequence of around 120 amino acids long. FGF ligands have different affinities towards the receptors and the interpretation of its signalling output and cellular response are highly complex. Affinity of FGF ligands towards its receptor is modulated by heparin/heparin sulphate proteoglycans binding to FGF ligands extracellularly (Eswarakumar et al., 2005). Table 1 summarises the receptor specificity of FGF ligands.

Subfamily	FGF	Cofactor	Receptor Affinity
	FGF1	Heparin or Heparin Sulphate	ALL FGFRs
FGF1	FGF2		FGFR1c, 3c > 2c, 1b, 4
FGF4	FGF4 FGF5 FGF6		FGFR1c, 2c > 3c, 4
FGF7	FGF3 FGF7 FGF10 FGF22		FGFR2b > 1b
FGF8	FGF8 FGF17 FGF18		FGFR3c > 4 > 2c >1c >3b
FGF9	FGF9 FGF16 FGF20		FGFR3c > 2c > 1c, 3b > 4
	FGF15/19		FGFR1c, 2c, 3c, 4
	FGF21	βKlotho	FGFR1c, 3c
FGF15/19	FGF23	αKlotho	FGFR1c, 3c, 4

Table 1: FGF ligand affinities.

Data assembled from Ornitz and Itoh, 2015.

FGFRs are receptor tyrosine kinases (RTKs) dimers consisting of an extracellular binding domain, transmembrane domain and a tyrosine protein kinase located intracellularly. The extracellular portion of the receptor consists of three immunoglobulin-like loops (IgI, DI-DIII) each possessing unique functions. In particular, the DII and DIII domains serve as the major ligand-binding site. The DIII loop determines the different isoforms of FGFRs and is therefore ligand specific. Alternative splicing of mRNA transcripts in the 3' (C-terminal) half of DIII loop determines the expression of 'IIIb' and 'IIIc' isoforms, occurring solely in FGFR1, FGFR2 and FGFR3. The 'IIIb' and 'IIIc' isoforms are encoded by exons 8 and 9 respectively, whilst exon 7 codes for the N-terminal of DIII ('IIIa') (Figure 6) (Eswarakumar et al., 2005). In addition, expression of the 'IIIb' and 'IIIc' isoforms are tissue specific: while the 'IIIb' isoform is expressed in epithelial tissue, the 'IIIc' isoform is mainly expressed in the mesenchyme (Orr-Urtreger et al., 1993). Receptor activation usually involves FGF ligands expressed in the tissue complementary to its receptor establishing a paracrine loop between the epithelium and mesenchyme (Eswarakumar et al., 2005, Ornitz and Itoh, 2015). An example for this interaction can be found in the developing limb bud, between *Fgfr2b* (epithelial) and *Fgf10* (mesenchymal) (Li et al., 2007). One of the key regulatory elements for FGFR2 splice forms lies in intron 8, located in the intragenic region between exons 8 and 9 of FGFR2 (Warzecha et al., 2010). Alternative splicing of IIIb and IIIc isoforms is effected by Epithelial Splicing Regulatory Protein (ESRP) 1 and ESRP2, which were originally identified in a high throughput cDNA screen (Warzecha et al., 2010). Both variants of ESRPs were enriched in epithelial cell lines (e.g. PNT2) with high endogenous expression of *Fgfr2b*. ESRPs coordinate alternative splicing of FGFR2 primarily towards the IIIb isoform, overexpression of ESRPs in mesenchymal cell lines that result in a splice switch from IIIc to IIIb (Warzecha et al., 2010). These splice switches have important implications in development, where they help to control the temporal ligand-mediated response of the tissue (Warzecha et al., 2010).

1.4.1-Cytosolic signalling pathways of FGFR

FGFR signal transduction is mediated through three major pathways: RAS-MAPK, PI3K-AKT and PLCγ-PKC pathways (Figure 7). Upon ligand binding, the receptor dimerises

and is autophosphorylated, leading to the recruitment and coupling of the anchor protein FRS2α (Fibroblast Growth Factor Substrate) at the receptor. FRS2 is required for FGFR signal transduction, as FRS2α null embryos exhibit embryonic lethality at E7.5 (Hadari et al., 2001). It is responsible for assembling a multiprotein complex consisting of docking and effector proteins which transduce signals to downstream kinases leading to transcriptional activation: Formation of the Grb2-Sos (Growth factor receptor bound 2-Son of Sevenless) complex is common to activate both RAS-MAPK and PI3K-AKT pathways. In addition to these, FGFR can also convey their signals via PLCγ-PKC pathway through a series of calcium signalling intermediates (Eswarakumar et al., 2005, Ornitz and Itoh, 2015). FGF signalling can be negatively regulated at multiple levels of the cascade. For example, Sprouty (Spry) family proteins regulate both the sensitivity of RAS-MAPK pathway and PI3K-AKT pathway through inhibition of Grb2. Downstream of the cascade, MAPK can be inactivated by Dusp6 (Dual Specificity Phosphatase 6). The most common transcriptional targets for FGF signalling pathway include *ETS* (E-Twenty Six; RAS-MAPK pathway), *FOXO1* (Forkhead box protein 1; P13K-AKT pathway) and *STAT* (Signal Transducer and Activator of Transcription; PLCγ-PKC pathway), each playing a handful of roles (Ornitz and Itoh, 2015). In the RAS-MAPK pathway, ETS expression leads to transcriptional activation of downstream genes associated with FGF signalling whilst in the P13K-AKT pathway, FOXO1 inhibition has anti-apoptotic effect. Expression of STAT by the PLCγ-PKC pathway activates target gene expression in the STAT pathway (Ornitz and Itoh, 2015). Collectively, cellular response towards FGF target gene expression is associated with controlling proliferation, differentiation, survival and migration (Ornitz and Itoh, 2015).

Activation of FGF signalling also drives signal transduction via non-canonical cascades. STAT1, STAT3 and STAT5 can directly bind to the receptor and translocate to the nucleus to initiate gene expression. In regards to cellular function, STAT proteins play an important role in FGFR3 signalling to modulate cellular proliferation via expression of cell cycle inhibitor p21 (Sahni et al., 1999). Other pathways that FGFRs influence include p38, Src and Jnk albeit the mechanisms are less well characterised (Brewer et al., 2015). Interestingly, a

novel signalling mechanism has been implicated for FGF signalling whereby the receptor and ligand are co-translocated to the nucleus after receptor internalisation (Maher, 1996, Reilly et al., 2004). This process has been mainly studied in FGFR1 and is shown to be clathrin dependent endocytosis (Reilly et al., 2004). This nuclear translocation mechanism is also reported in FGFR2 and FGFR3 (Zhou et al., 2015a, May et al., 2016). Upon reaching the nucleus, the complex is imported into the nucleus interior via the cargo protein importin β (Reilly and Maher, 2001). The consequence of FGFR1 nuclear localisation is believed to be related to regulation of cell proliferation, for which it facilitates expression of c-Jun and cyclin D1 (Reilly and Maher, 2001). From a clinical perspective, mis-translocation is implicated in cellular transformation in cancers (Coleman et al., 2014, May et al., 2016). The signals that initiate nuclear entry remain elusive, but the signal peptide is believed to be within the transmembrane domain of the receptor (Myers et al., 2003).

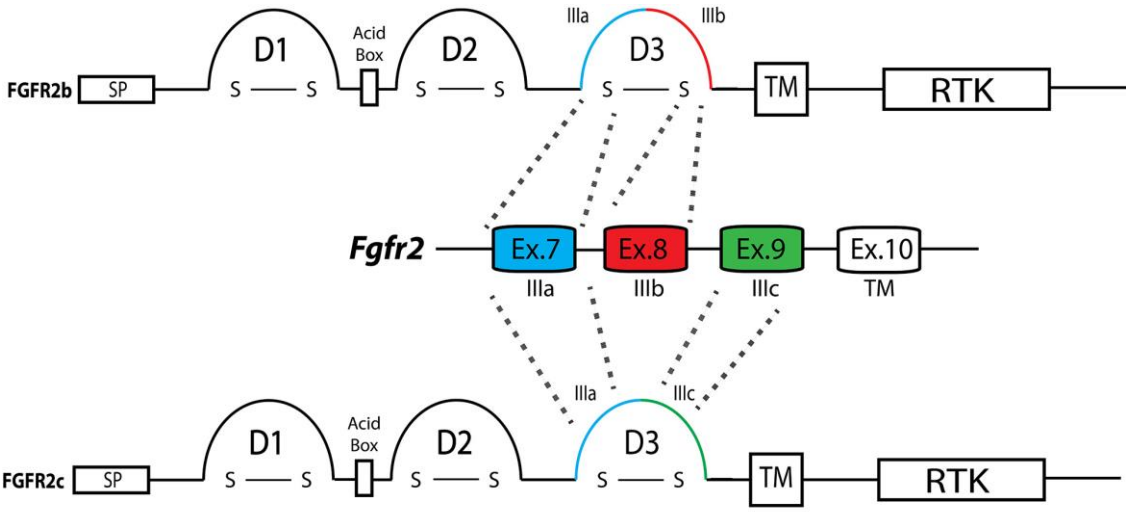

Figure 6: Alternative splicing of human and mouse *FGFR2*

Exons 8 and 9 encode for the posterior portion of the D3 Ig loop, and produce the two *FGFR2* isoforms. *FGFR2b* is produced from alternative splicing of exon 8, and *FGFR2c* from exon 9 respectively. Exon 7 is common to both isoforms and accounts for the anterior portion (IIIa) of the D3 loop. TM: transmembrane domain, RTK: (receptor) tyrosine kinase domain.

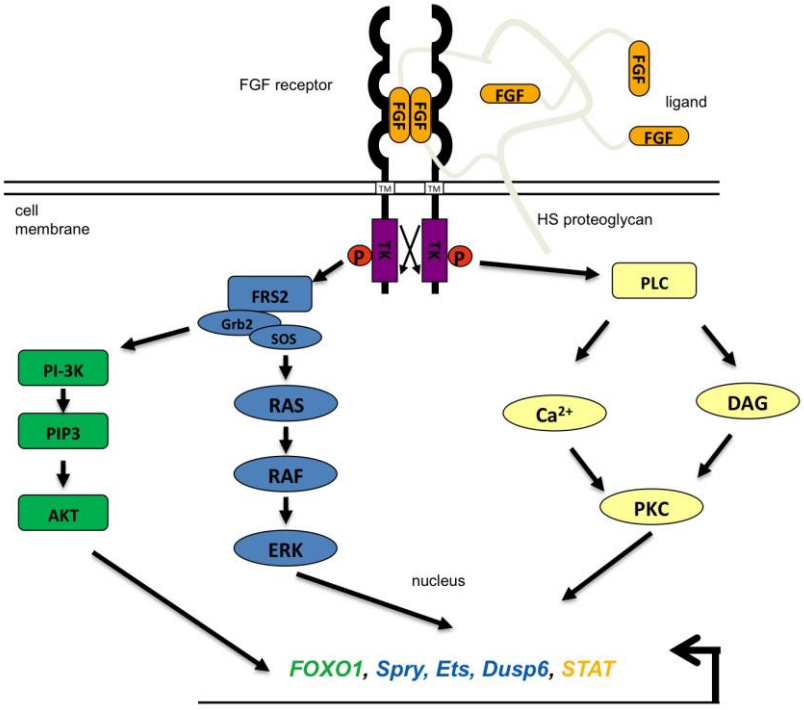

Figure 7: FGF signalling pathway.

Activation of FGFRs activates the PI3K-AKT (Green), RAS-MAPK (Blue) and PLCγ-PKC (Yellow) pathways. The respective colour of each target gene corresponds to the pathway. Image courtesy and modified from: Erwin Pauws.

1.4.2-Kinetics of FGF signalling

1.4.2.1-Autophosphorylation domains of FGFRs

FGFRs dimerize and induce trans-phosphorylation of the tyrosine kinase (TK) domain upon ligand binding. The first phase of phosphorylation involves the Y653 tyrosine residue, followed by Y583, Y463, Y766 and Y785 in the second phase. The last phase of phosphorylation requires activation of Y654 (Ornitz and Itoh, 2015). This sequential phosphorylation of tyrosine residues leads to amplification of tyrosine kinase activity by a factor of 500-1000 fold (Ornitz and Itoh, 2015). In addition to signal amplification, phosphorylation of distinct tyrosine residues results in recruitment of binding proteins required for downstream signalling transduction via RAS-MAPK, PI3K-AKT and PLCγ-PKC cascades (Figure 8) (Ornitz and Itoh, 2015). RAS-MAPK and PI3K-AKT activation requires the FGFR kinase FRS2α phosphorylation, which is constantly bound to the juxtamembrane of FGFR (Ornitz and Itoh, 2015). Upon receptor activation, FRS2α is activated by CRKL (CRK-Like protein) that is bound to Y463 (Figure 8; 1). Phosphorylated FRS2α consequently recruits Grb2 to the receptor to initiate downstream signal transuction (Figure 8; 2) (Ornitz and Itoh, 2015). The Y766 residue is required for the activation of the PLCγ-PKC pathway, whilst a docking site is present on Y677 for STAT proteins respectively. (Ornitz and Itoh, 2015) Therefore, differential activation of these tyrosine residues will result in diverse cellular response. This is elegantly shown *in vivo* where introduction of a point mutations in the transmembrane domain (L424A and R426A; $Fgfr2^{CLR}$ allele) prevented FRS2α recruitment and abolished both RAS-MAPK and PI3K-AKT signalling (Eswarakumar et al., 2006). Furthermore, introduction of the Fgfr2-CLR allele into the Crouzon mouse model ($Fgfr2c^{C342Y/+}$) resulted in a rescue of craniofacial malformations implicating the role of RAS-MAPK and/or PI3K-AKT in its pathogenesis (Eswarakumar et al., 2006). Similar examples can be drawn in FGFR1 hypomorphs, where targeting of the Y766 site in *Fgfr1* gene led to defects of the axial skeleton due to abrogation of PLCγ-PKC signalling (Partanen et al., 1998). Therefore, targeting specific tyrosine residues downstream of receptors enable the elucidation of cascades contributing to a pathogenic phenotype. Similar work was performed in PDGFRα, whereby a series of autophosphorylation

mutants were generated by knockin technologies in order to understand activation of downstream cascades (Klinghoffer et al., 2002). One allele targeted Y731/Y742 residue that prevented activation of PI3K; whilst another targeted the Y572/Y574 residues that prevented recuitment of Src, a cytoplasmic tyrosine kinase (Klinghoffer et al., 2002). Although substantial efforts were made to understand the signal transduction, little is known about the consequences within an *in vivo* context. Differential activation of the TK domain is responsible to translate effects caused by ligand/independent receptor activation (next section). Signal transduction by receptor tyrosine kinases (RTKs) could either drive an additive or differential cellular response. For example, a cumulative response can be hypothesised when disrupting multiple tyrosine residues that lead to a similar, but subtle phenotypic spectrum (i.e. binding sites to FRS2 and PLCγ) (Brewer et al., 2015, Partanen et al., 1998). In contrast, differential cellular response is hypothesized when a receptor is able to drive two distinct cellular responses. This is evident in endochondral ossification where activation of FGFR3 can inhibit chondrocyte proliferation via STAT and hypertrophic differentiation is prevented by RAS-MAPK signalling (Li et al., 1999, Murakami et al., 2004). The mechanism for such differences, despite conserved RTK domains across FGFRs, is not well understood (Ornitz and Itoh, 2015). However, it is likely to be related on how the receptor perceives the signal, which in turn influences receptor activation (discussed in the next section 1.4.2.2).

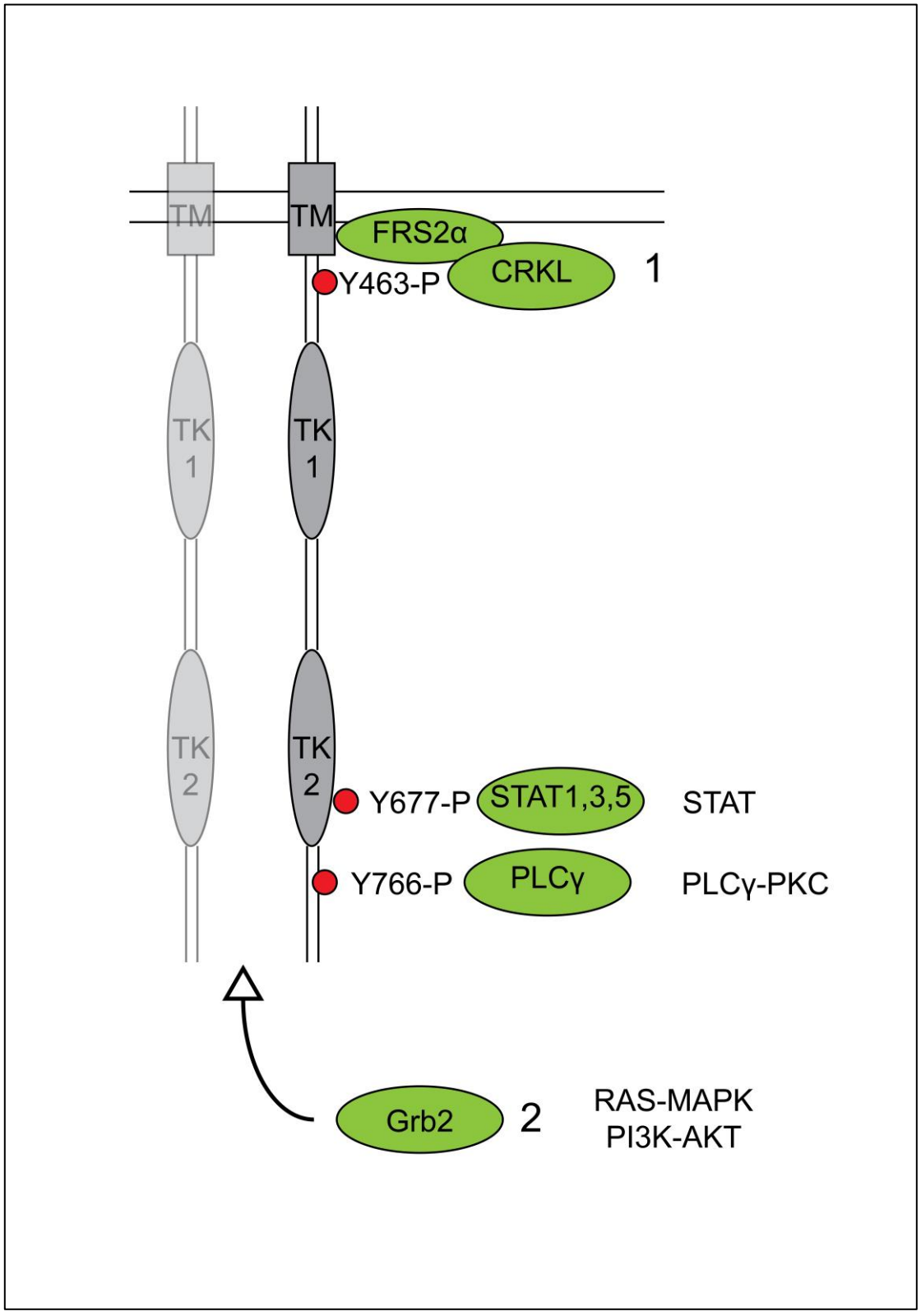

Figure 8: Tyrosine residues (red circles) required for RAS-MAPK, PI3K-AKT, STAT, PLCγ-PKC activation.

RAS-MAPK and PI3K-AKT: FRS2α is constantly bound to the juxtamembrane of FGFR. Upon receptor activation, FRS2α is activated by CRKL (CRK-Like protein) that is bound to Y463 (1). Phosphorylated FRS2α consequently recruits Grb2 to the receptor to initiate downstream signal transuction (2); STAT pathway activation requires Y677 phosphorylation and recruitment of PLCγ requires Y766 respectively. TM: transmembrane domain; TK: tyrosine kinase.

1.4.2.2-Intracellular response and dynamics of FGF signalling

Despite multiple ligands having affinities towards a given FGFR, it is possible that the nature of their signal transduction mechanisms is different. This is particularly important to address how signals are conveyed from the extracellular domain of the receptor to influence RTK activation. Receptor activation can be either ligand dependent or independent, which gives distinct signalling output and downstream interpretation. An example for the former instance can be drawn in the role of FGF7 and FGF10 in branching morphogenesis of the lung (Francavilla et al., 2013). Despite having affinities for FGFR2b, application of FGF7 in *ex vivo* lung cultures led to formation of cysts in contrast to that of FGF10, which promoted branching of the lung (Francavilla et al., 2013). This phenotypic consequence is due to receptor activation by FGF7 that led to cellular proliferation whilst FGF10 stimulated a migration response. On a molecular level, FGF10 facilitates activation of Y734 domain in the RTK that is the main driver causing these differences in cellular response. Specific activation of the Y734 tyrosine residue is responsible for promoting receptor recycling to the cell surface after endocytosis and concommitant downstream augmentation of PI3K-AKT signalling. However, binding of FGF7 to FGFR2b results in the opposite response where the receptor is degraded in the endosomes after endocytosis, which is independent of Y734 phosphorylation (Francavilla et al., 2013). This differential response caused by receptor trafficking ultimately determine amplitude and temporal dynamics of signal transduction. Here, application of FGF10 can be perceived as possessing a sustained response to receptor activation, whereby the signal elicited by FGF7 binding is transient due to increased receptor degradation (Francavilla et al., 2013). Altered trafficking dynamics were also reported in receptors independent of ligand activation. For example, a variant of the Crouzon mutation (C278F) has increased retention from the membrane due to increased ubiquitination by the E3 ubiquitin ligase Cbl (Hatch et al., 2006). The mechanisms causing aberrant receptor turnovers mutant FGFRs are yet to be investigated in detail even though a substantial cohort of craniofacial syndromes being caused by aberrant FGF signalling. Despite substantial efforts having been made to dissecting the pathway responsible for proliferation and differentiation (Ornitz and Marie, 2015, Marie, 2012), the mechanisms

controlling signalling dynamics concerning individual mutations on FGFRs still remain unclear. A particular focus could be to investigate signals and regulators required for protein sorting immediately after receptor activation. For example, cytoplasmic TKs such as Src, which is recruited to FRS2 immediately after FGFR activation, helps to internalise the receptor (Sandilands et al., 2007, Kaabeche et al., 2004). Of note, a comprehensive review on the effects of known TRK receptor trafficking has been published elsewhere (Miaczynska, 2013). Understanding the full picture for receptor trafficking will provide a critical insight to how signals are modulated and the subsequent effect on the transduction cascades.

How does two FGF ligands elicit a dissimilar response on the same receptor? This could relate to the FGF ligand affinities to co-factors such as Heparin Sulphate Proteoglycans (HSPGs). HSPGs are cell surface and extracelluar matrix (ECM) proteins that consists of a core protein, to which heparin sulphate glycosaminoglycan chains are attached (Lin, 2004). Core proteins of HSPG includes syndecan, perlecan, glypican and agrin. These can be anchored to the transmembrane (e.g. syndecan), localised on the cell surface (e.g. glypican) or diffusible in the ECM (e.g. perlecan or agrin) (Lin, 2004). FGFRs have a binding site for HSPG in the IglII loop to increase affinity of FGFs towards its receptor (Lin, 2004). HSPGs can modulate the morphogenic nature of FGFs that results in changing the binding affinity to receptors. FGF10 and FGF7 have different affinity towards HSPGs, and mutating a binding site (R187V) for HSPG on FGF10 mimicked the cellular events normally caused by FGF7 through FGFR2b signalling during branching morphogenesis. Together with Francavilla et al (2013), these results explain the role of HSPG in modulating the ligand's association with the receptor, which consequently elicit differential activation of the RTK domain and cellular response (Makarenkova et al., 2009). Other co-factors acting on the FGF signalling pathway include two Klotho family members, αKlotho and βKlotho, which act as binding partners for endocrine FGFs in place of HSPGs (Kuro-o, 2008). FGF15/19, FGF21 and FGF23 have low affinity towards HSPGs to that of paracine FGF ligands which allow the ligands to diffuse more freely across the ECM (Kuro-o, 2008). Indeed, disruption to endocrine FGFs is associated with a number of metabolic diseases. For example, FGF15 and FGF19 are secreted from intestines

modulate bile synthesis from the liver (Inagaki et al., 2005). Other modes of signalling include intracellular FGFs, comprising of the FGF11 family (FGF11, FGF12, FGF13 and FGF14). Little is known about their roles, but they are not known to bind to FGFRs (Olsen et al., 2003). However, they may assist on post-translational modifications and interaction with cytoskeleton (Wu et al., 2012).

Genetic ablation or gain of function (GOF) approaches to critical mediators of FGF signalling have provided substantial insights into the nature of downstream signalling. Therefore, it is widely accepted that the interactions between FGF ligands and FGFRs can function individually or in combination (See section; Mouse models). The latter is particularly notable since it is widely thought that FGF signals are conveyed through FGFR homodimers. However, additional research have provided insights into FGFRs that are capable of forming heterodimers. These studies include i) FGFR2 is able to transphosphorylate cells expressing a dominant negative form of FGFR (Bellot et al., 1991); ii) Overexpression of truncated FGFR1, lacking the cytoplasmic domain, is able to sequester activation of FGFR2-3 upon ligand binding (Ueno et al., 1992); iii) Recently, heterodimer interactions within FGFRs were confirmed via Forster Resonance Energy Transfer (FRET) (Del Piccolo et al., 2017). Here, the C-terminal domains of the FGFR1-3 were replaced with a respective fluorescent tag (e.g. mCherry). FGFR heterodimers were confirmed by FRET when a strong heterogenous signal was detected in proximity to each other. In the same study, the authors also investigated the effects of GOF mutations affecting FGFR3 (i.e. A391E and G380R) and found that they can also stabilise FGFR1 and FGFR2 (Del Piccolo et al., 2017). It is unknown as to the role of heterodimers in controlling the dynamics FGF signalling. A speculation could be to help increase the diversity for FGF signalling response. Similarities can be drawn in Platelet Derived Growth Factor (PDGF) signalling, where the α and β isoforms of Platelet Derived Growth Factor Receptor (PDGFR) are interchangable (Klinghoffer et al., 2001). However, downstream RTK signalling is likely to be conserved, whereby displacing the extracellular domain for one another (i.e. α to β and β to α) led to a largely redundant phenotype in PDGFRs (Klinghoffer et al., 2001).

In summary, to understand the kinetics of FGF signalling a multitude of factors must be considered ranging from the cell surface to intracellular signal transduction. Questions must be asked as to the immediate consequences after receptor activation that could influence subsequent signal transduction. This section has given examples on how phosphorylation of specific tyrosine residues can influence specific cascade activation and receptor turnovers. The complex interactions at the level of the receptor will therefore determine the outcome of the amplitude, and temporal dynamics of signal transmission.

1.5-Modes of bone formation

1.5.1-Endochondral ossification

Endochondral bones form from gradual displacement of cartilage template to bone. An intricate balance of chondrocyte specification, proliferation, differentiation and maturation are key to this process (Yeung Tsang et al., 2014). Chondrocytes lay down a series of ECM proteins as they mature, laying the foundation of the immature bone (Dreier et al., 2008, Kapyla et al., 2004). Deviation from normal chondrogenesis results in skeletal dysplasia and long bone defects ranging in phenotypic severity, which could be progressive or resulting in perinatal lethality (Yeung Tsang et al., 2014). Endochondral ossification can be summarized into three main processes: mesenchymal condensation (around E11.5), chondrocyte maturation (E13.5), primary (E15.5) and secondary ossification centre formation (P7) (Kozhemyakina et al., 2015). This is illustrated in Figure 9. Briefly, Mesenchymal stem cells (MSCs) cluster together to form osteo-chondroprogenitors which are bi-potential in nature (Barna and Niswander, 2007, Karuppaiah et al., 2016, Day et al., 2005). These cells are restricted in fate and adopt either an osteogenic or chondrogenic lineage to form osteoblasts and chondrocytes respectively (Day et al., 2005). Committed chondroprogenitors subsequently differentiate into chondrocytes that proliferate, matures and undergo cellular hypertrophy (Day et al., 2005). This series of events consequentially lead to the formation of the cartilage template ensheathed by the perichondrium (Colnot et al., 2004). The perichondrium is involved in formation of the bone collar, for which cells differentiate into osteoblasts to give rise to the future periosteum (Colnot et al., 2004).

During this time, primary ossification commences through vascular invasion of the periosteum, allowing blood vessels to penetrate into the calcifying cartilage (Colnot et al., 2004). Simultaneously, vascular invasion allows bone remodelling to occur, for which blood vessels carry cells (i.e. osteoclast and chondroclasts) involving in this process (Yeung Tsang et al., 2014). The consequent remodelling of the cartilage template allows osteoblasts to lay down calcified matrix allowing osteogenesis to occur, aiding the formation of the trabecular bone (Colnot et al., 2004). Gradually, the cartilage template is split into two ends by the calcified matrix, forming the epiphysis (Colnot et al., 2004).

The growth plate is absolutely essential for endochondral ossification as it controls the progressive events of chondrocyte proliferation, differentiation and maturation (Dreier et al., 2008, Dy et al., 2012). This enables the correct formation of the cartilage template required for the bone cellular architecture. The growth plate possesses a hierarchal structure and consists of four zones: Resting zone (RZ) consists of round chondrocytes that serves as a progenitor pool for proliferation and differentiation. In the proliferation zone (PZ), the rounded chondrocytes are flattened, reorganized and aligned into columns that are important for longitudinal growth (Kozhemyakina et al., 2015, Yeung Tsang et al., 2014). These cells continue to divide in columns. In the pre-hypertrophic zone, the cells begin to undergo hypertrophic differentiation through cell cycle exits (Beier et al., 2001, Beier et al., 1999). Finally, in the hypertrophic zone (HZ), pre-hypertrophic chondrocytes terminally differentiate and greatly increases in size (Colnot et al., 2004, Vortkamp et al., 1996). The lowermost boundary of the HZ is gradually calcified and replaced by bone (Colnot et al., 2004).

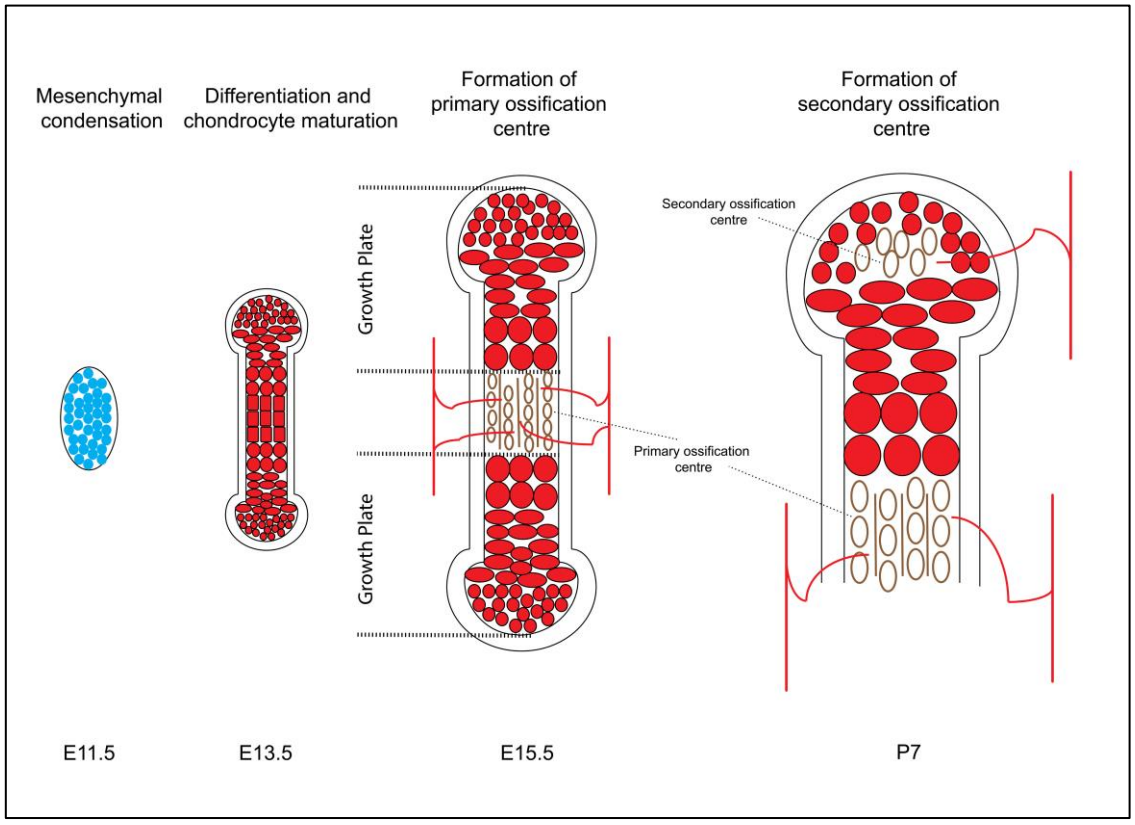

Figure 9: A schematic showing endochondral ossification.

Mesenchymal condensation occurs (blue cells) at E11.5 in the limb bud. MSCs differentiate into chondrocytes (red) at E13.5, and are surrounded by the perichondrium (white lining). As endochondral ossification progresses, the bone is separated by the osteoid, where vascularization (red lines) commences at roughly E15.5. This subsequently leads to formation of the primary ossification centre where chondrocytes are gradually displaced into bone. Gradually, the cartilage template is split into two ends by the calcified matrix (open circles), forming the epiphysis. The growth plate is essential for endochondral ossification as it controls the progressive events of chondrocyte proliferation, differentiation and maturation. Lastly, a secondary ossification centre forms at roughly P7, displacing the residual chondrocytes in the growth plate. Assembled from (Kozhemyakina et al., 2015).

1.5.1.1-Mesenchymal condensation

The first stage of endochondral condensation requires mesenchymal progenitors cells to be differentiated towards a chondrocytic lineage, which occurs around E11.5 (Kozhemyakina et al., 2015). The initiation of this process is highly dependent on transforming growth factor β (TGFβ) signalling (Barna and Niswander, 2007, Lim et al., 2015). The TGFβ superfamily comprises of bone morphogenic protein (BMP) and TGFβ, which bind to their receptor complexes to activate SMAD transcriptional cofactors. BMP signals are tranduced via SMAD1, SMAD5 and SMAD8 whilst TGFβ signals are conveyed through SMAD2 and SMAD3. These SMAD cofactors are classified as 'R-SMADS' (receptor activated SMADs), referring to the direct release from the receptor complex upon signalling activation. R-SMADs subsequently form heterodimers with SMAD4, which translocates to the nucleus to initiate downsteam gene expression (Derynck and Zhang, 2003). In a live imaging study conducted by Barna and Niswander (2007), BMP signalling was shown to be required for cellular compaction of mesenchymal condensates (Barna and Niswander, 2007). Failure to form this condensate, due to genetic ablation of both *Bmp2* and *Bmp4* in the mesenchyme, resulted in ulna and posterior digital malformation (Bandyopadhyay et al., 2006). BMP2 and BMP4 signals are likely to be conveyed through SMAD4 as its loss of function (LOF) led to loss of cellular condensates (Benazet et al., 2012). However, a largely normal phenotype is yielded should either one copy of *Bmp2* or *Bmp4* is available, implicating ligand redundancy. BMP signalling is critical to induce chondrocyte specification as $Smad4^{-/-}$ led to a reduction of Sox9 (Sry HMG Box 9) and Collagen (Col) 2 protein expression (Benazet et al., 2012).

Sox9 is the single most important transcription factor required for chondrogenesis, and its ablation leads to complete loss of cartilage elements (Bi et al., 1999, Akiyama et al., 2002). Lineage tracing of *Sox9* reveals it is expressed in the condensing mesenchyme and all cartilage primordia (Bi et al., 1999). In humans, LOF mutation to *SOX9* is associated with campomelic dysplasia, and is phenotypically described as hypoplasia of all endochondral elements (Foster et al., 1994). Chondrocytes express a multitude of collagens as they mature: Immature chondrocytes are characterized by high abundance of *Col2a1* and *Col9a1* expression together

with a series of matrix proteoglycans (Gomez-Picos and Eames, 2015, de Crombrugghe et al., 2001). In particular, deposition of these proteins by immature chondrocyte lays the foundation of the developing cartilage, whilst mature chondrocytes re-models the cartilage ECM and subsequently mineralizing it (Gomez-Picos and Eames, 2015). *Sox9* is critical to drive the downstream expression of *Col2a1 and Col9a1* and is therefore, important to drive the correct formation of cartilage primordia (Zhou et al., 1998). From a clinical point of view, skeletal dysplasia is caused by disruption to cartilage and bone development. There are approximately 400 skeletal dysplasias identified so far, which can be either a GOF or LOF, and are commonly associated with dwarfism and embryonic lethality (Yeung Tsang et al., 2014). Therefore, the correct formation of cartilage is critical for normal bone development, particularly being reliant on the intricate balance of chondrogenesis at the growth plate.

1.5.1.2-Chondrogenesis in the growth plate

Chondrocytes continue to mature, becoming hypertrophic and ultimately form the basis of the cartilage template as mesenchymal condensation progresses. This highly coordinated temporal-spatial control of chondrogenesis essentially forms the basis of the growth plate. The growth plate can be loosely defined as chondrocytes in their different stages of maturation, and is characterized by an array of markers expressed in the different zones (Figure 10) (Kozhemyakina et al., 2015). In addition to the master regulator for chondrocyte differentiation, *Sox9* is important to sustain chondrocyte identity (Bi et al., 1999, Akiyama et al., 2002). *Sox9* is upstream of *Sox5* and *Sox6* (Akiyama et al., 2002), and the trio coordinate chondrocyte specification through regulation of genes that define its function such as *Col2a1* (Smits et al., 2004, Smits et al., 2001, Lefebvre et al., 2001). The importance of *Col2a1* has been highlighted in a mouse model in which its conditional inactivation led to the loss of the growth plate (Li et al., 1995). As *Col2a1* defines immature and mature chondrocytes across the growth plate, its ablation led to insufficient chondrocytes being amplified and resulted in truncation of the axial skeleton (Li et al., 1995). Control of the cell cycle is critical to progress onto subsequent stages of the maturation process. Whether the cell decides to continue proliferating or exit the cell cycle for events such as differentiation, lies with G_1 phase of the cell cycle (Beier et al., 1999).

Progression in the cell cycle requires cyclin dependent kinase (CDKs), which is partnered with specific cyclin proteins to elicit target gene expression for cell cycle response and DNA replication. Chondrocytes express all of the D-type cyclins (D1, D2 and D3), which are involved in facilitating cellular proliferation (Beier et al., 1999). A comprehensive review on cell cycle mediators in chondrocytes is described elsewhere (Beier et al., 1999). However, *in vivo* literature on the role of cyclin in bone development is limited. Nonetheless, the growth plate of mice lacking cyclin D1 is considerably smaller, in particular to the proliferation zone (Beier et al., 2001). It is understood that cyclin D1 integrates signals from multiple pathways such as Parathyroid Hormone Related Peptide (PTHrP) and Hedgehog (Indian hedgehog, Ihh) (Beier et al., 2001, Long et al., 2001), linking their roles in controlling cellular proliferation. It is well understood that paracrine factors such as FGFs and IHH are expressed at the outer edges of the bone i.e. perichondrium/periosteum, to facilitate endochondral growth and chondrocyte survival (Figure 10) (Kozhemyakina et al., 2015). The next section will focus on the main pathways that facilitate chondrocyte proliferation and differentiation.

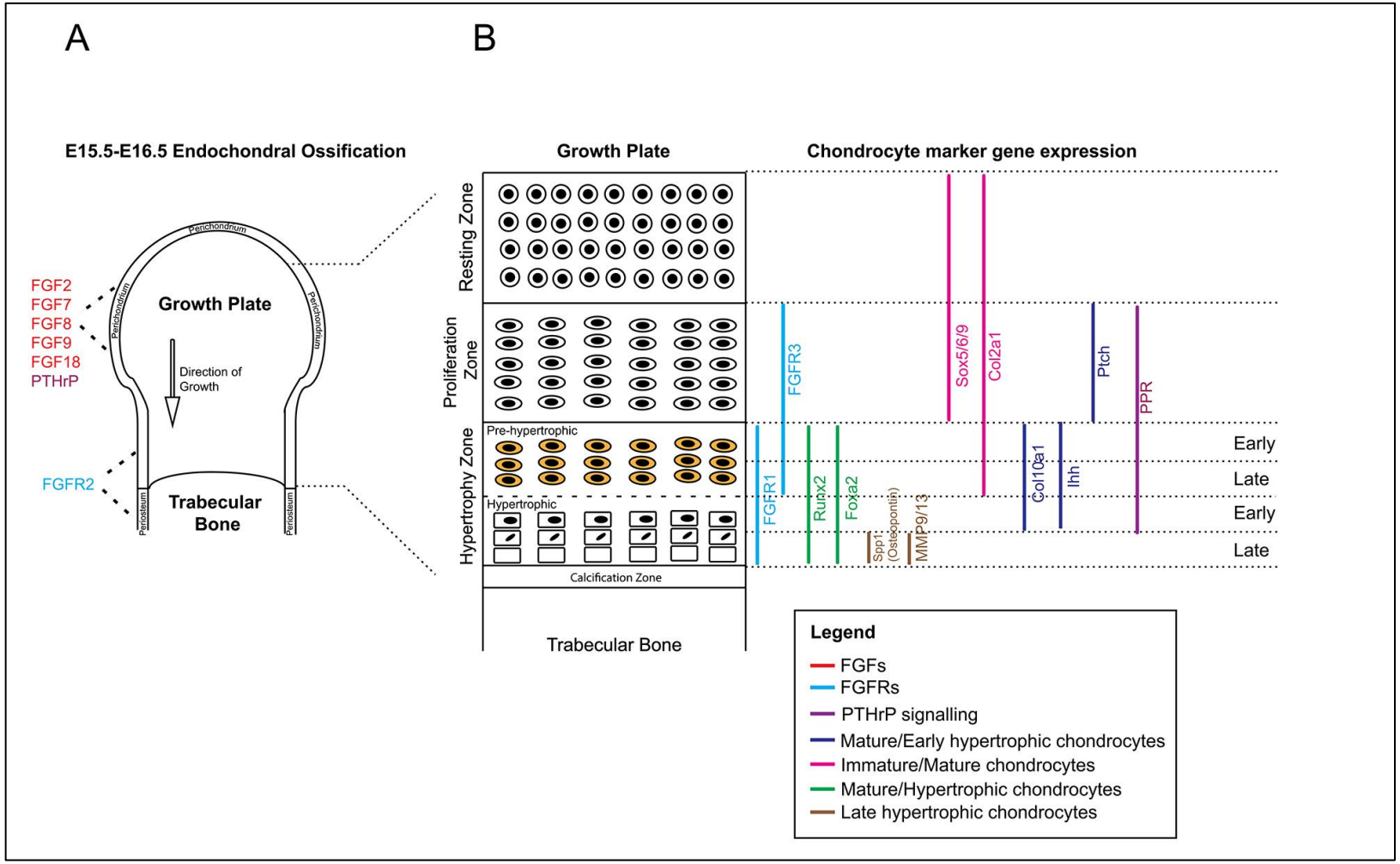
A
B
E15.5-E16.5 Endochondral Ossification
Growth Plate
Chondrocyte marker gene expression
FGF2
FGF7
FGF8
FGF9
FGF18
PTHrP
FGFR2
Perichondrium
Growth Plate
Direction of Growth
Periosteum
Trabecular Bone
Resting Zone
Proliferation Zone
Pre-hypertrophic
Hypertrophy Zone
Hypertrophic
Calcification Zone
Trabecular Bone
FGFR1
FGFR3
Runx2
Foxa2
Spp1 (Osteopontin)
MMP9/13
Sox5/6/9
Col2a1
Col10a1
Ihh
Ptch
PPR
Early
Late
Early
Late
Legend
FGFs
FGFRs
PTHrP signalling
Mature/Early hypertrophic chondrocytes
Immature/Mature chondrocytes
Mature/Hypertrophic chondrocytes
Late hypertrophic chondrocytes

Figure 10: Markers of endochondral ossification in the growth plate.

(A) is a schematic of the epiphyseal bone showing the expression of FGF ligands (red), PTHrP (purple) and FGFR2 (blue) in the perichondrium; (B) is an enlargement of the growth plate showing the expression of chondrocyte markers along different zones. Notice that respective ligands and receptors are expressed in complementary domains to facilitate paracrine loop (e.g. Ihh in hypertrophic zone and its receptor Ptch in proliferation zone). Data assembled from (Kozhemyakina et al., 2015)

1.5.1.3-Hedgehog and PTHrP signalling: A major feedback loop for chondrocyte maturation

Hedgehog and PTHrP signalling form a complex regulatory feedback loop controlling the rate of chondrocyte proliferation and differentiation (Yeung Tsang et al., 2014). In general, the ligand and receptor are expressed in zones complementary to each other with little overlap. For example, IHH is expressed in mature chondrocytes, located in the prehypertrophic and early-hypertrophic chondrocytes (Figure 10) (Iwasaki et al., 1997). IHH ligands are secreted and conveyed through the Patched (Ptch) receptor expressed in mature chondrocytes (Mak et al., 2008). These signals are conveyed through Gli proteins, which are expressed prominently throughout the growth plate, juxtaposing IHH expression (Koziel et al., 2005). Meanwhile, PTHrP is expressed in the perichondral chondrocytes, whilst its receptor (PTHrP Receptor; PPR) is expressed in the proliferating and prehypertrophic zones (Figure 10) (Iwasaki et al., 1997). The IHH-PTHrP paracrine loop is graphically illustrated in Figure 11: IHH is secreted from the hypertrophic zone and induces the expression of *Pthrp* in the perichondrium (Vortkamp et al., 1996), which maintains the expression of PTHrP, a negative regulator of chondrocyte differentiation. In response, PTHrP feeds back to *Ihh* expressing chondrocytes in the hypertrophic zone, preventing the differentiation of proliferating chondrocytes to pre-hypertrophic chondrocytes (Vortkamp et al., 1996). Therefore, this tightly regulated paracrine loop is important to i) maintain the correct balance of chondrocytes entering hypertrophy, and ultimately determining the ossification rate and ii) to ensure correct formation of the bone architecture. Indeed, disruption to downstream elements of the Hedgehog or PTHrP cascade, has consequences on the cellular architecture of the growth plate. For example, overexpression of IHH has resulted in the ectopic expansion of cartilage in the growth plate due to insufficient chondrocytes going into hypertrophy. In contrast, ablation of PTHrP led to an enlarged

hypertrophic zone due to an overabundance of cells going into hypertrophy (Kobayashi et al., 2005). It is believed Gli3 is the main transducer of IHH signalling (Koziel et al., 2005). A characteristic of *Ihh*$^{-/-}$ is premature chondrocyte differentiation and expansion of the hypertrophic zone (See Figure 11), and genetic ablation of *Gli3* partially restores chondrocyte proliferation and reverses excessive chondrocyte hypertrophy (Koziel et al., 2005).

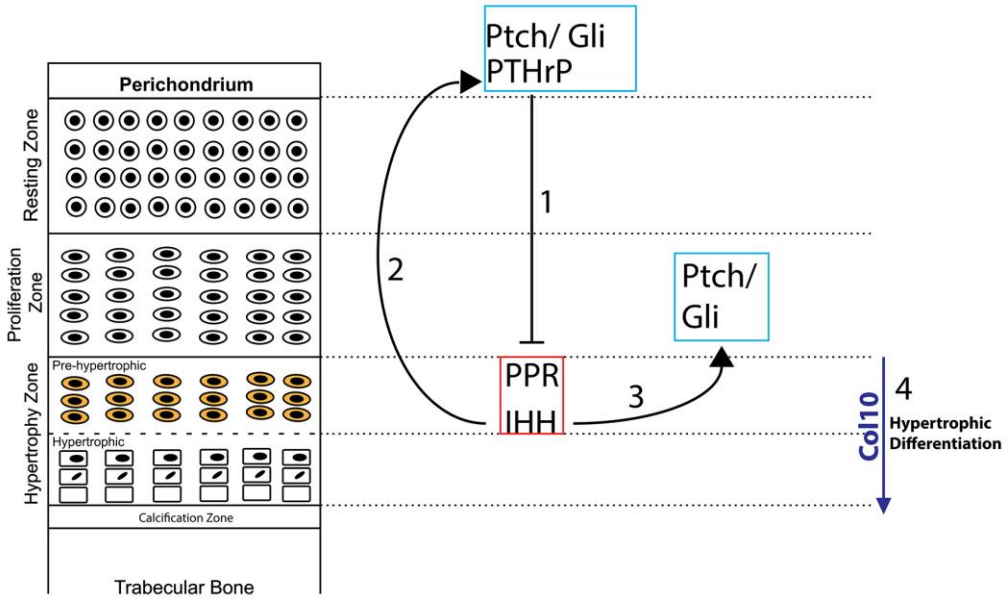

Figure 11 :PTHrP-IHH regulatory loop in the growth plate.

(1) Chondrocytes in the perichondrium secretes PTHrP and acts on PTHrP-Receptors (PPR) in the pre-hypertrophic zone. PTHrP maintains chondrocyte proliferation and represses/delays expression of *Ihh*. This prevents hypertrophic differentiation of chondrocytes. PTHrP is likely to suppress *Ihh* expression in a dose dependent manner; (2) IHH is secreted from the pre-hypertrophic zone and binds to Ptch receptors in perichondrial chondrocytes to maintain the expression of PTHrP. As this process in Hedgehog dependent, the signals are conveyed through Gli proteins; (3) IHH secreted from the pre-hypertrophic chondrocytes also act on the proliferation zone to maintain the amount of chondrocytes entering hypertrophy. (4) As the bone elongates, PTHrP repression decreases linearly resulting in the upregulation of *Ihh* leading towards hypertrophic differentiation (Col10). This highly intricate loop is important to regulate the size of growth plate and correct formation of the bone architecture. Furthermore, the growth plate provides a robust model to study organogenesis due to the presence of intricate feedback loops. Assembled from (Vortkamp et al., 1996).

1.5.1.4-The role of FGF signalling in endochondral ossification

FGFR3 is the principal mediator for endochondral growth in the long bone (Deng et al., 1996). Expression of *Fgfr3* commences after mesenchymal condensation, situated in the core of the mesenchyme (Ornitz and Marie, 2015). *Fgfr1* is expressed when the epiphyseal plates are formed, and when chondrocytes further mature (Ornitz and Marie, 2015). Both *Fgfr1* and *Fgfr3* have distinctive expression pattern where the former is mainly expressed in pre-hypertrophic and hypertrophic chondrocytes, the latter is expressed in proliferating chondrocytes (RZ and PZ) (Figure 10) (Kozhemyakina et al., 2015). The distinctive expression pattern directly infers their roles in growth plate, as *Fgfr1* seeks to maintain the survival of hypertrophic chondrocytes, whilst *Fgfr3* in proliferation and differentiation. Indeed, disruption of FGFR3 function (GOF mutation) in humans is associated with long bone defects such as achondroplasia and thanatophoric dysplasia, which are closely examined in mouse models (discussed in detail in Section 1.7.3). FGFR3 is a negative regulator of bone formation and as such, GOF-FGFR3 is commonly associated with dwarfism (Li et al., 1999). Interestingly, it is believed the undergrowth phenotype is conveyed through STAT, as FGFR3 activation is associated with increased STAT1, STAT5a and STAT5b expression and cell cycle repressors (p21, p18 and p19) (Li et al., 1999). Conversely, removal of $Fgfr3^{-/-}$ is associated with bone overgrowth (Deng et al., 1996). This is associated with expansion of the PZ in the growth plate and therefore, resulted in the amplification of chondrocytes (Deng et al., 1996). This loss of FGFR3 is complemented with the increase of Hedgehog genes such as *Ihh* and *Ptch* implying excessive chondrocytes undergoing hypertrophy and that FGFR3 is upstream of Hedgehog signalling (Chen et al., 2001, Iwata et al., 2000, Ornitz and Marie, 2015, Zhou et al., 2015b). Moreover, it has recently been shown that GOF mutation of FGFR3 (Y367C) has a direct consequence on cilia length, the primary location for Hedgehog signalling (Martin et al., 2018). FGF ligands are expressed in the perichondrium and diffuse into the growth plate to facilitate growth (Ornitz and Marie, 2015). The major binding partner for FGFR3 is likely to be FGF18, as the growth plate histology of $Fgf18^{-/-}$ yielded a similar cellular consequence to $Fgfr3^{-/-}$ (Ohbayashi et al., 2002, Deng et al., 1996). This included increased chondrocyte proliferation together with upregulation of Hedgehog signalling (*Ihh* and *Ptch*) during early development (around E15.5) (Ohbayashi et

al., 2002, Liu et al., 2002). However, in contrast to *Fgfr3*$^{-/-}$, *Fgf18*$^{-/-}$ mice display delays in ossification in both endochondral and intramembranous bones (Ohbayashi et al., 2002). In particular to the former, this observation suggests FGF18 expressed in the perichondrium may act on hypertrophic chondrocytes expressing FGFR1 in the HZ (Liu et al., 2002). It is believed that FGFR3 plays dual roles in maintaining chondrocyte proliferation and initiation of hypertrophy (Murakami et al., 2004, Sahni et al., 1999). This is related to the nature of growth factor signalling itself whereby activation of FGFRs initiate signal transduction through multiple cascades (Ornitz and Itoh, 2015). In particular, activation of FGFR3 led to phosphorylation of STAT1, which repressed proliferation of chondrocytes *in vitro* (Sahni et al., 1999, Li et al., 1999). Moreover, overactivation of the RAS-MAPK pathway through MEK1 reversed skeletal overgrowth phenotype in *Fgfr3* nulls (*Fgfr3*$^{-/-}$*; Col2a1 (MEK1)*) through restoration of chondrocyte proliferation (Murakami et al., 2004). Altogether, results obtained by Murakami et al (2004) suggest activation of FGFR3 is important to maintain the pool of chondrocyte undergoing proliferation and hypertrophic differentiation that is critical for subsequent ossification process in the PZ and HZ.

Historically, FGF2 was the first ligand identified in the growth plates (Ornitz and Marie, 2015). However, conditional deletion of FGF ligands does not appear to impact significantly on bone development likely due to compensatory effects of FGFs, such as conditional ablation of *Fgf2*$^{-/-}$ or *Fgf9*$^{-/-}$ resulted in a redundant phenotype (Montero et al., 2000, Colvin et al., 2001a, Colvin et al., 2001b). Despite FGFR2 being a positive regulator of bone formation, it appears to facilitate osteoblast differentiation. For example, the Crouzon mutation (C342Y) affects the mesenchymal (IIIc) variant of FGFR2 and has enhanced expression of osteogenic markers such as *Runx2* and *Osteopontin* without significant consequence on limb development (Eswarakumar et al., 2004). This is similar to isoform specific knockout of *Fgfr2c* (*Fgfr2c*$^{-/-}$), which led to delays in ossification due to a reduction of chondrocytes in the PZ (Eswarakumar et al., 2002). Despite FGFR2 functioning as a positive regulator of bone formation, its role is far more significant during the early stages of limb development. FGFR2 is expressed in both the apical epidermal ridge (AER) and the condensing mesenchyme of the

limb bud, and is confined to the periosteum during the late stages of embryogenesis (Delezoide et al., 1998). Further elucidation of its role came from isoform specific knockouts, and reveals that the epithelial IIIb isoform is required for limb bud outgrowth (De Moerlooze et al., 2000, Revest et al., 2001). These *Fgfr2b*$^{-/-}$ display a complete loss of limb structures (De Moerlooze et al., 2000, Revest et al., 2001). *In situ* hybridization also reveals a complete loss of transcripts expressed in the AER such as *Fgf8*, and *Shh* in the zone of polarizing activity (ZPA) (Revest et al., 2001). Furthermore, it is understood that the early stages of limb bud initiation requires FGF10 (mesenchyme) signalling to FGFR2b in the AER, which subsequently induces epithelial FGF8 signalling back to FGFR1c to establish the paracrine axis (Ornitz and Marie, 2015). In contrast, conditional inactivation of *Fgfr2c*$^{flox/-}$ in the mesenchyme using *Dermo1*$^{CRE/+}$ only yielded minor shortening of long bones (Yu et al., 2003). These results imply FGFR2b plays critical roles in patterning the limb, and that FGFR2c is less critical in this process. Whilst the role of FGFR2c in the early limb bud remains elusive, it can be said that FGFR2c is a determinant of longitudinal bone length and ossification rates through controlling osteoblast differentiation.

1.5.1.5-*Sox9* and *Runx2*: molecular switches for hypertrophic differentiation

The HZ expresses a multitude of markers including *Runx2*, *Ihh*, *Col10a1*, *Osteopontin* and *Mmp13* matrix metalloprotease. In particular to *Runx2*, it is the master regulator of osteoblast differentiation and its LOF (*Runx2*$^{-/-}$) results in the loss of calcified bone (Komori et al., 1997). Expression of *Runx2* is required for hypertrophic differentiation and *Runx2*$^{-/-}$ have smaller HZ and impaired *Col10a1* expression (Kim et al., 1999). Importantly, the inverse relationship between *Sox9* and *Runx2* determine fate transition from chondrocytes into osteoblasts (Dy et al., 2012, Zhou et al., 2006). Moreover, Sox9 directly interacts with the *Runx2* promoter and suppresses its expression in a dose dependent manner (Zhou et al., 2006). Overexpression of *Sox9* under the control of the osteoblast promoter *Col1a1*, is therefore able to prevent osteoblastogenesis, leading towards decreased bone mass (Zhou et al., 2006). In addition to its role as a master regulator for chondrocyte differentiation, it is also important to maintain chondrocyte identity throughout the maturation process. Along with Myocyte

Enhancer Factor 2c (*Mef2c*), *Sox9* can also directly facilitate expression of *Col10a1* to drive hypertrophic differentiation (Dy et al., 2012). *Sox9* is a target of multiple pathways that is subjected to potentiation (FGFs, BMP/TGFβ, Hedgehog) and repression (Wnt) (Kozhemyakina et al., 2015). As a consequence, this allows *Sox9* to maintain its expression in chondrocytes, and to enable correct transition between different phases of maturation. As *Sox9* is a master regulator for chondrocyte specification and to maintain its identity, it could be said that the intricate spatial-temporal control of *Sox9* determines the fate of cartilage and bone formation (Bi et al., 1999). Therefore, depletion of *Sox9* expression spells the end of chondrocyte fate. In addition to *Sox9,* Forkhead box A (FOXA) transcription factors also play a part in facilitating hypertrophic differentiation (Ionescu et al., 2012). The binding site for FoxA2 factors was first characterized through identification of regulatory elements upstream of the chicken Collagen X (Ionescu et al., 2012). Augmentation of FoxA2 has been shown to potentiate expression of hypertrophic marker genes *Col10a1* and *Mmp13 in vitro*. Together with LOF to *Foxa3*, disruption to *Foxa2* (*Foxa3*$^{-/-}$*; Foxa2*$^{flox/-}$*; Col2a1*$^{CRE/+}$) has been shown to delay hypertrophic differentiation. FoxA2 possess a similar binding site to Sox9, which could imply either competition or displacement with Sox9 during hypertrophic differentiation (Ionescu et al., 2012).

This section has discussed major pathways that trigger transition into hypertrophic differentiation in the growth plate (PTHrP, IHH and FGFR3), however, epigenetic factors may also facilitate this transition. It is well understood that histone modifications are critical to modulate gene expression by changing chromatin structure (Bannister and Kouzarides, 2011). In particular, transcriptional activity is repressed through tightening chromatin structure, which is performed through histone deacetylases (HDACs) (Bannister and Kouzarides, 2011). Hypertrophic differentiation is conveyed through HDAC4, downstream of PTHrP signalling (Vega et al., 2004, Correa et al., 2010). In fact, *Hdac4*$^{-/-}$ resulted in ectopic expression of *Ihh* and expansion of the HZ (Vega et al., 2004). Despite increased chondrocytes entering hypertrophy, these cells were not able to switch to an osteogenic fate. This is due to *Runx2* being directly repressed by HDAC4 in a dose dependent manner (Vega et al., 2004).

In summary, there are multiple triggers that drive hypertrophic differentiation. This is summarized in Figure 12 below. Ultimately, the entry into the hypertrophic programme requires downregulation of Sox9, which suppresses expression of *Runx2* linearly and it's downstream targets that are required for hypertrophic differentiation (Zhou et al., 2006). As Sox9 integrates with multiple pathways, the intricate signalling balance upstream of *Sox9* is required for smooth transition into hypertrophic chondrocytes.

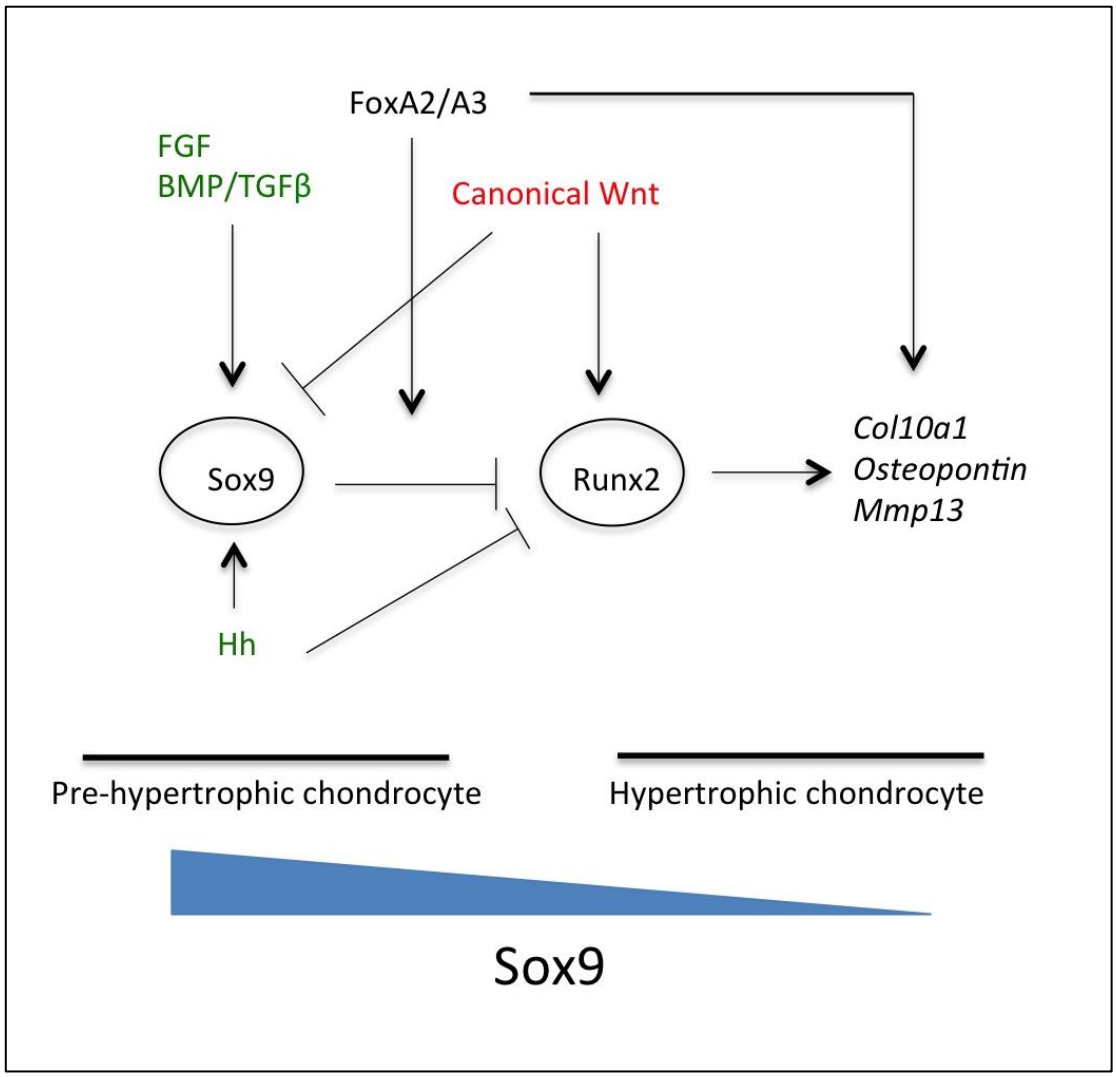

Figure 12: Molecular triggers for hypertrophic differentiation in chondrocytes.

Chondrocyte identity is dependent on the expression of Sox9 (blue wedge). Here, high *Sox9* expression is required to maintain chondrocyte identity and it represses *Runx2* expression in a dose dependent manner. *Sox9* expression is upregulated (green) by Hedgehog signalling (Hh), FGF, and BMP/TGFβ signalling and therefore, maintaining chondrocyte proliferation and identity. The transition to hypertrophic chondrocytes requires activated Wnt signalling, which represses (red) *Sox9* and promote *Runx2* expression. Other transcription factors promoting this transition include FoxA2/A3 where it is important to upregulate hypertrophic gene expression.

1.5.2-Intramembranous ossification

The calvarium is an intramembranous bone that is formed by condensation and mineralization of the craniofacial mesenchyme (Teven et al., 2014). This is in contrast to endochondral ossification where the bone is gradually displaced from a cartilaginous template (section 1.5.1) (Ornitz and Marie, 2015). Calvarial osteogenesis begins at around E13.5, osteoblast precursors express *Runx2,* a member of the Runt transcription factor family (Peskett et al., 2017). *Runx2* is a critical master regulator for osteoblast differentiation and its loss leads to significant skeletal hypoplasia, dwarfism and defects to the gross skeletal system (Komori et al., 1997). Mineralisation of the calvaria occurs at around E16.5 and progresses in a ventral to dorsal direction, a fully ossified calvaria can be perceived by E18.5 (Iseki et al., 1997) (Figure 13).

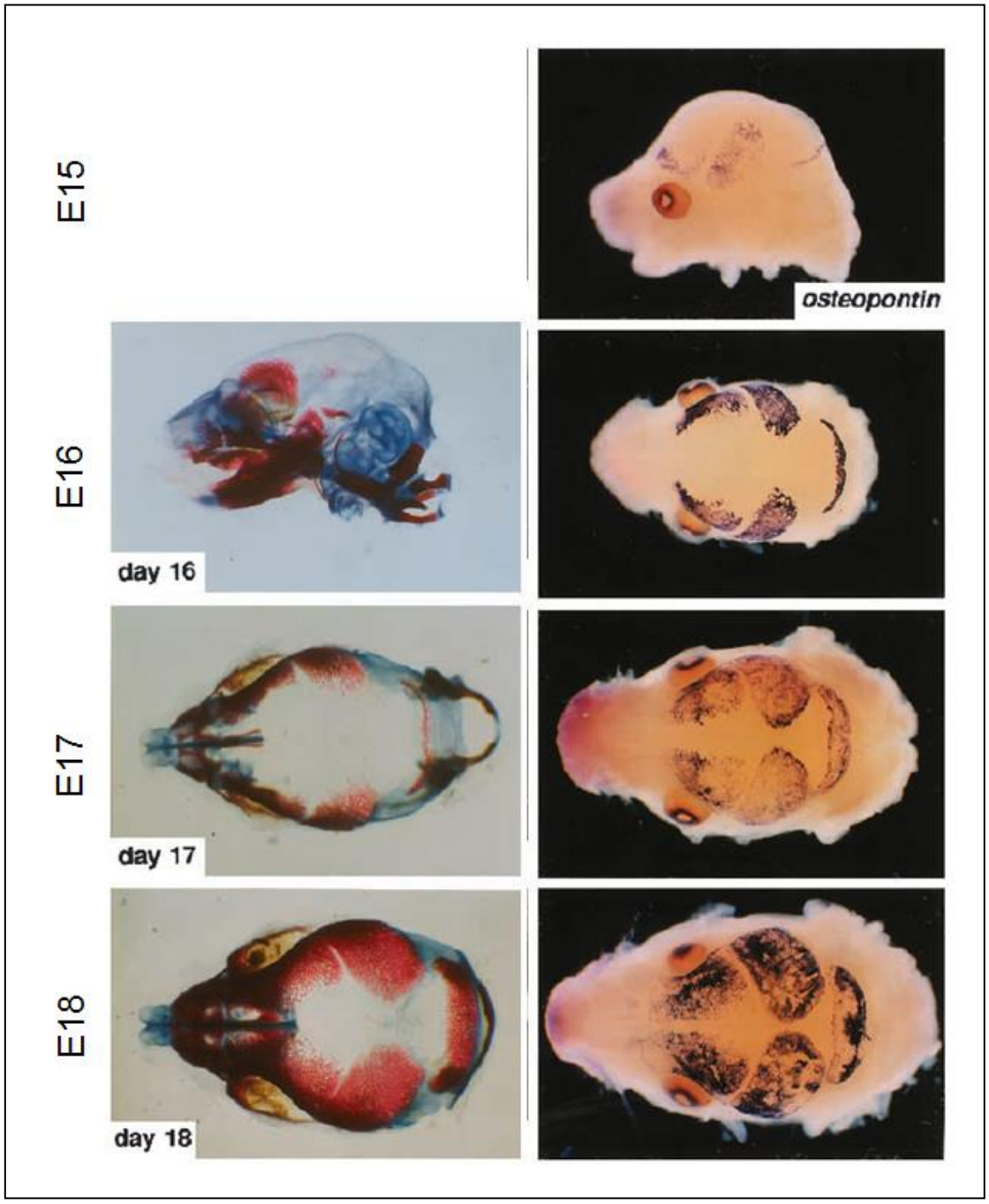

Figure 13-Mineralization of the calvaria.

Calvarial osteogenesis begins at E15 in a ventral to dorsal direction. Bone mineralization occurs at E16, as indicated by Alizarin Red staining on the left panel. Modified from Iseki et al., 1997.

Calvarial osteoblasts are derived from two distinct embryonic lineages, the mesoderm and NC (Yoshida et al., 2008, Quarto et al., 2010). Differentiated osteoblasts lay down the osteoid matrix of the calvarium during this process, consisting mainly of Col1 (Teven et al., 2014). This deposition of osteoid matrix extends outwards from the ossification centre. The outer edges of the bones develop into wedged shaped groups of cells that form the osteogenic front, which extend into the adjacent mesenchyme to recruit cells and advance the growth of cranial bones. The cranial suture is defined by the limits of the cranial bones coming into proximity with each other, bisected by a sea of undifferentiated mesenchyme. Cranial sutures remain unossified and patent during normal development, whilst new bones are formed at the osteogenic fronts. The suture mesenchyme needs to remain undifferentiated to maintain suture patency (reviewed in: (Teven et al., 2014). Generally speaking, osteoblast differentiation requires high levels of FGF signalling that is reflective of bone formation (Iseki et al., 1997, Iseki et al., 1999). Therefore, active FGF signalling is found along the bones and most active at the osteogenic fronts, whilst the suture mesenchyme has low levels of FGF signalling (Rice et al., 2000).

FGFs and FGFRs are differentially expressed in the cranial sutures (Hajihosseini and Heath, 2002). FGFs are mainly expressed in the mesenchyme, the surrounding dura and pericranial mesenchyme (Rice et al., 2000). The ligands common in both sagittal and coronal suture include *Fgf2, Fgf9* and *Fgf18* between E15-E17 (Hajihosseini and Heath, 2002, Kim et al., 1998, Rice et al., 2000, Deckelbaum et al., 2005). FGF18 in particular appears to be a major ligand regulating cranial bone development, as conditional knockout resulted in delays to ossification and coronal morphogenesis (Ohbayashi et al., 2002). Furthermore, *Fgf18* is expressed strongly in the osteogenic fronts of the frontal and parietal bones, potentially involved in commitment of progenitor cells towards an osteoblast lineage (Hajihosseini and Heath, 2002). FGF18 has a high affinity to the IIIc isoform of FGFRs and is likely to be a binding partner of FGFR1c and FGFR2c in differentiating osteoblasts (Ornitz and Itoh, 2015, Rice et al., 2000).

Fgfr1, Fgfr2 and Fgfr3 are co-expressed in osteoprogenitors and differentiating osteoblasts of the cranial bones between E15-E17 (Figure 14) (Rice et al., 2000, Iseki et al., 1999). In addition to osteoprogenitors, *Fgfr3* is mainly expressed in the underlying dura mater and calvarial cartilage (Delezoide et al., 1998, Rice et al., 2000, Iseki et al., 1999). Despite the expression of *Fgfr3* in the cranial bones, it does not appear to play major roles in craniofacial development. This is due to LOF since *Fgfr3*$^{-/-}$ resulted in a redundant phenotype (Deng et al., 1996). Furthermore, evidence from the human genetics and mouse models generated by knock in technologies, point towards the importance of craniofacial development in FGFR1 and FGFR2 signalling. This is discussed in detail in section 1.7, together with mouse models that contribute towards the understanding of craniofacial syndromes.

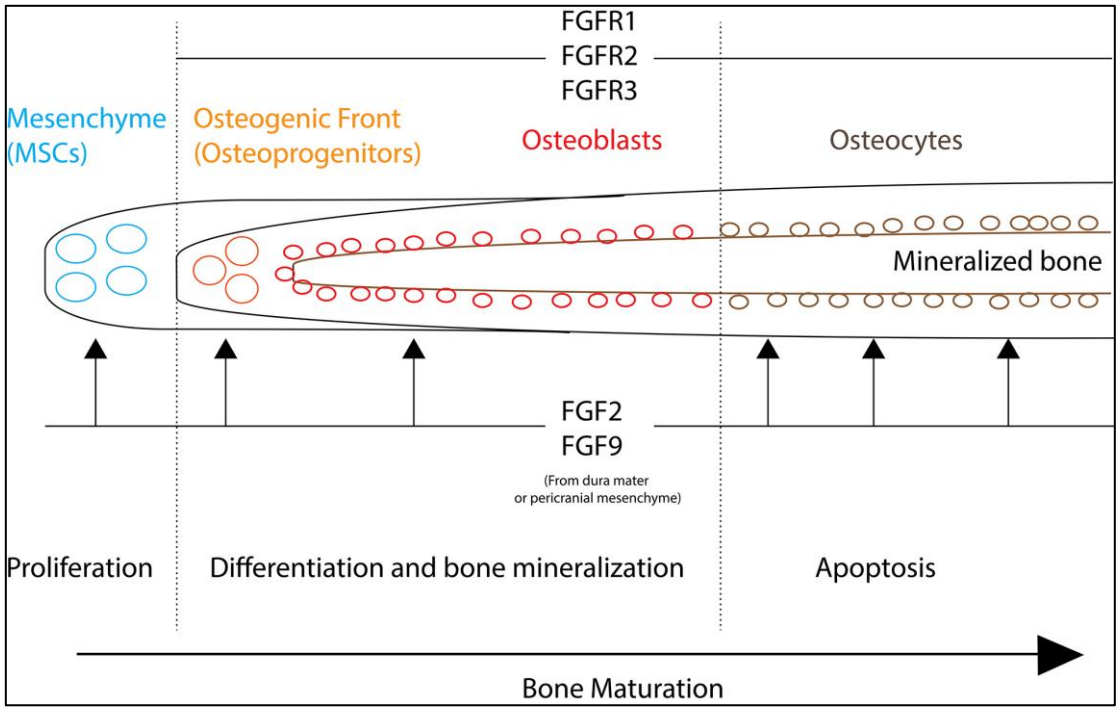

Figure 14: Overview of FGF ligand-FGFR interaction in osteogenesis.

High FGF signalling is required for MSC (blue circles) commitment into an osteoblast lineage. Cells in the osteogenic front are osteoprogenitors (pre-mature osteoblasts, orange circles), and progress through a series of maturation steps to become osteoblasts (red circles) and osteocytes (brown circles) that is FGF signalling dependent. Cranial sutures express a series of FGFs. FGF2 and FGF9 are used in this illustration as they are common to both sagittal and coronal sutures. Both of these ligands are expressed prominently in the suture mesenchyme, dura mater and pericranial mesenchyme. Consequently, these ligands diffuse to the cranial bones (arrows), binding to osteoprogenitors and maturing osteoblasts expressing FGFR1, FGFR2 and of an extent FGFR3. This highly coordinated maturation process is required to generate the correct amount of osteoblasts for bone formation.

1.5.2.1- Osteoblast maturation programme

Runx2 expression is directly downstream of FGFR2 (Miraoui et al., 2009), and a series of skeletal dysplasia and craniofacial syndromes are directly related to aberrations to FGF signalling (Ornitz and Itoh, 2015). Osteoblasts are derived from MSCs during intramembranous ossification. Figure 15 highlights the main transcription factors responsible for osteoblast differentiation and maturation. FGF signalling is upstream of all these process (Ornitz and Marie, 2015). In order for MSCs to differentiate into the osteoblast lineage, a combination of transcription factors is required. *Runx2* is fundamental for osteoblast differentiation as *Runx2* deletion results in a complete loss of skeletal elements (Komori et al., 1997). Maintaining a balance of *Runx2* expression is therefore crucial to normal skeletogenesis. *Osterix* is directly downstream from *Runx2* and is also required for osteoblast differentiation (Takarada et al., 2016). Osteoblasts progress through multiple stages of maturation process, and mature osteoblasts express different markers to those immature precursors. For example, committed osteoblasts express *Osteopontin*, *Alkaline Phosphatase* (*ALP*), *Osteocalcin* and *Col1α1*, important for bone mineralisation process (Hirakawa et al., 1994, Malaval et al., 1994, Iseki et al., 1997). These proteins provide the groundwork for subsequent bone mineralisation through calcium phosphate deposition, and are directly driven by *Osterix* expression (Nakashima et al., 2002). Mature osteoblasts demarcate the bone lining and can undergo apoptosis to help bone remodelling, while a cohort of osteoblasts can further mature into osteocytes, mainly situated in the bone matrix and marked by the expression of *Sclerostin* and *Activating Transcription Factor 4* (*Atf4)* (Long, 2012). These cells constitute around 95% of mature bone, forming an intricate network with osteoblasts subject for bone remodelling (Long, 2012).

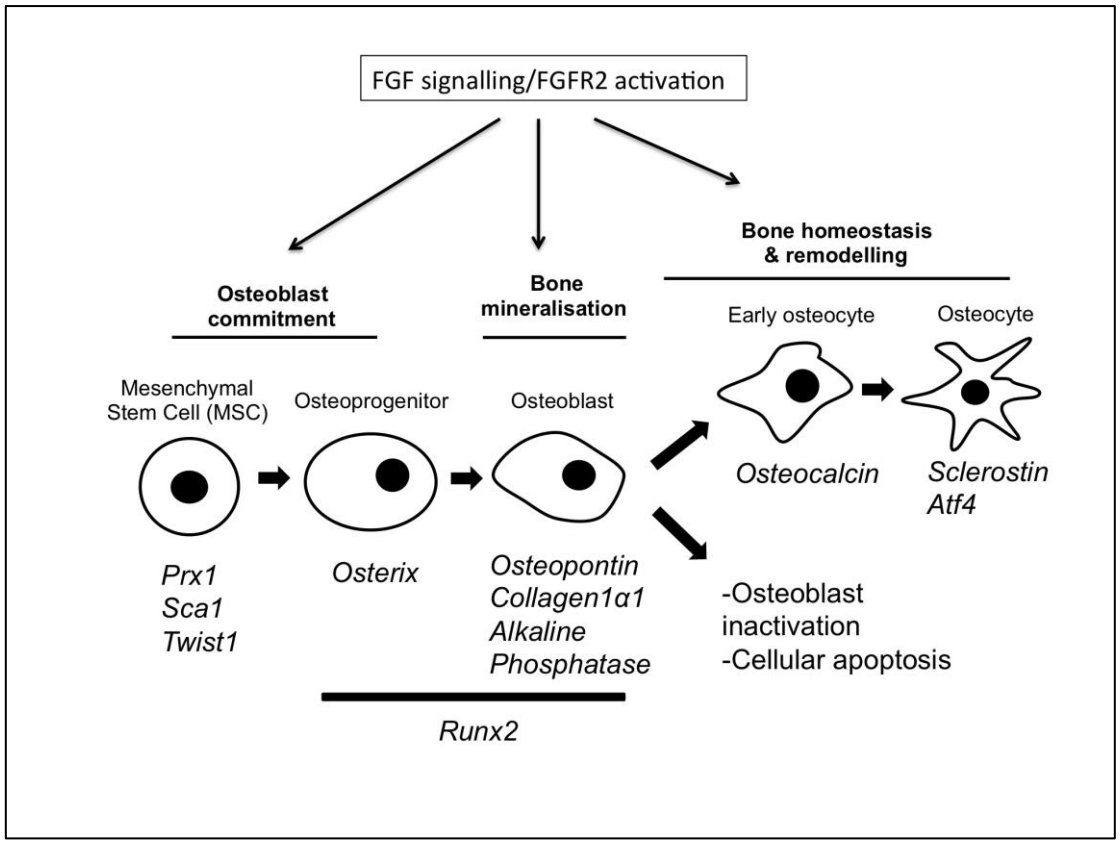

Figure 15: Osteoblast maturation programme.

MSCs are characterised by the expression of *Twist1, Prx1* and *Sca1*. Commitment of MSCs require the master regulator *Runx2*, and is concomitantly expressed with *Osterix* (*Osx*) in early osteoblasts. As the osteoblast matures, it starts to express mineralizing factors such as Osteopontin, Collagens, and Alkaline Phosphatase (ALP). Here, the osteoblasts can undergo inactivation or apoptosis, or aid remodelling through differentiation into osteocytes, characterised by the expression of *Osteocalcin, Sclerostin* and *Atf4*. Depending on the stage of the maturation process, FGF/FGFR2 signalling is responsible for proliferation, differentiation and apoptosis.

1.5.2.2-Effects of FGF signalling on osteoblast maturation programme

FGF signalling plays a wide range of roles concerning cellular proliferation, differentiation, survival and apoptosis (Ornitz and Itoh, 2015). Generally speaking, it has a stimulatory effect on osteoblasts and bone formation. Exposure to FGF signalling is able to commit MSCs into the osteogenic lineage through expression of *Runx2* (Miraoui et al., 2009, Valta et al., 2006). As GOF mutations in FGFRs are associated with increased osteogenesis (e.g $Fgfr2c^{C342Y/+}$; See mouse models in section 1.7) (Eswarakumar et al., 2004), it is possible that a proportion of patients with craniofacial syndromes may be associated with mis-specification of

MSCs towards an osteogenic lineage. However, as yet the contribution of these embryonic lineages towards pathogenesis remains elusive. This section will comment on *in vitro* data that have contributed to the understanding of osteoblast biology.

The effect of FGF signalling is complex and is dependent on a multitude of factors that modulate spatial-temporal dynamics. The overall effect of FGF signalling is linked to the stage of maturation in osteoblasts. For example, differentiation is increased in osteoblasts of *Fgfr1*$^{-/-}$, whereas both proliferation and differentiation is delayed in osteoprogenitors (Jacob et al., 2006). However, prolonged exposure of FGF2 and FGF9 to mature calvarial osteoblasts attenuated osteoblast differentiation and mineralization (Fakhry et al., 2005). These alterations in cellular response may be related to changes to receptor expression. For example, differentiating osteoblasts having higher levels of *Fgfr1* expression to that of osteoprogenitors, which are dominated by *Fgfr2* expression (Iseki et al., 1999). The changes in FGFR expression therefore yield distinct cellular consequences in response to endogenous ligands during the maturation process. The biochemical changes that alter FGF signalling dynamics can also change temporally. For example, *Fgfr2b* transcript levels are significantly higher in the frontal bone of adult mice compared to that of embryonic stages, which could determine the overall sensitivity of the receptor towards FGF ligands (Quarto et al., 2009). The combination of FGF ligands expressed *in vivo* will also drive the cellular response. FGF2 and FGF18 are example of ligands required for osteoblast maturation and are also present in the developing suture (Rice et al., 2000, Ohbayashi et al., 2002, Montero et al., 2000). For instance, deficiency in *Fgf2* (*Fgf2*$^{-/-}$) is related to osteopenia due to reduced osteoblastogenesis and bone mineralization (Montero et al., 2000). Similarly, *Fgf18*$^{-/-}$ resulted in delayed suture closure and calvarial ossification (Ohbayashi et al., 2002). These FGFs also play an important role in MSC commitment towards an osteoblast lineage in culture (Byun et al., 2014). Altogether, these results suggest FGF signalling is essential for specification, growth and maintenance of osteoblasts.

In addition to regulating cellular proiferation and differentiation, FGF signalling is also responsible to facilitate apoptosis. This event is stage dependent, as exposure to FGF1 in immature calvarial osteoblasts resulted in proliferation to that of late osteoblasts which

facilitated apoptosis (Mansukhani et al., 2000). Similar observations were reported in osteoblasts in the presence of GOF mutations (i.e. S252W) (Mansukhani et al., 2000). *In vivo* analysis revealed that the amount of cells undergoing programmed cell death is progressive over late gestational to early postnatal development (Rice et al., 1999). This is particularly interesting in deciphering the mechanics for suture closure. For example, GOF mutations such as FGFR2-C342Y are known to have premature cellular proliferation and differentiation in the coronal suture. However, it is likely that apoptosis plays an integral part in suture abolishment in latter stages of embryogenesis (Eswarakumar et al., 2004, Rice et al., 1999).

1.5.2.3-Cytosolic signalling cascades responsible for osteoblastogenesis

Signals are conveyed from the membrane via the RAS-MAPK, PI3K-AKT and PLCγ-PKC cascades in the FGF signalling pathway (Ornitz and Itoh, 2015). Figure 16 summarizes the roles of these cascades in osteoblastogenesis. Activation of these pathways individually or in combination yields distinctive cellular responses. Therefore, due to the complexity of RTK signal transduction, *in vitro* studies have focused on dissecting the biochemical cascades responsible for osteoblastogenesis. Treatment of FGF2 and FGF4 can faciliate cellular proliferation in osteoblast progenitors via the RAS-MAPK and PI3K-AKT pathways (Choi et al., 2008). Activation of RAS-MAPK pathway alone is also sufficient to induce osteoblast differentiation through FGFR2 via *Runx2* expression (Suzuki et al., 2012, Shukla et al., 2007, Miraoui et al., 2009). Indeed, ectopic osteoblast activity caused by an overactive FGFR2 pathway (e.g. FGFR2-S252W) can be reversed through ERK or p38 inhibition (Suzuki et al., 2012). In addition to understanding craniofacial development, the nature of GOF mutations affecting FGFRs helps to dissect the complex aetiology of growth factor signalling. For example, ectopic osteogenesis caused by the S252W mutation can cause transactivation of *Runx2* via the PLCγ-PLC cascade in MSCs and osteoblasts (Miraoui et al., 2009, Kim et al., 2003a). Exposure to FGF signalling also result in the concommitant activation of the PI3K-AKT cascade. The role of PI3K-AKT may aid cellular proliferation through survival, as pharmacological inhibition of AKT is sufficient to increase apoptosis (Raucci et al., 2008, Tran et al., 2003). In the absence of AKT, Forkhead Box O (FOXO) transcription factors facilitate

expression of pro-apoptotic genes (e.g. Caspase 9) (Tran et al., 2003). Furthermore, constitutive activation of AKT in early osteoblasts is sufficient to force differentation via expression of *Osterix* (Raucci et al., 2008). This observation is consistent in the presence of a FGFR2-C342Y mutation (Raucci et al., 2008). The ectopic differentiation of osteoblasts, due to augmentation of PI3K-AKT pathway has been found to be beneficial in healing of fractured endochondral and membrous bones (Burgers et al., 2013). It is also possible that the PI3K-AKT signalling pathway modulates the sensitivity of FGF signalling. In calvarial osteoblasts, augmentation of pAKT through knockdown of PTEN, a negative regulator of the AKT pathway, led to upregulation of *Fgf18* and downregulation of the RAS-MAPK feedback antagonist *Spry2* (Guntur et al., 2011). This observation is consistent with that of ectopic expression of osteoblast markers *in vitro*, which implies positive reinforcement of FGF signalling under pathogenic conditions (Guntur et al., 2011). FGF signalling is also able to facilitate crosstalks with multiple growth factor signalling pathways such as Epidermal Growth Factor (EGF) and PDGF to control osteogenesis (Miraoui et al., 2010a). Osteoblasts carrying mutant FGFR2-S252W has upregulated expression of EGFR and PDGFRα. This event is mediated by Cbl, as activated Spry2 interacts with ubiquitin ligase Cbl to prevent degradation of EGFR and PDGFRα. Furthermore, pharmacological inhibition of either EGFR or PDGFR is sufficient to reverse ectopic osteoblast differentiation normally caused by the S252W mutation. This cellular response is conveyed through the PLCγ-PKC pathway (Miraoui et al., 2010a). Similarly, expression of the Src family Lyn and Fyn, is shown to have negative effect on osteoblast differentiation (Kaabeche et al., 2004). Src family proteins are known to transduce signals directly from active RTKs (Schwartzberg, 1998). Constituative active FGFR2 causes increased ubiquitination and degradation of FGFR2 that resulted in premature osteoblast differentiation (Kaabeche et al., 2004). Ultimately, these studies highlight the aberrant crosstalks and downstream feedback loops in changing the dynamics of FGF signalling and osteoblast differentiation. Furthermore, It appears that the importance of positive feedback loops, such as those involved with PDGFR and EGFR, puts compensatory effect into context. In the above example, the upregulation of both PDGFR and EGFR could be a compensatory response to downregulation of the FGFRs in order to achieve the same cellular response (i.e.

differentiation). In addition to crosstalk with growth factor signalling pathways, FGF signalling is also sufficient to induce a positive effect on osteoblast differentiation with Wnt signalling. FGF2 is upstream of canonical Wnt signalling, and that endogenous FGF2 is able to supress degradation of βcatenin to facilitate osteogenic gene expression (Fei et al., 2011, Raucci et al., 2008). Similar applies to BMP/TGFβ signalling, where osteoblast differentiation is potentiated in the presence of FGF2/FGF9 (Fakhry et al., 2005). Ultimately, these results indicate that FGF signalling has a positive effect to potentiate bone formation, but more importantly, functioning upstream as the main regulator controlling osteoblastogenesis. Other modulators of bone formation include Twist1, which acts as a negative regulator (Bialek et al., 2004). On a clinical level, haploinsufficiency of Twist1 is associated with complex craniosynostosis in Saethre-Chotzen syndrome (Howard et al., 1997). Knockdown of *Twist1* is implicated in premature osteoblast differentiation (Miraoui et al., 2010b). This is due to Twist1 haploinsufficiency resulting in the upregulation of PI3K-AKT pathway, which is responsible for driving the expression of osteogenic markers (Guenou et al., 2006). PI3K-AKT cascade misregulation is caused by an attenuation of PI3K tagged for degradation by Cbl (Guenou et al., 2006). Accordingly, Twist1 is involved in promoting stemness and survival of MSCs and osteoblasts (Miraoui et al., 2010b, Yousfi et al., 2001). Twist1 has the ability to dampen cell death by suppressing the p53 apoptotic pathway (Maestro et al., 1999). Expression of tumor suppressor genes such as p19-ARF are reduced in the presence of Twist1 (Maestro et al., 1999). Furthermore, Twist1 is able to prevent cell death mediated by Caspase-3 and Tumour Necrosis Factor α (TNFα) (Maestro et al., 1999, Yousfi et al., 2002). In particular, it has been demonstrated that Twist1 can bind to *Tnfα* promoters to modulate its expression (Sosic et al., 2003). Twist1 is likely to form a negative regulatory loop with FGFR2 (Guenou et al., 2005). Indeed, it is able to directly interact with the *Fgfr2* promoter, and that calvarial osteoblasts obtained from Saethre Chotzen patients have decreased expression of *Fgfr2 in vitro* (Guenou et al., 2005). Furthermore, *Twist1*$^{+/-}$ mice have ectopic expression of *Fgfr2* normally absent from the suture mesenchyme, implying it is a negative regulator of FGFR2 signalling (Rice et al., 2000). The role of Twist1 *in vivo* is further examined in section 1.7.5 from *in vivo* data, but it is

likely that premature suture closure is associated with excessive osteoblastogenesis from the suture mesenchyme.

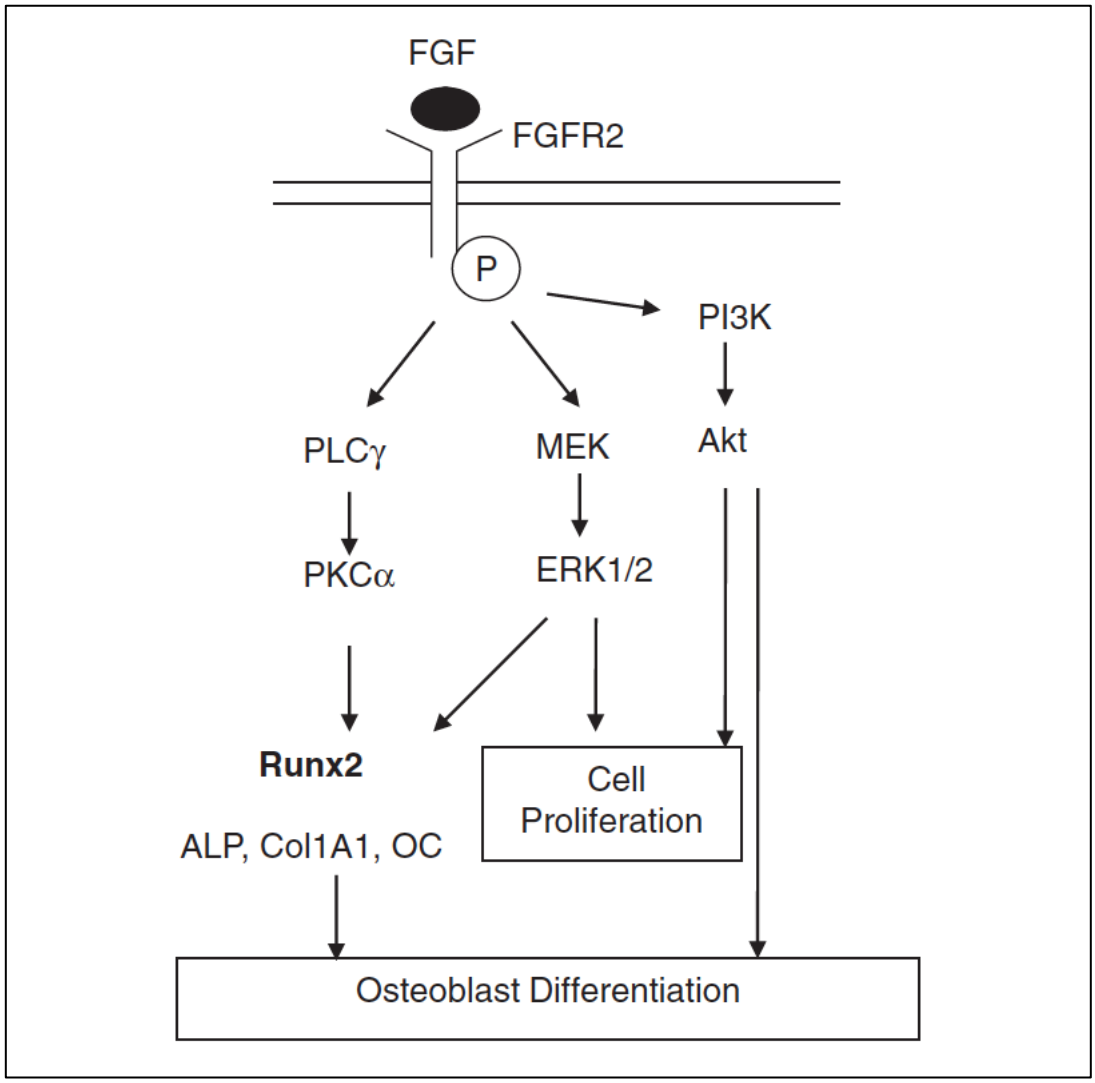

Figure 16: A summary of FGFR2 signalling cascades regulating cellular proliferation and differentiation.

FGFR2 activation leads to potentiation of RAS-MAPK, PI3K-AKT and PLCγ-PKC cascades. In general, RAS-MAPK induces cellular proliferation and differentiation, whilst PI3K-AKT and PLCγ-PKC drives differentiation. *Runx2* is downstream of both RAS-MAPK and PLCγ-PKC cascades, responsible drive expression of osteogenic genes (*Alp*, *Col1a1* and *Osteocalcin* (OC)). It should be noted that cellular differentiation caused by PI3K-AKT cascade is independent of *Runx2*. Adapted from: (Marie, 2012)

1.6-Human genetics of syndromic craniosynostosis and mouse models

1.6.1-Craniosynostosis

Craniosynostosis is a common feature of craniofacial birth defects, with a prevalence of 1:2500 births (Cohen and Krelborg, 1992). It is characterized by premature fusion of calvarial bones and could occur along multiple cranial sutures. Around 30% of craniosynostosis occurs within a characterised craniofacial syndrome ('syndromic craniosynostosis') with a genetic cause, whilst the majority of non-syndromic cases have a *de novo* cause ('non syndromic craniosynostosis') (Johnson and Wilkie, 2011). The molecular basis for craniosynostosis is complex: A dominant mutation within one of the FGFR 1, 2 and 3 genes are common to syndromic craniosynostosis, while intra-uterine constraint is the likely cause to the latter (Muenke et al., 1997, Muenke et al., 1994, Reardon et al., 1994, Johnson and Wilkie, 2011). The phenotypic consequence of craniosynostosis is skull distortion with secondary sensory-neurological deficits through an increase of intracranial pressure (Figure 18) (Derderian and Seaward, 2012). Typically, FGFR mutations are responsible for the 'Crouzonoid' phenotype comprising of complex craniosynostosis, midfacial hypoplasia, strabismus and brachycephaly (Figure 17). Figure 18 summarizes the skull distortions observed in humans according to the type of suture fusion. As a result of craniosynostosis, symptoms include optic atrophy, blindness and hearing deficits (Derderian and Seaward, 2012). There is currently no pharmacological treatment for craniosynostosis, with repeating surgical modalities the primary option to accommodate normal brain growth by correcting skull dysmorphology and reducing intracranial pressure, a procedure known as craniectomy (Johnson and Wilkie, 2011). Specifically, surgical interventions aim to re-open the suture ('distraction osteogenesis') with calvarial remodelling (Park and Yoon, 2012). Figure 19 illustrates the surgical modalities used to remodel the calvaria.

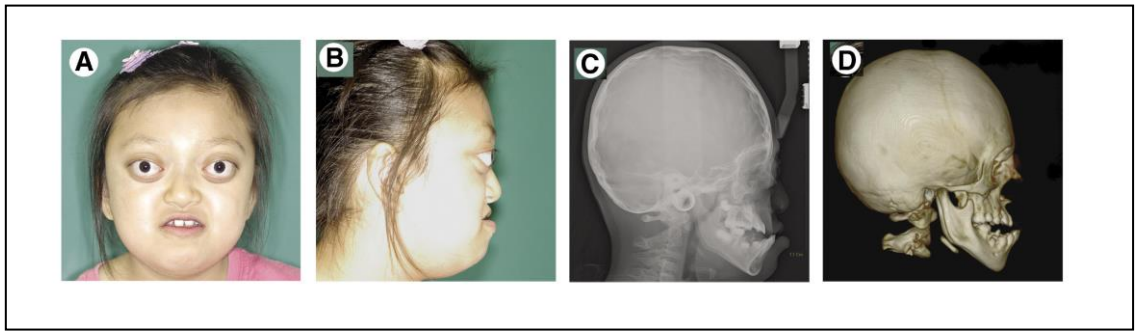

Figure 17: Presentation of a patient with Crouzon syndrome.

(A) Frontal view, (B) lateral view, (C) Cephalogram and (D) CT-scan. Notable phenotypes include midfacial hypoplasia, strabismus, brachycephaly. Modified from (Lee et al., 2012).

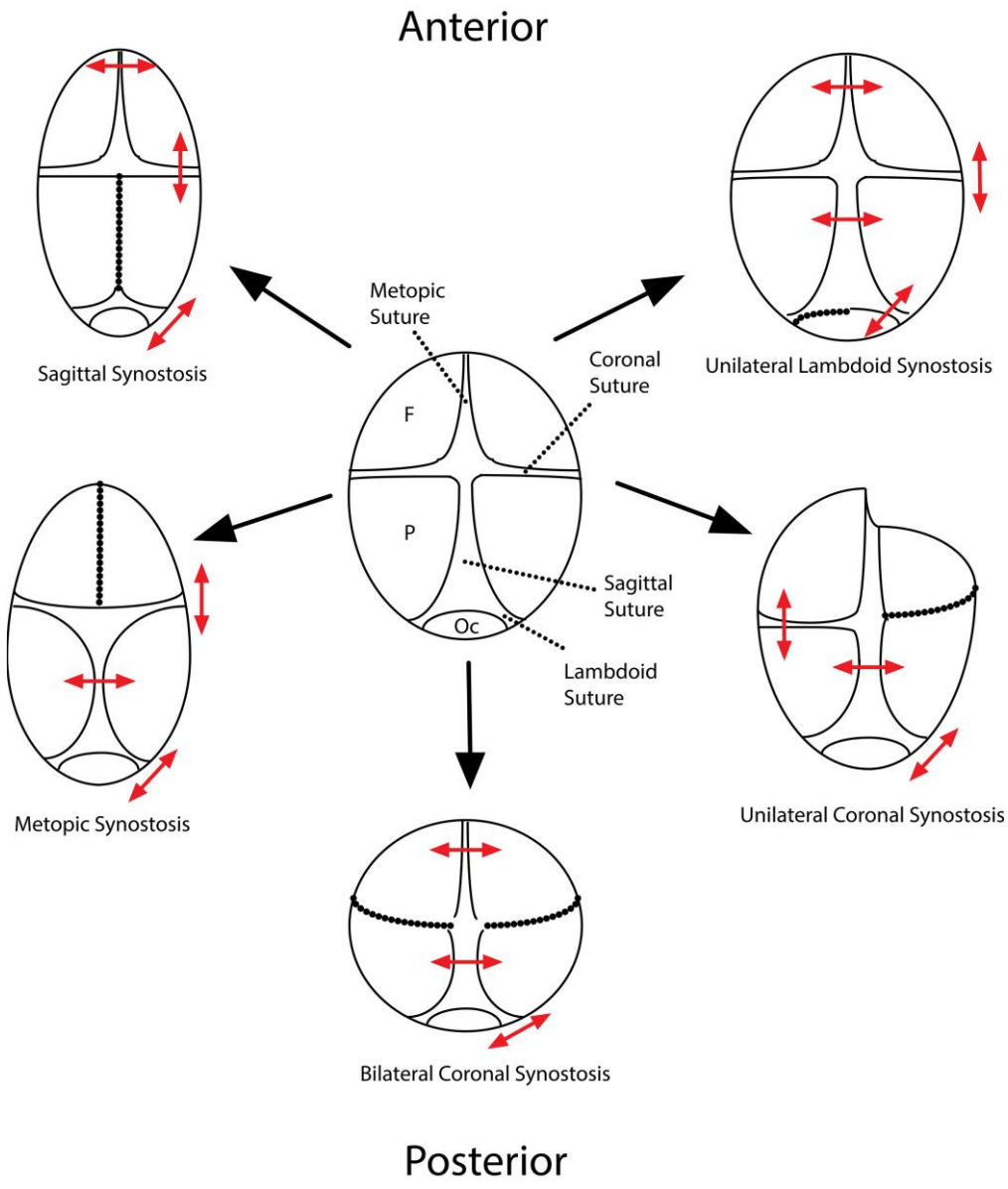

Figure 18: Craniosynostosis affects skull dysmorphology.

Red arrows indicate the direction of growth. Jagged line illustrates location of fused suture.

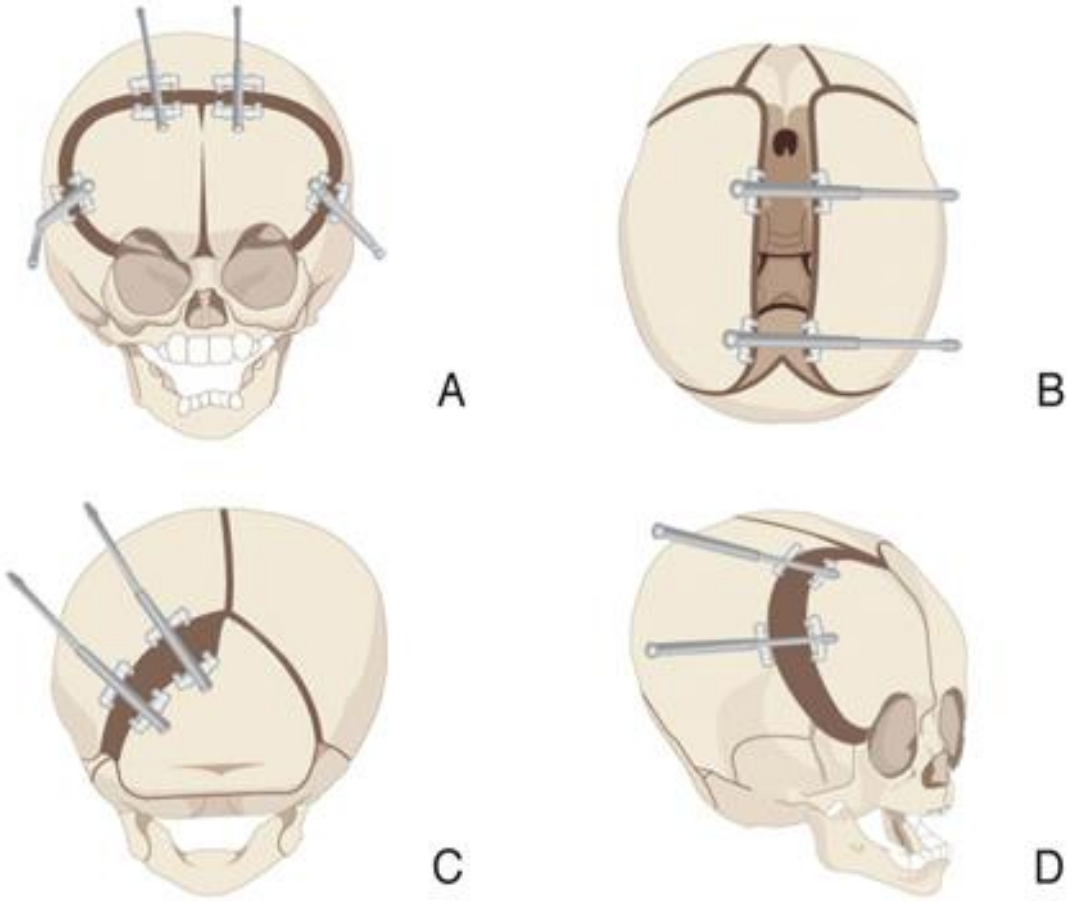

Figure 19: Distraction osteogenesis on the human calvaria

(A) to reopen the coronal suture, (B) sagittal suture, (C) lambdoid suture and (D) unilateral coronal suture. Adapted from Park and Yoon, 2012.

1.6.2-Human genetics of FGFRs and craniosynostosis

Historically, mutation to *MSX2* (Msh homeobox 2) gene was first to be identified associated with syndromic craniosynotosis, eliciting a clinical phenotype known as 'Boston-type craniosynostosis' (Jabs et al., 1993). Mutations on FGFRs were later identified. Perhaps the most common gene involved in syndromic craniosynostosis is the FGFR (Wilkie, 2005). The most notable characteristics of craniofacial dysmorphology is the 'Crouzonoid phenotype' with coronal synostosis being the most common type of suture fusion (Wilkie and Morriss-Kay, 2001). In general, mutations affecting FGFRs are activating ('gain-of-function'; GOF), allowing it to be constitutively active e.g. C342Y (Wilkie, 2005). Moreover, they have an autosomal dominant inheritance pattern (Wilkie, 2005). A generalisation is that the craniofacial spectrum elicited by FGFRs signalling misregulation depends on the tissue specificity and allelic mutations along the receptor gene (Wilkie, 2005) (Figure 20). Table 2 summarises all the clinical outcomes affected by common FGFR mutations. Interestingly, allelic mutations affecting the linker region (S252, P253, C278 and C342) accounts for 80% of all craniosynostosis. In fact, an interesting observation illustrated by Wilkie (2005) is that identical substitutions across FGFR paralogues are conserved at equivalent positions along the gene. For example, amino acid changes to linker regions of the receptors such as, proline to arginine (Pro250Arg), gives rise to Pfeiffer (FGFR1), Muenke (FGFR1) and Apert (FGFR2) syndromes (Figure 20), with coronal synostosis being a common phenotype of mutant FGFR1-FGFR3 (Wilkie, 2005). FGFR1-FGFR3 is expressed along the edges of the calvarial bones with FGFR2 predominantly in the osteogenic front (Figure 21) (Johnson et al., 2000, Iseki et al., 1999). However, the spatial localisation of the splice forms is not well characterised due to its high sequence homology and instead, it is mainly through isoform specific knockouts in mouse models that their functions have been delineated. Undeniably, mouse models offer a significant platform to study human disease progression, and generating models carrying knock in mutations can help to address questions concerning the phenotypic diversity caused by various mutations. To date, a large cohort of craniofacial research is focussed on the genomic landscape, but little delineates the biochemical and transcriptomic events that influence cellular activity *in vivo*. In order to advance translation, it is critical to address the aberrant mechanisms that lead

toward craniofacial abnormalities. An example of such a model is the *Fgfr2c*$^{C342Y/+}$ mouse model for human Crouzon syndrome that is used throughout this project (Figure 22) (Eswarakumar et al., 2004).

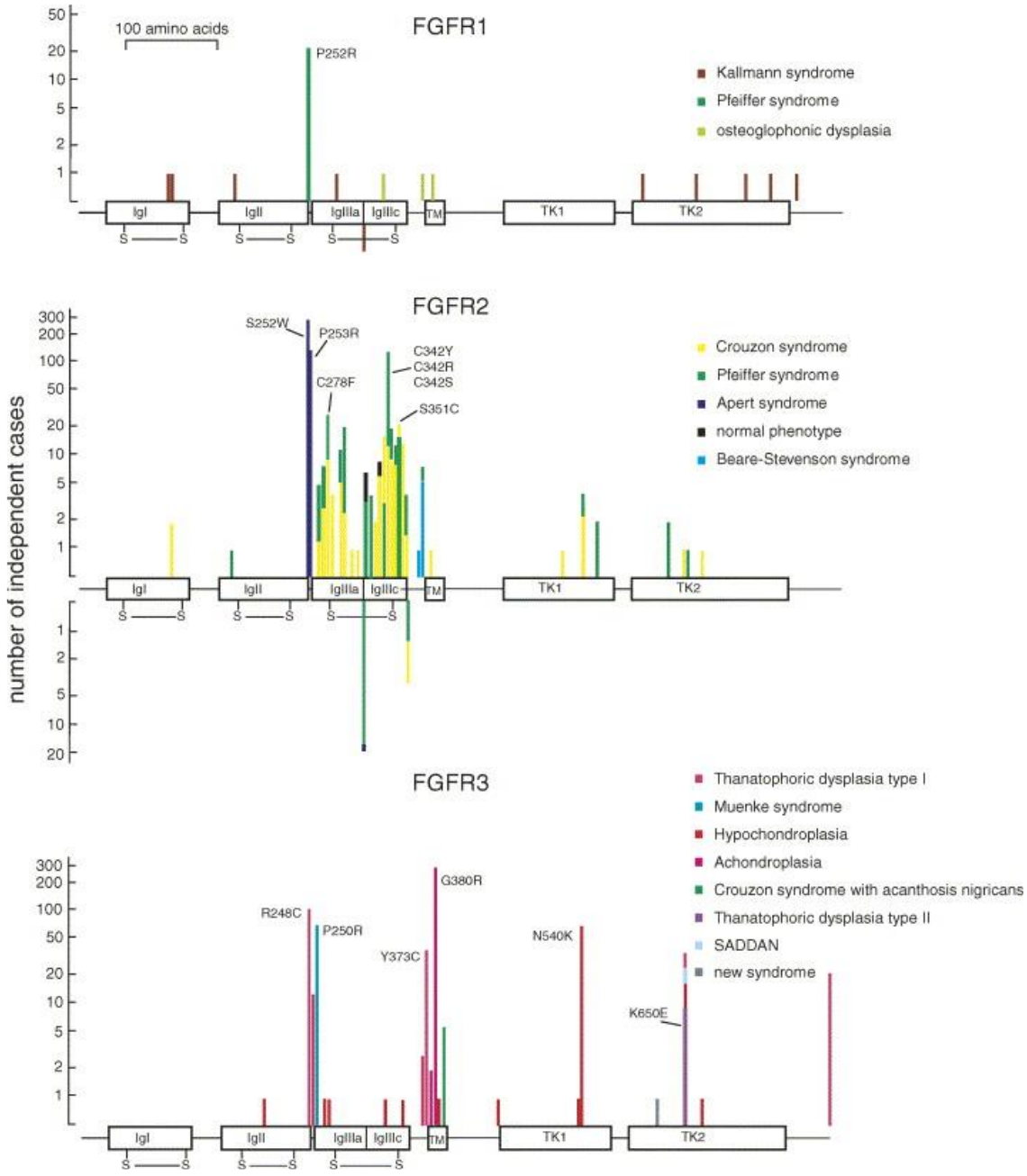

Figure 20: Frequency and distribution of mutations identified on the FGFRs.

Note the frequency of FGFR mutations are located in the linker region (IgIIIa, IgIIIc), in particular to FGFR1 and FGFR2. FGFR3 mutations have a strong prevalence in the transmembrane domain. Adapted from Wilkie 2005.

Gene	Mutations/location	Clinical syndrome	Key clinical features
	Widespread (haploinsufficiency)	Kallmann syndrome	Anosmia, hypogonadotrophic hypogonadism
	P252R (100%)	Pfeiffer syndrome (mild)	Craniosynostosis, cutaneous syndactyly
FGFR1	N330I, Y374C, C381R	Osteoglophonic dysplasia	Short stature, craniosynostosis, bone demineralisation
	S252W (66%), P253R (32%)	Apert syndrome	Craniosynostosis, crouzonoid faciesa, bony syndactyly
	IgIIIc (71%), IgIIIa (23%), TK, IgI	Crouzon/Pfeiffer/Jackson–Weiss/Antley–Bixler syndromes	Craniosynostosis, crouzonoid facies, graded severity of limb anomalies (nil, broad first digits, elbow fusion)
FGFR2	Y375C (>85%), S372C	Beare Stevenson syndrome	Severe craniosynostosis, cutis gyrata
	P250R (>99%)	Muenke syndrome	Coronal craniosynostosis, clinically not diagnostic
	HCH: N540K (42%). ACH: G380R (99%). TDI: R248C (56%), Y373C (22%), stop codon (12%). TDII: K650E (100%). SADDAN: K650M (100%)	Hypochondroplasia/achondroplasia /SADDAN/thanatophoric dysplasia I and II (TDI, TDII)	Short-limbed bone dysplasia of graded severity from mild short stature to neonatal lethality; acanthosis nigricans in severely affected survivors; craniosynostosis in TDII and some TDI
	A391E (100%)	Crouzon syndrome with acanthosis nigricans	Craniosynostosis, crouzonoid facies, acanthosis nigricans
FGFR3	R621H	New syndrome	Sensorineural hearing loss, camptodactyly, tall stature, kyphoscoliosis, microcephaly, developmental delay

Table 2: Summary of mutation affecting FGFRs and its clinical outcome. SADDAN: Severe achondroplasia with developmental delay and acanthosis nigricans.

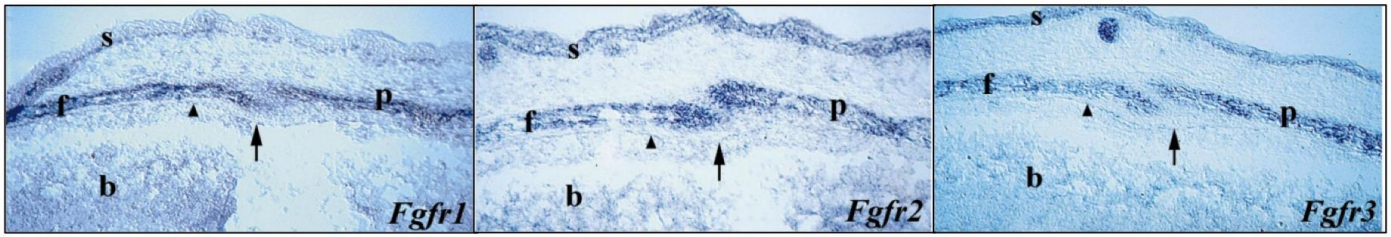

Figure 21: Expression of FGFRs in the coronal suture

Note the predominance of *Fgfr2* in the osteogenic front of the embryonic suture. F: Frontal bone, P: Parietal bone, b: brain, s: skin. Adapted from Johnson et al., 2000.

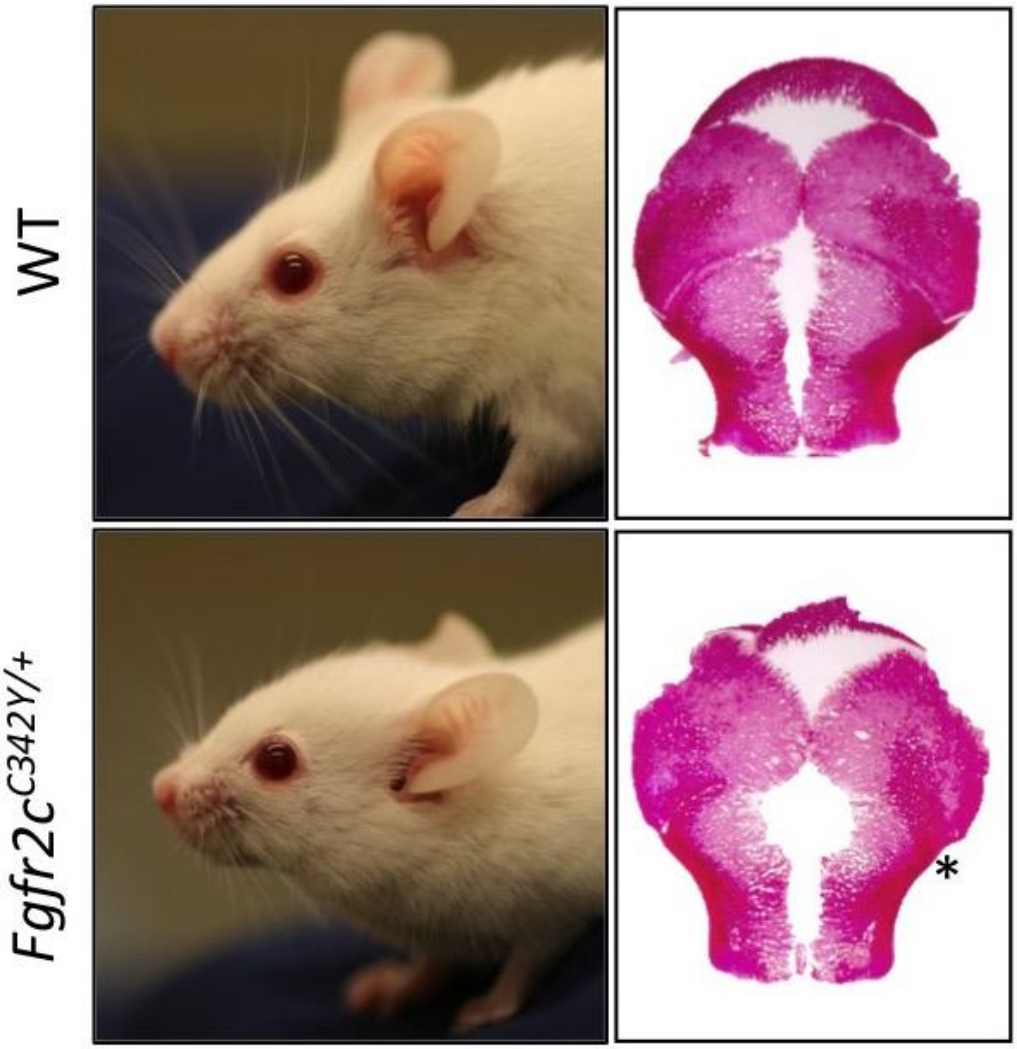

Figure 22: Mouse model for human Crouzon syndrome, *Fgfr2c*$^{C342Y/+}$.

Brachycephaly, midfacial hypoplasia and coronal synostosis (*) is a phenotypic hallmark for both patient and mouse model. Image courtesy: Erwin Pauws.

1.7-Mouse models for craniosynostosis

Mouse models associated with craniosynostosis and bone diseases are compiled in Table 3 and Table 4.

1.7.1-FGFR1

Mutations in FGFR1 are hallmarks for Kallman, Jackson-Weiss and Pfeiffer syndromes (Ornitz and Itoh, 2015). In addition to the common craniofacial abnormalities, severe Pfeiffer syndrome patients exhibit limb and digit abnormalities (Muenke et al., 1994). Specifically, these patients have varying degrees of syndactyly, finger truncation, broad digits and short limbs (Muenke et al., 1994). The P252R substitution responsible for Pfeiffer syndrome was originally identified in the early 1990s, affecting exon 5 of *FGFR1*, common to both splice forms (Muenke et al., 1994). The mutation was eventually reproduced in the mouse genome, creating a model for Pfeiffer syndrome ($Fgfr1^{P250R/+}$) with bi-coronal craniosynostosis along with enhanced expression of osteogenic genes (Zhou et al., 2000). Additionally, these mice have increased cell proliferation at P5 in the sutures. On the other hand, loss of function mutations (e.g. G237S, P722H, N724K) to this receptor is more associated with hormone dysregulation than with skeletal defects, and is related to Kallman syndrome (Pitteloud et al., 2006). *Fgfr1* is expressed prominently in the distal limb bud between E8.5-E12.5, and is required for its correct initiation and outgrowth (Verheyden et al., 2005, Li et al., 2005). Conditional inactivation of $Fgfr1^{-/-}$ in the limb bud mesenchyme ($T^{Cre/+}$) do result in long bone and digital defects during later stages of development, similar to those in Pfeiffer patients (Verheyden et al., 2005, Li et al., 2005). Therefore, the differential phenotype elicited by LOF mutations in humans and knockout mice suggest dosage sensitivity of FGFR1 signalling.

Complete removal of FGFR1 signalling leads to embryonic lethality and is seen comprehensive throughout the literature (Deng et al., 1994, Yamaguchi et al., 1994). Multiple strategies have been adopted to ameliorate this problem, including generation of hypomorphs by reducing the expression of full length FGFR1, mutating binding sites for Frs2 on *Fgfr1*, or preventing Trk autophosphorylation (Partanen et al., 1998). Additionally, Partanen and

colleagues (1998) have achieved isoform specific knockout to exons 8 (IIIb) and 9 (IIIc) by inserting a stop codon into these exons. *Fgfr1b* appears to be the major player in axial skeleton development, as *Fgfr1b*$^{-/-}$ display vertebrate column truncations and limb abnormalities, despite the craniofacial skeleton remains largely normal (De Moerlooze et al., 2000). Thus, the lack of craniofacial phenotype exhibited by FGFR1 LOF implies its role in craniofacial development is minor. *Fgfr1c* knockout is embryonic lethal suggesting the importance of the mesenchymal isoform in embryogenesis (Partanen et al., 1998).

1.7.2-FGFR2

FGFR2 is a positive regulator for osteoblast differentiation and manipulating this signalling pathway has adverse consequences to osteoblast differentiation. It is well characterised that *Runx2*, the master regulator for osteoblast differentiation, is downstream of FGFR2 signalling (Miraoui et al., 2009). Therefore, a substantial proportion of clinical syndromes and bone diseases have been related to FGFR2 misregulation. The role of FGFR2 in osteogenesis was characterised using knockout models. Several groups have generated *Fgfr2* knockout lines with similar phenotypes, yielding a series of gastrulation, placental and osteogenesis defects (Yu et al., 2003, Arman et al., 1998, Arman et al., 1999, Xu et al., 1998). The first FGFR2 knock out was generated by targeted disruption to the kinase domain of the receptor, preventing autophosphorylation (Arman et al., 1998). Other *Fgfr2* knockouts followed, by disrupting immunoglobulin loops along the receptor gene (Xu et al., 1998). Xu et al., (1998) generated a knockout by removing exons encoding the IgIII loop responsible for ligand specificity. Despite homozygous lethality at E10.5, this study was the first to provide insights into the role of FGFR2 in limb development as these mutants fail to develop limb buds, owing to a loss of paracrine signalling responsible for tissue outgrowth (Xu et al., 1998). It was later discovered through *Fgfr2b*$^{-/-}$ that the IIIb isoform is critical for limb outgrowth, as these mice have a complete loss of the appendicular skeleton (De Moerlooze et al., 2000, Revest et al., 2001). Fgf10 is a likely candidate for limb outgrowth as *Fgf10*$^{-/-}$ mice exhibit striking similarities to *Fgfr2b*$^{-/-}$ mice (Sekine et al., 1999, Min et al., 1998). Similarly, *Fgfr2c*$^{-/-}$ mice show this isoform is required for normal craniofacial development (Eswarakumar et al., 2002).

Others have also generated conditional *Fgfr2* knockouts to study tissue specific effects: Conditional knockout in the mesenchyme using *Dermo1*$^{Cre/+}$ leads to defects in both axial and craniofacial skeleton (Yu et al., 2003). Specifically, these mice have decreased bone density, truncated femur owing to insufficient chondrocyte and osteoblast proliferation, brachycephaly and dwarfism (Yu et al., 2003).

A large cohort of characterised craniofacial syndromes are commonly associated with *FGFR2* germline mutations (Figure 20) (Wilkie, 2005). GOF mutations in the *FGFR2* gene are characteristic of Apert, Crouzon, and Beare-Stevenson syndromes (Wilkie, 2005). FGFR2 signalling is a key player in craniofacial development. Crouzon syndrome is caused most commonly by a substitution mutation in FGFR2c (FGFR2c-C342Y; at the DIII Ig loop) and is autosomal dominant (Reardon et al., 1994). The substitution of a cysteine to a tyrosine residue results in the stabilization of intermolecular disulphide bonds at the receptor extracellular domains, leading to constitutive activation (Eswarakumar et al., 2005). The phenotypes affecting the IIIc isoform in Crouzon syndrome are mainly craniofacial, whilst those in Apert syndrome have additional limb phenotypes such as truncation and syndactyly, as the mutation (e.g. FGFR2-S252W) affects both FGFR2 splice variants (Johnson and Wilkie, 2011). Mouse models are available for the most common FGFR2 craniofacial syndromes: *Fgfr2c*$^{C342Y/+}$ (Crouzon), *Fgfr2c*$^{W290R/+}$ (Crouzon) and *Fgfr2*$^{S250W/+}$ (Apert), *Fgfr2*$^{S252W/+}$ (Apert) (Wang et al., 2005b, Eswarakumar et al., 2004, Mai et al., 2010, Chen et al., 2003). A common characteristic in these models are shortened midface, brachycephaly and coronal suture obliteration, which mimicks the human disease phenotype. On a cellular level, these mutations affect FGFR2 function by altering osteoblast proliferation, differentiation and apoptosis in the suture. Eswaraskumar et al 2004 reported an early increase (around E13.5) in cellular activity at the osteogenic front that is responsible for suture obliteration in *Fgfr2c*$^{C342Y/+}$ (Eswarakumar et al., 2004). On the other hand, Chen et al., 2003 reported increased apoptosis is a key player for coronal synostosis development in a separate mouse model for Apert syndrome (*Fgfr2*^{S250W}) (Chen et al., 2003).

It is not well understood how a separate allelic mutation also affecting the transmembrane domain of FGFR2 gives rise to Beare-Stevenson syndrome (*Fgfr2*$^{Y394C/+}$) (Wang et al., 2012). Similar to the C342Y mutation, FGFR2-Y394C stabilises intermolecular bonds of unpaired cysteine residues leading towards constitutive activation. However, despite some craniofacial similarities, Beare-Stevenson patients have additional skin abnormalities including cutis gyrate (thickened scalp) and acanthosis nigricans (hyper pigmentation) (Wang et al., 2012). A mouse model has also been generated to study this mutation (*Fgfr2*$^{Y394C/+}$), but the pathogenic origins of the cutaneous phenotype remains unclear (Wang et al., 2012). Increasing gene dosage also allows the identification of novel phenotypes in animal models. For example, a detailed analysis of *Fgfr2c*$^{C342Y/C342Y}$ identified exencephaly, overt cleft of the secondary palate and a series of segmentation defects along the axial skeleton (Peskett et al., 2017).

Due to a common craniofacial phenotype elicited in animal models for syndromic synostosis, they provide a robust platform to test novel therapeutic approaches and evaluate the safety of treatment. For instance, Shukla et al., 2007 attempted to rescue the coronal suture through knockdown of the RAS-MAPK pathway with short-hairpin RNA (shRNA) and ERK inhibitor (U0126) in the Apert mouse model. Despite rescuing the suture, longitudinal monitoring of these mice revealed a series of growth restrictions and unknown causes of death post-treatment (Shukla et al., 2007). Indeed, the activating nature of FGFR2 has led to the assumption that attenuation of downstream signalling is sufficient to rescue craniofacial malformations (Shukla et al., 2007, Pfaff et al., 2016). Several studies were able to demonstrate this *in vivo*: Firstly, craniofacial morphology was rescued when a mutant *Frs2α* allele was introduced onto the *Fgfr2c*$^{C342Y/+}$ mouse, which prevented activation of the downstream RAS-MAPK pathway (Eswarakumar et al., 2006). Secondly, systematic ERK knockdown using shRNA was also sufficient to rescue craniosynostosis in *Fgfr2*$^{S252W/+}$ (Shukla et al., 2007). However, the view of dampening the signal may well be over-simplistic given the complexity of pathogenic FGFR2 signalling. Snyder-Warwick et al 2010 examined the nature of FGF signalling output in the palates of the Crouzon mouse model (Snyder-Warwick et al., 2010). The authors have found *Spry2*, *Spry4*, *Etv5* and *Dusp6*, all direct targets of FGF signalling, to be

downregulated across multiple developmental stages (Snyder-Warwick et al., 2010). On the cellular level, these embryos had reduced cellular proliferation that was the cause of palatal shelf elevation delays. Moreover, isoform specific knockout of *Fgfr2c* (*Fgfr2c*$^{-/-}$) is sufficient to phenocopy that of *Fgfr2c*$^{C342Y/+}$ with apparent coronal synostosis (Eswarakumar et al., 2002). The paradoxical nature of FGFR2c signalling remains to be elucidated, but it is accepted that an intricate balance of signalling activity is required for normal development.

1.7.3-FGFR3

FGFR3 is a negative regulator for bone formation (Deng et al., 1996). Several groups have successfully created multiple FGFR3 knockout lines with different targeting methods, all showing consistent bone overgrowth phenotypes (Deng et al., 1996, Colvin et al., 1996, Eswarakumar and Schlessinger, 2007). The most notable characteristic is that these mice have a larger appearance as a consequence of ectopic chondrogenesis (Deng et al., 1996, Colvin et al., 1996). Despite this, their bones have increased porosity, likely due to a reduction in bone mineralisation. Further development of isoform specific knockouts revealed that the *Fgfr3c* isoform is responsible for this hyperplastic phenotype (Eswarakumar and Schlessinger, 2007). Interestingly, a hyperactive FGFR3 pathway leads to opposite effects where GOF mutations in FGFR3 were associated with short-limbed dwarfism caused by skeletal dysplasias such as achondroplasia and thanatophoric dysplasia (Rousseau et al., 1994, Shiang et al., 1994, Bellus et al., 1995). The missense mutation for achondroplasia was originally identified as glycine to arginine substitution (FGFR3-G380R) within the transmembrane domain of FGFR3 (Shiang et al., 1994, Bellus et al., 1995). This mutation decreases receptor trafficking from the membrane, resulting in increased levels of phosphorylation during exposures to FGF ligands and signalling activation (Monsonego-Ornan et al., 2000). Histological analysis reveals a saturation of FGFR3 at mutant mouse growth plates, coincided with fewer chondrocytes in growth plates and hypertrophic zones (Monsonego-Ornan et al., 2000, Segev et al., 2000). Several mouse models have been made for achondroplasia such as *Fgfr3*$^{G374R/+}$ and *Fgfr3*$^{G369C/+}$ using knock in approaches to the transmembrane domain (Wang et al., 1999, Chen et al., 1999). Others integrated the human FGFR3-G380R cDNA into the mouse genome, phenocopying the human

disease (Segev et al., 2000, Lee et al., 2017). In addition to the dwarfism phenotype, these mice also display brachycephaly and brain distortion (Wang et al., 1999). Thanatophoric dysplasia is the most severe form of dwarfism (Tavormina et al., 1995). The genetic differences that separate achondroplasia and thanatophoric dysplasia lies within receptor activation. Mutations that result in achondroplasia are caused by ligand dependent receptor overactivation, whilst mutant FGFR3 variants for thanatophoric dysplasia are constitutively active (Ornitz and Itoh, 2015). Mutations responsible for thanatophoric dysplasia stabilise intramolecular bonds of FGFR3 at either the transmembrane domain (*Fgfr3*$^{S365C/+}$) or the ligand specific domain (*Fgfr3*$^{Y367C/+}$) (Chen et al., 2001, Pannier et al., 2009, Ornitz and Itoh, 2015). In humans, a further mutation affecting the TK domain i.e. FGFR3-K650E was identified, but a mouse model is not yet available for this, perhaps owing to the potency of mutations affecting the kinase domain (Ornitz and Itoh, 2015). There have been reports linking craniosynostosis to achondroplasia and thanatophoric dysplasia in the literature; however, these links are not well established. For example, thanatophoric dysplasia patients exhibit a cloverleaf skull, suggestive of severe craniosynostosis (Tavormina et al., 1995), a separate mutation for achondroplasia-FGFR3-A391E, is identified in Beare-Stevenson patients (Meyers et al., 1995) and similarly in the mouse, an isolated study reports coronal synostosis in *Fgfr3*$^{G380R/+}$ (Lee et al., 2017).

The P250R mutation is the most common mutation identified in the three FGFR paralogues (Wilkie, 2005). Muenke syndrome is a consequence of FGFR3-P250R mutation, where unilateral or bicoronal synostosis is an apparent characteristic (Muenke et al., 1994). The P250R mutation affects both FGFR3 isoforms, which increases affinity for FGF ligands (Muenke et al., 1994, Wu et al., 2009). A knock-in of this mutation in the mouse recapitulated Muenke syndrome (*Fgfr3*$^{P244R/+}$) (Twigg et al., 2009). However, the craniosynostosis phenotype was incompletely penetrant due to background differences between mouse strains. Despite the variability observed in the general craniofacial skeleton, it was nevertheless a consistent mouse model for studying inner ear development (Mansour et al., 2009, Mansour et al., 2013). Muenke individuals were reported to have poor sensory reception towards the low end of the auditory spectrum (Mansour et al., 2009). Analysis of the *Fgfr3*$^{P244R/+}$ mouse identified multiple

disruptions to the cochlear duct cytoarchitecture with alterations to the overall balance of support cells, with bias towards Dieter cell fate differentiation (Mansour et al., 2013, Mansour et al., 2009). This change of fate was largely due to the mutation causing the receptor losing ligand specificity, allowing ligands to bind promiscuously to both *Fgfr3b* and *Fgfr3c* isoforms (Mansour et al., 2013). Genetic rescue of the ear phenotype can be achieved by reducing a copy of *Fgf10*, a ligand specific to both isoforms, in compound mutants (*Fgfr3*$^{P244R/+}$*; Fgf10*$^{+/-}$) (Mansour et al., 2013). Perhaps this study offers perspectives into the reason why craniosynostosis does not develop in the Muenke mouse: it could be a consequence of the precise ligands available in the coronal suture which are required to induce the phenotype, and may explain the inconsistencies observed in the original study.

1.7.4-FGF ligands and craniosynostosis

The embryonic coronal sutures express a repertoire of FGF ligands (Hajihosseini and Heath, 2002). However, it is not known how FGF ligands coordinate craniofacial development or regulate suture patency. The difficulty largely stems from FGF ligands having multiple affinities toward their receptors (Table 1) (Zhang et al., 2006). Therefore, abrogation of FGF genes *in vivo* is likely to result in a redundant phenotype (Zhang et al., 2006, Barak et al., 2012, Wright and Mansour, 2003). In light of this, determining whether a phenotype is a consequence from a single FGF ligand or a combination working synergistically remains a challenge. The FGF ligand is abundant during development and any genetic perturbation will most likely result in defects to organogenesis. One of the main purposes of FGF signalling in development is to mediate cross talks between the mesenchyme and epithelium (Ornitz and Itoh, 2015). The most common FGF ligands involved in this process include epithelial expressed FGF9 and FGF10 in the mesenchyme, each signalling reciprocally to their tissue specific FGFR isoforms (Ornitz and Itoh, 2015). An example of tissue specific interaction is in the developing limb bud, instituting a positive feedback loop for its outgrowth (Li et al., 2007, Revest et al., 2001). Thus, disrupting the tight coordination genetically results in a series of skeletal dysplasias in the axial skeleton, largely affecting bone mass, densities and stunted growth (De Moerlooze et al., 2000, Revest et al., 2001, Eswarakumar et al., 2002, Eswarakumar et al., 2004). In addition to genetic

approaches, surgical bead implantations soaked in known FGF ligands have been fundamental to understanding osteogenesis *in vivo* (Iseki et al., 1999). Explicitly, this classical embryology approach is well characterised to investigate the impact of specific ligands on the calvaria e.g. FGF2, to probe for ectopic osteogenesis (Iseki et al., 1999). All the FGF ligands are expressed in the coronal suture with the exception of FGF3 and FGF4 (Hajihosseini and Heath, 2002). There has not been a report of syndromic craniosynostosis associated with ligand function other than FGF9 to date (Harada et al., 2009). However, mutations to *FGF3*, *FGF8* and *FGF10* are sufficient to cause craniofacial malformations, but the mechanisms responsible for their pathogenesis lie beyond the scope of this section (Ornitz and Itoh, 2015).

Multiple synostoses syndrome (MSS) is characterised by multiple fusion of synovial joints in the axial skeleton (Wu et al., 2009). It is autosomal dominant and is caused by a missense mutation in FGF9 (FGF9-S99N) (Wu et al., 2009). A phenotype closely resembling MSS in the mouse, with fusion in the elbow and knee, has been reported upon substitution of arginine-143 to threonine ($Fgf9^{N143T/+}$) (Harada et al., 2009). In addition to elbow-knee synostoses (EKS), these mice exhibit coronal synostosis. The consequence of the mutation has led to a loss-of-function to FGF9 binding to heparin, affecting overall FGFR signalling potency. This protein interaction impairment resulted in hyper diffusibility of the ligand in the extracellular matrix, encroaching into the joint and suture mesenchyme to induce synostosis. Additionally, mouse mutants carrying the missense mutation have ectopic expression of multiple osteoblast precursor markers such as *Runx2* and *Osteopontin* in the coronal suture mesenchyme at E16.5 (Harada et al., 2009). FGF9 has high affinity towards the IIIc isoforms, in particular to FGFR3c (Zhang et al., 2006). Thus, coronal synostosis for Muenke syndrome is indirectly linked to FGF9, as the mutation affecting Muenke syndrome (FGFR3-P250R) is a consequence of FGFR3c having high affinities towards FGF9 (Harada et al., 2009, Muenke et al., 1997).

Due to the promiscuity of ligand-receptor interaction, it is possible that ectopic expression of FGF ligands can also drive tissue specific phenotypes provided the receptors are expressed in the right tissue. In this scenario, Carlton and colleagues successfully phenocopied

the Crouzon mouse model (*Fgfr2c*$^{C342Y/+}$) by disrupting the intergenic regions of *Fgf3* and *Fgf4*, normally absent from the wild-type (WT) suture, with midfacial hypoplasia, brachycephaly and bi-coronal synostosis (Carlton et al., 1998). Phenotypic redundancy is a consequence of ligand compensation. For example, in respect to FGF9, a fully penetrant urogenital tract defect is only observed when both *Fgf9* and *Fgf20* are knocked out (Barak et al., 2012). This is similar during cardiovascular morphogenesis, with partial penetrance when single deletions to *Fgf3* and *Fgf10* occurred at one time (Urness et al., 2011).

In summary, the marginal nature of syndromic craniosynostosis related to FGF ligands is likely associated with ligand redundancies, especially when the coronal suture expresses 20 of the 22 FGF ligands. The spatial-temporal dynamics of FGF signalling, along with the diversity of FGF ligands functioning synergistically, will therefore make biological data difficult to interpret. As biological signals are conveyed through the receptors, targeting FGFRs yield more substantial phenotypes to that observed in ligands while giving direct interpretation to its function.

1.7.5-Other mouse models with syndromic craniosynostosis

1.7.5.1-*Twist1, Msx2*

The Twist family genes encode two basic-helix-loop-helix (bHLH) transcription factors: *Twist1* and *Twist2* (also known as *Dermo1*) (Qin et al., 2012). Originally, *Twist1* was demonstrated to be required for neural tube morphogenesis whilst *Twist2*, involved in regulating cytokine gene expression (Chen and Behringer, 1995, Sosic et al., 2003). *Twist1* plays a variety of roles in mesoderm development focussing mainly in mesenchymal tissue and is expressed in the cranial mesenchyme (Bildsoe et al., 2013). *Twist1* is expressed prominently in the suture mesenchyme and its inactivation in mice results in coronal synostosis (Behr et al., 2011a, Carver et al., 2002). This is due to *Twist1* functions as a negative regulator of bone formation where it prevents osteoblast differentiation through *Runx2* inhibition (Bialek et al., 2004). *Runx2* deficient mice display delayed osteogenic activity *in vivo*, but introducing a copy of *Twist1* null allele into *Runx2*$^{+/-}$ (*Runx2*$^{+/-}$*; Twist1*$^{+/-}$) was sufficient to spare a hypoplastic

phenotype (Bialek et al., 2004, Komori et al., 1997). Conversely, *in vitro* analysis of *Twist1* knockdown revealed decreased *Runx2* expression with increased apoptosis (Yousfi et al., 2001, Maestro et al., 1999). Additionally, mutant *Twist1* drives increased expression of *FGFR2 in vitro* and *in vivo*, perhaps as a compensatory effect, to upregulate the sensitivity of FGF signalling for cellular survival (Miraoui et al., 2010b, Connerney et al., 2008). In regards to disease pathogenesis, autosomal inheritance of mutations in *TWIST1* is representative of Saethre-Chotzen syndrome and is a LOF mutation (Howard et al., 1997, el Ghouzzi et al., 1997). Saethre-Chotzen patients display complex suture abolishment most notably coronal, posterior frontal and lambdoid sutures with digit duplication (el Ghouzzi et al., 1997, Howard et al., 1997). The first *Twist1* mutant was described in 1995 to study cranial neural tube closure, with deletions in the protein-coding region of the gene by substituting exon 1 with a neo-cassette (Chen and Behringer, 1995). However, these *Twist1* homozygotes were embryonic lethal at E11.5 due to an open neural tube. *Twist1*$^{+/-}$ mice were viable with partial penetrance of limb and craniofacial phenotypes that replicated human disease according to the to genetic background of the animals (Bourgeois et al., 1998). In addition to *Twist1* being a negative regulator for osteogenesis, it also functions to inhibit chondrocyte differentiation. *Twist1*$^{+/-}$ demonstrates enhanced chondrocytic activity in the coronal suture mesenchyme with upregulation of chondrocyte markers such as *Sox9*, *Collagen II* and *Collagen X*, but its significance is currently elusive (Behr et al., 2011a). Contact inhibition also appears to play important roles in mediating Saethre-Chotzen syndrome, as both the Notch ligand *Jagged1* (*Jag1*) and the ephrin receptor-*EphA4* are downstream of *Twist1*. Conditional knockout of either *Jag1* or *EphA4* on a *Twist1*$^{+/-}$ background augments the craniosynostosis phenotype, whilst removal of either *Jag1* or *EphA4* is not sufficient to derive this pathogenesis (Ting et al., 2009, Yen et al., 2010). Both these studies stress the importance of contact inhibition in controlling osteoblast differentiation in the mesenchyme, conditional removal of which leads to mis-specification, and loss of positional information in specifying the suture boundary. Additionally, LOF mutations in *JAG1* in humans is linked to Alagille syndrome, bridging the pathogenesis with Saethre-Chotzen syndrome (Yen et al., 2010). bHLH proteins plays a plethora of roles in development and functions in hetero/homo-dimers (Massari and Murre, 2000). bHLH proteins

are classified by its tissue distribution, ability to dimerize and DNA binding specificities. Class I bHLH proteins are known as 'E proteins' and are abundant in multiple tissue types to that of Class II e.g. Twist, that has restricted expression domains. Both Class I and Class II HLH proteins contain the basic domain and is therefore DNA binding to that of the Class III factors. Examples of Class III proteins include Id (Inhibitor of DNA binding), which facilitates dimerization with E proteins and perturb formation of heterodimer formation between ClassI/II proteins (Massari and Murre, 2000). The degree of *Twist1* syndromic craniosynostosis is related to their binding partners and the dimers they form. For example, a severe craniosynostosis phenotype is caused by a frameshift in *Tcf12* in a *Twist1* background ($EIIa^{CRE/+}$; $Tcf12^{flox/-}$; $Twist1^{+/-}$) (Sharma et al., 2013). Transcription factor 12 (*Tcf12*) is an E protein, and the inability to form the Twist1-Tcf12 heterodimer results in a severe phenotype. The same scenario occurs to LOF of bHLH inhibitors *Id1* and *Id3* under a *Twist1* heterozygous background, with the former showing greater penetrance ($Id1^{+/-}$; $Twist1^{+/-}$) (Connerney et al., 2008).

Mutations in *MSX2* are associated with Boston type craniosynostosis (Jabs et al., 1993). Substitution of a histidine to a proline at position 148 on the MSX2 protein increases binding affinity towards the DNA (Ma et al., 1996). *Msx2* is expressed in the sagittal and lambdoid sutures of the mouse, and its overexpression-either WT or through a GOF mutation-$Msx2^{P7H/+}$, leads to narrowing of the sagittal suture and abnormal bone overgrowth, particularly to the parietal bone (Liu et al., 1995). In contrast, *MSX2* haploinsufficiency in humans leads to ectopic calvarial foramen and delayed suture closure, due to the loss of binding affinity to target DNA (Wilkie et al., 2000). Similar observation is reported upon knockout of *Msx1* and *Msx2 in vivo* (Roybal et al., 2010). The ectopic foramen was not a consequence of embryonic patterning defect but rather, a mitotic decrease in the bone, likely from the ossification centre (Roybal et al., 2010, Ishii et al., 2003). *Msx2* and *Twist1* interact to coordinate cellular proliferation and differentiation: Firstly, haploinsufficiency of both genes lead to ectopic frontal foramen formation and secondly, knockout of both alleles result in increased phenotypic severity (Ishii et al., 2003). Analysis of embryos between E12.5 and E14.5 revealed the pathogenesis is mainly a reduction of osteoblast differentiation beginning at E12.5. It is interesting to note that the

transcripts of these genes do not display the same expression pattern embryonically, but lead to the same phenotypic outcome. Therefore, this suggests these transcription factors may work synergistically as a co-factor to derive the same phenotype at the protein level (Ishii et al., 2003).

1.7.5.2-Hedgehog related genes

Gli3 is associated with Greig cephalopolysyndactyly (GCP). GCP is an autosomal dominant disorder affecting both limb and craniofacial development, and is associated with *Gli3* LOF (Hui and Joyner, 1993). The most notable characteristics include supernumeric fingers (polydactyly), macrocephly and a broad forehead. Additional phenotype includes lambdoid synostosis (Rice et al., 2010). Gli3 is primarily a repressor of Hedgehog signalling, which its LOF exacerbates, resulting in GCP. Specifically, GCP is caused by deletions to 7p13 on the human chromosome, and is also mapped to the same region in the mouse genome (Hui and Joyner, 1993). Johnson (1967) developed the first mouse model 'Xtra Toes', $Gli3^{Xt\text{-}J/Xt\text{-}J}$ (Xt-J), carrying an intragenic deletion of *Gli3* (Johnson, 1967, Hui and Joyner, 1993).

Augmented Hedgehog signalling is related to Carpenter syndrome, through LOF to *RAB23* (Ras-related protein Rab23)- a separate negative regulator of Hedgehog signalling preventing signalling transduction through Gli2 repression (Jenkins et al., 2007, Eggenschwiler et al., 2006). Carpenter syndrome patients display complex synostosis, but $Rab23^{-/-}$ mice do not recapitulate this phenotype and is lethal embryonically (Eggenschwiler et al., 2001). Thus, the $Gli3^{Xt\text{-}J/Xt\text{-}J}$ was used to study Hedgehog misregulation in craniosynostosis instead (Rice et al., 2010). Further analysis of $Gli3^{Xt\text{-}J/Xt\text{-}J}$ reveals ectopic osteoblast differentiation in the lambdoid sutures, which leads to early suture abolishment. Lambdoid synostosis can be rescued however, through augmentation of FGF signalling, which upregulates expression of *Twist1* (Rice et al., 2010, Rice et al., 2000). Interestingly, missense mutations to human *MEGF8* (multiple EGF like domain 8), a single pass membrane protein, phenocopies those observed in Carpenter syndrome (Twigg et al., 2012). Additional features include left-right asymmetry and cardiac defects, which was also reported in a mouse mutant generated as a result of a large-scale mutagenesis screen ($Megf8^{C193R/+}$) (Zhang et al., 2009, Aune et al., 2008). However, craniofacial or skeletal

defects were not analysed in this paper. It is unclear to the role of *Megf8* during development, but the close resemblance between *MEGF8* and Carpenter syndrome suggests the mechanism responsible is highly similar. A speculation as such could affect early development, and given by the abnormalities in left right-asymmetry, it is likely to affect both Nodal and Hedgehog signalling. In particular to the latter, it has been shown recently that *Megf8* dampens Hedgehog signalling in the primary cilia that could explain the phenotypic similarities to Carpenter syndrome caused by *RAB23* mutation (Pusapati et al., 2018).

1.7.5.3-Transforming growth factor beta (TGFβ) signalling misregulation

TGFβ signalling misregulation is associated with Marfan syndrome, a rare disorder occurring between 1:5,000 individuals (Judge and Dietz, 2005). Marfan syndrome is a complex disease affecting multiple systems. It is associated with craniofacial and skeletal dysmorphology, cardiovascular abnormalities, tissue fibrosis, ocular, and mental deficits (Judge and Dietz, 2005). Loeys-Dietz disease and Shprintzen-Goldberg syndrome, have a varying phenotypic spectrum of the described 'Marfanoid phenotype' (MacCarrick et al., 2014, Carmignac et al., 2012, Loeys et al., 2005, Judge and Dietz, 2005). In particular, patients with Marfanoid phenotype and craniosynostosis are commonly referred to as 'Shprintzen-Goldberg syndrome'. Missense mutations in the extracellular matrix protein Fibrillin 1 (*FBN1*) was first identified to be associated with Marfan syndrome, and has been implicated in craniosynostosis (Dietz et al., 1991, Sood et al., 1996). However, multiple knock-ins were generated in the mouse without craniosynostosis together with phenotypic variations between mouse strains in visceral organ systems (Carta et al., 2006, Judge et al., 2004, Ng et al., 2004, Pereira et al., 1999). LOF to the TGFβ signalling repressor- *SKI* (SKI proto-oncogene) was later identified, linking craniosynostosis in Shprintzen-Goldberg to TGFβ signalling (Doyle et al., 2012, Carmignac et al., 2012). Mutations in the genes encoding the transforming growth factor beta receptors (TGFBR), *TGFBR1* and *TGFBR2* are associated with Loeys-Dietz disease (Loeys et al., 2005). Loeys-Dietz patients typically have cardio-ventricular and outflow tract abnormalities, cleft palate, hypertelorism and occasionally craniosynostosis (Loeys et al., 2005). Substitution mutation in *TGFBR1* and *TGFBR2* augment TGF signalling activity, given by

increase of pSMAD readout, and is therefore a GOF mutation (Loeys et al., 2005). Craniosynostosis can be a phenotype of mutations in either of the receptors, and several mouse models have been generated to mimic this syndrome with varying degrees of phenotypic severity (i.e. *Tgfbr1*$^{M318R/+}$ and *Tgfbr2*$^{G357W/+}$) (Gallo et al., 2014). In particular, *Tgfbr1*$^{M318R/+}$ has partial coronal synostosis with additional kyphosis in the thoracic region (Gallo et al., 2014).

1.7.5.4-Other mouse models with craniosynostosis phenotype

The previous section described mouse models that have a strong correlation to syndromic craniosynostosis. There are also mouse mutants that possess craniosynostosis but do not fall within a categorised syndrome or bone disease. Substantial cohorts of these mutants are related to growth factor signalling misregulation (See below). Further to *Fgfr2*$^{C342Y/+}$, isoform specific knockouts such as *Fgfr2b*$^{-/-}$ and *Fgfr2c*$^{-/-}$ also display craniosynostosis phenotype (Eswarakumar et al., 2002, De Moerlooze et al., 2000). In particular, *Fgfr2c*$^{-/-}$ mutants harbour coronal synostosis that phenocopies the *Fgfr2c*$^{C342Y/+}$ (Eswarakumar et al., 2002). The main difference between both models lies within the disease progression, where the latter possesses the accelerated phenotype during early embryogenesis (Eswarakumar et al., 2002, Eswarakumar et al., 2004). *Fgfr2b*$^{-/-}$ displays a subtle form of craniosynostosis, with fusion of the parietal and squamous temporal bones (De Moerlooze et al., 2000). It is established that a hallmark of craniosynostosis is the upregulation of the RAS-MAPK pathway (Shukla et al., 2007). Indeed, knockout of (*Dusp6*$^{-/-}$) a negative regulator of ERK, results in coronal synostosis (Li et al., 2007). Similarly, LOF mutations to Ets2 repressor factor (*ERF*) is also implicated in compound craniosynostosis affecting the coronal and sagittal sutures (Twigg et al., 2013). ERF is responsible for the export of active ERK from the nucleus to attenuate its transcriptional activation activities, and conditional knockout of ERF (*ERF*$^{\Delta/-}$) recapitulates its phenotype (Twigg et al., 2013).

Although not commonly associated with craniosynostosis, Platelet derived growth factor (PDGF) signalling has also been related to craniofacial malformations and coronal synostosis (He and Soriano, 2017, Moenning et al., 2009, Soriano, 1997). This is most likely due to the conserved nature of growth factor signalling downstream of the receptor. Signalling

misregulation in an isoform of the platelet derived growth factor receptor (PDGFR)-PDGFRα, is implicated in midline defects and a split face (*Pdgfrα*$^{-/-}$) (Soriano, 1997). Moreover, over-activation of PDGFRα (*Pdgfrα*$^{D842V/+}$) drives ectopic chondrogenesis that elicits coronal and lambdoid synostosis through the P13K-AKT cascade (He and Soriano, 2017). A similar phenotype is replicated in a transgenic over-expression model located at the *Rosa26* locus (*R26R*$^{Pdgfrα\text{-}D842V/+}$) (Moenning et al., 2009).

In addition to growth factors, Wnt/β-catenin signalling is also a key player in regulating osteoblast proliferation and differentiation, whereby potentiation of signalling favours these conditions (Yu et al., 2005). In the absence of signalling activation, β-catenin is prevented from being translocated to the nucleus through degradation. Therefore, Wnt signalling modulators are critical to modulate signalling sensitivity: Axin serves as a scaffold for formation of a β-catenin degradation complex, and its degradation is therefore Axin dependent (Logan and Nusse, 2004). Augmentation of Wnt signalling by *Axin2*$^{-/-}$ results in coronal and interfrontal synostosis (Yu et al., 2005). Similarly, overexpression of a osteoinductive protein, Nel-like type 1 molecule (*Nell1*) elicits posterior frontal suture craniosynostosis, along with the partial closure of sagittal and coronal sutures (Zhang et al., 2002). *NELL1* was originally isolated from samples obtained from unilateral (non-syndromic) coronal synostosis patients, and is expressed in the mesenchyme and osteogenic fronts (Ting et al., 1999). *NELL1* expression is upregulated in sutures undergoing premature fusion, and is believed to augment Wnt/ β-catenin signalling, through interactions with β-integrins in osteoblasts (Ting et al., 1999, James et al., 2015).

Other mutants reported in the literature include the following: Growth differentiation factor 6 (*Gdf6*) is a secreted morphogen associated with the BMP signalling pathway (Ducy and Karsenty, 2000). Mutants lacking both alleles of *Gdf6* (*Gdf6*$^{-/-}$) display coronal synostosis and appendicular skeleton abnormalities, with fusion of the tarsals and carpals (Settle et al., 2003). *Runx2* is indispensable for osteoblast differentiation, and overexpression of *Runx2* in the mesenchyme, driven under the endogenous promoter *Prx1* (*Prx1-Runx2*), elicits multiple synostosis, inclusive of multiple joint fusions in the appendicular skeleton (Maeno et al., 2011). Metopic suture synostosis is caused by LOF mutations to Fras1 related extracellular related

gene 1 (*FREM1)*, and is a cause of trigonocephaly in humans (Vissers et al., 2011). *Frem1* encodes a protein secreted by mesenchymal cells that aids extracellular matrix remodelling (Smyth et al., 2004). In the mouse, Frem1 is expressed along the periphery of the frontal bone, immediately adjacent to the interfrontal suture (metopic eqivalent) (Vissers et al., 2011). The orginal mouse model generated-*Frem1*$^{Bat/+}$ is a hypomorph, with the mutation mapped through ENU mutagenesis (Smyth et al., 2004). The mouse harbours a substitution mutation (T>C) which causes exon skipping to occur during transcription (Smyth et al., 2004). A knockout is also available, *Frem1*$^{qbrick/+}$, which includes exon 2 deletion (Kiyozumi et al., 2006, Vissers et al., 2011). Both mouse models harbour interfrontal synostosis, with the latter mutant possessing a stronger phenotype (Vissers et al., 2011).

1.7.6-Evaluation of mouse models in the literature

Mouse models have been central to study human diseases. Together with lineage tracing reporters, the phenotypes caused by knock in mutations have been critical to understand the pathways required for craniofacial development. Furthermore, mouse models provide a platform to test novel therapeutic strategies and management techniques (Wang et al., 2015, Perlyn et al., 2006, Maruyama et al., 2016). However, it is well discussed in the murine research community that significant discrepancies in expected phenotypes may be the result of genetic differences between species, genetic redundancies and sensitivities. An example of this can be seen for *RAB23* mutation responsible for human Carpenter syndrome (Eggenschwiler et al., 2001, Jenkins et al., 2007). LOF of the mammalian homologue of *RAB23*, results in exencephaly and early embryonic lethality (Eggenschwiler et al., 2001). Other examples include Ets domain-containing transcription factor (*ERF*), where craniosynostosis is only observed in a mouse model harbouring a conditional allele ($Erf^{\Delta/-}$) in contrast to that of a deletion ($Erf^{dl1/-}$) (Twigg et al., 2013, Papadaki et al., 2007). The difference in phenotype is due to the conditional allele having a greater efficiency in abrogating *Erf* gene expression (Twigg et al., 2013). Similar can be said of those mouse models related to Marfan syndrome that do not recapitulate a craniofacial phenotype (Gallo et al., 2014, Judge et al., 2004, Ng et al., 2004, Pereira et al., 1999).

The ability to generate gene knockout models has been pivotal in our understanding of gene function, and this in turn is dependent upon successful and accurate targeting of the specific allele of interest. Therefore, it makes sense that the overall design of a targeting vector is vital to reproducibly produce a consistant phenotype. However, there are instances in the literature where a wide phenotypic spectrum can be produced. Examples of this can be seen in the *Fgfr2* knockouts, as the receptor protein has multiple functionalities (Molotkov et al., 2017, Yu et al., 2003). A common strategy to generate an *Fgfr2* knockout is through the removal of the ligand-binding domain (exons 8-9, IgI loop3). However, this mutant did not result in the complete removal of the FGFR2, but yielded a truncated, albeit non functional, receptor instead. On the other hand, removal of exon 5, common to both *Fgfr2b* and *Fgfr2c* isoforms, did not

lead to the expression of a truncated receptor (Yu et al., 2003, Molotkov et al., 2017). In fact, there are slight phenotypic differences too between the knockouts, with the latter *Fgfr2c* knockout appearing less severe (Yu et al., 2003, Molotkov et al., 2017). Targeting constructs recombined between intragenic regions also have an effect on gene expression. Here, removal of exon 9 encoding *Fgfr2c* is able to cause a splice switch that results in ectopic *Fgfr2b* expression (Hajihosseini et al., 2001). LoxP sites were inserted in *Fgfr2* intergenic regions of exons 8-10, and conditional removal of the loxP sites through recombination could have increased susceptibility to alternative splicing alterations (Hajihosseini et al., 2001). The upregulation of *Fgfr2b* subsequently shifted the phenotype from a Crouzon spectrum to that of Apert (Hajihosseini et al., 2001). Nonetheless, the successful targeting of specific genes has been vital to determine gene function contributing towards human disease.

Mouse models for characterised syndromes and developmental bone diseases

Gene	Mutation/Insertion/recombinants	Bone disease/Syndrome	Synostosis	Model	Reference
Fgf9	N143T	EKS/MSS		LOF	Harada et al 2009
Fgf3 ***Fgf4***	Intragenic retroviral insertion mutagenesis	Crouzon phenocopy	Coronal	Overexpression	Carlton et al 1998
Fgfr1	P250R	Pfeiffer	Coronal, interfrontal, sagittal		Zhou et al 2000
Fgfr2	C342Y	Crouzon			Eswarakumar et al 2004
	W290R	Crouzon	Coronal		
	S252W				Wang et al 2005
	S250W	Apert	Coronal, sagittal, lambdoid		Chen et al 2003
	Y394C	Beare-Stevenson			Wang et al 2012
Fgfr3	P244R	Muenke	Coronal		Twigg et al 2009
	G374R				Wang et al 1999
	G369C				Chen et al 1999
	G380R	Achondroplasia			Segev et al 2000
	S365C				Lee et al 2017
	Y367C	Thanatophoric dysplasia	N/A	GOF	Pannier et al 2009
Twist1	Gene trap, *Twist1*$^{+/-}$				Chen and Behringer 1995
					Behr et al 2011
Id1	*Id1*$^{+/-}$*; Twist1*$^{+/-}$				
Id3	*Id3*$^{+/-}$*; Twist1*$^{+/-}$	Saethre-Chotzen	Coronal, sagittal, lambdoid	LOF	Connerney et al 2008
Msx2	*Timp1-P7H*				
	CMV-P7H			GOF	
	CMV-WT	Boston-type craniosynostosis	Coronal, sagittal, lambdoid	Overexpression	Lin et al 1995
Jag1	Gene trap, *Jag1*$^{+/-}$		No phenotype	LOF	
	Jag1$^{+/-}$*; Twist1*$^{+/-}$*; Mesp1*$^{CRE/+}$	Alagille	Coronal, sagittal, lambdoid	LOF	Yen et al 2010
Gli3		Greig cephalopolysyndactyly/Carpenter Syndrome			Hui and Joyner 1993
	Intragenic deletion, *Gli3*$^{Xt\text{-}J/Xt\text{-}J}$		Lambdoid	LOF	Rice et al 2010
Tgfbr1	M318R	Loeys-Dietz disease	Coronal	GOF	Gallo et al., 2014

Table 3: Mouse models for characterised syndromes and developmental bone diseases.

Gene	Mutation/Insertion/recombinant	Synostosis	Model	Reference
Fgfr2c	Exon 9 STOP, *Fgfr2c*$^{-/-}$			Eswarakumar et al 2002
	Exon 9 flox, *Fgfr2c*$^{\Delta/+}$	Coronal		Hajihosseini et al 2001
Fgfr2b	Exon 8 STOP, *Fgfr2b*$^{-/-}$	Squamous temporal-parietal	LOF	De Moerlooze et al 2000
Nell1	WT (CMV*)	Coronal, sagittal, posterior frontal	Overexpression	Zhang et al 2002
Axin2	Gene trap, *Axin2*$^{-/-}$	Coronal, Interfrontal		Yu et al 1995
Dusp6	Exon3 STOP, *Dusp6*$^{+/-}$			
	Dusp6$^{-/-}$			Li et al 2007
Gdf6	Gene trap, *Gdf*$^{-/-}$	Coronal	LOF	Settle et al 2003
Pdgfrα	D846V (R26*)	Coronal, interfrontal	Overexpression	Moenning et al 2009
	Pdgfrα$^{D842V/+}$*; Meox2*$^{CRE/+}$	Coronal		
	Pdgfrα$^{D842V/+}$*; Mesp1*$^{CRE/+}$	Coronal, lambdoid	GOF	He and Soriano 2017
EphA4	*EphA4*$^{-/-}$			
	Twist1$^{+/-}$*; EphA4*$^{+/-}$	Coronal	LOF	Ting et al 2009
Runx2	*Prx1-Runx2*	Pan-synostosis	Overexpression	Maeno et al 2011
Erf	Exon 2+3 deletion, *Erf*$^{-/-}$			Papadaki et al 2007
	Erf flox, *Erf*$^{\delta/+}$	No phenotype		
	Erf flox, *Erf*$^{\delta/-}$	Coronal, sagittal, lambdoid	LOF	Twigg et al 2013
Frem1	Frameshift (T>C) at intron 25, *Frem1*$^{bat/+}$		Hypomorph	Smyth et al 2004
	Exon 2 deletion, *Frem1*$^{QBrick/+}$	Posterior frontal	LOF	Vissers et al 2011

*=Promoter

Table 4: Mouse models with craniosynostosis but do not fall within a characterised syndrome

1.8-Aim of project

Despite the large cohort of studies where mutations were identified to contribute towards craniofacial birth defects, questions remain as to the developmental and molecular events that contribute to syndromic craniosynostosis. This PhD project therefore provides a comprehensive and comparative analysis of a novel transgenic mouse model generated in the Pauws lab (*R26R*$^{Fgfr2cV5/Fgfr2cV5}$) with that of the more widely studied *Fgfr2c*$^{C342Y/+}$. The following objectives for this PhD were:

i) To identify the embryonic lineage sensitive to *Fgfr2c* signalling in the craniofacial skeleton.

ii) To examine the nature of *Fgfr2c* signalling misregulation at the protein and RNA level.

iii) To explore the phenotypic impact of *Fgfr2c* overexpression on *Fgfr2c*$^{C342Y/+}$ (*R26R*$^{Fgfr2cV5/+}$;*βactin*$^{CRE/+}$;*Fgfr2c*$^{C342Y/+}$).

iv) To investigate the consequences of over-activating the downstream cascade commonly associated with syndromic craniosynostosis (RAS-MAPK), using an oncogenic mouse model (*KRas*$^{LSL-G12D/+}$).

v) To identify novel genes contributing to syndromic craniosynostosis using transcriptomic profiling.

The overall aim is to generate a detailed understanding of the molecular events that occur during normal and abnormal suture morphogenesis, which ultimately lead to the identification of novel therapeutic opportunities aimed at reducing recurrent surgeries for syndromic craniosynostosis.

Chapter 2

Materials and Methods

2.1-Animals

All the animals used in this thesis are summarized in Table 5. Generation of the *Fgfr2c* overexpression mouse *($R26R^{Fgfr2cV5/Fgfr2cV5}$):* To target the *Rosa26* genomic locus (*$Gt(ROSA26)^{tm1Sor}$*), *Fgfr2c-V5* construct was inserted 3' to a targeting vector carrying the *loxP-PGK-neo-tPa-loxP* cassette (Soriano, 1999). The V5 epitope tagged to the *Fgfr2c* is unique to transgene expression and differentiates transgenic from endogenous FGFR2c protein expression. Following selection, the construct was linearised and injected into embryonic stem cells using standard procedures at UCL Transgenic Services. The founders (CD1) were maintained as homozygotes (*$R26R^{Fgfr2cV5/Fgfr2cV5}$*).

$\beta actin^{CRE/+}$ was previously described in Sakai et al., 1997 (Sakai and Miyazaki, 1997). CRE recombinase is driven under the control of the *βactin* promoter to generate ubiquitous expression. *$Mesp1^{CRE/+}$* was previously described in Saga et al., 1999 (Saga et al., 1999). CRE recombinase is driven under the control of Mesoderm posterior 1 (*Mesp1*) promoter to elicit conditonal expression in the mesoderm. *$Wnt1^{CRE/+}$; $R26R^{YFP/+}$* was previously described in Freem et al., 2010 (Freem et al., 2010). CRE recombinase is driven under the control of the *Wnt1* promoter to generate conditional expression in the NCC lineage. *$Wnt1^{CRE/+}$* mice were crossed with *$R26R^{YFP/YFP}$* reporter to generate *$Wnt1^{CRE/+}$; $R26R^{YFP/+}$* offspring. Cells positive with the *CRE* allele will also express the reporter protein, thus labeling cells from the NCCs lineage. *$Wnt1^{CRE/+}$; $R26R^{YFP/+}$*. *$Wnt1^{CRE/+}$; $R26R^{YFP/+}$*animals were bred with WT to lineage trace cells from NCC lineage in the calvaria. *$R26R^{mTmG/mTmG}$* was previously described in (Muzumdar et al., 2007). This reporter line was chosen to show CRE activity in the sutures in Chapter 3. The *mTmG* allele was crossed with *$R26R^{Fgfr2cV5/Fgfr2cV5}$* to generate a double conditional mouse that overexpresses both *mTmG* and *Fgfr2cV5* (*$R26R^{Fgfr2cV5/mTmG}$*) upon conditional overexpression. The breeding strategy is shown in Figure 23.

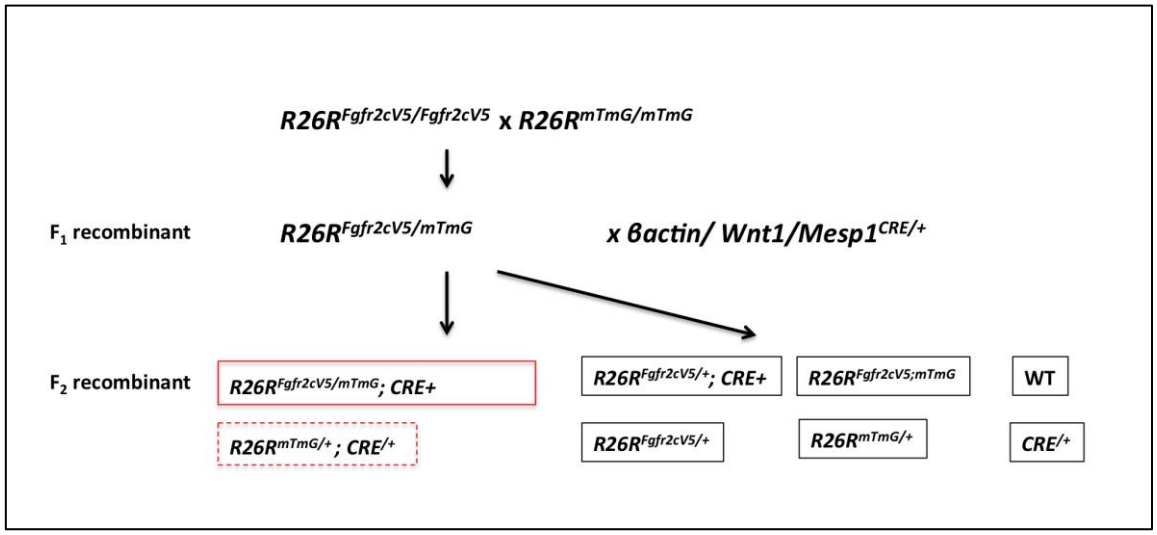

Figure 23: Interbreeding strategy to introduce mTmG allele into the *Fgfr2c* overexpression mouse.

R26R$^{mTmG/mTmG}$ were crossed with *R26R*$^{Fgfr2cV5/Fgfr2cV5}$ to produce *R26R*$^{Fgfr2cV5/+}$*; R26R*$^{mTmG/+}$. The F_1 recombinants were subsequently bred with conditional CRE lines to drive *Fgfr2c-V5* overexpression and reporter activity. A total of 8 genotypes were expected from the F_2 recombinants. This was a method attempted to indirectly show the expression of FGFR2c-V5 when IHC failed to address the localization of the transgenic protein in the calvaria. Red box is indicates the desired genotype but however, due to the nature of trans-heterozygotes, only the genotype with CRE reporter activity was selected (dotted box).

Fgfr2c$^{C342Y/+}$ was previously described in Eswarakumar et al., 2004, with the colony re-derived through the EMMA (European Mouse Mutant Archive) consortium. *Fgfr2c*$^{C342Y/+}$ was crossed with CD1-WT to derive *Fgfr2c*$^{C342Y/+}$ embryos. *KRas*$^{LSL-G12D/+}$ was previously described in Tuveson et al., 2004 (Tuveson et al., 2004). *KRas*$^{LSL-G12D/+}$ was paired with a *Wnt1*$^{CRE/+}$ to conditionally over-activate mutant *KRas-G12D* in the NCC lineage. *R26R*$^{Fgfr2cV5/Fgfr2cV5}$ allele was introduced into the *Fgfr2c*$^{C342Y/+}$ to generate a double mutant; all littermates were genotyped for both *Fgfr2c*$^{C342Y/+}$ and *Fgfr2c-V5* allele (*R26R*$^{Fgfr2cV5/+}$; *Fgfr2c*$^{C342Y/+}$) prior to any experimental proceedings. *Fgfr2c*$^{C342Y/+}$*; R26R*$^{Fgfr2cV5/+}$ was subsequently crossed with *βactin*$^{CRE/+}$ to generate ubiquitous overexpression (*R26R*$^{Fgfr2cV5/+}$; *βactin*$^{CRE/+}$*;Fgfr2c*$^{C342Y/+}$), with embryos harvested at E18.5. The breeding strategy is illustrated in Figure 24. *R26R*$^{Fgfr2cV5/+}$*; Fgfr2c*$^{C342Y/+}$*; βactin*$^{CRE/+}$ is to be presented with an underline (*R26R*$^{Fgfr2cV5/+}$*;βactin*$^{CRE/+}$*;Fgfr2c*$^{C342Y/+}$) from here on to aid visual clarity.

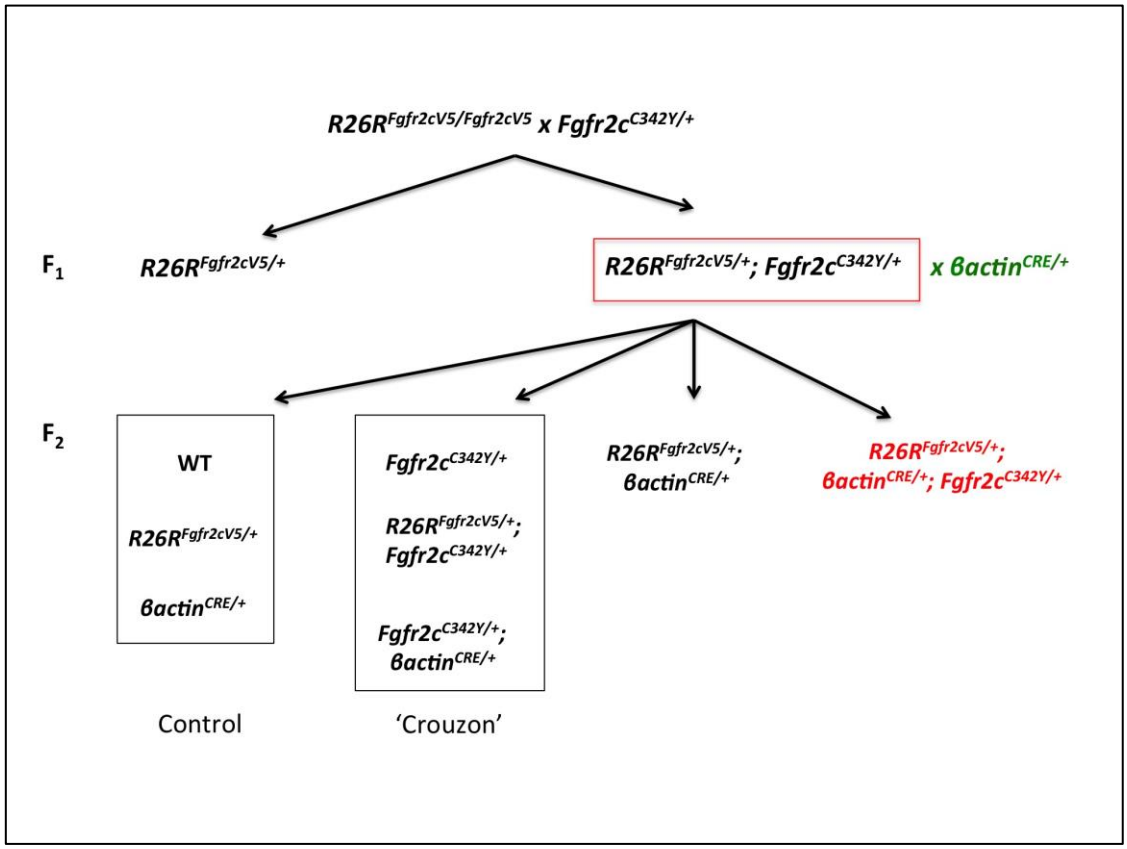

Figure 24: Introduction of the *Fgfr2c* overexpression allele into *Fgfr2c*$^{C342Y/+}$.

R26R$^{Fgfr2cV5/Fgfr2cV5}$ was crossed with *Fgfr2c*$^{C342Y/+}$ to generate *R26R*$^{Fgfr2cV5/+;}$ *Fgfr2c*$^{C342Y/+}$. These F_1 recombinants were subsequently matched with *βactin*$^{CRE/+}$. A total of 8 genotypes were expected from the cross, and the desired recombinant carries all three alleles in *R26R*$^{Fgfr2cV5/+}$; *βactin*$^{CRE/+}$;*Fgfr2c*$^{C342Y/+}$ (Red)

Mouse Lines	Strain	Description	References	MGI
βactin$^{CRE/+}$	Mixed CD1	Ubiquitous expression	Sakai et al., 1997 (Biochem Biophys Res Commun)	1919410
Wnt1$^{CRE/+}$; *R26R*$^{YFP/+}$	C57BL/6	NCCs specific expression with eYFP reporter allele	Danielian et al., 1998 (Curr. Biol)	2386570
Mesp1$^{CRE/+}$	Mixed CD1	Core mesoderm specific expression	Saga et al., 1999 (Development)	2176467
R26R$^{Fgfr2cV5/Fgfr2cV5}$		*Fgfr2cV5* overexpression under *Rosa26* transgene	This lab	6150825
R26R$^{mTmG/mTmG}$	C57BL/6	Dual reporter mouse. Expresses eGFP post excision and tdTomato prior to recombination	Muzumdar et al., 2007 (Genesis)	3716464
R26R$^{Fgfr2cV5/mTmG}$	Mixed CD1	Dual reporter mouse with *Fgfr2cV5* allele	This lab	N/A
Fgfr2c$^{C342Y/+}$		Mouse model for human Crouzon syndrome	Eswarakumar et al., 2004 (PNAS)	3053095
WT		Wild type on a CD1 background	Charles River Laboratories	N/A
KRas$^{LSL-G12D/+}$	C57BL/6	Conditional oncogenic KRas-G12D with Lox-STOP-Lox (LSL) minigene cassette	Tuveson et al., 2004 (Cancer Cell)	2429948
R26R$^{Fgfr2cV5/+}$; *Fgfr2c*$^{C342Y/+}$	Mixed CD1	Mouse model for human Crouzon syndrome carrying the *Fgfr2cV5* flox transgene	This lab	N/A

Table 5: Mouse lines used in this thesis.

2.2- Genotype determination

2.2.1-DNA extraction

A biopsy sample was obtained from recombinants for genotyping. A cocktail of lysis buffer[1] and Proteinase K (Roche) was applied to the samples and incubated for 1 hour 30 mins at 55 ^{o}C, followed by 10 mins incubation at 85^{o}C to inactivate the enzyme. An equal proportion of isopropanol was added to the lysate to precipitate the DNA, followed by a brief wash in 70% EtOH. The lysate was air dried thoroughly and reconstituted in 20-50µl H_2O.

2.2.2-Genotype determination for *Rosa26* or CRE

Genotyping primers span the *Rosa26* short arm to determine the presence of the $R26R^{Fgfr2cV5/Fgfr2cV5}$ floxed allele (Figure 25 A). To determine *Fgfr2c-V5* overexpression recombinants, mice carrying the *Fgfr2c-V5* floxed allele were crossed with respective CRE recombinase animals ($\beta actin^{CRE/+}$; $Wnt1^{CRE/+}$ or $Mesp1^{CRE/+}$) and analysed at desired embryonic stages as required per experiment. Littermates were genotyped for *CRE* and *LoxP* excision on the transgene, where the primers span the *Rosa26* short arm and 5' of the *Fgfr2c-V5* transgene. The expected amplicon for the *Fgfr2c-V5* overexpressing recombinants was 0.64kb for the excised transgene (Figure 25 B) and 0.50kb for CRE recombinase (Figure 25 C). Table 6 and Table 7 describe the primers and PCR parameters used to determine respective genotypes of the mouse lines driven under the *Rosa26* promoter respectively.

[1] 100mM Tris-HCL pH 8.5, 5mM EDTA, 0.2% SDS, 200mM NaCl

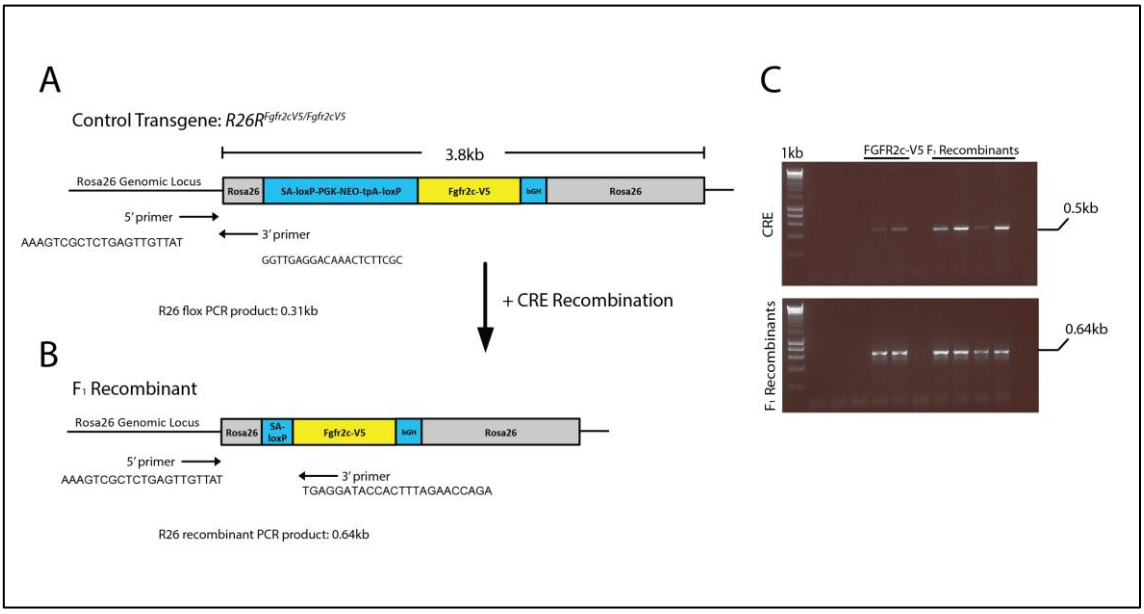

Figure 25: Strategy for R26R recombinants genotyping.

Primers specific for the recombinants span the *Rosa26* short homology arm and the excision junction between the *LoxP* site and *Fgfr2c-V5*. Expected amplicon: 0.5kb (CRE); 0.64kb (R26R-FGFR2cV5).

Primers	Sequence	Amplicon
CRE (Forward)	accctgatcctggcaatttcgg	0.5kb
CRE (Reverse)	gatgcaacgagtgatgaggttc	
R26R-FGFR2cV5 (Common Forward)	aaagtcgctctgagttgttat	0.64kb
R26R-FGFR2cV5 (Reverse)	tgaggataccactttagaaccaga	
R26R-FGFR2cV5 (flox) (Reverse)	ggttgaggacaaactcttcgc	0.31kb
R26R-mTmG (Forward)	ctctgctgcctcctggcttct	0.25kb
R26R-mTmG (Reverse)	cgaggcggatcacaagcaata	
R26R-YFP (Forward)	aaagtcgctctgagttgttat	0.32kb
R26R-YFP (Reverse)	aagaccgcgaagagtttgtc	

Table 6 Genotyping primers for Rosa26 or CRE

PCR Steps	CRE	R26R-Fgfr2cV5	R26R-mTmG	R26R-YFP
Initial denaturation	94ºC, 2mins	94ºC, 5mins		
Denaturation	94ºC, 30 secs	94ºC, 30secs	94ºC, 20secs	94ºC, 30secs
Annealing	63ºC, 45secs	60ºC, 30secs	58ºC, 25secs	60ºC, 30secs
Extension	72ºC, 45 secs	72ºC, 40secs	72ºC, 45secs	72ºC, 40secs
Final Extension	72ºC, 5mins			
Total Cycles	29	37	32	37

Table 7: PCR parameters for *Rosa26* and CRE primers

2.2.3-Genotyping for the *Fgfr2c*$^{C342Y/+}$ knock in mutation

A set of primers amplifies the WT *Fgfr2* fragment (Table 8). Table 9 denotes PCR cycling parameters for the *Fgfr2* primer pairs. The C342Y mutation inserts a restriction site on the *Fgfr2* construct for RSAI enzyme (Eswarakumar et al., 2004). Therefore, a further enzymatic digest using RsaI (New England Biolabs) is required to determine the mutation in *Fgfr2*. The PCR products were subsequently incubated at 37ºC, 1 hour before enzymatic denaturation at 85ºC. Two bands were expected for CD1-WT (373bp/136bp) and three for heterozygotes (311/136/62bp).

Primers	Sequence	Amplicon
Fgfr2 (Forward)	cggtgtctcttcgtgtctctc	550bp (WT) 370bp/136bp (WT + RsaI) 311bp/136bp/62bp (Het + RsaI) 311bp/62bp (HOM+ RsaI)
Fgfr2 (Reverse)	gaggggtcatttggaacattt	

Table 8: *Fgfr2* genotyping primers and expected amplicon after RSAI digestion to determine knock in mutation.

Step	FGFR2-C342Y
Initial denaturation	95°C, 2mins
Denaturation	95 °C, 2mins 30 secs
Annealing	60 °C, 20s (-1°C/cycle)
Extension	72 °C, 1min
Final Extension	72°C, 5mins
Total Cycles	15

Table 9: PCR cycling parameters for *Fgfr2* primers.

2.2.4-Genotyping for the *KRas*$^{G12D/+}$ mice

The genotyping strategy for *KRas*$^{LSL\text{-}G12D/+}$ is illustrated below (Figure 26) (Table 10 and Table 11). The *KRas-LSL-G12D* is conferred by a transcriptional termination stop element (loxP-STOP-loxP) upstream of the oncogenic *KRas* (*), characterized by a substitution mutation from GGT to GAT in exon 1.

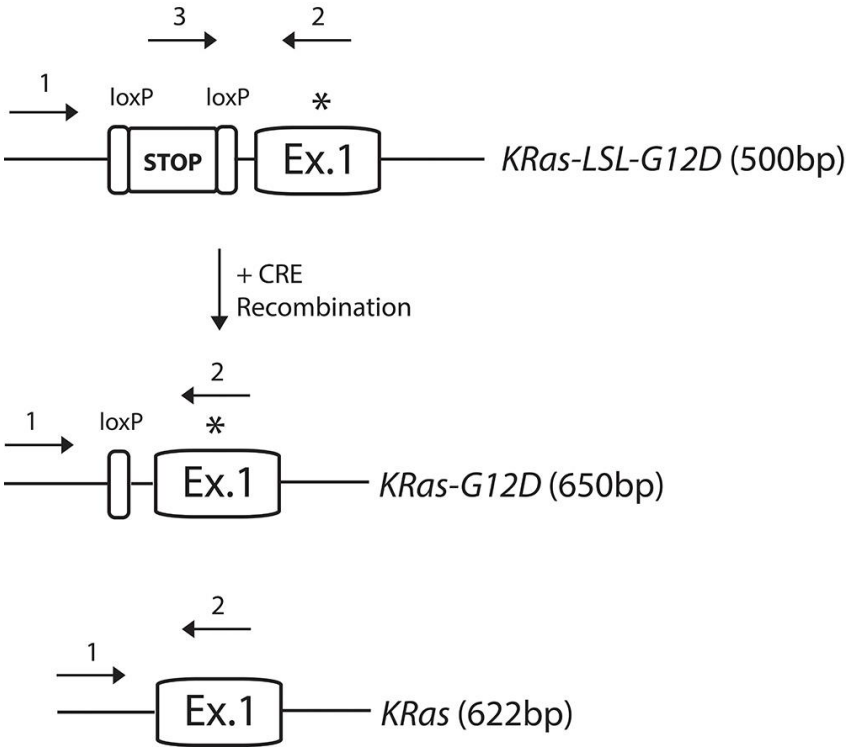

Figure 26: Genotyping strategy of *KRas*$^{LSL\text{-}G12D/+}$ and its recombinants.

Common primers (1+2) flank the exons and intragenic regions, whilst primer 3 is specific for stop element (*) G12D mutation.

Primers	Sequence	Amplicon
KRas 1 (Common Forward)	gtctttccccagcacagtgc	WT: 622bp
KRas 2 (Common Reverse)	ctcttgcctacgccaccagctc	G12D: 650bp
KRas 3 (Flox)	agctagccaccatggcttgagtaagtctgca	LSL: 500bp

Table 10: Genotyping primers for KRas.

Step	KRas
Initial denaturation	95°C, 2mins
Denaturation	95°C, 30secs
Annealing	61°C, 30secs
Extension	72°C, 45secs
Final Extension	72°C, 5mins
Total Cycles	34

Table 11: PCR cycling parameters for KRas.

2.3-Culture systems

2.3.1-Cells

HEK293T (immortalized human embryonic kidney cells) were cultured in Dulbecco Minimum Essential Medium (DMEM) alpha culture medium (Gibco) supplemented with 10% Fetal Bovine Serum (FBS) and 1% Penicillin-Streptomycin.

2.3.2-Cell transfection

Cells were transfected with plasmids carrying the FGFR2c-V5 construct (*pFgfr2c-V5*), *Fgfr2c*$^{C342Y/+}$ (*pFgfr2c-C342Y-V5*) or control *pcDNA* in 6 well plates when they have reached 50% confluence. A cocktail of 100µl Optimem culture medium (Gibco), 1ul FuGENE transfection reagent (Promega) and 1ug of DNA was added to each well prior to 48 hours incubation at 37°C, 5% CO_2. Success of cellular transfection was determined by the V5 epitope on the *Fgfr2* plasmids.

2.3.3-*Ex vivo* calvarial explant cultures

Embryos were harvested at E17.5 and dissected in PBS. The calvaria was dissected from the skin and brain and cultured in Dulbecco's Modified Eagle Medium (DMEM, Sigma) supplemented with 10% Fetal Bovine Serum (FBS, Sigma) and 5% Penicillin-Streptomycin. The medium was refreshed every other day and cultured for 2 weeks at 37°C, 5% CO_2. Calvaria were fixed in 70% ethanol and processed for 0.01% Alizarin Red stain upon experimental completion.

2.4-Quantitative RT-qPCR

2.4.1-RNA extraction

RNA was extracted using the Trizol method (Invitrogen). E12.5 whole embryos, E16.5 calvaria, or HEK293T cells were homogenized in 1ml Trizol and incubated at room temperature (RT) for 5mins, prior to phase separation with chloroform (Sigma). The aqueous phase was isolated in a new tube, and RNA precipitated in 500ul of isopropanol. The samples were centrifuged to pellet the RNA, with the supernatant discarded. The RNA was washed in 70% Ethanol (EtOH) and re-pelleted. EtOH was subsequently removed with the RNA allowed to air-dry, and resuspended in RNAse free water (Sigma) in appropriate volumes (around 100ul). A full protocol is found in Appendix 1.

2.4.2-cDNA synthesis

cDNA was synthesized using the QuantiTect Reverse Transcription Kit (Qiagen) according to the manufacturer's protocol. cDNA synthesis was performed at 2ug with all the reagents doubled linearly. Briefly, genomic DNA was eliminated from the RNA extraction process using the supplied 'gDNA wipeout buffer'. The cocktail was incubated at 42^{o}C for 2 mins before resting on ice. The RNA was subsequently incorporated with the reverse transcription reaction cocktail consisting of reverse transcriptase, primers and reaction buffer. Reverse transcription was performed at 42^{o}C for 15 mins and at 95^{o}C for 3 mins to inactivate the enzyme. The cDNA was diluted 1:2 to reach a final concentration of 1ug for RT-qPCR.

2.4.3-Quantitative RT-qPCR

Expression analysis was performed using Taqman assays (Applied Biosystems). RT-qPCR was achieved using the 7500 Fast Real Time PCR System (Applied Biosystems) or StepOne Real-Time PCR System (Applied Biosystems) on a 96-well plate at 1ug. The reaction was set up at 12ul per well (Table 12), with a minimum of three technical replicates per genotype, with *Rn18* chosen as the reference gene. Table 13 illustrates all the assays used for the RT-qPCR. The collected dataset was analysed and exported into the 7500 Fast Real-Time and StepOne PCR Software (Applied Biosystems). Amplification efficiencies were checked in

target genes and controls prior to data analysis using the ΔΔCt method normalized to the controls.

RT-qPCR reaction (/well)	Volume (µl)
TaqMan Fast Universal Master Mix (Applied Biosystems)	6
Assay	0.6
cDNA (1ug)	1
H_2O	4.4
Total	12

Table 12: RT-qPCR reaction

Reference Genes	Company	Assay ID	Specie
Fgfr2c	Applied Biosystems	Mm01269938_m1	Mouse
Fgfr2b		Mm01275520_m1	Mouse
Rn18		Mm03928990_g1	Mouse
SPRY2		Hs01921749_s1	Human
SPRY4		Hs01935412_s1	Human
ETV5		Hs00927557_m1	Human
Rn18		Mm03928990_g1	Mouse
Col9a1		Mm00483836_m1	Mouse
Map3k6		Mm00522235_m1	Mouse
Pcyt1b		Mm00616920_m1	Mouse
Papln		Mm01307240_m1	Mouse
Pdgfb		Mm00440677_m1	Mouse
Rsad2		Mm00491265_m1	Mouse

Table 13: RT-qPCR assays

2.5-Immunoblots

All the stock reagents required for immunoblotting can be found in Appendix 2.

2.5.1-Protein extraction for whole embryos

E12.5 embryos were dissected under ice cold PBS and homogenized in RIPA buffer[2] with MINI complete protease inhibitor cocktail (Sigma) and centrifuged to obtain protein lysates. Protein concentration was determined using Bradford reagent (Biorad) and spectrophotometry. Protein lysates were prepared at 30ug in a cocktail of 4x Lamelli buffer (Biorad) and dithiothrethiol, and were denatured at >80^{o}C for 8 mins. Samples were immediately stored in -20^{o}C until required.

[2] 150mM NaCl, 1% Triton X-100 (Fisher), 0.5% sodium deoxycholate (Sigma), 0.1% SDS (Sigma), 50mM Tris-pH 8.0 (Fisher)

2.5.2- Protein extraction for cells

Cells were washed in ice cold PBS and harvested on ice. Cells were resuspended in a specialized lysis buffer[3] optimized for cells and lysed by pipetting. Cell lysates were harvested by centrifugation and aqueous phase isolated. Protein concentration was determined using Bradford reagent (Biorad) and spectrophotometry. Protein lysates were prepared at 10ug in a cocktail of 4x Lamelli buffer (Biorad) and Dithiothrethiol, and were denatured at >80^{o}C for 8 mins. Samples were immediately stored in -20^{o}C until required.

2.5.3-Transfer and antibody blotting

V5 immunoblot: Lysates were resolved in 10% gel at 130V in Tris/Glycine/SDS Running Buffer (Biorad). Gels were transferred using a semi-dry cell, Trans Blot Turbo Transblot Transfer System (Biorad) onto prepacked PVDF membranes optimized for the system (Transblot Turbo Mini PVDF Transfer Packs; Biorad). Blots were washed in 0.1% Tris buffered saline with 0.1% Tween (TBST) before blocking in 5% Milk-TBST for 2 hours at RT. Anti-V5 antibody was incubated at 1:1000 overnight at 4^{o}C in 1% Milk-TBST (Table 14 and Table 15). Following washes in 0.1% TBST the following day, blots were incubated with appropriate anti-specie horseradish peroxidase (HRP) secondary antibodies (1:3000) for 1 hour. Membranes were washed thoroughly in TBST and developed using Enzymatic Chemiluminescence (ECL) reagents (General Electric).

2.5.4-Re-blotting membranes

Immunoblots can be stripped of its antibodies and reblotted with a subsequent antibody of interest, such as Glyceraldehyde-3-Phosphate Dehydrogenase (GAPDH) loading control (Millipore). Blots were washed in H_2O prior to antibody stripping with 0.2M Sodium hydroxide (NaOH) at 37^{o}C. Membranes were blocked in 5% Milk-TBST, and re-blotted with GAPDH 1:5000 in 1% Milk-TBST overnight at 4^{o}C. Secondary HRP antibodies were applied the following day at 1:3000 and subsequently redeveloped, with all blotting procedures maintained as described above.

[3] 50mM pH7.6 Tris-Base; 150mM NaCl, 1% Triton X-100, 0.02% Sodium Azide, 1mM MINI protease inhibitor (Roche), 1mM sodium orthovanadate, 25mM sodium fluoride

2.5.5-pERK/tERK immunoblots

V5 immunoblots were stripped of its antibodies and reblotted with the subsequent antibody of interest (Table 15). Blots were washed in H_2O prior to antibody stripping with 0.2M sodium hydroxide (NaOH) at 37ºC. Membranes were blocked in 5% BSA-TBST, and re-blotted with pERK (1:2000, Cell Signalling Techologies), in 1% BSA-TBST overnight at 4ºC. Secondary HRP antibodies were applied the following day at 1:3000 and redeveloped as above. The strip and re-blot cycle is performed two more times, such that tERK (1:2000; Cell Signalling Technologies) and GAPDH (1:10,000; Millipore) can be applied.

Primary Antibodies	Concentration	Host and Class	Company	Cat. No.	Secondary Antibody (1:3000)	Company	Host and Class
αV5	1.1000	Mouse Monoclonal IgG	Invitrogen	R960-25	αMouse HRP	Dako	Rabbit Polyclonal IgG
αGAPDH	1.5000		Millipore	MAB374			

Table 14: Immunoblot conditions for E12.5 whole embryos

Antibodies	Company	Catalogue No.	Host specie	Primary concentrations	Secondary antibody (1:3000)
αV5	Invitrogen	R960-25	Mouse	1.1000	anti-mouse HRP
αGAPDH	Millipore	MAB374		1.10000	
α-pERK	Cell Signalling Technologies	D13.14.4E XP	Rabbit	1.2000	anti-rabbit HRP
α-tERK		9102			

Table 15: Immunoblot conditions for cells

2.6-Histology

2.6.1-Embryo embedding for frozen sections

Embryos were harvested at E16.5 or E18.5 with the heads removed from the axial skeleton. Heads were mounted on a cork disc, embedded in OCT compound (VWR) on the axial plane, and snap frozen using the dry ice isopentane (VWR) method. Heads were stored in -80^{o}C until required for cryosectioning. Cryosections were cut between 15-20um on the Model OTF Cryostat (Bright), with sections mounted on Superfrost Plus slides (VWR).

2.6.2-Paraffin embedding

E16.5 embryo heads were skinned and fixed in 4% Paraformaldehyde (PFA) or 10% formalin overnight before graded dehydration in EtOH. Embryos were cleared in analytical grade xylene (Fisher) before paraffin wax displacement in a 60^{o}C oven. The samples were embedded and sectioned on a microtome (Leica) between 8-10um on the axial plane.

2.6.3-Bone and cartilage histology

E18.5 embryos were skinned and eviscerated after phenotypic analysis. Embryos were dehydrated in 75% EtOH overnight at 4^{o}C and stained with 0.01% alcian blue (Sigma) working reagent[4] overnight, room temperature (RT). Embryos were washed in 75% EtOH for a further 24 hours and cleared in 1% potassium hydroxide (Fisher) (KOH) the following day. After sufficient clearing, 0.01% alizarin red working solution[5] was added to the embryos. The embryos were processed overnight and washed in 1% KOH the following day. Samples were transferred to a graded glycerol (Sigma) gradient and were eventually stored in 80% Glycerol. The wholemount protocol can be found in Appendix 3.

2.6.4-Wholemount alizarin red stain

Calvarial explants were fixed in 70% EtOH overnight at 4^{o}C before transferring to 1% KOH. After sufficient clearing to remove residual tissue surrounding the calvaria, 0.01% alizarin red working solution (0.01% Alizarin Red-1% KOH) was added to the calvaria and

[4] 0.01% Alcian blue (Sigma); 20% acetic acid; 80% of 75% EtOH

[5] 0.01% Alizarin red (Sigma)-1% KOH

stained overnight. This was followed by subsequent washes in 1% KOH prior to graded glycerol in preparation to storage. Stained calvaria is stored in 80% Glycerol-H_2O.

2.6.5-Wholemount alcian blue staining of calvaria

E18.5 embryos were skinned and eviscerated. Embryos were dehydrated in 75% EtOH overnight at 4^{o}C and stained with alcian blue working reagent[6] overnight-RT. Embryos were washed in 75% EtOH for a further 24 hours and cleared in 1% KOH (Fisher) the following day. The embryos were processed overnight and washed in 1% KOH the following day. The embryos were eventually processed for graded glycerol-H_2O (Sigma) equilibration after sufficient washes in 1% KOH. The calvaria was eventually dissected for in 80% Glycerol-H_2O.

2.6.6-Cartilage histology (sections)

E16.5 embryo heads were paraffin embedded as previously described in section 2.6.2 and cut on the coronal plane between 10-12um on the microtome (Leica). Sections were dewaxed in Histoclear (National Diagnostics) and redehydrated in graded EtOH. Sections were processed for 0.01% alcian blue working reagent[6] and counter-stained using 1% Nuclear Fast Red (Sigma) to visualise the nucleus. Sections were dehydrated in graded EtOH and mounted in DPX.

2.6.7-Alkaline phosphatase (ALP) assay

Cryosectioned embryos were thawed and immediately fixed in 4% PFA before permeablised in 0.1% TBST. Samples were equilibrated in NTMT before developing in NBT-BCIP-NTMT solution[7]. To allow even developing times, all samples were processed at once. Developed samples were counterstained with 1% nuclear fast red (Sigma) and mounted in Mowiol mounting media (Sigma) (Appendix 4).

2.6.8-Wholemount alizarin red stain

Calvarial explants were fixed in 70% EtOH overnight at 4^{o}C before transferring to 1% KOH. After sufficient clearing to remove residual tissue surrounding the calvaria, 0.01% alizarin red working solution (0.01% Alizarin Red-1% KOH) was added to the calvaria and

[6] 0.01% alcian blue (Sigma); 20% acetic acid; 80% of 75% EtOH

[7] NBT: 4.5ul/ml, BCIP: 3.5ul/ml, NTMT

stained overnight. This was followed by subsequent washes in 1% KOH prior to graded glycerol in preparation to storage. Stained calvaria is stored in 80% Glycerol-H_2O.

2.6-*In situ* hybridisation (ISH)

2.6.1-Cloning the mV5 transgene for RNA *in situ* probe

Transgenic mouse V5 (*mV5*) was cloned in the Pauws lab. Primers spanning a unique portion of the V5 transgene were designed using Primer 3 plus software (http://www.bioinformatics.nl/cgi-bin/primer3plus/primer3plus.cgi), and validated using *in silico* PCR software (http://rohsdb.cmb.usc.edu/GBshape/cgi-bin/hgPcr) (Figure 27). DNA was extracted from $R26R^{Fgfr2cV5/Fgfr2cV5}$ ear biopsies to use as the template DNA for PCR amplification. Primers were obtained from Sigma and amplified with standard PCR protocol (expected amplicon: 155bp). The PCR product derived from ear biopsies yielded two bands close to the band of interest (Figure 28 A). To determine the correct band, a second PCR reaction was set up against a plasmid (pcDNA3) already carrying *Fgfr2cV5* in the lab (Figure 28 B). Subsequently, the specific band was extracted using the Gel Extraction Kit (Qiagen), and was cloned into the pGEMT-Easy Vector (Promega) according to the manufacturers' protocol. The cloned plasmids were transformed into XL1-Blue competent cells (Agilent) and starting cultures amplified in SOC medium (Thermo). The cultures were spread onto ampicillin agar plates for selection. A total of 6 colonies were picked and processed for MINI overnight inoculation containing Luria Broth and ampicillin (1:1000 dilution). Plasmids were extracted using the QIAprep Spin MINIprep kit (Qiagen) according to the manufacturer's protocol the following day. An additional diagnostic digest was performed with EcoRI (Promega) to visualize the insert. However, the insert was not detected in the gel, and a diagnostic PCR using the *mV5* primers were implemented to confirm the presence of the insert (Figure 28 C). Extracted plasmids were sent for sequencing at Barclay House (UCL), and the sequence aligned using BLAST (NIH) to determine the success of the cloning and direction of the insert (Figure 29). Meanwhile, Plasmid DNA containing the V5 insert was processed for an overnight MIDI inoculation, and extracted using the QIAprep MIDIprep kit (Qiagen) according to the manufacturer's protocol the following day. The same controls were applied to the MIDIprep plasmids as for the MINI using enzyme and PCR reactions for quality assurance.

GGGCAATTCTGCAGATATCCAGCACAGTGGCGGCCGCTCGAGTCTAGAGGGCCC
GCGGTTCGAAGGTAAGCCTATCCCTAACCCTCTCCTCGGTCTCGATTCTACGCGT
ACCGGTCATCATCACCATCACCATTGAGTTTAAACCCGCTGATCAGCCTCGACTG
TGCC

V5: GGTAAGCCTATCCCTAACCCTCTCCTCGGTCTCGATTCTACG
Forward Primer: AGATATCCAGCACAGTGGCG
Rev Primer: GCACAGTCGAGGCTGATCAG

Figure 27: Primer design against *mV5* transgene.

mV5 primers spanning unique portion of *Rosa26* transgene with *V5* epitope. The expected amplicon is 155bp.

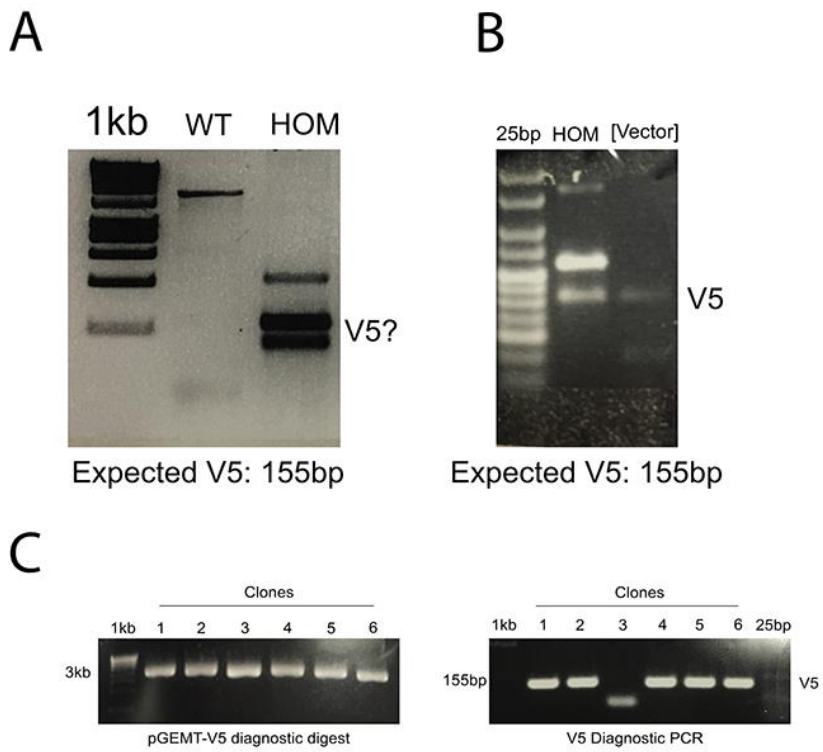

Figure 28: Resolving the correct *mV5* band.

(A) Multiple bands yielded in the ear biopsies of *R26R*$^{Fgfr2cV5/Fgfr2cV5}$ (HOM); (B) A second PCR was set up against a plasmid vector (pcDNA3) already carrying *Fgfr2c-V5* to determine the correct band. (C) No dropout was detected in any of the clones, and PCR was adopted to amplify the insert using *mV5* primers. Note that clone 3 did not carry the insert.

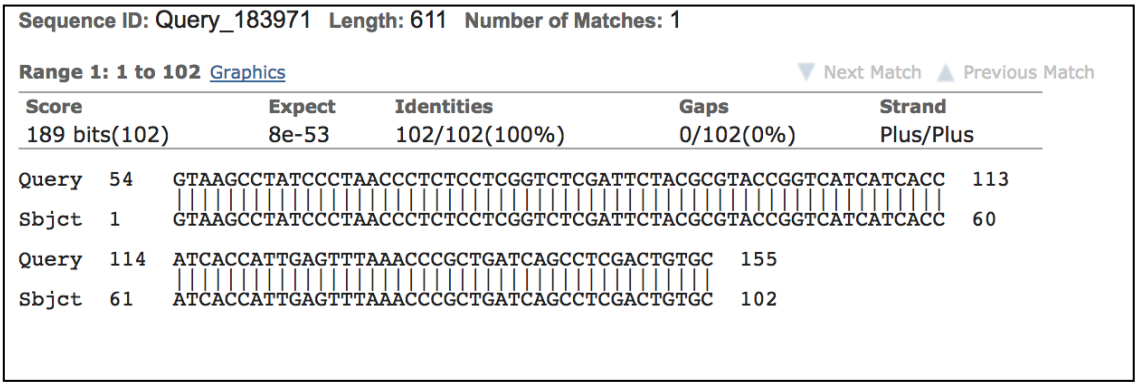

Figure 29: Sequence alignment of an *Fgfr2c-V5* clone containing the mV5 insert.

The output here is a screenshot from BLAST (NCBI).

2.6.2-*In vitro* transcription

mV5 plasmid was linearized with either Sal1 or NCO1 enzyme (Promega) to generate the respective sense and antisense RNA probes. PCR Cleanup Kit (Qiagen) was utilized to remove restriction enzymes prior to *in vitro* transcription according to the manufacturer's protocol. Figure 30 illustrates the plasmid map. *mV5* probes were transcribed at 37^{o}C in a cocktail of Digoxigenin (DIG) (Roche) with T7 RNA polymerase for sense, and SP6 for antisense probes respectively. DNAse1 (Roche) treatment was applied to the transcription cocktail to remove any plasmid DNA, and passed through a Chroma Spin Column (Clontech) to clean the products according to the manufacturer's protocol. RNA probes were quantified by gel electrophoresis (Figure 31) and concentrations determined by Nanodrop (Thermo). Specific protocols for plasmid linearization and *in vitro* transcription can be found in Appendix 5.

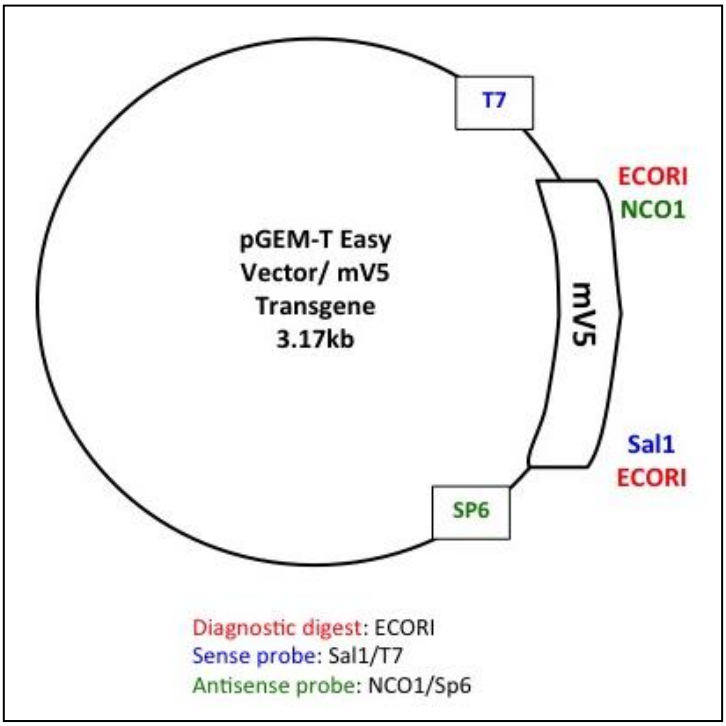

Figure 30: Plasmid map of *mV5*

Plasmid map is shown with the enzymes required for diagnostic digest, linearization and *in vitro* transcription.

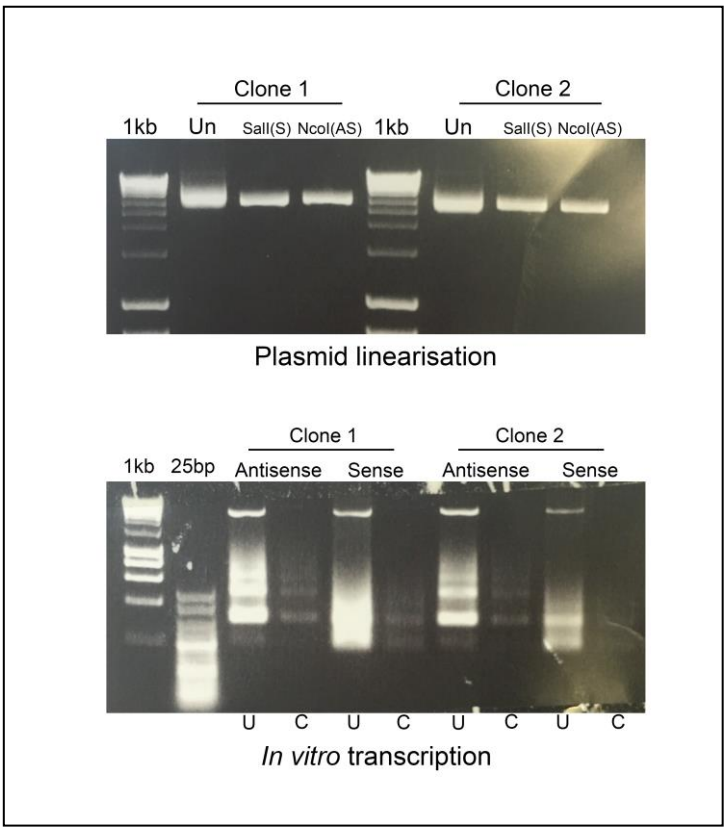

Figure 31: Plasmid linearization (Top) and *in vitro* transcription of *mV5* probes using appropriate enzymes (Bottom). U: uncleaned probes; C: Cleaned probes using Chroma Spin Columns.

2.6.3-*mV5* wholemount ISH

E12.5 whole embryos were harvested and fixed in 4% Paraformaldehyde (PFA) overnight prior to graded dehydration in methanol (MeOH). Embryos were bleached in 6% H_2O_2-MeOH before serial rehydration. Embryos were washed in phosphate buffered saline (PBS)-0.1% Tween (Sigma) (PTW), and treated with 1:1000 Proteinase K in PTW to permeabilise embryos for roughly 30 minutes. Post-fix[8] was applied to stop the Proteinase K activity before further washes in PTW. Subsequently, embryos were equilibrated in hybridisation buffer[9] before sense or antisense *mV5* probes hybridisation. *Sox9* antisense probe (Lovell Badge group), were used as a positive control for experiment. Hybridisation was attempted at 65^{o}C and 70^{o}C for these probes. Following hybridisation, embryos were washed in Solution 1[10] and Solution 2[11] at respective hybridization temperatures and washed in Tris buffered saline- 1% Tween-20 (TBST). Hybridised probes were detected with alkaline phosphatase-coupled Anti-DIG antibodies (1:2000, Roche), and was incubated overnight in 5% Heat Inactivated Sheep Serum (HISS) in TBST at 4^{o}C. Post antibody washes were performed in TBST, before transferring to NTMT[12] for probe development. For detection of DIG probes, a cocktail of BCIP (5-Bromo-4-chloro-3-indolyl phosphate, Sigma) and NBT (Nitro Blue Tetrazolium Chloride, Sigma) was applied in alkaline phosphatase buffer NTMT. Subsequently, specimens were washed briefly in PTW before storage in 4% PFA. The full protocol and stock reagent are available in Appendix 6.

2.6.4-*In situ* hybridisation on tissue sections

For paraffin sections, sections were dewaxed in Histoclear (National Diagnostics) and rehydrated in graded EtOH, while frozen sections were immediately rehydrated in DEPC-H_2O. Briefly, sections were fixed in 4% PFA and permeabilised in Proteinase K solution at 10 mg/ml. Proteinase K reaction was stopped by fixing in 4% PFA, and subsequent electrostatic attractions neutralised in a cocktail of 0.1M Triethaloamine solution with acetic anhydride prior to further

[8] 0.1% Gluteraldehyde (Sigma) in 4% PFA

[9] 50% Formamide, 5x Saline Sodium Citrate (SSC) pH4.5, 1%SDS, 50ug/ml yeast tRNA, 50ug/ml heparin

[10] 50% Formamide, 5x SSC, 1% SDS and DEPC-H_2O

[11] as Solution 1, but with 2x SSC

[12] pH9.5, 5M NaCl; 1M Tris-HCl (Hydrochloric Acid); 1M $MgCl_2$ (Magnesium Chloride); 0.1% Tween-20

washes in DEPC-PBS. Tissue sections were dehydrated in graded ethanol and left to air dry prior to hybridisation process. Digoxigenin (DIG) RNA ISH was achieved at 300ng/ml probes in hybridisation mix[13] with DIG antisense RNA probes overnight at 65ºC in a humidified chamber. The plasmids used to synthesise *Spry2*, *Spry4* and *Etv5* ISH probes were a gift from the Basson Lab. Post hybridisation washes were performed in a temperature-controlled water bath at 65°C and washed in a series of formamide and graded SSC[14] solutions (2x and 0.2x SSC). The sections were subsequently washed in Buffer 1[15] and blocked in 10% HISS, and incubated with anti-DIG antibody (1:2000, Roche) in 1% HISS overnight at 4°C. Sections were developed in NBT/BCIP the following day in a cocktail of Buffer 2[16] and 10% Polyvinylacetate. The slides were allowed to develop in the dark at room temperature until sufficient signal was visualized. Developed slides were mounted in Mowiol mounting media. Protocol is available in Appendix 7.

[13] Formamide, 5M NaCl, 1M Tris pH 8.5, 0.5M EDTA pH 8, Denharts solution, RNase inhibitor, tRNA

[14] NaCl, sodium citrate, adjusted to pH 7.0. See appendix 8 for details

[15] 1M Tris-HCl pH7.6, 5M NaCl, H_2O. See appendix 8 for details

[16] 1M Tris pH9.5, 5M NaCl, 2M $MgCl_2$. See appendix 8 for details

2.7-Immunohistochemistry (IHC)

2.7.1-IHC for frozen sections

2.7.1.1-Detection of V5 epitope and YFP: Cryosections were thawed at RT in a humidified chamber and rehydrated in PBS before fixation in 4% PFA. Sections may proceed to antigen retrieval at 110ºC, 2 mins in 10mM pH6.5 Sodium citrate buffer[17] in a decloaking chamber (Biocare Medical) at 110ºC-2 mins after brief washes in PBS to remove the fixative. Sections were then permeabilised in 0.1% PBST and non specific binding quenched in blocking buffer[18] and 10% HISS prior to incubation of αV5 primaries (between 1:100-1:500) in working antibody solution (blocking buffer + 1% HISS) overnight at 4ºC. YFP was detected using an antibody specific for GFP (Invitrogen) at a concentration of 1:500. After several washes in 0.1% PBST, appropriate anti specie biotinylated (Dako), or Alexa Fluor-488 (Life Technologies) conjugated secondary antibodies were incubated for 1 hour RT in working antibody solution. Samples incubated with biotinylated secondary antibodies were subject to streptavidin-555 conjugate amplification (1:500, Life Technologies), and 0.1% Sudan black-70% EtOH incubation to reduce auto-fluorescence if necessary. Further washes in 0.1% PBST was performed to remove excess secondary antibodies before counterstaining nuclei in 4, 6-diamidino-2-phenylindole (DAPI; Life Technologies) at a concentration of 1:10,000 in PBS. Sections were subsequently washed in PBS and coverslipped in Mowiol mounting media. Table 16 and Table 17 summarise the conditions for IHC on frozen sections, and a full protocol is available in Appendix 8.

[17] 10mM Sodium Citrate, 0.05% Tween-20, adjusted to pH6.5 with HCl

[18] 0.1% PBST, 0.15% Glycine and 2mg/ml BSA

Antibodies	Company	Catalogue No.	Host specie	Primary concentrations	Secondary, anti specie IgG	Streptavidin 555 amplification
Anti-V5 Tag	Invitrogen	R960-25	Mouse	1.100 1.250 1.500	1.250 (Biotinated)	1.500
Anti-V5 Tag-ChIP Grade	Abcam	ab9116	Rabbit	1.100 1.250	1.500 (Biotinated) 1.250 (Biotinated)	1.500
Anti-Fibronectin	Abcam	ab23750	Rabbit	1.100 1.250 1.500	1.250 (Biotinated)	1.500
Anti-GFP tag	Invitrogen	A-11120	Mouse	1.500	1.250 (Alexa Fluor-488)	N/A

Table 16: V5 IHC for frozen sections

Antibodies	Company	Catalogue No.	Host specie	Primary concentrations	Secondary, anti specie-biotinayted IgG	Streptavidin 555 amplification
Anti-V5 Tag	Invitrogen	R960-25	Mouse			
Anti-Fibronectin	Abcam	ab23750	Rabbit	1.500	1.500	1.500

Table 17: V5 IHC for frozen sections with antigen retrieval (10mM Sodium Citrate Buffer, pH 6.5) at 110ºC, 2mins

2.7.2-IHC on paraffin sections

2.7.2.1-Detection of V5 epitope: Paraffin sections were dewaxed in Histoclear (National Diagnostics) before graded EtOH rehydration. Antigen retrieval was executed in a decloaking chamber (BioCare Medical) at 110ºC for 2 mins in 10mM Sodium Citrate pH6.5 buffer or Declere solution (Sigma). Sections were permeabilised in 0.1% PBST and blocked in 10% sheep serum (Sigma) and blocking buffer. αV5 antibody (CST or Invitrogen) were tested at multiple concentrations, and incubated overnight in 1% HISS and blocking buffer Table 18. Appropriate secondary antibodies were incubated for an hour the following day. A goat-anti-mouse Alexa Fluor-488 secondary (Life Technologies, 1:500) was used to detect V5 directly without amplification, whilst a goat-anti-rabbit biotinylated antibody was used to boost V5 signal (1:250, Dako). Signals were subsequently amplified using Streptavidin 555 (1:500, Life Technologies) conjugates that recognize biotin. Sections were washed several times in 0.1% PBST, and stained for DAPI (1:10,000, Thermo Fisher) in PBS before coverslipped in Mowiol mounting medium (Sigma). Conditions are summaried in Table 18, and a full protocol is available in Appendix 9.

Antibodies	Company	Cat.	Host specie	Antigen Retrieval	Primary	2º anti specie IgG	Amplification	Notes
αV5 Tag	Invitrogen	R960-25	Mouse	Declere	1.500 1.2000	1.500, Alexa Fluor-488	N/A	Emma Peskett, c.2013
αV5 Tag	Cell Signalling Technologies	D3H8Q	Rabbit	10mM Sodium Citrate pH6.5	1.100 1.250	1.250, anti-rabbit biotinayed IgG	1.500 (Steptavidin 555)	

Table 18: V5 IHC on paraffin sections

2.7.2.2-pERK and osteopontin IHC

Paraffin sections were dewaxed in Histoclear (National Diagnostics) before graded EtOH rehydration. Antigen retrieval was executed in a decloaking chamber (BioCare Medical) at 110ºC for 10 minutes in 10mM Sodium Citrate pH6.5 buffer. Sections were permeabilised in 0.1% PBST and blocked in 10% sheep serum (Sigma) and blocking buffer[19]. Primary antibodies were incubated on the sections overnight in 1% sheep serum (Sigma) and blocking buffer. pERK (rabbit mIgG, Cell Signalling Technologies) was used at 1:250 and anti-osteopontin (Mouse mIgG, Developmental Studies Hybridoma Bank) at 1:200, and appropriate secondary antibodies were incubated for an hour the following day. Goat-anti-mouse Alexa Fluor 488 secondary antibodies were used against osteopontin and whilst biotin goat-anti-rabbit secondary antibodies (Dako) were used against pERK. The pERK signals were amplified using Streptavidin 555 conjugates (Life Technologies) at 1:500. 0.1% Sudan black was applied onto tissue sections for 5 minutes to quench any autofluorescence, and rinsed briefly in PBST to relieve any excess staining. Lastly, tissue sections were stained in DAPI (Thermo Fisher) at 1:10,000 in PBS before coverslipped in Mowiol mounting medium (Sigma) (Appendix 9). Table 19 illustrates conditions required of pERK/osteopontin IHC.

Antibodies	Company	Cat.	Host specie	Antigen Retrieval	Primary concentrations	Secondary, anti specie IgG	Amplification
Anti-pERK	Cell Signalling Technologies	D13.14.4 E XP	Rabbit	10mM Sodium Citrate pH6.5 at 110ºC, 2mins	1.250	1.250, anti-rabbit biotinayed IgG	1.500 Steptavidin 555
Anti-Osteopontin	DSHB	MPIIIB10 (1)	Mouse		1.200	1.200, Alexa Fluor-488	N/A

Table 19: pERK/Osteopontin IHC conditions

[19] 0.15% Glycine, 2mg/ml BSA (Bovine Serum Albumin) in 0.1% PBST

2.8-Phenotypic analysis

2.8.1-Gross analysis of phenotype

Embryos harvested at E18.5 and were weighed on a fine balance. An electronic caliper (Fisher) was used to measure the crown-rump length and head length of the embryo. Data were subsequently transformed and processed for statistical analysis.

2.8.2-Morphometric analysis of the craniofacial skeleton

E18.5 calvaria stained with bone and cartilage stain were subjected to 'Region of Interest' (ROI) analysis using FIJI software (NIH). The craniofacial skeleton was dissected for the frontal, parietal and nasal bones in 80%-glycerol and flat mounted onto frosted slides (Fisher). Images were taken for surface area measurements of frontal, parietal and nasal bones using FIJI. Two measurements were made from both hemispheres of the bone, and the results were expressed as an average value. The quantification was performed blind without knowledge of the embryo's genotype beforehand in order to eliminate any bias. The mandibles were also quantified in the same manner with the length measured instead. As embryo sizes vary between litters, data normalisation was necessary to reduce signal to noise ratio and allow comparisons between litters to occur. Quantified data were normalized to an endogenous structure that was not affected by FGFR2c signalling, and the length of the appendicular skeleton was chosen for this purpose (Figure 32 A & B) (Eswarakumar et al., 2002, Eswarakumar et al., 2004). Measurements were taken from both forelimbs, measured from the scapula to the wrist. The results were expressed as the average length acquired from both limbs. The result indicates that *Fgfr2c* overexpression has no influence on limb length (p=0.271; control: n=9; $R26R^{Fgfr2cV5/+}$; $\beta actin^{CRE/+}$: n=4), and was therefore chosen as the endogenous control for data transformation of litters (See section 3.2.9). The results were subsequently processed for statistical analysis.

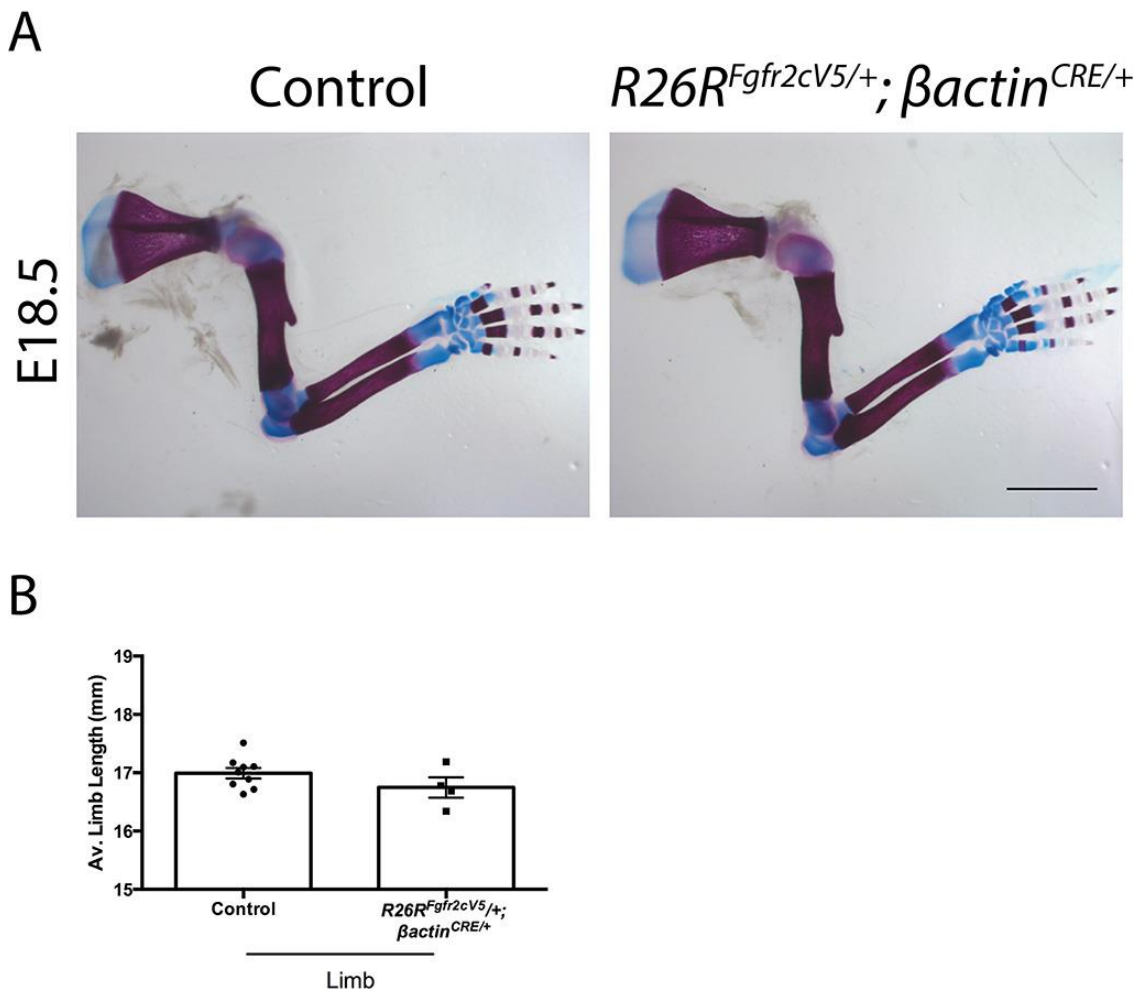

Figure 32: *Fgfr2c* overexpression does not have an effect on limb length and is used as an endogenous control for data transformation.

(A) Images of the mouse forelimb; (B) Graph showing the average forelimb length measured from the scapula to the wrist (p=0.271; Control: n=9; *R26R*$^{Fgfr2cV5/+}$*; βactin*$^{CRE/+}$: n=4). Statistics: Student's t-test with Welch's correction. Error bars depict SEM. Scale bar: 2mm.

2.8.3-Data transformation for littermates

1) **Find sample mean** ($\bar{x}$)
   -Let m1 and m2 be raw measurements

$$\frac{m1 + m2}{2} = \bar{x}$$

2) **Find population (n) mean of littermate (**$L\mu$)

$$\frac{\sum \bar{x}}{n} = L\mu$$

3) **To minimize sample variability between littermates, normalize littermates against a constant (i.e average limb length)**

   i) Find normalization factor (*L.nf*) against average limb length

   -Let Average limb length constant be 16.9162
   -Let L.nf be normalization factor

$$\frac{16.9162}{L\mu} = L.\,nf$$

   ii) Normalize the mean measurements ($\bar{x}$) of each littermate to average limb length (*L.nf*) to obtain transformed data ($T\bar{x}$)

$$\bar{x}\ x\ L.\,nf = T\bar{x}$$

4) **Find relative percentage change in respect to controls**

   i) Find total average of controls across all littermates (Con$T\mu$), given by the sum of all control samples (Con$T\bar{x}$) to population (n)

$$\frac{\sum Con.T\bar{x}}{n} = Con.\,T\mu$$

   ii) Compare mutant samples (Mut.$T\bar{x}$) relative to total average of control group (Con.$T\mu$). Overall change in mutants is expressed as a relative percentage to Con.$T\mu$

$$\left[\frac{Mut.\,\bar{x}}{Con.\,T\mu}\right]\ x\ 100 = \text{relative change (\%)}$$

2.9-Statistical analysis

SPSS Statistics 22 (IBM) software was used as the primary statistical package for data analysis. First, the data was tested for normality using Shapiro-Wilk test to determine the use of parametric or non-parametric tests. Independent samples t-test ('Student's t test') with Welch's correction (parametric) or Mann Whitney U (non-parametric) tests were used to compare the difference of means between the control and mutant groups where appropriate. One-way ANOVA with Tukey posthoc or non-parametric Kruskal Wallis with Dunn-Bonferroni posthoc test was adopted for analysis of three or more groups. A p-value of <0.05 was considered significant. The analysed data were plotted using Prism 6.0 software (GraphPad).

2.10-Image acquisition

Images concerning phenotype or embryology were acquired on the Zeiss Steni SV6 Stereoscope mounted with a camera (Leica DFC 490). For sections, fluorescent images were captured on the Leica DM1000 microscope mounted with a camera (Photometrics CoolSnap CF). Brightfield images were acquired on the Zeiss Axioplan 2 microscope attached with a camera (Zeiss Axiocam HRc).

2.11-Profiling the coronal suture

2.11.1-Histology for LCM

E16.5 CD1-WT and *Fgfr2c*$^{C342Y/+}$ embryo heads were embedded in OCT Compound (VWR) and snap frozen using -80ºC isopentane method. The heads were sectioned at 20µm along the axial plane using a cryostat (Bright), and mounted on Arcturus PEN membrane glass slides (Life Technologies). Sections were dried and stored at -80ºC until required. Mounted sections were subjected to 1% Alizarin Red/0.06% Fast Green (Sigma) to visualise the coronal suture. Sections were rehydrated and stained in 1% alizarin red for 5 mins and washed in H_2O. The sections were subsequently counterstained with 0.06% fast green until sufficient prior to further washes in H_2O to remove excess staining. Finally, sections were dehydrated in graded EtOH and stored in -80ºC until use.

2.11.2-Performing laser capture microdissection

Coronal sutures were microdissected on the PALM-Axiovert 200M Microscope (Zeiss). The ROI of the coronal suture is defined by the appositional growth limits of the frontal and parietal bones. The ROI is selected manually on the PALMRobo software (Zeiss), which defines the laser path of the LCM. Bilateral coronal sutures from the same embryo were captured along the dorsal-ventral profile down to the level of the eye. Samples were collected using Adhesive Cap 500 collection tubes (Zeiss). Subsequently, 200µl of lysis buffer RLT (Qiagen) was added to the samples immediately after collection, and stored at -80^{o}C until RNA extraction.

2.11.3-RNA preparation and sequencing

RNA was extracted using the RNeasy micro-kit (Qiagen) according to the manufacturer's protocol. Sample quality was determined with the 2200 Tapestation (Agilent). RNA samples were amplified, and cDNA library constructed using the Clonetech SMART-Seq v4 Ultra Low Input RNA Kit (Takara) in accordance to the manufacturer's protocol. The cDNA libraries were sequenced paired end at a depth of 30 millions reads per sample on the Illumina NextSeq 500 platform. A total of three biological replicates per genotype within the same litter (CD-1 WT and *Fgfr2c*$^{C342Y/+}$) were sequenced. The sequenced data (FASTQ files) were aligned using TopHat and Cufflink software to generate Binary Alignment Map (BAM) files for subsequent analysis on Strand NGS softwre. Alignments were visualised on the BaseSpace platform (Illumina). All procedures were carried out at UCL Genomics with the exception of RNA extraction and data interpretation on BaseSpace.

2.11.4-Expression analysis

Figure 33 is a diagrammatic representation of the RNAseq pipeline. BAM files were uploaded and analysed on the Strand NGS software. Samples were categorised for their genotype, with a cut off threshold of 10 folds applied for differential expression analysis based on the DeSeq2 algorithm. Additional filters were applied to ensure alignment quality against the reference genome: Reads must have both mates present such that it improves mapping to a

precise region. Any reads that were not paired, too far apart, missing, translocated, misorientated or unaligned were excluded from the analysis. To select the genes for expression validation, read counts must be consistent across all three biological replicates to ensure accuracy. A subsequent PubMed search was conducted to determine its role and relevance to craniofacial development. A total of six genes were selected for expression validation. On a separate analysis, BAM files were run against a FGF entity list (Table 20) serving as an *in silico* experimental control, and data prepared for Gene Set Enrichment Analysis (GSEA). The entity list was assembled from multiple FGF signalling readouts described in (Ornitz and Itoh, 2015).

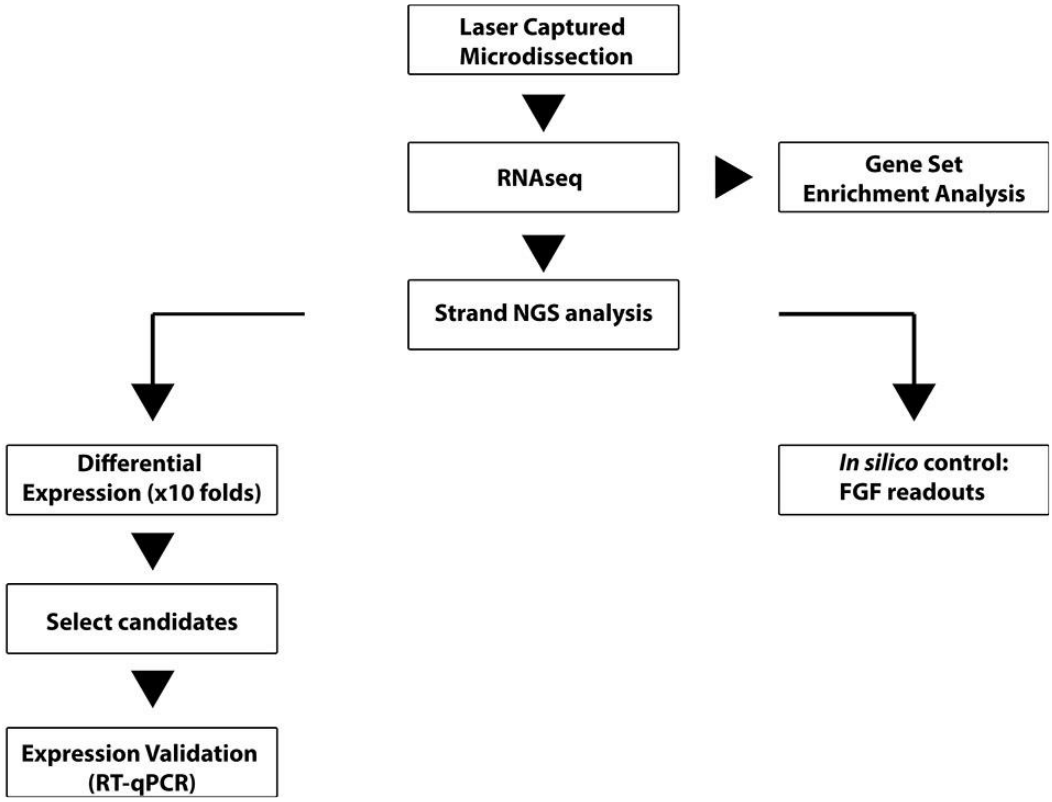

Figure 33: Pipeline for RNAseq analysis.

Gene Symbol	ENSEMBL
Stat1	ENSMUSG00000026104
Fgf7	ENSMUSG00000027208
Fgf2	ENSMUSG00000037225
Spry1	ENSMUSG00000037211
Foxo1	ENSMUSG00000044167
Fgf5	ENSMUSG00000029337
Fgf6	ENSMUSG00000000183
Fgf23	ENSMUSG00000000182
Fgf21	ENSMUSG00000030827
Fgfr2	ENSMUSG00000030849
Fgf3	ENSMUSG00000031074
Fgf4	ENSMUSG00000050917
Fgf15	ENSMUSG00000031073
Fgf20	ENSMUSG00000031603
Fgf22	ENSMUSG00000020327
Dusp6	ENSMUSG00000019960

Gene Symbol	ENSEMBL
Fgf18	ENSMUSG00000057967
Fgf11	ENSMUSG00000042826
Stat5a	ENSMUSG00000004043
Stat3	ENSMUSG00000004040
Etv4	ENSMUSG00000017724
Fgf10	ENSMUSG00000021732
Fgf9	ENSMUSG00000021974
Fgf17	ENSMUSG00000022101
Spry2	ENSMUSG00000022114
Fgf14	ENSMUSG00000025551
Etv5	ENSMUSG00000013089
Fgf12	ENSMUSG00000022523
Tsc2	ENSMUSG00000002496
Spry4	ENSMUSG00000024427
Fgf1	ENSMUSG00000036585
Fgf8	ENSMUSG00000025219
Fgf13	ENSMUSG00000031137
Fgf16	ENSMUSG00000031230

Table 20: FGF entity list

2.11.5-Gene set enrichment analysis (GSEA)

The initial output of the RNAseq dataset from Illumina was processed for GSEA to determine the molecular signature in *Fgfr2c*$^{C342Y/+}$. Genes were pre-ranked in 'R' statistic programme based on Wald's test statistic with the help of Dr John Apps (UCL). The ranked genes were subsequently uploaded onto the GSEA software (http://software.broadinstitute.org/gsea/index.jsp), and ran against the hallmark gene set database on MSigDB. Gene sets must be at least 75% confident, through their False Discovery Rate (FDR, $q<0.25$), and display 95% ($p<0.05$) confidence for their enrichment.

Chapter 3

Results (Part I)

Investigation of *Fgfr2c* expression levels in the *Fgfr2c-V5* transgenic mouse

3.1-Introduction

The aim of the *Fgfr2c* overexpression model (*R26R*$^{Fgfr2cV5/Fgfr2cV5}$) is to perturb molecular events downstream of FGFR2c. This section gives an introduction to the *Fgfr2c* overexpression transgenic mouse, and the approaches adopted to confirm its overexpression in specific tissue types. Expression validation is critical to show that the overexpression allele is functional both at the RNA and protein level. The following methods have been employed to demonstrate this:

i) Use of real time quantitative polymerase chain reaction (RT-qPCR) to investigate the expression of *Fgfr2c*.

ii) Detection of the V5 epitope using immunoblots, immunohistochemistry (IHC) and *in situ* hybridisation (ISH), unique to the transgenic FGFR2c-V5 protein.

iii) Use of transgenic reporter mice to detect CRE recombinase activity *in vivo*.

3.2-Results

3.2.1-Evaluation of *FGFR2c-V5* expression

To investigate the impact of FGFR2c signalling in the craniofacial skeleton, the Pauws laboratory generated a transgenic mouse that conditionally overexpresses the WT form of *Fgfr2c* (*R26R*$^{Fgfr2cV5/Fgfr2cV5}$) in collaboration with the UCL Transgenic Service. RT-qPCR was used to confirm the relative expression of *Fgfr2c* in the overexpressing recombinants (Figure 34 A). Figure 34 A shows an upregulation of FGFR2c expression by 1.8 folds in whole E12.5 embryos overexpressing *Fgfr2c* ubiquitously (n=3) (courtesy: Emma Peskett). In addition to RT-qPCR, the overall purpose of the V5 epitope is to tag conditional FGFR2c overexpression at the protein level, in order to distinguish the transgenic receptor protein from endogenous FGFR2c in the embryo (Figure 34 B). A indicates the expression of the V5 tag in E12.5 *R26R*$^{Fgfr2cV5/+}$; *βactin*$^{CRE/+}$ wholemount embryos (n=3).

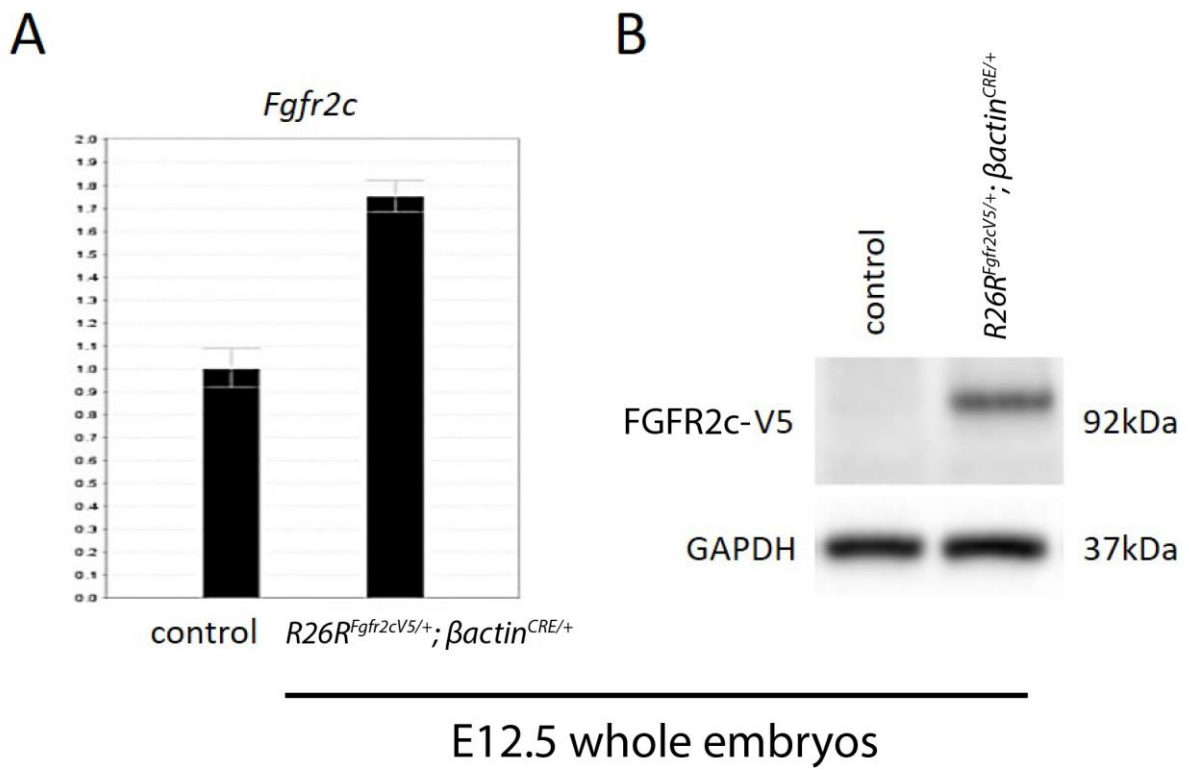

Figure 34 Expression validation of *Fgfr2c* overexpression in E12.5 *R26R$^{Fgfr2cV5/+}$; βactin$^{CRE/+}$*

RT-qPCR of *Fgfr2c*, there is roughly a 1.8 folds of transcript upregulation; (B) Immunoblot of the V5 epitope. Control is *R26R$^{Fgfr2cV5/+}$*; Error bars: SEM; RT-qPCR courtesy: Emma Peskett.

3.2.2-Strategies to determine conditional *FGFR2c-V5* overexpression

R26R$^{Fgfr2cV5/Fgfr2cV5}$ was crossed with the following CRE lines to delineate the role of FGFR2c in craniofacial development: *βactin*$^{CRE/+}$ (ubiquitous), *Wnt1*$^{CRE/+}$ (NCCs), *Mesp1*$^{CRE/+}$ (mesoderm). Therefore, it is crucial to demonstrate the correct embryonic compartment expresses transgenic *Fgfr2c-V5*. As the calvaria derives from the NCC and mesoderm, conditional overexpression is expected in the frontal bone (NCC, *R26R*$^{Fgfr2cV5/+}$*; Wnt1*$^{CRE/+}$) and parietal bone (mesoderm, *R26R*$^{Fgfr2cV5/+}$*; Mesp1*$^{CRE/+}$). In regards to the *R26R*$^{Fgfr2cV5/+}$*; βactin*$^{CRE/+}$, overexpression is expected in both lineage derivatives. E16.5 was chosen as the ideal stage to perform this experiment, due to the earliest morphological appearance of the calvaria.

3.2.3-Expression validation in *R26R*$^{Fgfr2cV5/+}$*; Wnt1*$^{CRE/+}$ and *R26R*$^{Fgfr2cV5/+}$*; Mesp1*$^{CRE/+}$

There was an increase of *Fgfr2c* transcripts in the frontal bone upon conditional overexpression using the *Wnt1*$^{CRE/+}$ (*R26R*$^{Fgfr2cV5/+}$*; Wnt1*$^{CRE/+}$) (A). *Fgfr2c* transcript was upregulated by 2.07 fold (p=0.0203; n=4) relative to the controls (*R26R*$^{Fgfr2cV5/+}$), whilst no difference was detected in the parietal bone and the limb negative control (Figure 35 A & B). Next, expression validation was attempted for conditional overexpression in the mesoderm (*R26R*$^{Fgfr2cV5/+}$; *Mesp1*$^{CRE/+}$) (Figure 35 C & D). Surprisingly, there was a significant increase of *Fgfr2c* transcripts in the frontal bone (p=0.0245; n=4) by 0.73 folds relative to the controls (Figure 35 C), but not in the parietal bone in these mutants. Despite the fact that the limb is a derivative of mesoderm, RT-qPCR analysis indicated that limb *Fgfr2c* transcripts did not differ at E16.5 between *R26R*$^{Fgfr2cV5/+}$; *Mesp1*$^{CRE/+}$ and controls (Figure 35 D) (Loebel et al., 2012).

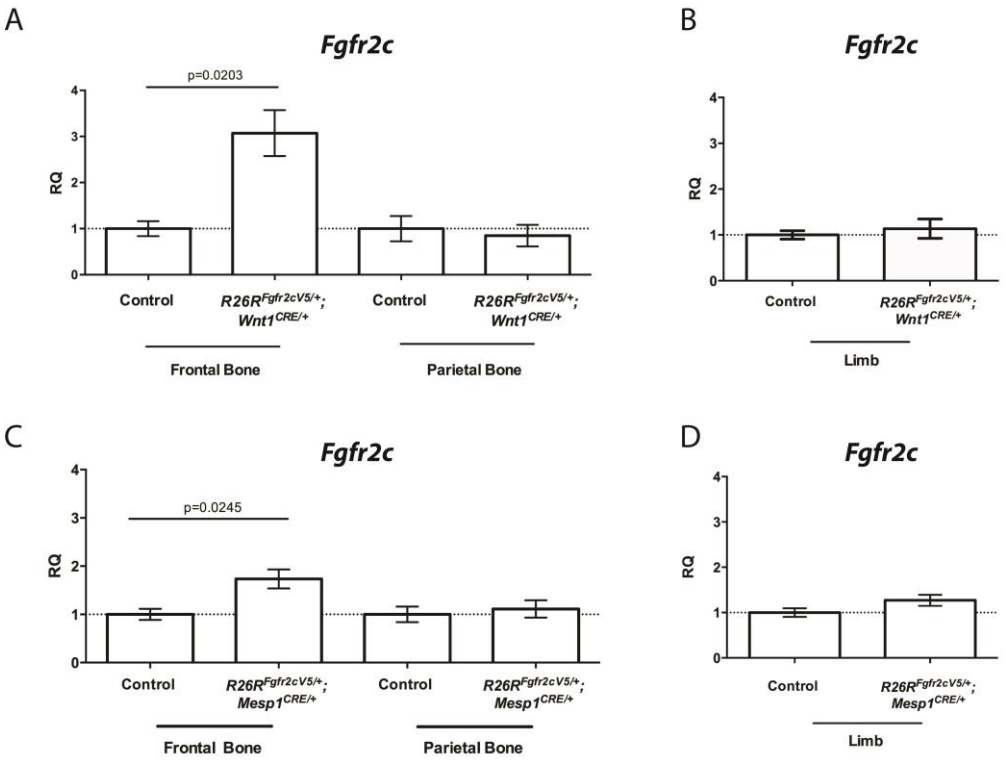

Figure 35: Expression validation of *Fgfr2c* in the E16.5 calvaria and limb

(A) Significant increase of *Fgfr2c* transcript in the frontal bone of $R26R^{Fgfr2cV5/+}; Wnt1^{CRE/+}$ and (B) no changes in transcript levels in the limb. (C) Significant increase of the *Fgfr2c* transcript was detected in the frontal bone of $R26R^{Fgfr2cV5/+}; Mesp1^{CRE/+}$ and (D) no changes in expression in the limb. Statistics: Student's t-test with Welch's correction. Error bars: SEM.

3.2.4-Expression validation in *R26R*$^{Fgfr2cV5/+}$; *βactin*$^{CRE/+}$

The lack of overexpression observed in *R26R*$^{Fgfr2cV5/+}$; *Mesp1*$^{CRE/+}$ prompted the need to investigate the mesoderm lineage further. *R26R*$^{Fgfr2cV5/+}$; *βactin*$^{CRE/+}$ was selected as a control for this purpose to elucidate whether there are any transcript upregulation in the mesoderm (Figure 36). In particular, *Fgfr2c* overexpression is to be expected in both frontal and parietal bones. Unexpectedly, the same trend is observed in *R26R*$^{Fgfr2cV5/+}$; *βactin*$^{CRE/+}$ to that of *R26R*$^{Fgfr2cV5/+}$; *Mesp1*$^{CRE/+}$: there was no difference in transcript levels observed in the parietal bone, but only in the frontal bone of 1.48 folds (n=3) (Figure 36 A). Statistical test was not performed owing to an error during the planning of the experiment. Instead of processing the samples individually for RNA extraction, the samples were pooled together based on their lineage derivatives in a single tube. RT-qPCR analysis was also performed in the limb, where there was a significant upregulation of *Fgfr2c* transcripts in the limb by 1.96 folds (p=0.05; n=2) (Figure 36 B).

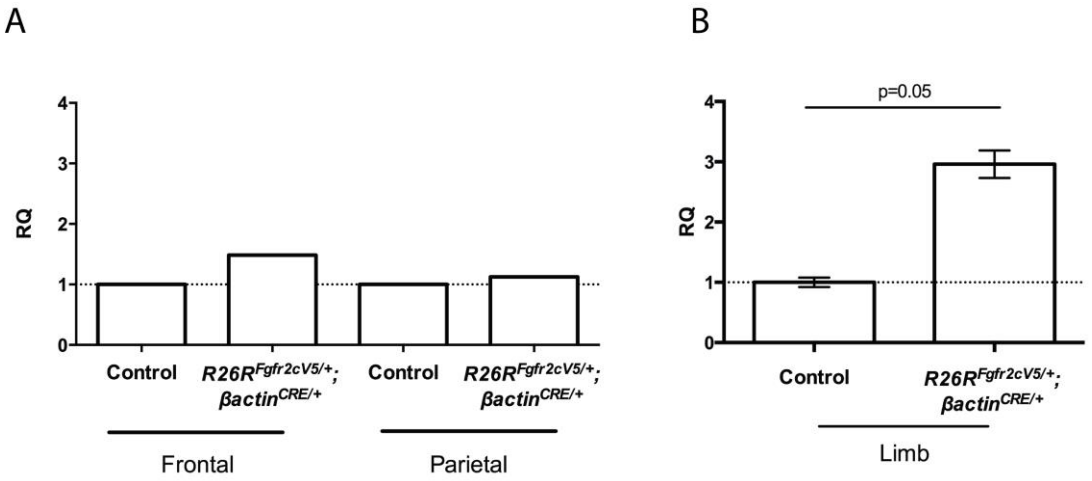

Figure 36 Expression validation in E16.5 *R26R*$^{Fgfr2cV5/+}$; *βactin*$^{CRE/+}$ calvaria.

(A) No differences in *Fgfr2c* transcripts in the parietal bone of *R26R*$^{Fgfr2cV5/+}$; *βactin*$^{CRE/+}$; (B) Significant increase of *Fgfr2c* transcript in the limb of *R26R*$^{Fgfr2cV5/+}$; *βactin*$^{CRE/+}$. Statistics: Student's t-test with Welch's correction. Note: no statistical analysis was performed in (A).

3.2.5-Visualizing the V5 epitope *in vivo*

Visualising the V5 epitope was integral to understanding the spatial localization of cells expressing transgenic FGFR2c. Table 16 and Table 17 summarise the IHC conditions performed on frozen sections of controls and $R26R^{Fgfr2cV5/+}$; $\beta actin^{CRE/+}$ (n > 2) for each condition described). This study, along with a previous member of the Pauws lab (Emma Peskett c.2013), also attempted IHC on paraffin sections (Data not shown). Conditions were as described in Table 18 for paraffin sections. Unfortunately, the V5 epitope was not detected over the course of this study in $R26R^{Fgfr2cV5/+}$; $\beta actin^{CRE/+}$. The results obtained were either non-specific or lacking positive signal (Figure 37). Panel A shows IHC performed on frozen sections with varying concentrations of the V5 antibody. All conditions were performed in adjunct with a control antibody against fibronectin, where specific signals for blood vessels in the telencephalon were detected in all conditions attempted (Figure 37 B). Antigen retrieval with 10mM sodium citrate buffer was also attempted, but yielded the same results as without unmasking for the V5 antibody (Figure 37 C). ISH was subsequently attempted to detect the V5 epitope, with a unique portion of the *mV5* transgene cloned into the pGEM-T vector (Figure 30). The *mV5 in situ* probe was tested in embryos where conditional expression can be distinguished from background staining. For this reason, ISH was attempted in E12.5 $R26R^{Fgfr2cV5/+}$; $Mesp1^{CRE/+}$. This experiment was only partially successful, with 1 out of 6 embryos yielding positive hybridization in the limb bud under the conditions attempted (Figure 38; arrow). Due to the difficulty to optimize the *in situ* probe, ISH was not continued.

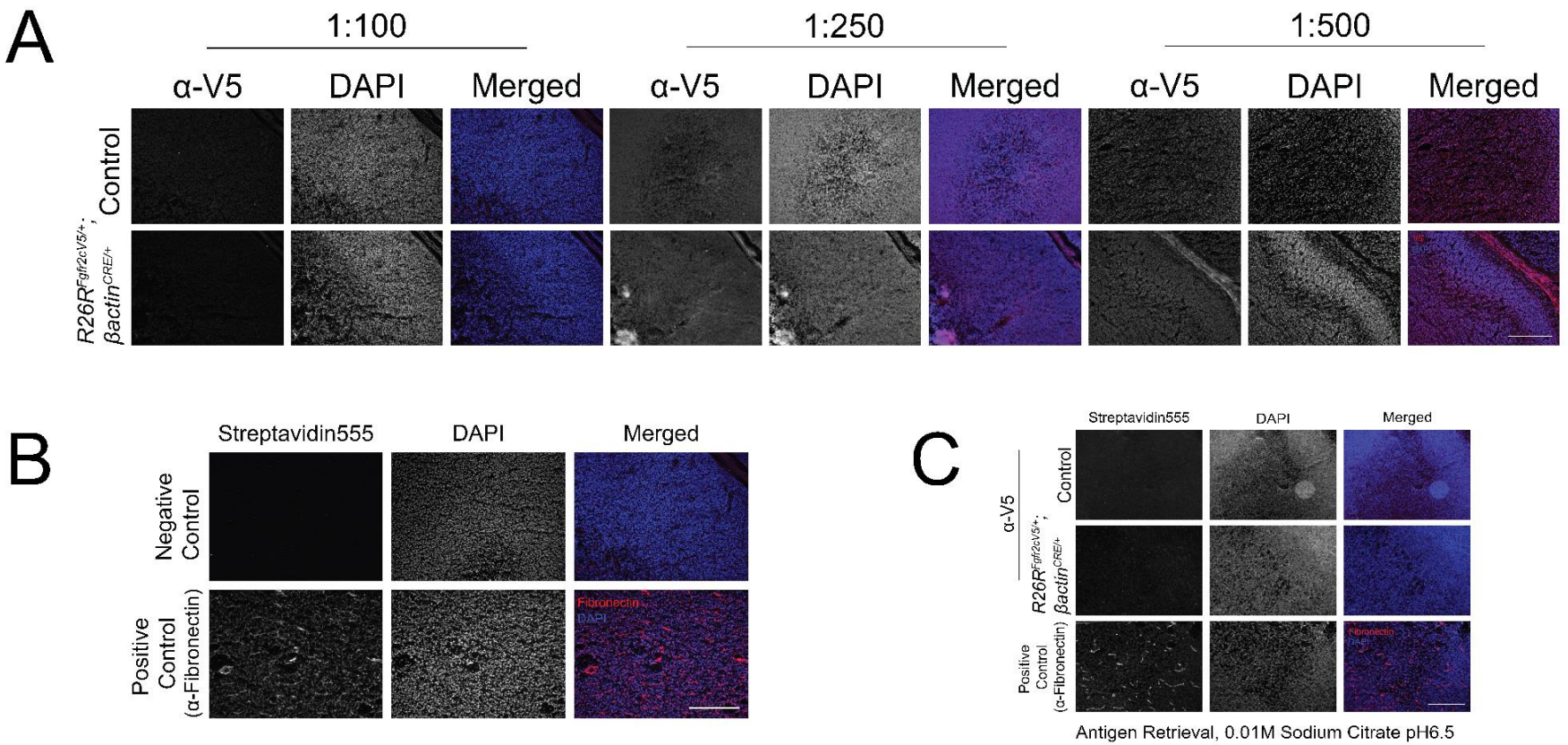

Figure 37: V5 IHC on frozen sections with images showing axial sections of the telencephalon (n>2 for all conditions described).

(A) αV5 IHC performed at multiple concentrations (1:100-1:500), note the lack of specific staining in these sections; (B) All conditions were carried out with a positive (αFibronectin) and a negative control (Secondary antibodies only), this panel is a representative from this cohort of attempts; (C) αV5 performed with 0.01M sodium citrate antigen retrieval buffer. Scale bar: 200um.

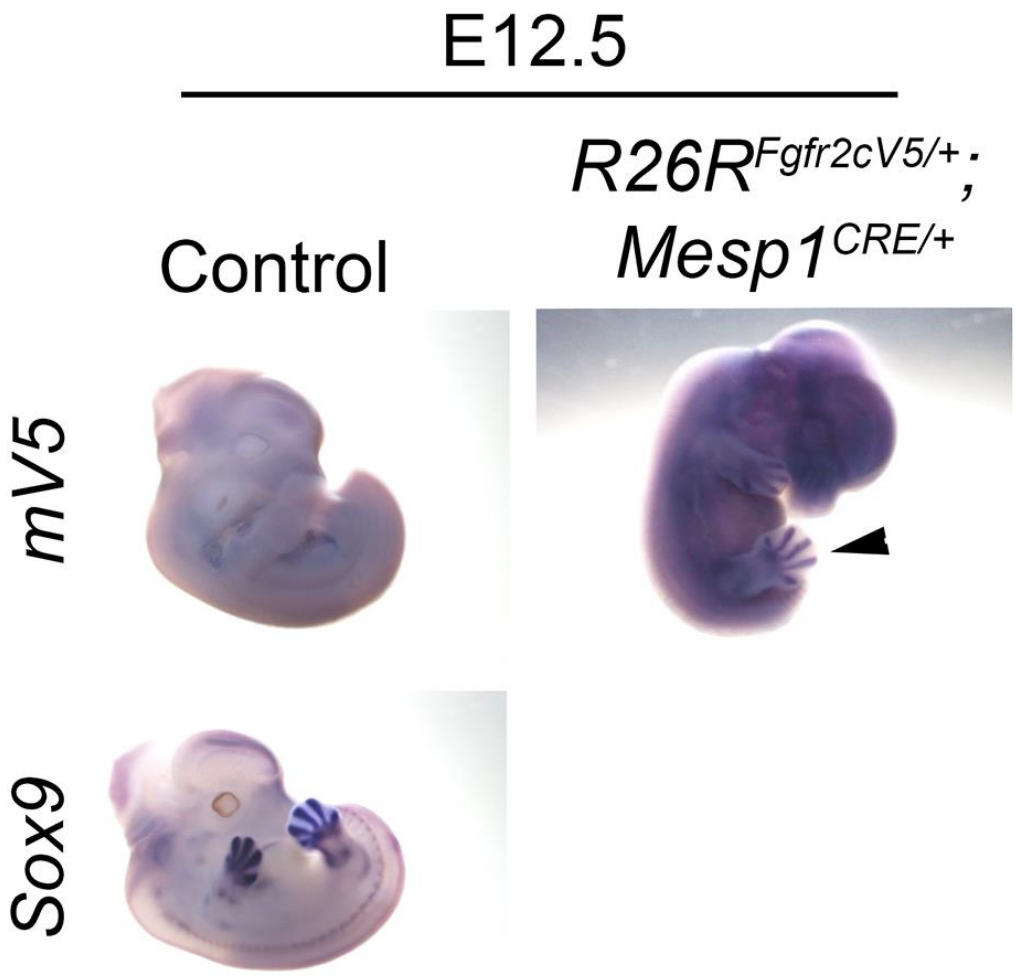

Figure 38: *mV5* wholemount ISH on E12.5 *R26R*$^{Fgfr2cV5/+}$; *Mesp1*$^{CRE/+}$ (n=1/6).

Arrow denotes an embryo with positive hybridization of *mV5 in situ* probe in the limb (arrow) (1/6). *Sox9* is adopted as an experimental control, showing positive staining in the somites and limbs.

3.2.6-Use of reporter lines to indirectly show *Fgfr2c-V5* overexpression

This experiment sets out to address two aims: Firstly, to show *Fgfr2c* overexpression indirectly through reporter activity and secondly, to demonstrate that the CRE lines were not compromised due to the results obtained thus far. Yoshida and colleagues have previously lineage traced the calvaria, providing a reference control for this study (Yoshida et al., 2008). $R26R^{mTmG/mTmG}$ was introduced into the $R26R^{Fgfr2cV5/Fgfr2cV5}$ ($R26R^{Fgfr2cV5/mTmG}$) in an attempt to visualize the *Fgfr2c-V5* expressing cells (Figure 23). The *mTmG* reporter was previously described in Muzumdar et al 2007, consisting of a *R26R-loxP-tdTomato-tPA-loxP-eGFP* construct with the ability to generate mosaic expression upon recombination. Unfortunately, it was difficult to collect sufficient embryos owing to the low expectancy of Mandelian ratio (1:8) obtained from the resultant genotypes. Eventually, a heterozygous reporter allele recombined with a respective CRE (i.e $R26R^{mTmG/+}$; $CRE^{/+}$) was chosen instead (Figure 39). Control embryos ($R26R^{mTmG/+}$) did not display any evidence for recombination and tdTomato was expressed globally across tissue as expected (Figure 39 A-D). Consistent with previous literature, reporter activity for $R26R^{mTmG/+}$; $Mesp1^{CRE/+}$ was only detected in the parietal bone (n=2) (Figure 39 I-L), whilst $R26R^{mTmG/+}$; $\beta actin^{CRE/+}$ was in both frontal and parietal bones (n=2) (Figure 39 E-H). Due to the presence of the *Rosa26-YFP* reporter allele already present in the $Wnt1^{CRE/+}$; $R26R^{YFP/+}$, interbreeding with the $R26R^{mTmG/mTmG}$ was not necessary. $Wnt1^{CRE/+}$; $R26R^{YFP/+}$ was eventually crossed with WT to visualize *YFP* reporter in embryos. As expected, cells positive for the $Wnt1^{CRE/+}$ and YFP was only detected in the frontal bone (n=3) (Figure 39 M-P).

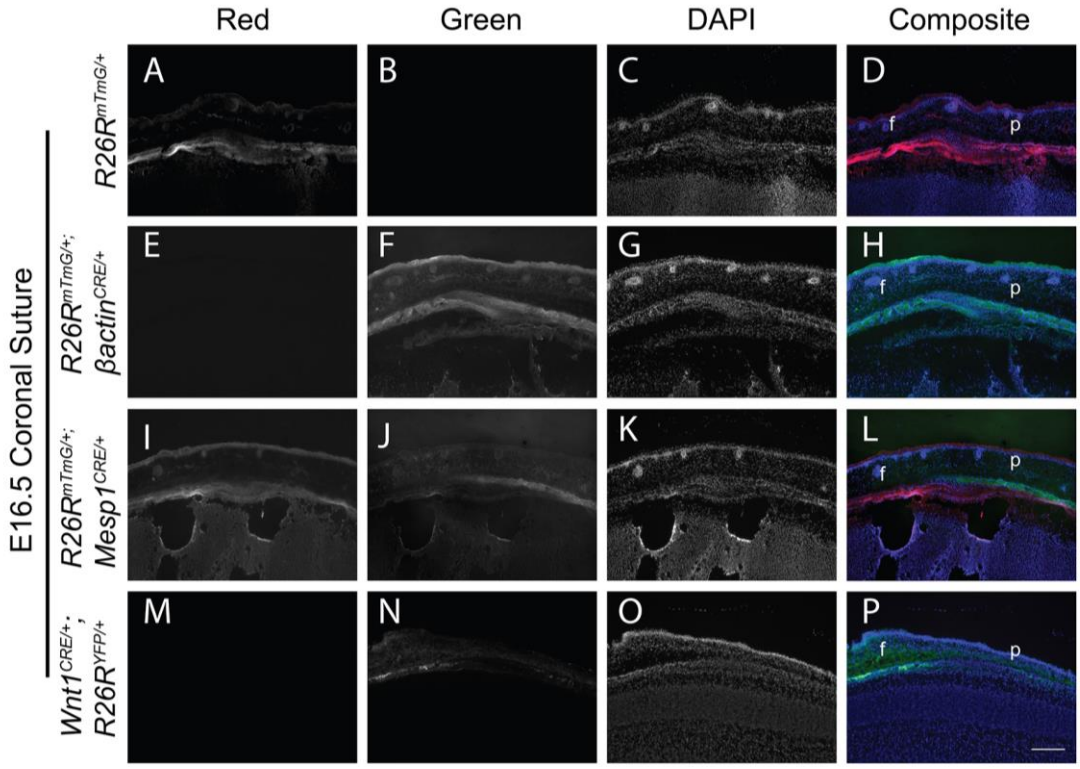

Figure 39: Reporter lines to show CRE activity in the E16.5 coronal suture.

(A-D) Control embryos (*R26R*$^{mTmG/+}$) did not show any evidence of CRE recombination and tdTomato is expressed throughout the cranial bones; (E-H) Complete recombination is present in *R26R*$^{mTmG/+}$*; βactin*$^{CRE/+}$ and eGFP is expressed throughout the cranial bones; (I-L) Cells derived from the mesoderm only expresses eGFP in the parietal bone of *R26R*$^{mTmG/+}$*; Mesp1*$^{CRE/+}$. (M-P) Cells derived from the NCC lineage only express YFP in *Wnt1*$^{CRE/+}$*; R26R*$^{YFP/+}$ mice; Coronal sutures are shown on the axial plane; Single channels are displayed in false colour; f: Frontal bone, p: Parietal Bone; Scale bar: 200um.

3.3-Discussion

This section deals with experiments to investigate and confirm expression of the *Fgfr2c-V5* in the embryo. However, this task faced multiple challenges that encompass the conditional overexpression in specific lineages, in particular to the mesoderm (discussed below), and the localization of the V5 epitope *in vivo*. The significance of the latter aim is of specific importance, as the spatial localization of the V5 epitope directly corresponds to the cells that express transgenic FGFR2c-V5. Due to the difficulties in visualizing the V5 epitope, an alternative strategy was to detect RNA expression using an antisense ISH probe designed against a unique portion of the transgene containing the *V5* sequence. This was partially successful as conditional expression was observed in the $R26R^{Fgfr2cV5/+;}$ $Mesp1^{CRE/+}$. Subsequently, reporter mice were used to indirectly infer the localization of overexpressing cells *in vivo,* and to confirm that there was no compromise to the CRE lines used in this study. Given these issues, the following discussion will focus on the potential shortcomings as well as detailing the techniques that could be adopted to address the problems.

3.3.1-Expression validation in the mesoderm lineage

An interesting observation was the lack of *Fgfr2c* transcript upregulation in the parietal bone for $R26R^{Fgfr2cV5/+;}$ $Mesp1^{CRE/+}$ and $R26R^{Fgfr2cV5/+;}$ $\beta actin^{CRE/+}$. The effects observed in the mesoderm are likely due to the nature of the *Rosa26* transgene acting on specific tissue types. It is characterised that the transgene does not elicit uniform expression across all tissue types, given by the fluorescent intensity of reporter proteins (Tchorz et al., 2012, Kisseberth et al., 1999, Mao et al., 1999). This is reflective of the low *Fgfr2c* RNA expression in the parietal bone upon conditional expression. It is unknown as to the mechanism contributing to this molecular event, but it could either suggest i) attenuated transgene expression in or ii) augmented RNA degradation in the parietal bone tissue. As we shall see, the lack of *Fgfr2c* overexpression in the parietal bone may have an impact on the phenotype yielded in the phenotypic experiments later in this study (See Chapter 3, Results part II).

To determine the molecular discrepancy of the mesoderm, limb tissue was adopted as a control to demonstrate *Fgfr2c* overexpression. However, *Fgfr2c* transcript levels remain similar to controls in $R26R^{Fgfr2cV5/+;}$ $Mesp1^{CRE/+}$. *Mesp1* is an early cranial mesoderm marker, able to give rise to multiple progenitors within the lineage (Chan et al., 2013, Gopalakrishnan et al., 2015, Lescroart et al., 2010). It has been shown that *Mesp1* activity, which is detectable in the early limb bud, is absent by E17.5 (Gopalakrishnan et al., 2015, Saga et al., 2000). In this regard, expression validation should be carried out at the appropriate embryonic stage. Cellular heterogeneity may also contribute to temper with late stage expression validation in the limb tissue, as muscle tissue express multiple markers (Gopalakrishnan et al., 2015, Chan et al., 2013). Therefore, the expression of *Mesp1* is restricted to a specific cell type (i.e. satellite cells) (Chan et al., 2013), making it difficult to distinguish positive results from the bulk tissue mass. The *Mesp1* limb results contrasts that of $R26R^{Fgfr2cV5/+;}$ $\beta actin^{CRE/+}$, where *Fgfr2c* expression is expected in every cell. The heterogeneity of the tissue is also related to the abundance of *Fgfr2c* transcripts observed in the frontal bone of $R26R^{Fgfr2cV5/+;}$ $Mesp1^{CRE/+}$. This could be explained by the prominence of mesodermal progenitors derived from the paraxial mesoderm lining the periphery of the frontal bone by E18.5 (Deckelbaum et al., 2012). As *Mesp1* is sufficient to give rise to the paraxial mesoderm, the intermixing of cells in the frontal bone would have led to a false positive for *Fgfr2c* overexpression in this tissue.

Two possible methods to tackle these issues include:

i) Use fluorescence activated cell sorting (FACS) to enrich for the specific cells of interest within the dissected tissue sample. This could be achieved through the use of antibodies such as αV5 or αCRE. The results could then be expressed as a total number of cells positive for the antigen of interest within the tissue, backed up with expression data from any primary cultures generated.

ii) Expression validation was performed at a late stage for $Mesp1^{CRE/+}$ recombinants. Future experiments could attempt to isolate structures from an earlier embryonic stage. A potential

tissue to perform this experiment would be the developing heart, as the endocardium and myocardium strongly express *Mesp1* (Saga et al., 2000)

3.3.2-The V5 epitope

An advantage of the V5 epitope is the small size as the polypeptide is 14 amino acids long. The V5 is tagged at the C-terminal of the transgenic FGFR2c, and the minimal size of the tag reduces potential interference with protein function, whilst still serving as a robust marker for transgenic protein expression. However, the V5 epitope was not easily visualized by IHC methods. The difficulties to detect the epitope may be due to a very specific protocol being required for the antibody. Few other studies that have reported successful visualizion of the V5 *in vivo* are likely due to ectopic or particularly high levels of expression levels of the tag. For example, one study used a viral vector to drive expression in the mouse hippocampus (Verbeeck et al., 2012). In this respect, expression levels are likely to exceed those of the *Rosa26* locus. The widely available *Rosa26* construct (*Gt(Rosa26)*^{tm1Sor}) achieves moderate levels of transgene expression (Mao et al., 1999). As mentioned previously, it is speculated that the *Rosa26* transgene elicits broad, albeit not uniform reporter activity across different tissue (Kisseberth et al., 1999, Mao et al., 1999). Several groups have criticized the construct over the moderate levels of expression, and have substituted the endogenous promoter for one that exacerbates transgene expression (e.g. pCAGG) to accelerate phenotypic severity (Nyabi et al., 2009, Tchorz et al., 2012). The 'moderate' expression can be reflected in immunoblots in this study, as the V5 epitope was only detected between 30-50ug of *R26R*$^{Fgfr2cV5/+}$*;* *βactin*$^{CRE/+}$ lysates. Therefore, it is likely to pose greater difficulties to detect the protein using IHC methods and as shown in Figure 37, yielded negative results even in the presence of streptavidin signal amplification. Despite the fact that reporter lines were used to indirectly show the transgene expression, there are tools that could help with detecting the epitope. For example, undertaking Tyramide Signal Amplification (TSA) in IHC provides significant signal amplification for proteins with low expression. Other considerations such as placement of the epitope, could also affect the overall function of the protein (Park et al., 2015). Placement of the tag should be away

from any functional domains. In this study, V5 is tagged towards the C-terminal of FGFR2c, adjacent to the catalytic domain of the terminal, which could be disadvantages to the overall catalytic function of the receptor. Any potential disruptions to the receptor could be determined by immunobloting, such as appreciating the phosphorylation of Frs2α, or the catalytic domains of FGFR2c-V5. The *mV5* ISH probe was initially tested on $R26R^{Fgfr2cV5/+;}$ $Mesp1^{CRE/+}$ wholemounts, with expression expected in the mesoderm e.g. limb. Despite partial success, the majority of attempts appeared to yield non-specific binding, which was potentially due to the small size of the probe, being under 200bp long. Ideally, an ISH probe should be greater the 500bp to increase hybridization specificity. Due to the lack of success with the wholemount ISH, section ISH with the *mV5* was not carried out.

Chapter 4

Results (Part II)

Phenotypic analysis of the craniofacial skeleton in *Fgfr2c* overexpression mice

4.1-Introduction

To analyse the complexity of FGFR2c signalling in craniofacial development, the Pauws lab generated a novel transgenic mouse model (*R26R*$^{Fgfr2cV5/Fgfr2cV5}$). The craniofacial skeleton was thoroughly examined using a series of morphometric analyses as described in this section. By using a conditional receptor overexpression approach, lineage sensitivities to FGFR2c signalling can be identified. A large proportion of the craniofacial skeleton is derived from the NCCs and mesoderm (Jiang et al., 2002). Firstly, a constitutively active *βactin*$^{CRE/+}$ was crossed with *R26R*$^{Fgfr2cV5/Fgfr2cV5}$ to identify the regions sensitive to FGFR2c signalling. Secondly, *Mesp1*$^{CRE/+}$ and *Wnt1*^{CRE} were adapted as lineage specific controls for the *R26R*$^{Fgfr2cV5/Fgfr2cV5}$. The latter CRE lines were important as they serve to identify ectopic expression of *Fgfr2c-V5* generated by the *βactin*$^{CRE/+}$.

4.2-Results

4.2.1-*Fgfr2c* overexpression causes growth restriction

R26R$^{Fgfr2cV5/Fgfr2cV5}$ were crossed with either *βactin*$^{CRE/+}$ (Ubiquitous), *Wnt1*$^{CRE/+}$ (NCC) or *Mesp1*$^{CRE/+}$ (Mesoderm) to induce conditional overexpression of *Fgfr2c* (Figure 40 A). *R26R*$^{Fgfr2cV5/+}$; *βactin*$^{CRE/+}$ embryos were examined at E18.5 for their size (head length and crown rump length-'CRL') and weight (Figure 40 B-E). Results were expressed as an average percentage change (Av.Δ %) relative to controls (*R26R*$^{Fgfr2cV5/+}$). Ubiquitous *Fgfr2c* overexpression (n=9) led to a significant reduction in the head length (Av.Δ 7.19%; $p<0.0001$; $t(17.78)=7.74$) (Figure 30 D), CRL (Av.Δ 4.83%; $p=0.0018$; $t(13.23)=3.90$) (Figure 30 C) and weight (Av.Δ12.26%; $p=0.0001$; $t(22.16)=5.39$) (Figure 30 E) to the controls (n=17). *R26R*$^{Fgfr2cV5/+}$; *βactin*$^{CRE/+}$ embryos also display a fully penetrant microtia in the outer ear (n=6/6) (Figure 40 B; arrow). The calvaria are derived from the NCC and mesoderm (Yoshida et al., 2008). *R26R*$^{Fgfr2cV5/Fgfr2cV5}$ were subsequently crossed with *Wnt1*$^{CRE/+}$ or *Mesp1*$^{CRE/+}$ with their phenotypes corroborated with *R26R*$^{Fgfr2cV5/+}$; *βactin*$^{CRE/+}$ to identify any ectopic effects generated by the ubiquitous CRE line. *R26R*$^{Fgfr2cV5/+}$; *Wnt1*$^{CRE/+}$ embryos (n=6) yielded significant decrease in weight (Av.Δ6.72%; $p=0.0028$; $t(9.23)=4.05$) (Figure 30 E) while head length (Figure 30 D) and CRL were not significantly reduced (Figure 30 C). Moreover, ears were normal in *R26R*$^{Fgfr2cV5/+}$; *Wnt1*$^{CRE/+}$. No significant reduction was seen in embryos upon *Fgfr2c* overexpression in the mesoderm using *Mesp1*$^{CRE/+}$ (*R26R*$^{Fgfr2cV5/+}$; *Mesp1*$^{CRE/+}$) (n=9) to the controls (n=4) (Figure 40 B-D). Altogether, ubiquitous and conditional *Fgfr2c* overexpression in the NCC lineage causes skeletal hypoplasia with overall stunted growth.

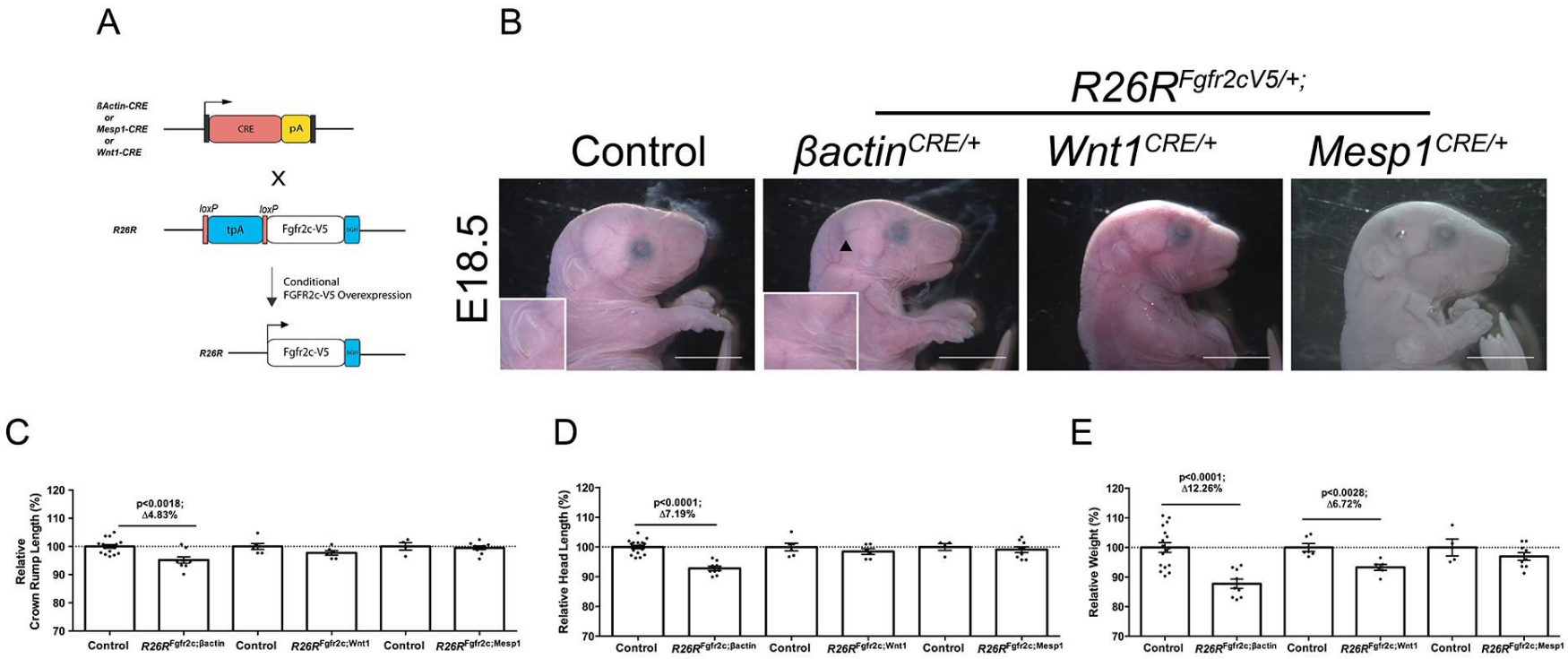

Figure 40: Gross phenotype of embryos with *Fgfr2c* overexpression.

(A) Schematic of $R26R^{Fgfr2cV5/Fgfr2cV5}$ breeding schematic; (B) Microtia (n=6/6) (Arrow) observed in E18.5 $R26R^{Fgfr2cV5/+}$; $\beta actin^{CRE/+}$ and not $R26R^{Fgfr2cV5/+}$; $Wnt1^{CRE/+}$ and $R26R^{Fgfr2cV5/+}$; $Mesp1^{CRE/+}$. Inserts are magnified images of the external ear; (C) Significant reduction in body length of $R26R^{Fgfr2cV5/+}$; $\beta actin^{CRE/+}$ ($p<0.0018$; n=9); (D) Significant reduction in head length in $R26R^{Fgfr2cV5/+}$; $\beta actin^{CRE/+}$ ($p<0.0001$; n=9); (E) Significant reduction in weight in $R26R^{Fgfr2cV5/+}$; $\beta actin^{CRE/+}$ ($p<0.0001$, n=9) and $R26R^{Fgfr2cV5/+}$; $Wnt1^{CRE/+}$ ($p<0.0028$, n=6). Statistics: Student's t-test with Welch's correction. Error bars depict SEM. Scale bar: 5mm.

4.2.2- *Fgfr2c* overexpression leads to frontal bone hypoplasia and patent suture

Craniofacial structures were assessed at E18.5 and quantified for the surface area and length for mandibles. Figure 41 is a panel showing the craniofacial skeleton, and areas affected in the *Fgfr2c* overexpression mutants are highlighted in arrows and asterisks (Figure 41). Quantitative data were expressed as an average percentage change in the mutants relative to the controls ($R26R^{Fgfr2cV5/+}$) normalized to 100% (Av.Δ %) (Figure 42). Frontal bones of $R26R^{Fgfr2cV5/+}$; $\beta actin^{CRE/+}$ were significantly smaller (Av.Δ11.4%; $p<0.0001$; $t(22.98)=6.99$; $n=9$) (Figure 41 E green arrow; Figure 42 A) along with other NCC derivatives such as nasal bones (Av.Δ12.90%; $p<0.0001$; $t(22.06)=7.91$; $n=10$) (Figure 41 D open arrow; Figure 42 C) and mandibles (Av.Δ5.77%; $p<0.0001$; $t(20.64)=7.30$; $n=9$) (Figure 41 D black arrow; Figure 42 D). No significant reduction was observed in the mesoderm derived parietal bone (Figure 42 B). Moreover, these mutants had notable hypoplasia of the tympanic ring in the middle ear (Figure 41 F orange arrow; n=9/10), overt cleft palate (Figure 41 F, asterisk; n=4/10) and a wider interfrontal suture (Figure 41 E line; n=9/9). Similarly, $R26R^{Fgfr2cV5/+}$; $Wnt1^{CRE/+}$ embryos followed a similar trend with significant decreases in NCC derivatives: Frontal bone (Av.Δ9.12%; $p=0.0131$; $t(6.89)=3.32$; $n=6$) (Figure 41 H, green arrow; Figure 42 B), nasal bones (Av.Δ7.91%; $p=0.0024$; $t(9.077)=4.17$; $n=6$) (Figure 41 G, open arrow; Figure 42 C); and mandibles (Av.Δ3.71%) ($p=0.0007$; $t(9.96)=4.82$; $n=6$) (Figure 41 G black arrow; Figure 42 D). Moreover, the clefting phenotype was heterogeneous in its severity: 1 out of 6 embryos exhibit an overt cleft (Figure 41 I, asterisk) whilst 3 out of 6 display palatal shelf hypoplasia (data not shown). No middle ear defects were present in this cohort of embryos (n=0/3). In $R26R^{Fgfr2cV5/+}$; $Mesp1^{CRE/+}$, calvarial bone size appeared unchanged (Figure 41 K; Figure 42 D) and no defects were present in the ear or the palate (n=0/9) (Figure 41 L). In summary, *Fgfr2c* overexpression causes skeletal hypoplasia.

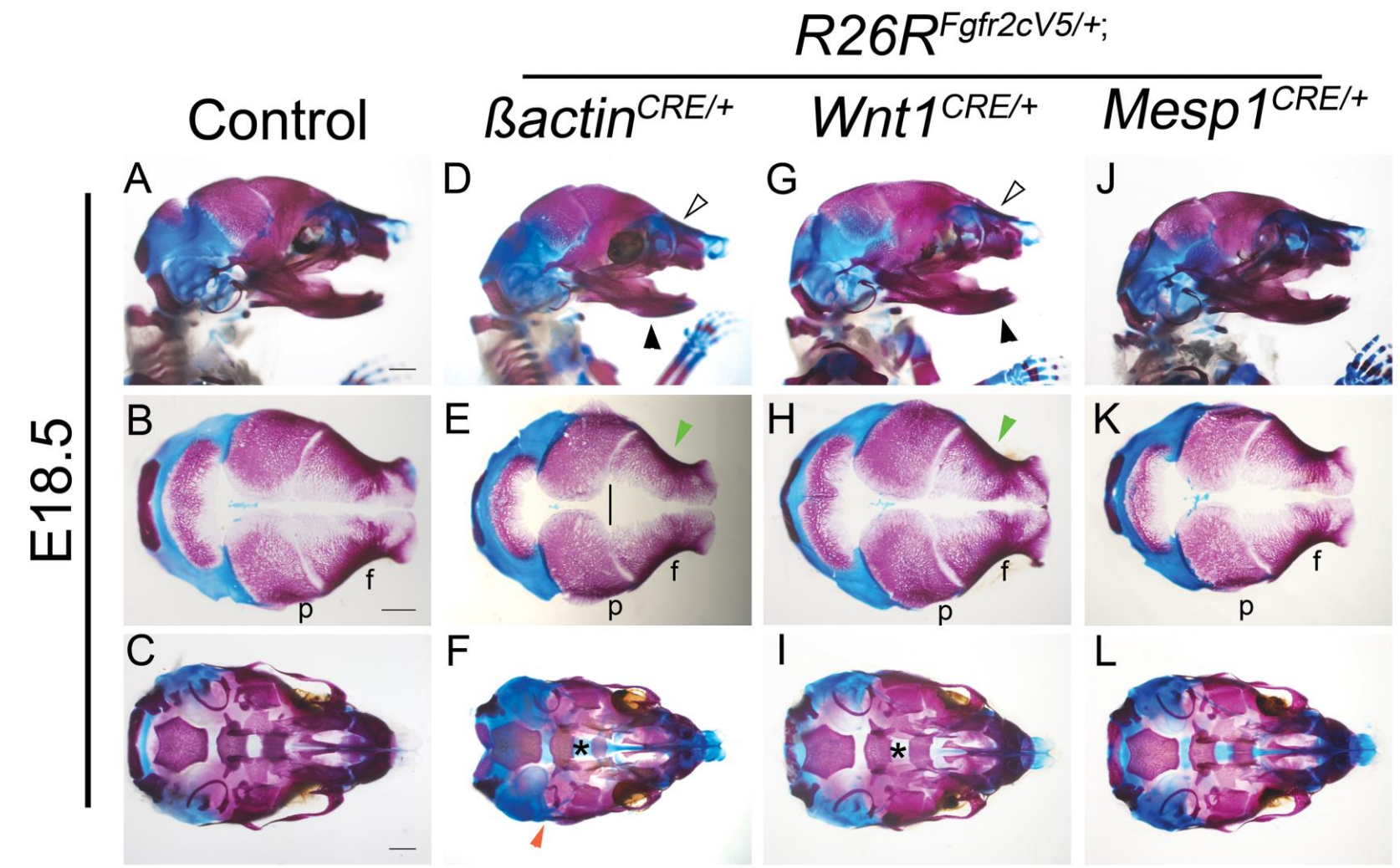
R26R Fgfr2cV5/+;
Control
ßactin CRE/+
Wnt1 CRE/+
Mesp1 CRE/+
E18.5
A
B
C
D
E
F
G
H
I
J
K
L
f
p
*

Figure 41 Craniofacial phenotypes of *Fgfr2c* overexpressing mutants at E18.5.

Wholemount bone and cartilage histology of (A-C) Controls (*R26R*$^{Fgfr2cV5/+}$); (D-F) *R26R*$^{Fgfr2cV5/+}$; *βactin*$^{CRE/+}$; (G-I) *R26R*$^{Fgfr2cV5/+}$; *Wnt1*$^{CRE/+}$; (J-L) *R26R*$^{Fgfr2cV5/+}$; *Mesp1*$^{CRE/+}$; *R26R*$^{Fgfr2cV5/+}$; *βactin*$^{CRE/+}$ display smaller in frontal bones (E, green arrow; n=9), nasal bones (D, , open arrow; n=6) and mandibles (D, black arrow; n=9). Tympanic ring hypoplasia (F, orange arrow; n=9/10), wider frontal suture (E, line; n=9/9) and overt cleft palate (F, *; n=4/10) were also present; *R26R*$^{Fgfr2cV5/+}$; *Wnt1*$^{CRE/+}$ (G-I) also exhibit smaller frontal bones (H, green arrow; n=6), nasal bones (G, open arrow; n=6) and mandibles (G, black arrow; n=6). Clefting phenotype is heterogenous (I, *; Overt: 1/5, palatal shelf hypoplasia: 3/5). No obvious phenotypic differences were observed in *R26R*$^{Fgfr2cV5/+}$; *Mesp1*$^{CRE/+}$ (J-L; n=9). f=Frontal bone, p=Parietal bone; Scale bar: 1mm.

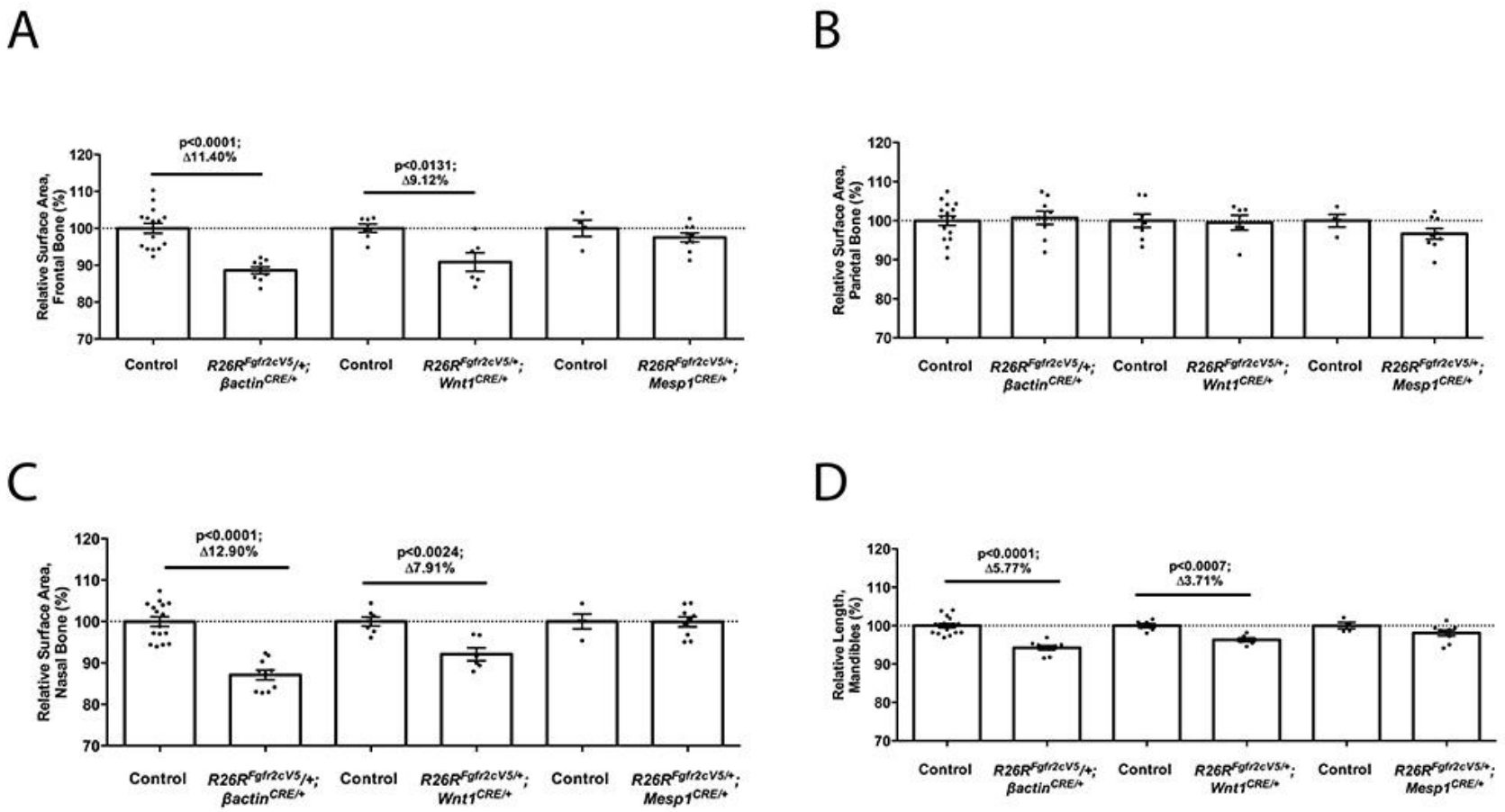

Figure 42 Craniofacial bones of the NCC lineage display hypoplasia.

(A) *R26R*$^{Fgfr2cV5/+;}$ *βactin*$^{CRE/+}$ ($p<0.0001$; n=9) and *R26R*$^{Fgfr2cV5/+}$; *Wnt1*$^{CRE/+}$ ($p<0.0131$; n=6) shows significant insufficienies of the frontal bone; (B) No phenotypic differences in the parietal were observed across all genotypes; (C) Significant reduction in size of the nasal bone in *R26R*$^{Fgfr2cV5/+;}$ *βactin*$^{CRE/+}$ ($p<0.0001$; n=9) and *R26R*$^{Fgfr2cV5/+}$; *Wnt1*$^{CRE/+}$ ($p<0.0024$; n=6); (D) Significant reduction in the mandibles of *R26R*$^{Fgfr2cV5/+;}$ *βactin*$^{CRE/+}$ ($p<0.0001$; n=9) and *R26R*$^{Fgfr2cV5/+}$; *Wnt1*$^{CRE/+}$ ($p<0.0007$; n=6). Data was normalized to the limb endogenous control and expressed as an average percentage change (%). Statistics: Student's t-test with Welch's correction; Error bars: SEM; Δ: Difference of means in respect to the control group.

4.2.3-Ubiquitous *Fgfr2c* overexpression does not result in coronal synostosis

Coronal synostosis is a hallmark of Crouzon-Pfeiffer syndrome and can be observed in the *Fgfr2c*$^{C342Y/+}$ mouse model as well as the *Fgfr2c* knockout (Eswarakumar et al., 2004, Eswarakumar et al., 2002). Strikingly, none of the aforementioned embryos with *Fgfr2c* overexpression show signs of coronal synostosis. While subtle changes in the *Fgfr2c*$^{C342Y/+}$ coronal suture morphology are visible from E17.5, full fusion of frontal and parietal bones is not visible until three weeks after birth (Eswarakumar et al., 2004). Due to the presence of a cleft palate in *R26R*$^{Fgfr2cV5/+}$; *βactin*$^{CRE/+}$ embryos, mice do not survive after birth, making it impossible to assess the postnatal synostosis phenotype. *Ex vivo* explant cultures were adopted to overcome this problem (Figure 43). Previous explant cultures in our lab showed that evidence for coronal synostosis could be achieved after one week of culture in *Fgfr2c*$^{C342Y/+}$ E17.5 calvaria. In *R26R*$^{Fgfr2cV5/+}$; *βactin*$^{CRE/+}$ calvaria, coronal synostosis was not observed, while *Fgfr2c*$^{C342Y/+}$ calvaria appears to be undergoing fusion compared to that of the control (n=7) and *R26R*$^{Fgfr2cV5/+}$; *βactin*$^{CRE/+}$ (n=6) at T15 (Figure 43; Arrow). Upon culture within this time window, there was no evidence for coronal synostosis in *R26R*$^{Fgfr2cV5/+}$; *βactin*$^{CRE/+}$ after 15 days of culture. Additionally, the effect of FGFR2 perturbation on osteoblast maturation at a pre-synostosis embryonic stage (E16.5) was examined by analysing alkaline phosphatase (ALP) activity (Figure 44). *Fgfr2c*$^{C342Y/+}$ sutures display increased suture overlap and ectopic ALP in the sutural mesenchyme (n=3) (Figure 44; arrow), whilst ALP activity in *R26R*$^{Fgfr2cV5/+}$; *βactin*$^{CRE/+}$ appear less, and the frontal and parietal bones are spaced normally that resemble controls (n=3) (Figure 44; asterisk). This data implies that FGFR2c overexpression does not cause coronal craniosynostosis and does not mimic FGFR2 activation in the *Fgfr2c*$^{C342Y/+}$ suture.

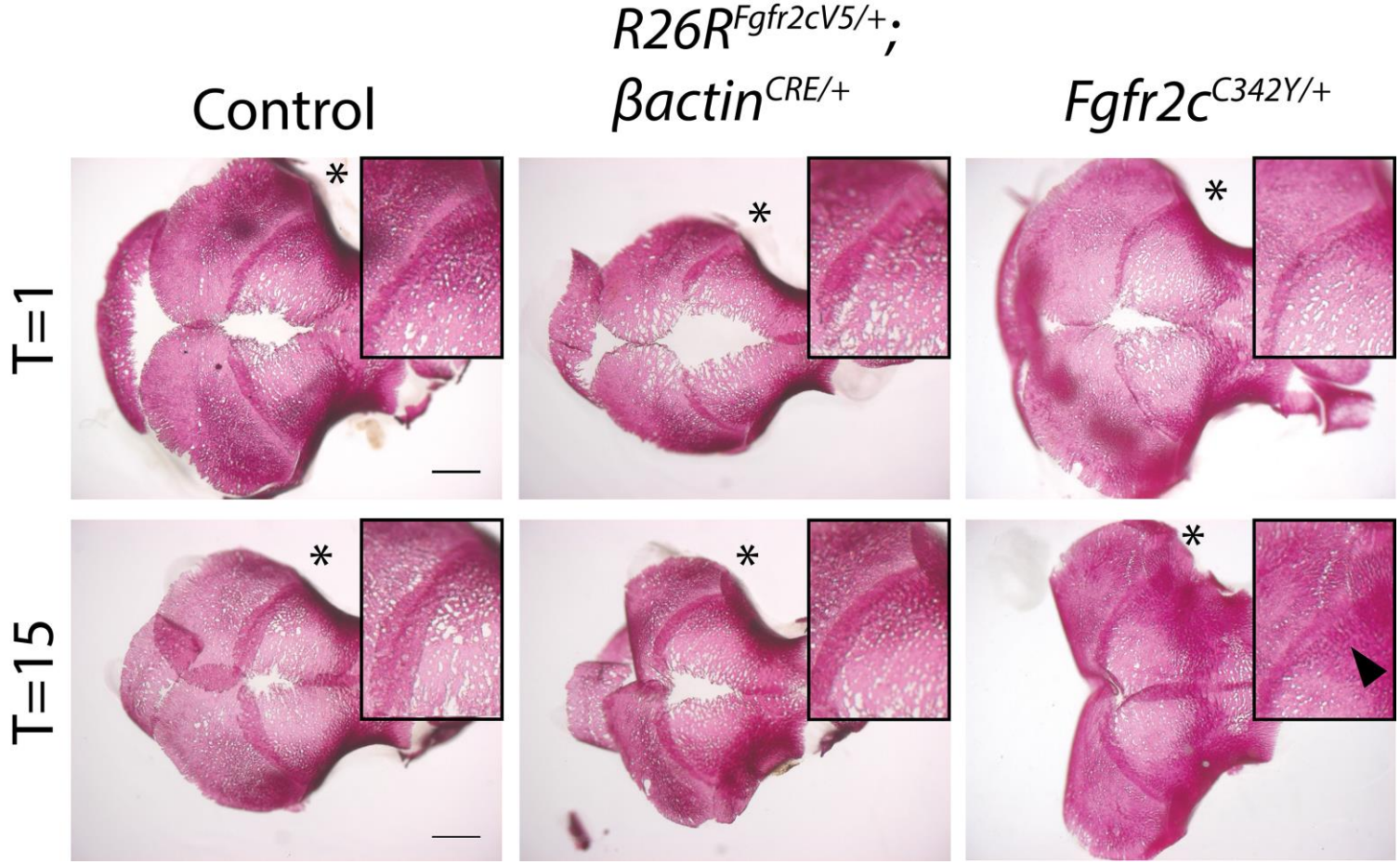

Figure 43: Absence of coronal synostosis in *R26R*$^{Fgfr2cV5/+;}$ *βactin*$^{CRE/+}$ *ex vivo* after culture.

Suture overgrowth had increased after 15 days of culture. *Fgfr2c*$^{C342Y/+}$ was used as a control for the assay to demonstrate the synostosis process, where suture fusion was apparent (arrowhead, insert). Insert is a magnified image of the representative coronal suture in the respective explants (*). Scale bar: 1mm.

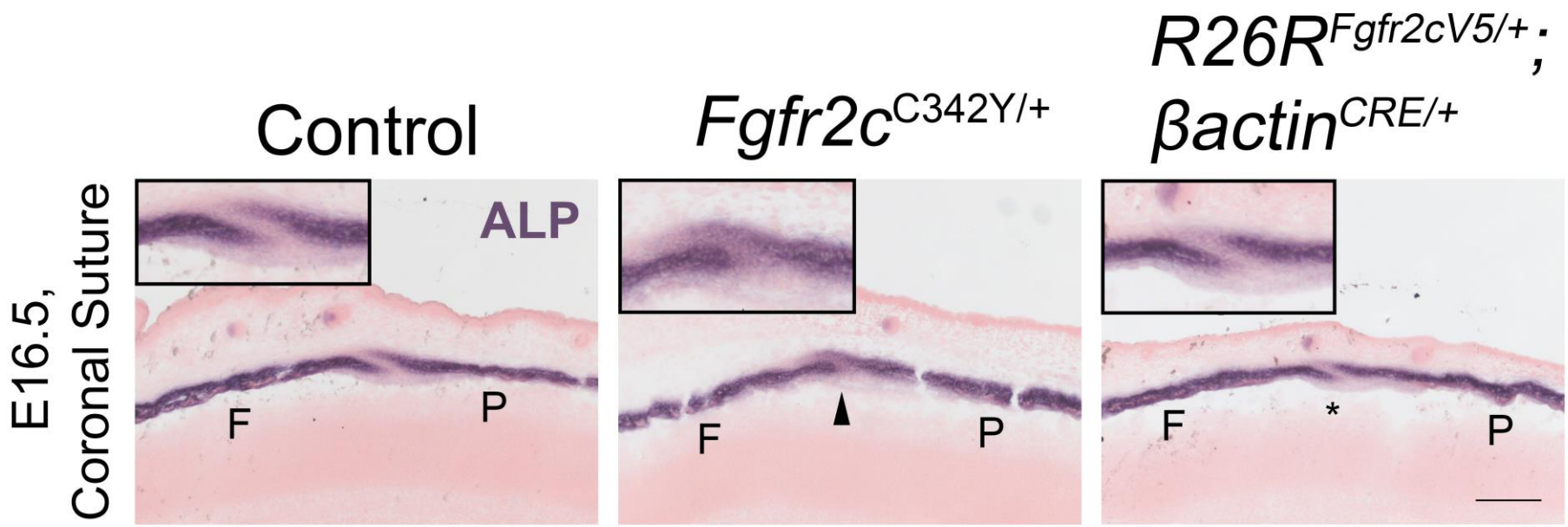

Figure 44: Comparison of osteoblast activity in the coronal suture.

Note the increased overgrowth in the osteogenic fronts of *Fgfr2c*$^{C342Y/+}$ and ectopic expression of ALP in the suture mesenchyme (arrow). Notice the extension of the osteogenic fronts in *R26R*$^{Fgfr2cV5/+}$; *βactin*$^{CRE/+}$appears underdeveloped to that of *Fgfr2c*$^{C342Y/+}$ (*). N=3 analyzed for each genotype; F: Frontal Bone; P: Parietal bone; Insert is a magnified crop of the suture; Scale bar: 200um.

4.3-Discussion

FGFR2c signalling misregulation was examined through *Fgfr2c* overexpression and compared that to *Fgfr2c*$^{C342Y/+}$. This section reports global *Fgfr2c* overexpression yielded craniofacial hypoplasia, microtia along with a clefting phenotype. Strikingly, this cohort of mutants did not develop coronal synostosis as opposed to *Fgfr2c*$^{C342Y/+}$ and *Fgfr2c*$^{-/-}$ (Eswarakumar et al., 2004, Eswarakumar et al., 2002). Furthermore, growth restriction is a hallmark phenotype in the overexpression model. However, analysis of the appendicular skeleton (i.e. the limb, Figure 32) in *R26R*$^{Fgfr2cV5/+}$; *βactin*$^{CRE/+}$, rules out intrauterine constriction as the probable cause for global growth restriction.

4.3.1-*Fgfr2c* overexpression yields skeletal hypoplasia in the NCC lineage

This study reports craniofacial hypoplasia of the NCs lineage upon conditional *Fgfr2c* overexpression. A previous morphometric analysis of the adult *Fgfr2c*^{C342Y} reports smaller frontal and nasal bones, accompanied by a short anterior cranial base (Liu et al., 2013). Diminished calvarial bone volume was also reported in other mouse models for syndromic craniosynostosis most notably in *Fgfr2*$^{S252W/+}$ and *Fgfr3*$^{P244R/+}$ (Muenke syndrome) (Twigg et al., 2009, Chen et al., 2003). This is consistent with our finding that hypoplasia of NC-derived bones is present in E18.5 *R26R*$^{Fgfr2cV5/+}$; *βactin*$^{CRE/+}$ mice. However, *Fgfr2c*$^{C342Y/+}$ embryos at E18.5 do not show similar signs of hypoplasia at this stage (See Figure 53). The nature of the C342Y mutation itself plays different roles in both early and late stages of development (Liu et al., 2013, Mansukhani et al., 2000). The C342Y mutation favours early osteoblast commitment but however during late stages of gestation, it inhibits bone mineralisation and facilitates cellular apoptosis (Liu et al., 2013, Mansukhani et al., 2000, Rice et al., 1999). Any phenotypic effects of remodelling in the frontal bone by the C342Y mutation will be too early to be perceived at this stage. Overall, the similarities observed between both mouse models suggest shortening of the frontal bone is a contributor to mid-facial hypoplasia. Despite similarities observed in the frontal bone of *Fgfr2c*$^{C342Y/+}$ and *R26R*$^{Fgfr2cV5/+}$; *βactin*$^{CRE/+}$, it is likely that the

derived phenotype is mechanistically different: $R26R^{Fgfr2cV5/+}$; $\beta actin^{CRE/+}$ implies frontal hypoplasia is a result of early embryonic defect whereby in $Fgfr2c^{C342Y/+}$ is a progressive disorder, as the phenotype elicited is only reported postnatally, suggesting bone remodelling could be the main player contributing to hypoplasia (Hatch et al., 2006, Eswarakumar et al., 2004, Liu et al., 2013).

The changes to the frontal bone architecture provide insights into coronal synostosis and NCC misregulation. NCs dominate the head mesenchyme during early embryogenesis, and require constant re-positioning with cells derived from the mesoderm to compartmentalise the calvaria (Yoshida et al., 2008, Jiang et al., 2000). As such, loss of cellular polarity in NCs has been reported to drive craniosynostosis via the ectopic expansion of the frontal bone (Tabler et al., 2016, Tabler et al., 2013, Merrill et al., 2006). Others have also investigated the skeletogenic potentials of NCCs, where it has greater response to FGF signalling and osteogenic potentials compared to the mesoderm derived osteoblasts (Li et al., 2010, Yu et al., 2005). Additionally, in humans, a set of genes involved in NCCs specification such as *SNAI1* and *ZIC2* have been identified to be involved in craniosynostosis, but their relationship with FGF signalling is less understood (Twigg et al., 2015, Twigg and Wilkie, 1999). Interestingly, *SNAI1* is not required for NCC specification in the mouse, as *SnaI1* conditional knockout only yielded defects to left-right asymmetry (Murray and Gridley, 2006). In contrast, $Zic2^{-/-}$ yielded significant loss of pre- and post- migratory NCCs, and led to a reduction of NCCs populating the head mesenchyme at E9 (Elms et al., 2003). *Zic2* is downstream of FGF8, as their expression patterns overlap in the midline of the telencephalon, and FGF8 overexpression can expand the expression domain of *Zic2* (Okada et al., 2008). Similarly, whole genome sequencing in humans uncovered a GOF mutation in human *ZIC1* as a novel player involved in coronal synostosis (Twigg et al., 2015). In *Xenopus*, *Zic1* and *Pax3* act synergistically in the surface ectoderm to commit cells towards a NCC fate. Co-injection of *Zic1* and *Pax3* mRNA into *Xenopus* animal caps lead to ectopic expression of NCC markers such as *Foxd3* and *Slug* (Sato et al., 2005). The function of *Pax3* and *Zic1* appear to integrate NCC inducing signals from multiple signalling pathways: FGFs functions upstream of *Pax3* and *Zic1* as an NCC inducer along with a low BMP and Wnt signal

(Sato et al., 2005, Mayor et al., 1997, LaBonne and Bronner-Fraser, 1998). These findings imply correct patterning of the head mesenchyme is essential for correct craniofacial development. As NCCs play substantial roles in craniofacial development, it is therefore not surprising when the elicited phenotype is a consequence of NCCs mis-specification by perturbed FGF signalling.

3.3.2-Role of the mesoderm in craniosynostosis

The lack of a coronal synostosis phenotype in $R26R^{Fgfr2cV5/+}$; $\beta actin^{CRE/+}$ suggests that the mechanisms contributing towards disease pathogenesis are different to that of $Fgfr2c^{C342Y/+}$. There is a speculation that there is insufficient ligand present endogenously to drive craniosynostosis. Coronal synostosis of $Fgfr2c^{C342Y/+}$ stems from the mesoderm, and is a consequence of enhanced cellular activity during the early stages of suture morphogenesis, as this is apparent to the increased appositional growth and hyperplasia of the parietal bone (See Figure 53) (Eswarakumar et al., 2004). Furthermore, the enhanced ALP expression mimics those in the Apert mouse model ($Fgfr2^{P253R/+}$), with increased overlap from the parietal bone (Wang et al., 2010). Interestingly, coronal synostosis is only sufficient to be developed in the mesoderm of a conditional mouse model for Apert syndrome ($Fgfr2^{S252W/+}$; $Mesp1^{CRE/+}$) (Holmes and Basilico, 2012, Holmes et al., 2009). Similar to the mechanisms of $Fgfr2c^{C342Y/+}$, suture abolishment in the Apert mouse model is primarily a consequence of increased cellular apoptosis in the osteogenic fronts and suture mesenchyme during late gestation stages (Holmes and Basilico, 2012, Deckelbaum et al., 2012, Rice et al., 1999). However, the lack of parietal bone phenotype in $R26R^{Fgfr2cV5/+}$; $\beta actin^{CRE/+}$ could hinder suture pathogenesis. Firstly, a possible explanation is the limited ligand availability in the mesoderm during early embryogenesis *in vivo*, and may require a higher response to FGF signalling to stimulate the osteogenic programme (Behr et al., 2010, Quarto et al., 2009). Secondly, the lack of a parietal bone phenotype in $R26R^{Fgfr2cV5/+}$; $\beta actin^{CRE/+}$ could be due to the efficiency of transgene, where transcript upregulation was absent from the parietal bone (Figure 35 and Figure 36).

4.3.2-Osteogenic potential in *R26R$^{Fgfr2cV5/+}$; βactin$^{CRE/+}$* and *Fgfr2c$^{C342Y/+}$*

Osteoblasts derived from both NCC lineage and mesoderm have different osteogenic potentials, where the former demonstrates greater sensitivity for osteoblast differentiation (Quarto et al., 2010, Liu et al., 2013). The difference is due to the molecular profile of these osteoblasts and their endogenous expression of *Fgfr2c* (Quarto et al., 2009). The frontal bone display higher endogenous expression of *Fgfr2c* during late gestation (E17.5), explaining greater sensitivities toward FGF ligands (Quarto et al., 2009). This would ultimately determine the threshold for osteoblast differentiation between the tissue types in respect to the endogenous FGF ligands available *in vivo* (Quarto et al., 2010, Hajihosseini and Heath, 2002). The parietal bone is known to have attenuated expression of *Fgfr2c* and its ligands to that of the frontal bone and therefore, the osteogenic potential is lessened relative to that of the frontal bone (Behr et al., 2010). Another point to consider is that receptor overexpression and *Fgfr2c$^{C342Y/+}$* are functionally distinct as the former is ligand dependent, and ligand will act as a limiting factor for receptor activation.

The dissimilar ALP activity in *R26R$^{Fgfr2cV5/+}$; βactin$^{CRE/+}$* and *Fgfr2c$^{C342Y/+}$* observed at E16.5 signifies the ossification process between both mouse models is functionally distinct. In line with previous report, suture overgrowth was identified in *Fgfr2c$^{C342Y/+}$* and this chapter further reports ectopic ALP activity in the mesenchyme (Eswarakumar et al., 2004). The ectopic expression of ALP in the mesenchyme echoes those in the Apert mouse model (*Fgfr2$^{P253R/+}$*), in parallel with increased osteoblast commitment in the osteogenic fronts (Wang et al., 2010). These reports suggest a common characteristic in GOF mutations, where these mutations drive ectopic osteoblast differentiation to aid premature suture closure. *R26R$^{Fgfr2cV5/+}$*; *βactin$^{CRE/+}$* displays insufficient osteoblast activity in the coronal suture at E16.5, implying insufficient osteoblastogenesis. FGFR2 signalling is a mitogenic factor and is involved in osteoblast maturation, the phenotype observed in *R26R$^{Fgfr2cV5/+}$*; *βactin$^{CRE/+}$* suggests delays to this program (Ornitz and Itoh, 2015). The master regulator for osteoblast differentiation- *Runx2*, is well characterised to be downstream of the FGF signalling pathway, and it would be ideal to

investigate whether there are aberrations to osteoblast commitment in these sutures, along with markers for early and late osteoblasts (Xiao et al., 2000, Miraoui et al., 2009).

It should be noted that WT-FGFR2 overexpression and FGFR2-C342Y are functionally distinct as the former is ligand dependent, and receptor activation will depend on the concentration of ligand available endogenously. Thus, these receptors are mechanistically different, and would drive distinctive signalling interpretations and characteristic phenotypes (Miraoui et al., 2009). For instance, Miraoui et al., 2009 reports that PLCγ-PKC is a major effector of osteoblast differentiation in mutant FGFR2-S252W to that of the WT, where the latter signals through RAS-MAPK cascade. Here, ectopic osteoblast differentiation was only rescued through the knockdown of the PLC-PKC pathway in cells carrying the mutant receptor (Miraoui et al., 2009). Given by the data reported *in vitro*, the functional basis of the receptor is distinct from one another, where mutations affecting the receptor drive preferential bias towards an effector cascade. Of note, mutant FGFR2 has greater stimulatory effect for osteoblast commitment and mineralization than receptor overexpression, where the latter express latent cellular activity (Miraoui et al., 2009).

Maintaining a correct balance of osteoblast proliferation-differentiation is critical for suture patency. $R26R^{Fgfr2cV5/+}$; $\beta actin^{CRE/+}$ display similarities with the $Fgfr2c^{-/-}$ in the coronal suture through decreased appositional growth (Eswarakumar et al., 2002). Specifically, $R26R^{Fgfr2cV5/+}$; $\beta actin^{CRE/+}$ have decreased osteoblast commitment in the coronal suture, whereas $Fgfr2c^{-/-}$ has decreased cell proliferation and bone formation in the suture (Eswarakumar et al., 2002). However, $R26R^{Fgfr2cV5/+}$; $\beta actin^{CRE/+}$ do not develop coronal synostosis that is in contrast to $Fgfr2c^{C342Y/+}$ and $Fgfr2c^{-/-}$ (Eswarakumar et al., 2004, Eswarakumar et al., 2002). It is likely that the overall signalling disruption by receptor overexpression is less extreme than that of complete signalling removal ($Fgfr2c^{-/-}$), and that of a constitutively active receptor ($Fgfr2c^{C342Y/+}$). This is reflected by the subtlety of the phenotype under ubiquitous receptor overexpression. As mentioned, a speculation that causes the suture undergrowth between $R26R^{Fgfr2cV5/+}$; $\beta actin^{CRE/+}$ and $Fgfr2c^{-/-}$ could lie within aberrations to osteoblast differentiation and maturation program (Yu et al., 2003). Ultimately, there will be less osteoblast generated for

bone formation resulting in underdevelopment of the suture. In contrast, sustained expression of C342Y mutation is likely to result in an amplification of osteoblasts prior to late stage apoptosis that augment pre-mature suture closure in the osteogenic front (Eswarakumar et al., 2004, Holmes and Basilico, 2012, Holmes et al., 2009, Liu et al., 2013). The master regulator for osteoblast differentiation- *Runx2,* is well characterised to be downstream of the FGF signalling pathway, and future efforts should aim to delineate osteoblast commitment in the sutures at multiple stages (Xiao et al., 2000, Miraoui et al., 2009).

Overall, the ALP data presented in this chapter provides a comparative analysis of osteoblast activity in the coronal suture between mouse models with coronal synostosis. The results presented are in line with previous literature, whereby receptor overexpression and FGFR2c-C342Y possess distinct signalling characteristics.

4.3.3-FGFR2c overexpression results in a cleft palate phenotype

Murine palatogenesis commences at E11.5 and is complete by E17.5. Morphogenesis of the murine palate occurs in three major morphogenic events concerning i) vertical outgrowth ii) shelf elevation iii) fusion (Bush and Jiang, 2012). The palate derives from the orofacial prominence, and initial shelf outgrowth occurs after the fusion of maxillary process and medial nasal processes. Of note, the facial prominence is predominantly populated by NCCs (Chai et al., 2000). During this time, the primary and secondary palates are formed as a result of paired outgrowth alongside the tongue. Palatal shelf elevation occurs between E14.5-E15.5 towards the midline, with fusion occurring along the seam after elevation (Bush and Jiang, 2012). Cleft palate is common pedigree to FGFR-related craniofacial syndromes, and a handful of genes have been implicated in syndromic cleft palate inclusive of FGFR2 (Stanier and Pauws, 2012, Bush and Jiang, 2012). However, the prevalence of cleft palate in human Crouzon syndrome is less than that in Apert patients, which may be owed to the mutation affecting both isoforms in the latter (Stanier and Pauws, 2012). Palatogenesis is a tightly regulated process of epithelial and mesenchymal interactions involving FGFR2: However, FGFR2b appears to be the major player involved in palatal shelf elevation as conditional knockout of this isoform or its corresponding ligand, *Fgf10,* led to an overt cleft. *Fgfr2b* expression is restricted to the

epithelium of the palatal shelf, whilst *Fgf10* is confined to the mesenchyme. Cellular analysis of the palatal shelf also shed light on the nature of proliferative activity. *Fgfr2b*$^{-/-}$ has greater impact on decreasing proliferative activity in the epithelium than the mesenchyme (Rice et al., 2004).

The overt cleft phenotype in both *R26R*$^{Fgfr2cV5/+}$; *βactin*$^{CRE/+}$ and *R26R*$^{Fgfr2cV5/+}$; *Wnt1*$^{CRE/+}$ were not fully penetrant: 40% (4/10) of *R26R*$^{Fgfr2cV5/+}$; *βactin*$^{CRE/+}$ embryos display an overt cleft whilst 20% (1/5) for *R26R*$^{Fgfr2cV5/+}$; *Wnt1*$^{CRE/+}$. The partial penetrance may boil down to a multitude of factors. FGF ligands have multiple affinities towards specific isoforms (Zhang et al., 2006). Therefore, ectopic expression of the receptors may have interacted with endogenous ligands in the tissue, especially in the case of *βactin*$^{CRE/+}$, the receptor would be expressed in the epithelium. Lineage tracing using the *R26R*$^{mTmG/+}$; *Wnt1*$^{CRE/+}$ indicates that the palatal shelf mesenchyme is derived from NCCs (Nik et al., 2016). The low penetrance of *R26R*$^{Fgfr2cV5/+}$; *Wnt1*$^{CRE/+}$ indicates that the mesenchyme may play secondary roles in elevation to that of the epithelium, an expected location of *Fgfr2b* expression. Moreover, any phenotypic consequences elicited by receptor overexpression will be determined by the availability of FGF ligands in the tissue. Altogether, the low penetrance of overt cleft in *Fgfr2c* overexpression suggests that the IIIc isoform is less critical than that of the IIIb in shelf elevation. This is evident in the lack of phenotype in *Fgfr2c*$^{-/-}$, which corresponded to the endogenous removal of the receptor *in vivo* (Eswarakumar et al., 2002). However, it is unclear as to the mechanism that leads towards a palatal phenotype in *Fgfr2c*$^{C342Y/C342Y}$ homozygote, but the similarities with *R26R*$^{Fgfr2cV5/+}$; *βactin*$^{CRE/+}$ is perhaps a consequence of insufficient cells generated for shelf elevation (Peskett et al., 2017, Snyder-Warwick et al., 2010).

4.3.4-Ear malformation in *R26R*$^{Fgfr2cV5/+}$; *βactin*$^{CRE/+}$ is an ectopic effect

There are no reports of external ear defects related to human Crouzon syndrome or in *Fgfr2c*$^{C342Y/+}$. However, isolated cases were reported in humans, such as a mutation responsible for Jackson-Weiss syndrome (FGFR2-C342R), which results in hearing loss and ear canal hypoplasia (Park et al., 1995). This study describes *R26R*$^{Fgfr2cV5/+}$; *βactin*$^{CRE/+}$ embryos have microtia with hypoplasia of the tympanic ring.

Interestingly, the microtia phenotype is reflective of lacrimo-auriculo-dento-digital (LADD) syndrome (Rohmann et al., 2006). The biochemical basis for LADD syndrome remains unclear, but appears to be related to FGF signalling via haploinsufficiencies of *FGFR2*, *FGFR3* and *FGF10* (Rohmann et al., 2006). In reference to FGFR2, a number of mutations identified in LADD syndrome affect the intracellular kinase domain of the receptor (Rohmann et al., 2006). Experimentally, mutant FGF10 has reduced binding affinity for FGFR2b and was increasingly susceptible to proteolytic degradation compared to WT-FGF10 (Shams et al., 2007).

However, the external ear phenotype observed in the $R26R^{Fgfr2cV5/+}$; $\beta actin^{CRE/+}$ is a likely consequence of ectopic expression of FGFR2c in the presence of ligands with high affinities for FGFR2b. The lack of ear external phenotype observed in mouse models of *Fgfr2c* suggests this (Eswarakumar et al., 2002, Eswarakumar et al., 2004). Moreover, $Fgfr2b^{-/-}$ leads to inner ear dysgenesis, owing to mispatterning of the otic vesicle (De Moerlooze et al., 2000, Pirvola et al., 2000). Specific features affected by the IIIb knockout include hypoplastic otic vesicle, with dysmorphology of the cochlea and vestibular apparatus during late gestation. Furthermore, cochleovestibular neurons fail to form and under development of the sensory epithelium (Pirvola et al., 2000). Despite no obvious visible defect in the $R26R^{Fgfr2cV5/+}$; $\beta actin^{CRE/+}$ cochlea during whole mount skeleton stains, functional aberrations to the inner ear cannot be ruled out given the prominent role of FGFs in ear development. Of note, a clear hypoplastic tympanic ring was seen in the $R26R^{Fgfr2cV5/+}$; $\beta actin^{CRE/+}$ that phenocopies to that of $Fgfr2c^{-/-}$ at E18.5, implying a role for FGFR2c in ossification of the auditory bulla (Eswarakumar et al., 2002).

4.3.5-Experimental considerations

Perhaps the most difficult aspect of the phenotypic analysis surrounds the subtlety of the phenotype. This is likely due to the phenotype being dependent on the presence of the endogenous ligand. On the quantitative front, post harvest analysis of E18.5 embryos was performed with an electronic caliper, which may not be able to detect any minute phenotypic changes. It was noted for $R26R^{Fgfr2cV5/+}$; $Wnt1^{CRE/+}$ that there was no significant decrease of embryo lengths. In particular, head size reduction was only observed using FIJI software that provided sufficient resolution for analysis. The stunted growth restriction in $R26R^{Fgfr2cV5/+}$; $\beta actin^{CRE/+}$ also promoted the investigation into whether this was a secondary defect of intrauterine constriction. The limb was previously reported to be independent of alterations to FGFR2c signalling in $Fgfr2c^{C342Y/+}$ (Eswarakumar et al., 2002, Eswarakumar et al., 2004). This serves as an internal control to investigate global growth restriction. It was determined in Figure 32 that there was no difference between appendage skeleton length in the mutants, ruling out the possibility of intrauterine constraints. However, it is also ideal to perform phenotypic analysis of placentas in adjunct to limb length in the future. Moreover, due to the lack of phenotypic variations in the limb, it serves a robust constant for data transformation during the morphometric analysis.

Evidence for craniosynostosis development *ex vivo* can be observed after 15 days in culture previously in this lab. It should be noted that calvarial explant cultures were not as robust as *in vitro* cultures. An example of this can be seen in $Fgfr2c^{C342Y/+}$ where a complete fusion of the suture was not observed. Therefore, $Fgfr2c^{C342Y/+}$ was cultured alongside $R26R^{Fgfr2cV5/+}$; $\beta actin^{CRE/+}$ calvaria where possible to serve as an experimental control. Two factors can account for the overall calvarial growth in i) the extent of the bone overlap and ii) the pH indicator in the culture media. Should the calvaria grow over time, the extent of the overlap would be more substantial than that before culture. In the latter case, the media turns yellow to indicate metabolic activity. A second strategy that could be used to bypass the perilethality in $R26R^{Fgfr2cV5/+}$; $\beta actin^{CRE/+}$ is a tamoxifen inducible CRE line. Ideally, tamoxifen would be administered after palatal closure at around E15.5 to induce *Fgfr2c* overexpression.

This is a plausible strategy to overcome the perilethality but ultimately, it depends on whether the research question is aimed at addressing suture formation or its patency. In the latter circumstance, along with the progressive nature of craniosynostosis, then using a tamoxifen inducible CRE line is desirable. However, suture formation commences between E12.5-E13.5 and using an inducible CRE would not address questions concerning early embryogenesis in this experiment (Iseki et al., 1997, Deckelbaum et al., 2012).

4.3.6-Future directions

For the duration of this project, efforts were focused upon the frontal and parietal bones of the calvaria. The next stage of the morphometric analysis should be migrated onto micro-CT and compare the phenotype to that of *Fgfr2c*$^{C342Y/+}$. Data obtained from micro-CT will have sufficient resolution to perform further analysis that concerns volume and bone density. The latter case is of particular interest as osteoblasts derived from the NCCs and mesoderm differs in their mineralisation potentials (Senarath-Yapa et al., 2013). Therefore, it would be informative to appreciate the overall porosity of *R26R*$^{Fgfr2cV5/+}$; *βactin*$^{CRE/+}$ and *Fgfr2c*$^{C342Y/+}$ to compare the ossification ratios. In regards to the calvarial explants, it would be interesting to observe whether craniosynostosis can be induced through FGF bead implants at the suture, given the increased number of receptors present through overexpression. This overall experiment would be sufficient to show that there is insufficient ligand present to drive suture closure in *R26R*$^{Fgfr2cV5/+}$; *βactin*$^{CRE/+}$.

Abnormal cellular activity is a consequence of signalling misregulation. A handful of studies examined the cellular proliferation directly in the coronal sutures of mouse models for syndromic craniosynostosis (Eswarakumar et al., 2004, Wang et al., 2005b, Holmes and Basilico, 2012). It is important to note that proliferative assays label cells at multiple stages of the cell cycle: markers such as Ki67 are abundant throughout the cell cycle, whereas BrdU only labels the S-phase (Iatropoulos and Williams, 1996). Future studies should aim to perform co-labelling of markers to fully clarify the ratio of cells undergoing proliferation and differentiation. For example, Ki67/EdU co-labelling can be used to understand the ratio of cells exiting the cell cycle for osteoblast differentiation in the suture, with an aim to address whether

there are aberrations to terminal differentiation (Haston et al., 2017). Therefore, the overall aim of this experiment is to improve clarity for cellular proliferation, and to fully determine whether is any disruption to the overall osteoblast differentiation program.

Chapter 5

Results (Part III)

Comparison of the FGFR2 signalling pathway in *Fgfr2c*$^{C342Y/+}$ and *R26R*$^{Fgfr2cV5/+}$*; βactin*$^{CRE/+}$ mice

5.1-Introduction

R26R$^{Fgfr2cV5/+}$*; βactin*$^{CRE/+}$ and *Fgfr2c*$^{C342Y/+}$ result in distinct phenotypes. It is well known that constitutive active FGFR2 leads to upregulation of the RAS-MAPK pathway, and that pERK serves as a readout for FGF signalling misregulation (Pfaff et al., 2016). Inspection of the RAS-MAPK cascade is mainly performed using immunoblots, with the spatial localization of pERK expressing cells remaining unclear in vivo. A single study shows the expression of pERK in the coronal suture but without sufficient clarity (Deckelbaum et al., 2005). In the current study, the phospho-epitope was found to be preserved *in vivo*, and pERK signal was amplified with streptavidin conjugates. Furthermore, this chapter demonstrates pERK is co-expressed in osteoblasts marked by the expression osteopontin. As FGFR2 plays multiple roles in proliferation, differentiation and survival, visualizing pERK activity allows the inference of biochemical activity during suture morphogenesis. Further to this, this study examined the expression of multiple FGFR2 RAS-MAPK target genes (*Spry2, Spry4, Etv5*) using ISH and RT-qPCR.

5.2-Results

5.2.1-FGFR2c overexpression and FGFR2c-C342Y mutation lead towards an overactive RAS-MAPK pathway *in vivo* and *in vitro*

To assess whether *Fgfr2c* overexpression leads to a similar activation of the RAS-MAPK pathway, the levels of pERK was investigated *in vivo* and *in vitro*. In this respect, expression of pERK was visualised in E16.5 coronal sutures using immunohistochemistry, at a stage where the sutures were morphologically similar (Control: n=4; $Fgfr2c^{C342Y/+}$: n=4; $R26R^{Fgfr2cV5/+}$; $\beta actin^{CRE/+}$: n=3) (Figure 45). pERK is expressed all along the perimeter of the frontal and parietal bones and upon closer inspection, cells positive for pERK co-express osteopontin, indicative of mature osteoblasts (Figure 45 A). Interestingly, both mutants show an increase of pERK expression as compared to controls (Figure 45 A). Both $Fgfr2c^{C342Y/+}$ and $R26R^{Fgfr2cV5/+}$; $\beta actin^{CRE/+}$ mutants display increased pERK expression at the osteogenic fronts of the bones flanking the suture (compare Figure 45 A and Figure 45). pERK activity was also modelled *in vitro* using HEK293Ts (n=4 independent transfections) (Figure 45 B). pERK 1 and 2 were activated upon transfection of pFGFR2cV5 ('IIIc-V5') (encoding the wild-type FGFR2-IIIc isoform) and pFGFR2c-C342Y-V5 ('C342Y-V5') (encoding the mutated receptor) relative to mock transfected cells. Further, there was an increase of ERK1 and ERK2 phosphorylation in both instances. Quantification of the blots using densitometry reveals significant upregulation of pERK in both FGFR2cV5 transfected conditions (Figure 45 C). Specifically, there was significantly more pERK activity in the C342Y-V5 ($p<0.0001$) and IIIc-V5 ($p=0.0101$) transfected cells relative to the pcDNA control cells as expected from the Western blot results. Cells transfected with C342Y-V5 has an increased pERK output by 8.1 units than that of WT-V5 transfected group ($p=0.0005$) likely due to the constitutive activation of the mutant receptor.

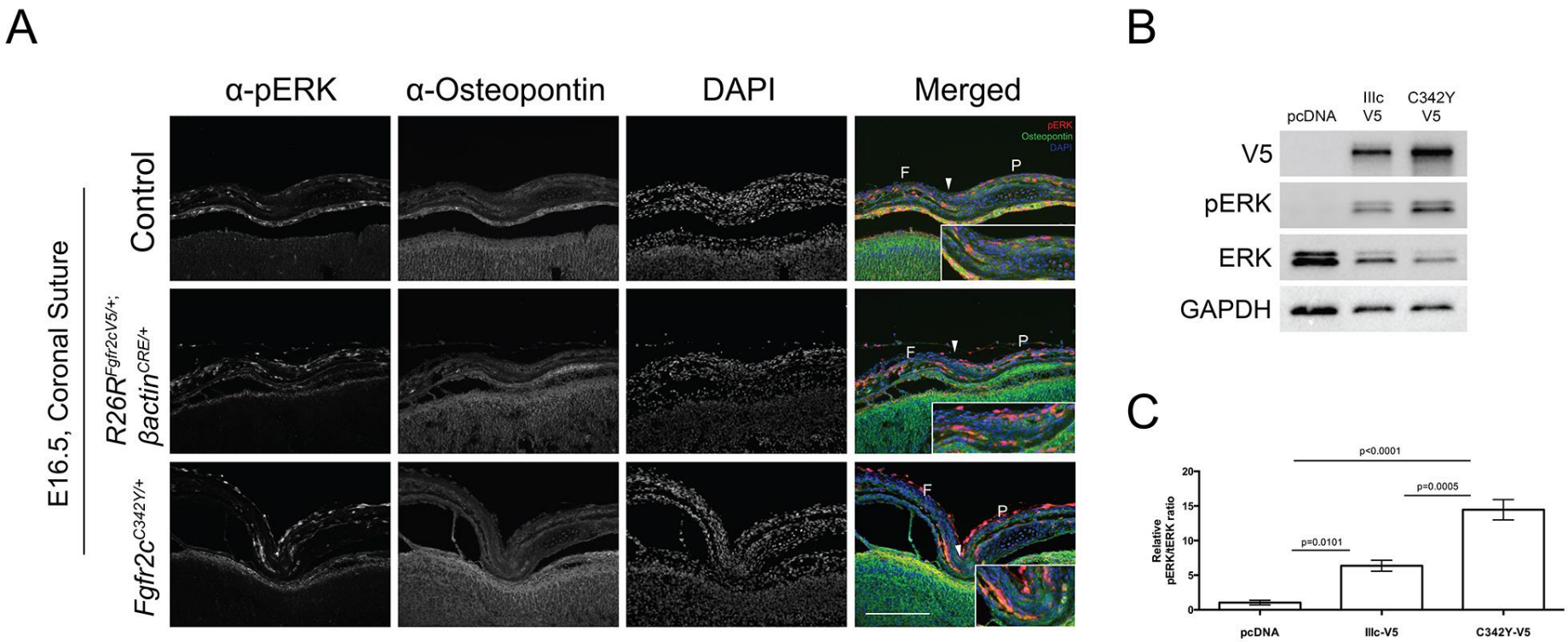

Figure 45: Upregulation of pERK *in vivo* and *in vitro* in $R26R^{Fgfr2cV5/+;}$ $\beta actin^{CRE/+}$ and $Fgfr2c^{C342Y/+}$.

(A) pERK (red) coincides with the expression of osteopontin along the periphery of the bone and the osteogenic front at E16.5, marking mature osteoblasts. Both $R26R^{Fgfr2cV5/+}$; $\beta actin^{CRE/+}$ and $Fgfr2c^{C342Y/+}$ have upregulated pERK (red) *in vivo* as compared to controls. The invagination in $Fgfr2c^{C342Y/+}$ was an artefact of tissue processing (B) Western blot to demonstrate upregulation of pERK upon cellular transfection of pFgfr2IIIc-V5 (IIIc-V5) and pFgfr2c-C342Y-V5 (C342Y-V5) plasmids in HEK293Ts. (C) Relative pERK:tERK ratio quantified by densitometry of transfected HEK293T cells. F: Frontal Bone; P: Parietal Bone; White arrow marks the location of the coronal suture; Insert is a magnified cropped of the coronal suture; Statistics: Oneway ANOVA with Tukey's posthoc. Error bars: SEM. Scale Bar: 200um.

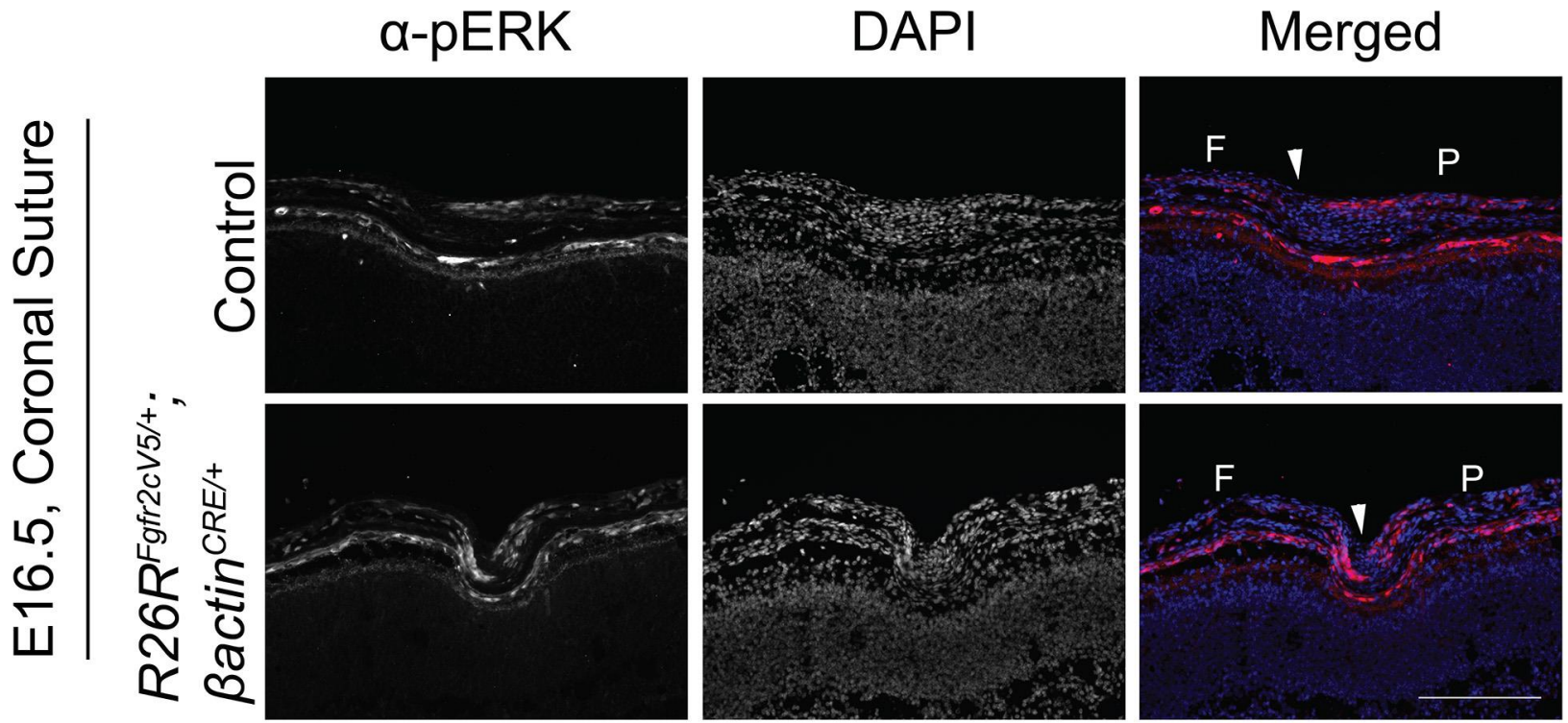

Figure 46: Expression of pERK in the osteogenic front is also present in *R26R$^{Fgfr2cV5/+}$; βactin$^{CRE/+}$*.

pERK expression is also detected in the osteogenic fronts of control and *R26R$^{Fgfr2cV5/+}$; βactin$^{CRE/+}$*. White arrowhead depicts the location of the coronal suture. F: Frontal bone; P: Parietal bone. Scale bar: 200um.

5.2.3-Expression of *SPRY2, SPRY4, ETV5* in HEK293T cells

In addition to relative biochemical activity, HEK293T cells were transfected with IIIc-V5 and C342Y-V5 to model the downstream activity of FGF signalling *in vitro*, and to compare the differences between receptor overexpression and the C342Y mutation. In general, there was an increase of readout transcript upon cellular transfection of IIIc-V5 and C342Y-V5 plasmids into HEK293Ts (n=4). Expression of *FGFR2c* was confirmed using assays for the *Fgfr2c* gene and a negative control of *Fgfr2b* (Figure 47). The raw data for the transfected plates are represented in Figure 47. There was a significant increase between pcDNA and C342Y-V5 transfected conditions in both *SPRY4* (Oneway ANOVA: $F(2,9)=9.85$, $p=0.005$; Tukey's: $p=0.004$) and *ETV5* (Oneway ANOVA: $F(2,9)=9.197$, $p=0.007$; Tukey's: $p=0.005$) expression (Figure 48 B and C). Expression was increased by an average of 37.8 units for *SPRY4* and 64.0 units for *ETV5* respectively (Figure 48 B and C). Transcript increase lies close to statistical significance pcDNA and IIIc-V5 conditions (*SPRY4*: Tukey's: $p=0.076$; *ETV5*: Tukey's: $p=0.084$) (Figure 48 B and C). No differences were detected between the IIIc-V5 and C342Y-V5 transfected groups for all readout assays. In regards to *SPRY2*, there were no expression changes between all transfected conditions (Figure 48 A). Moreover, the average RQ value was low upon all conditions suggesting the absence of *SPRY2* regulation in HEK293T cells.

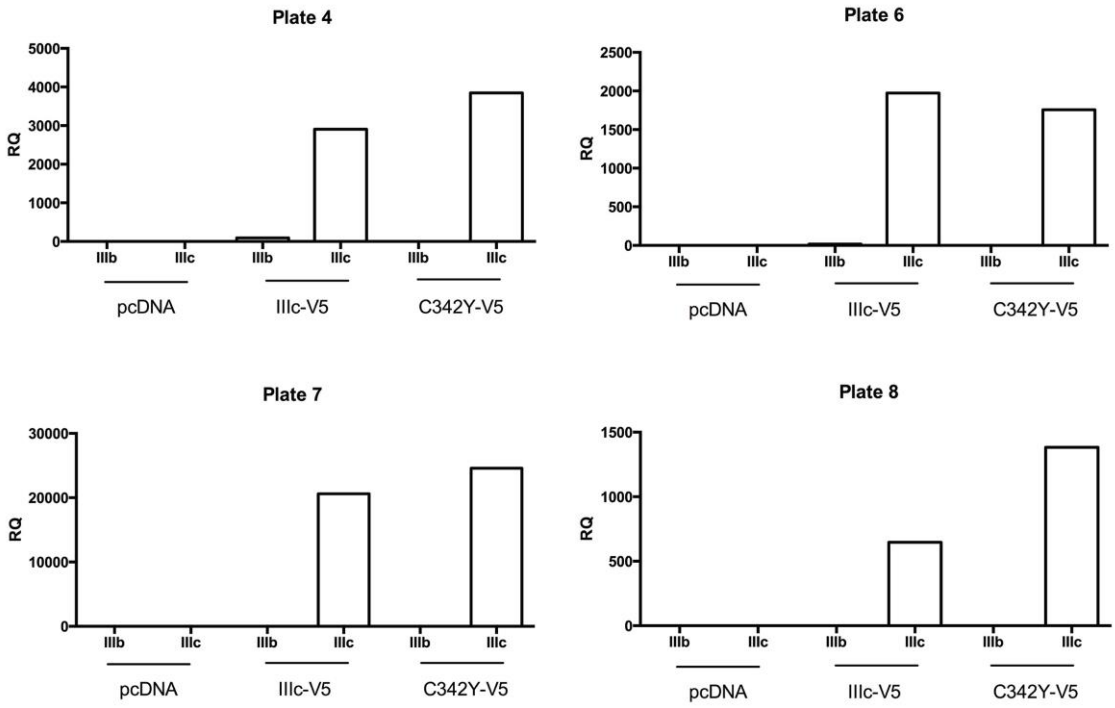

Figure 47: Expression validation of cells transfected with either IIIc-V5 or C342Y-V5 plasmids.

There is a marked increase of *Fgfr2c* (IIIc) transcripts but not *Fgfr2b* (IIIb), confirming the success of the transfection.

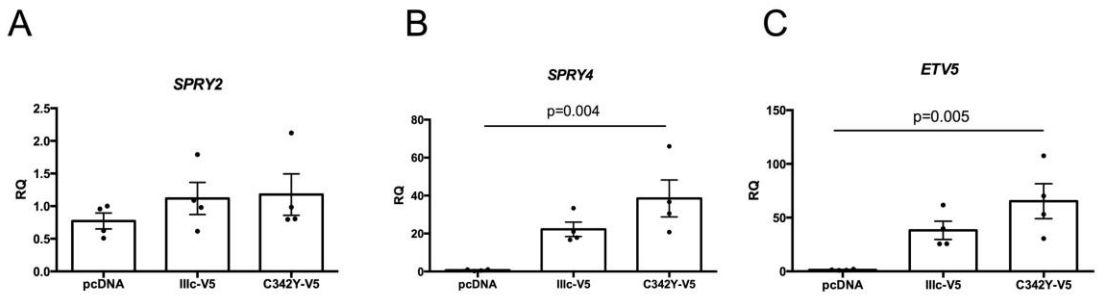

Figure 48: *SPRY2*, *SPRY4* and *ETV5* expression in transfected cells.

(A) Low RQ values between all transfected conditions suggest the absence of *SPRY2* regulation in HEK293Ts; (B) Significant increase in *SPRY4* transcript between C342Y-V5 and pcDNA conditions (p=0.004; n=4); (C) Significant increase in *ETV5* transcript between C342Y-V5 and pcDNA conditions (p=0.005; n=4). Statistics: Oneway ANOVA with Tukey's posthoc test. Error bars depict SEM.

5.2.4-No ectopic expression of FGFR2c signalling in E16.5 coronal sutures

Next, ISH was performed in sections to determine the expression of FGFR2 signalling target genes *in vivo* at E16.5 (Figure 49). *Spry2* (A-C), *Spry4* (D-F) and *Etv5* (G-I) are direct transcription targets of FGFR2c signalling and the RAS-MAPK cascade (Snyder-Warwick et al., 2010, Ornitz and Itoh, 2015). Due to the difficulty of preserving suture integrity in frozen sections, several biological replicates were performed using paraffin wax (Figure 49 C & F). *Spry2, Spry4* and *Etv5* were expressed along the frontal and parietal bones without any ectopic activity detected in the coronal suture of both $R26R^{Fgfr2cV5/+}$; $\beta actin^{CRE/+}$ (*Spry2*: n=3; *Spry4*: n=3; *Etv5*: n=5) and $Fgfr2c^{C342Y/+}$ (*Spry2*: n=4; *Spry4*: n=3; *Etv5*: n=3) to the controls (*Spry2*: n=5; *Spry4*: n=4; *Etv5*: n=3). Additionally, *Spry2* and *Spry4* expression were also detected in the epidermis of the skin. While both models show an activated RAS-MAPK pathway in the suture, the fact that only $Fgfr2c^{C342Y/+}$ activation results in craniosynostosis suggest that FGFR2c overexpression cascade activation is functionally distinct to that of the mutant receptor.

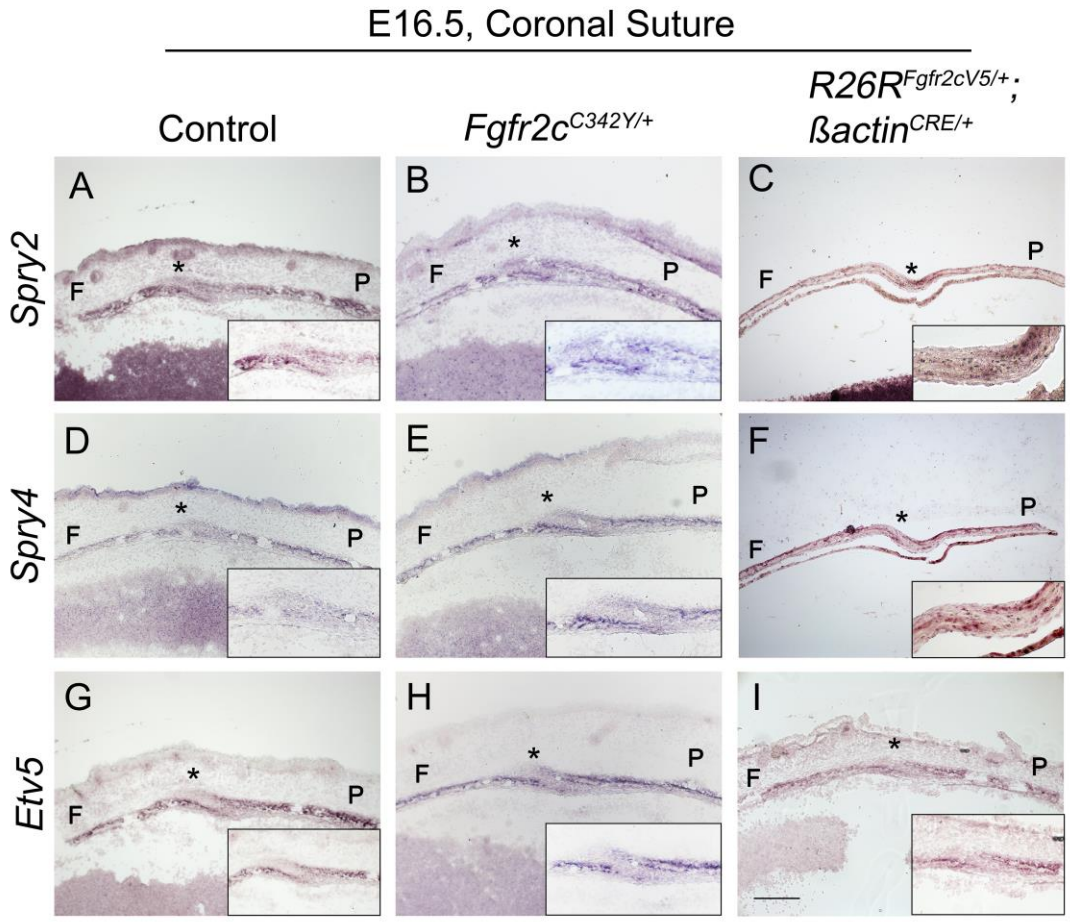

Figure 49 No ectopic expression of FGFR2 signalling readouts *in vivo*. (A-C) ISH of *Spry2*; (D-F) *Spry4*; (G-I) *Etv5*.

Inserts are high-resolution crop outs of the coronal suture (*). ISH was performed in paraffin sections in (C) and (F). F: Frontal bone, P: Parietal bone. Scale bar: 200um.

5.3-Discussion

5.3.1-Biochemical similarities between *R26R$^{Fgfr2cV5/+}$*; *βactin$^{CRE/+}$* and *Fgfr2c$^{C342Y/+}$*

FGFR2 signalling activation plays multiple roles in cellular proliferation, differentiation, and apoptosis (Miraoui et al., 2009, Mansukhani et al., 2000). The master regulator for osteoblast differentiation- *Runx2,* is well characterised to be downstream of the FGF signalling pathway (Xiao et al., 2000, Miraoui et al., 2009), and that exposures to FGF ligands are sufficient to drive osteoblast gene expression (Iseki et al., 1997, Miraoui et al., 2009, Xiao et al., 2000, Kim et al., 2003a). Interestingly, pERK cellular expression was not solely confined to the osteogenic front, but also along the outer edges of the bone. In general, both *R26R$^{Fgfr2cV5/+}$*; *βactin$^{CRE/+}$* and *Fgfr2c$^{C342Y/+}$* exhibited upregulated pERK readouts. A plausible explanation for the phenotypic differences observed in this study, albeit with similarities in RAS-MAPK signalling properties, is that activating mutations to FGFR2 elicit dissimilar cascade activation to that of WT-FGFR2 (Kim et al., 2003a, Miraoui et al., 2009). Miraoui et al., 2009 compared the differences in cascade activation and concluded that Apert-FGFR2-S252W transactivates the PLCγ-PKC pathway to drive ectopic osteoblast differentiation, whereas WT-FGFR2 predominantly signals through the RAS-MAPK in MSCs (Miraoui et al., 2009). Eventually, this misregulation by mutant FGFR2 drives elevated matrix mineralisation and ALP activity (Miraoui et al., 2009). Other growth factor pathways such as PDGFR also behave similarly, where increasing levels of PDGFR signalling is sufficient to drive ectopic osteogenesis and complex craniosynostosis via PLCγ-PKC pathway *in vivo* (Moenning et al., 2009). The skeletal hypoplasia, coronal suture patency and increased porosity observed in *R26R$^{Fgfr2cV5/+}$*; *βactin$^{CRE/+}$* suggests delayed osteoblast maturation, but it is unknown how *Fgfr2c* overexpression interrupts this harmony. As FGFR2 is critical for cell-renewal, one speculation is shifting the balance from osteoblast differentiation to proliferation in early development. This hypothesis is supported by *in vitro* cultures of MSCs, as exposure to FGF2 promotes stemness in the presence of osteoblast differentiation media (Baddoo et al., 2003).

The upregulated pERK in *R26R*$^{Fgfr2cV5/+}$; *βactin*$^{CRE/+}$ can also be explained by sensitization of signalling activity due to the over abundance of FGFR2c. In this respect, the ratio between receptor to endogenous FGF ligand is greatly bolstered. An example of signalling sensitization can be linked to pain and nociception, as glutamate receptors are upregulated to enable neurons to be hyperexcitable (Harris et al., 1996). This can be tested *in vitro*, by comparing the ratios between ligands tagged with radioisotope to surface receptors. Given the nature that ectopic osteogenesis can be achieved through constant exposure of FGF ligands *in vitro* and *in vivo*, the lack of coronal synostosis in *R26R*$^{Fgfr2cV5/+}$; *βactin*$^{CRE/+}$ is likely to be insufficient ligand present endogenously to drive the osteogenic program (Iseki et al., 1997, Sarkar et al., 2001). This property can be related to the decreased appositional growth and osteoblast activity observed in the sutures of *R26R*$^{Fgfr2cV5/+}$; *βactin*$^{CRE/+}$ (Figure 44).

5.3.2-Expression analysis of *SPRY2*, *SPRY4* and *ETV5 in vitro*

Spry2, *Spry4* and *Etv5* were previously described as direct readouts of the RAS-MAPK pathway (Snyder-Warwick et al., 2010, Pratilas et al., 2009). There are four Sprouty proteins identified in both mouse and humans, acting to suppress RTK signalling at multiple levels (Ornitz and Itoh, 2015). SPRY2 protein suppresses FGF signalling early on in the cascade through Grb2-Sos intervention, to prevent recruitment of FRS2, whilst SPRY4 acts downstream to inhibit Raf activation (Hanafusa et al., 2002, Sasaki et al., 2003). Together with ETV4, ETV5 constitute to the Erm family of proteins responsible for downstream FGFR2 gene expression (Firnberg and Neubuser, 2002, Chotteau-Lelievre et al., 2001). As these are driven directly by FGF signalling, they would provide a good marker for potential downstream signalling aberrations.

Cellular transfection of HEK293Ts was adopted to model the overall downstream activity of the RAS-MAPK pathway. Interestingly, cellular transfection did not affect *SPRY2* expression, suggesting it is not directly downstream of FGFR2c signalling in this cell line. However, *SPRY4* and *ETV5* did display transcript changes post transfection, indicating the presence of *SPRY4* and *ETV5* in HEK293Ts. The lack of statistical significance between pcDNA and IIIc-V5 conditions is related to the nature of the statistical test. The low sample

population and unequal variance (Levene's test, p=0.056 for *SPRY4* and p=0.064 for *ETV5*) between test groups would have influenced the outcome of Oneway ANOVA and Tukey's post hoc tests leading towards Type II error ('False negative') (e.g. pcDNA and IIIc-V5 conditions). Overall, the outcome of this experiment is a proof of concept that increased downstream readout activity is corresponded with *Fgfr2c* overexpression and those carrying GOF mutations i.e. $Fgfr2c^{C342Y/+}$.

5.3.3-Similar expression patterns of FGFR2 signalling readouts in the coronal suture

FGF signalling readouts were not ectopically expressed in either $Fgfr2c^{C342Y/+}$ and $R26R^{Fgfr2cV5/+}$; $\beta actin^{CRE/+}$. On the one hand, ISH is a qualitative assay and may not provide sufficient resolution to detect subtle changes at transcript levels. However, this experiment did provide information to show that FGF signalling is confined within a specific spatial domain, along the membranous bones and the osteogenic front. This is expected as the expression of readouts coincides with periosteoblasts-cells known to be expressing *Fgfr2* (Deckelbaum et al., 2005, Johnson et al., 2000). However, owing to the nature of ubiquitous overexpression and the morphogenic nature of FGFs, ectopic expression is to be expected in the $R26R^{Fgfr2cV5/+}$; $\beta actin^{CRE/+}$ suture mesenchyme. The lack of misexpression in these overexpressing mutants suggests FGFs act locally, perhaps confined to the osteogenic front, as opposed to long-range cues within the suture to govern osteogenesis. For example, *Fgf18* and *Fgf20* transcripts are detected in the osteogenic fronts of the coronal suture, coinciding with those genes involved in FGFR2 signalling, pointing towards potential autocrine interactions (Hajihosseini and Heath, 2002, Ornitz and Itoh, 2015).

As a high concentration of FGFs is required for osteogenesis and bone mineralisation, the spatial confinement of FGF signalling suggests craniosynostosis is a result of ectopic bone formation from the osteogenic fronts (Sarkar et al., 2001). The abundance of FGFs from the leading edge of the osteogenic front would have recruited additional MSCs from the suture mesenchyme to differentiate into this lineage. Therefore, the overall pool of MSCs in the

mesenchyme would be depleted over the course of development leading to premature suture abolishment.

5.3.4-Future direction

In vitro: A substantial number of experiments in this project are *in vivo* orientated. However, future work should be focused on *in vitro* assays as they offer a robust platform to dissect out molecular and cellular events. For instance, the expression analysis experiment using HEK293T cells is a proof of concept that qualitative (ISH) data can be backed up with quantitative approaches. HEK293T cells are however, immortalized and therefore not the optimal cell line to perform expression analysis, despite its advantage in modelling biochemical cascades. Therefore, using a more suited cell line such as MC3T3s, or through the generation of primary cultures from the calvaria of $Fgfr2c^{C342Y/+}$ and $R26R^{Fgfr2cV5/+}$; $\beta actin^{CRE/+}$, would help to ensure the relevance of future *in vitro* experiments. There is a protocol available to generate primary cultures from the calvaria (Appendix 10), which involves treating the tissue with a series of protease. However, the protocol does not account for lineage specific osteoblasts, and methods must minimize lineage mixing as they have different osteogenic potentials (Senarath-Yapa et al., 2013, Quarto et al., 2010). This could be achieved by using flow cytometry against relevant markers specific to lineage specific osteoblasts. Future experiments could include the molecular basis for osteoblast differentiation and maturation. This is achieved by performing expression analysis on markers such as *Runx2* and *Osterix*, or those involved in late stage differentiation such as *Sclerostin* or *Osteocalcin*. Next, cells from primary cultures could be assessed for the rate of ossification, which can be achieved through ALP and alizarin red assays.

In vivo: The *in vivo* experiments should aim to backup findings from the *in vitro* environment, and seek to understand the cellular events in the suture. For instance, these experiments would be accomplished by IHC, and should focus on the differences of osteoblast commitment and maturation between the mouse models. Moreover, it would be important to demonstrate the co-expression of FGFR2c and pERK in the suture, which shows the contribution of FGFR2c in suture morphogenesis. However, this was not achieved owing to the lack of a robust FGFR2c antibody. One of the feedback regulators not investigated in this study

is Dusp6, a direct inhibitor of activated ERK. Coronal synostosis is a hallmark of *Dusp6*$^{-/-}$, implying signalling augmentation in this pathology (Li et al., 2007). In particular, there is no literature that presents the activity of *Dusp6* in the suture. As negative feedback occurs at the protein level, it would be crucial to compare the active Dusp6 (p-Dusp6) expression in both mouse models.

Chapter 6

Results (Part IV)

Exploring RAS-MAPK pathway misregulation *in vivo*

6.1-Introduction

The results of this chapter are divided into two sections:

- Part A explores the impact of ubiquitous *Fgfr2c* overexpression on *Fgfr2c*$^{C342Y/+}$. This is because as *Fgfr2c* overexpression does not cause coronal synostosis, this experiment questions whether the addition of this allele to the *Fgfr2c*$^{C342Y/+}$ would modify the craniofacial phenotype.
- Part B focuses on over-activation of the RAS-MAPK pathway using the *KRas*$^{LSL\text{-}G12D/+}$ (Tuveson et al., 2004). The aim of oncogenic KRas is to examine the role of RAS-MAPK signalling in craniofacial development by minimizing cross talks at the level of the receptor.

6.2-Results: Part A

6.2.1-Gross phenotype of *R26R$^{Fgfr2cV5/+}$;βactin$^{CRE/+}$;Fgfr2c$^{C342Y/+}$*

To assess the impact of the overexpression allele on *Fgfr2c$^{C342Y/+}$*, a double mutant carrying both the *Fgfr2c-C342Y* and *Fgfr2c* overexpression allele was generated (*R26R$^{Fgfr2cV5/+}$;βactin$^{CRE/+}$;Fgfr2c$^{C342Y/+}$*). The most apparent external anomaly resulting from *Fgfr2c* overexpression alone was microtia (Figure 50; arrow). This was exacerbated in double mutants where anotia was present in 90% of mice (Figure 50; dotted box) (n=10/11). External ear development was normal in *Fgfr2c$^{C324Y/+}$* mutants (n=15). As expected, *R26R$^{Fgfr2cV5/+}$; βactin$^{CRE/+}$* (n=11) displayed shortened head length to controls (Oneway ANOVA with Tukey's post-hoc test: p=0.018; Δ3.43) (Figure 51A). This significant decrease was also present in *R26R$^{Fgfr2cV5/+}$;βactin$^{CRE/+}$;Fgfr2c$^{C342Y/+}$* embryos (n=8; p=0.001; Δ5.24). Head length remained normal in *Fgfr2c$^{C342Y/+}$* (n=10) in respect to the controls, but were significantly larger than that of *R26R$^{Fgfr2cV5/+}$;βactin$^{CRE/+}$;Fgfr2c$^{C342Y/+}$* (p<0.001; Δ6.50). Embryos carrying the overexpression allele were significantly lighter in weight: *R26R$^{Fgfr2cV5/+}$;βactin$^{CRE/+}$; Fgfr2c$^{C342Y/+}$* displayed significant weight attenuation in respect to the controls (p=0.009; Δ10.14) and *Fgfr2c$^{C342Y/+}$* (p=0.009; Δ10.14) (Figure 51 C). As expected, *R26R$^{Fgfr2cV5/+}$; βactin$^{CRE/+}$* displayed significant reduction in weight to the control group (p=0.001; Δ9.86), in addition to *Fgfr2c$^{C342Y/+}$* (p=0.028; Δ8.10). No significant difference was observed in crown-rump length between all genotypes (Figure 51 B).

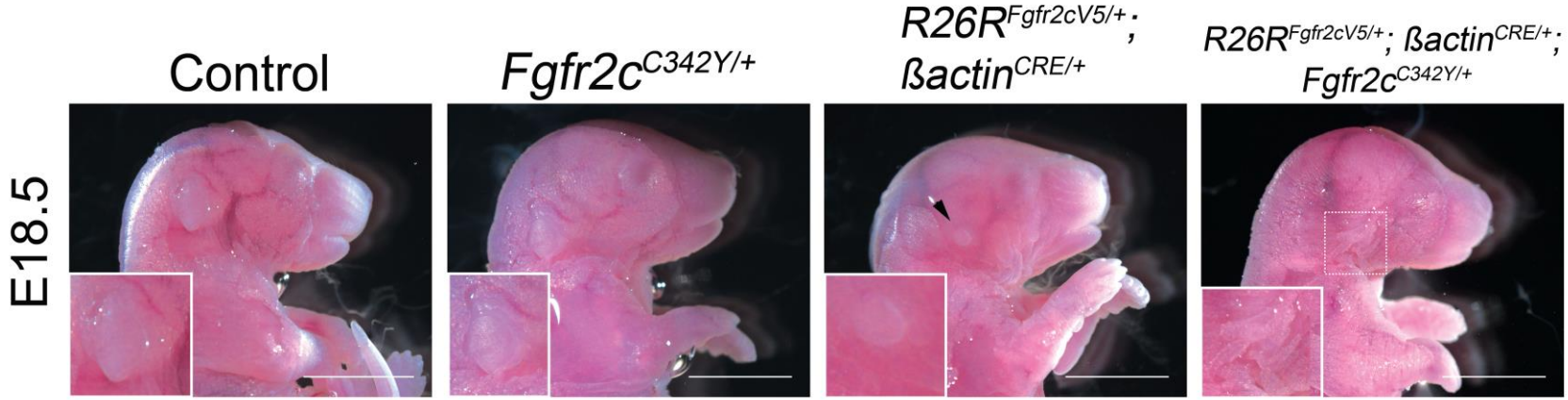

Figure 50 Gross phenotype of *R26R$^{Fgfr2cV5/+}$; βactin$^{CRE/+}$;Fgfr2c$^{C342Y/+}$*.

R26R$^{Fgfr2cV5/+}$; βactin$^{CRE/+}$;Fgfr2c$^{C342Y/+}$ embryos displays anotia (dotted box) compared to anotia seen in *R26R$^{Fgfr2cV5/+}$; βactin$^{CRE/+}$*. Inserts are cropped images of the external ear. Scale bar: 5mm.

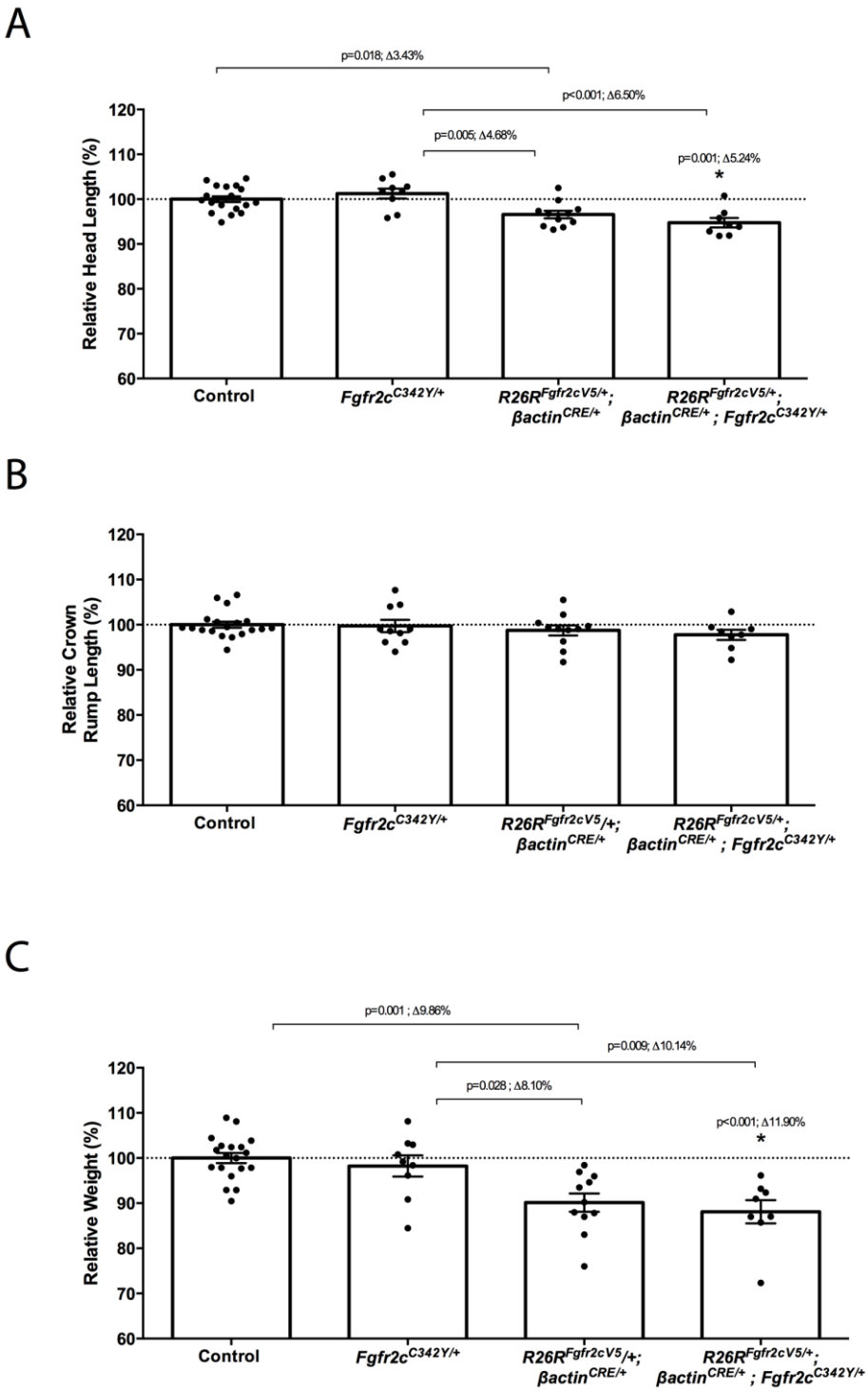

Figure 51: Post harvest quantification of *R26R$^{Fgfr2cV5/+}$;βactin$^{CRE/+}$;Fgfr2c$^{C342Y/+}$*.

(A) The head length of *R26R$^{Fgfr2cV5/+}$; βactin$^{CRE/+}$; Fgfr2c$^{C342Y/+}$* were significantly smaller than that of *Fgfr2c$^{C342Y/+}$* and control groups (*); (B) CRL was unchanged in *R26R$^{Fgfr2cV5/+}$; βactin$^{CRE/+}$; Fgfr2c$^{C342Y/+}$* relative to the controls; (C) *R26R$^{Fgfr2cV5/+}$; βactin$^{CRE/+}$; Fgfr2c$^{C342Y/+}$* were significantly lighter than the controls (*) and *Fgfr2c$^{C342Y/+}$*. Statistics: Oneway ANOVA with Tukey's posthoc test. Error bars depict SEM; Δ: Difference of means between the genotypes.

6.2.2-Introduction of the *Fgfr2c* overexpression allele into *Fgfr2c*$^{C342Y/+}$ partially rescues the Crouzon phenotype

As FGFR2c overexpression does not cause suture synostosis, the question remains whether the addition of this allele to the *Fgfr2c*$^{C342Y/+}$ mice would change the craniofacial phenotype. To assess the impact of the overexpression allele on *Fgfr2c*$^{C342Y/+}$, morphometric analysis on the calvaria was carried out as previously described in Section 2.8. Examination of the craniofacial skeleton reveal partial rescue of the Crouzon phenotype (Figure 52): An enlarged interfrontal wormian bone is characteristic of *Fgfr2c*$^{C342Y/+}$ (n=6/7) (Figure 52 E arrowhead), and these were generally smaller in *R26R*$^{Fgfr2cV5/+}$;*βactin*$^{CRE/+}$;*Fgfr2c*$^{C342Y/+}$ (n=4/5), combined with an enlarged widening of the posterior interfrontal suture (Figure 52; E and H line). However, an overt palate and tympanic hypoplasia were still present in these mutants (n=7/7 analysed) (Figure 52 F and I; arrowhead and * respectively).

6.2.3-*R26R*$^{Fgfr2cV5/+}$; *βactin*$^{CRE/+}$; *Fgfr2c*$^{C342Y/+}$ yields hypoplasia of the calvarial bones

Morphometric analyses of calvarial bones show that *R26R*$^{Fgfr2cV5/+}$;*βactin*$^{CRE/+}$;*Fgfr2c*$^{C342Y/+}$ frontal bones were smaller than that of the control (Δ11.86; p<0.001; Control: n=8, *R26R*$^{Fgfr2cV5/+}$;*βactin*$^{CRE/+}$;*Fgfr2c*$^{C342Y/+}$: n=6) (Figure 53 A). Significant size reduction was also present when *R26R*$^{Fgfr2cV5/+}$; *βactin*$^{CRE/+}$ frontal bones were compared to *Fgfr2c*$^{C342Y/+}$ (Δ9.19%; p=0.001; n=6). Also, there was a significant decrease in frontal bone size between both *R26R*$^{Fgfr2cV5/+}$;*βactin*$^{CRE/+}$;*Fgfr2c*$^{C342Y/+}$ (Δ14.80%; p<0.001; n=6) when compared with *Fgfr2c*$^{C342Y/+}$ (n=10). Morphometric analysis of the parietal bones indicates significant increase in the parietal bone of *Fgfr2c*$^{C342Y/+}$ (n=10) as compared to all other genotypes (Control: Δ6.54%, p=0.001, n=8; *R26R*$^{Fgfr2cV5/+}$; *βactin*$^{CRE/+}$: Δ6.08%, p=0.006, n=6; *R26R*$^{Fgfr2cV5/+}$;*βactin*$^{CRE/+}$;*Fgfr2c*$^{C342Y/+}$: Δ5.44%, p=0.016, n=6) (Figure 53 B). Other derivatives of the NCC lineage were also analysed such as the nasal bone and mandible (Figure 53 C and D). The nasal bone were smaller in the *R26R*$^{Fgfr2cV5/+}$;*βactin*$^{CRE/+}$;*Fgfr2c*$^{C342Y/+}$ (Δ18.38%; p=0.033; n=3) to that of *Fgfr2c*$^{C342Y/+}$ (n=5) (Figure 53 C). Inspection of the mandible revealed that embryos carrying the *Fgfr2c* overexpression allele exhibit micronagthia:

$\underline{R26R^{Fgfr2cV5/+};\beta actin^{CRE/+};Fgfr2c^{C342Y/+}}$ (n=7) has smaller mandibles when compared to that of the control (Δ9.50%; p<0.001) and $Fgfr2c^{C342Y/+}$ groups (Δ7.34%; p=0.013; n=9) (Figure 53 D). The same applies to $R26R^{Fgfr2cV5/+}$; $\beta actin^{CRE/+}$ when compared to the control group (Δ4.75%; p=0.002; n=11). Altogether, these results suggest the overexpression allele has exerted influence over $Fgfr2c^{C342Y/+}$, with potential rescue of the parietal bone.

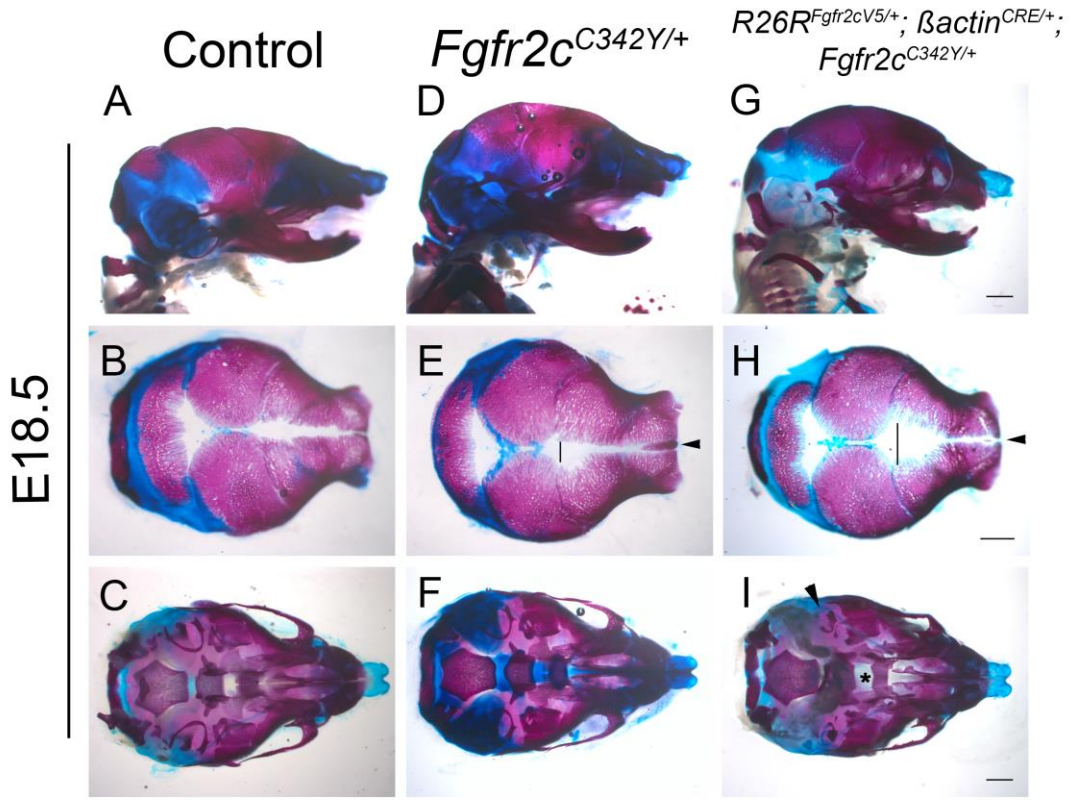

Figure 52: *Fgfr2c* overexpression partially rescues the *Fgfr2c*$^{C342Y/+}$ phenotype.

Control embryos are illustrated in (A-C); *Fgfr2c*$^{C342Y/+}$ (D-F) and *R26R*$^{Fgfr2cV5/+}$; *βactin*$^{CRE/+}$;*Fgfr2c*$^{C342Y/+}$ (G-I); The wormian bone in *R26R*$^{Fgfr2cV5/+}$; *βactin*$^{CRE/+}$;*Fgfr2c*$^{C342Y/+}$ appears comparatively smaller than in *Fgfr2c*$^{C342Y/+}$ mice (n=4/5; compare E and H arrowhead), and a wider frontal posterior interfrontal suture (compare E and H line). Other features include severe tympanic ring hypoplasia (I, arrow) and cleft palate (I, *); Scale bar 1mm.

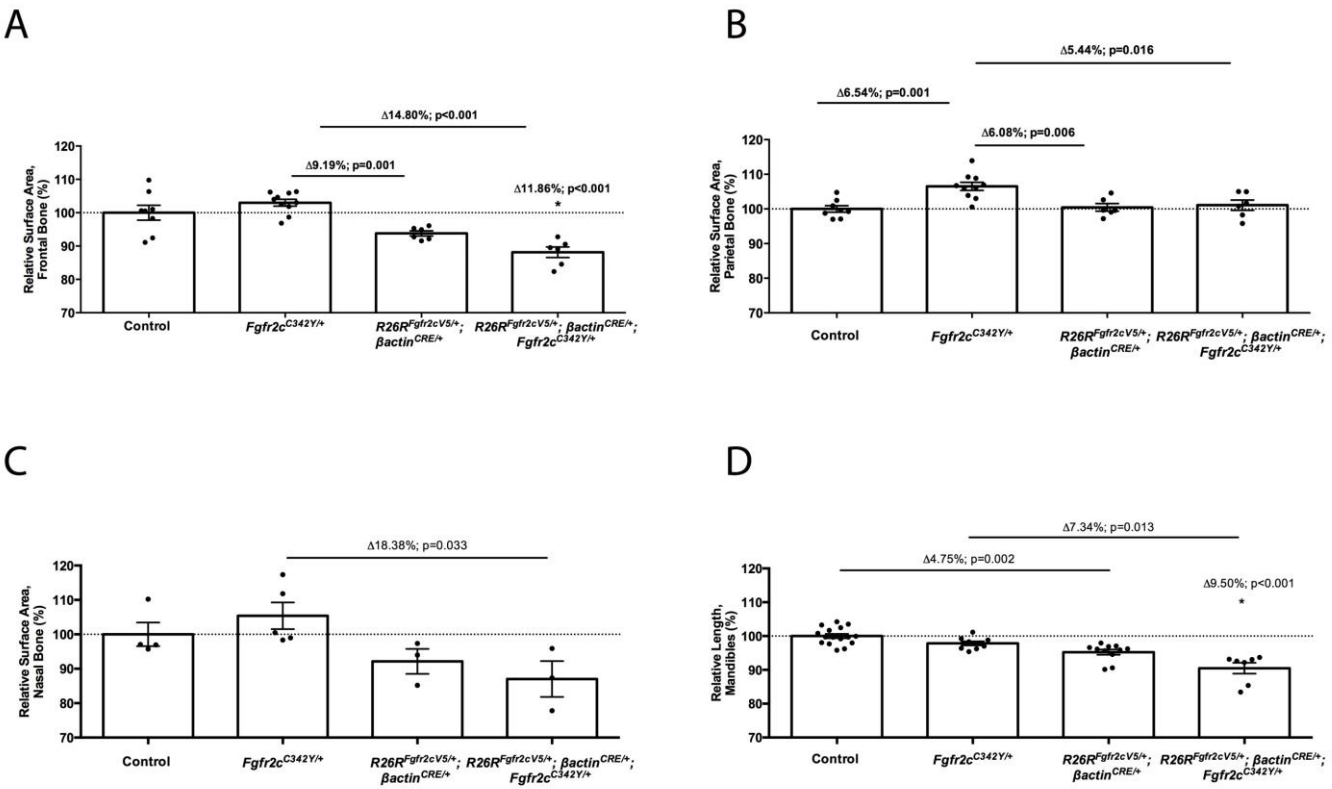

Figure 53: Morphometric analysis of the calvaria.

(A) *R26R*$^{Fgfr2cV5/+}$; *βactin*$^{CRE/+}$;*Fgfr2c*$^{C342Y/+}$ has frontal bone hypoplasia, and is significantly smaller than of the control groups (*) and *Fgfr2c*$^{C342Y/+}$; (B) *Fgfr2c*$^{C342Y/+}$ display parietal bone hyperplasia across all groups compared; (C) Comparatively smaller nasal bone in *R26R*$^{Fgfr2cV5/+}$;*βactin*$^{CRE/+}$;*Fgfr2c*$^{C342Y/+}$ in respect to *Fgfr2c*$^{C342Y/+}$; (D) Micronagthia in embryos carrying the *Fgfr2c* overexpression transgene. Asterisk (*) is statistical significance between the control and *R26R*$^{Fgfr2cV5/+}$;*βactin*$^{CRE/+}$;*Fgfr2c*$^{C342Y/+}$ groups; Statistics: Oneway ANOVA with Tukey's posthoc test for (A) and (B); Kruskal Wallis test with Dunn's posthoc for (C) and (D). Error bars depict SEM; Δ: Difference of means between the genotypes.

6.2.4-*Fgfr2c* overexpression delays coronal suture morphogenesis in *Fgfr2c*$^{C342Y/+}$

Due to the morphometric differences observed, ALP was used to determine osteoblast activity and suture morphology. The coronal sutures of *R26R*$^{Fgfr2cV5/+}$;*βactin*$^{CRE/+}$;*Fgfr2c*$^{C342Y/+}$ were inspected to determine its phenotypic severity in respect to *Fgfr2c*$^{C342Y/+}$ at E18.5 (Figure 54). The increased overlap observed in *Fgfr2c*$^{C342Y/+}$ sutures was ameliorated in the presence of the *Fgfr2c* overexpression allele (Figure 54; compare * to arrowhead) (Control: n=2; *Fgfr2c*$^{C342Y/+:}$ n=2; *R26R*$^{Fgfr2cV5/+}$;*βactin*$^{CRE/+}$;*Fgfr2c*$^{C342Y/+}$: n=3). However, it is important to note that suture abolishment remains a likely consequence as boundaries between the membranous bones and suture mesenchyme was less distinctive to that of a control in *R26R*$^{Fgfr2cV5/+}$;*βactin*$^{CRE/+}$;*Fgfr2c*$^{C342Y/+}$. Altogether, these results suggest the overexpression allele is possible to delay calvarial ossification in the presence of *Fgfr2c*$^{C342Y/+}$ allele.

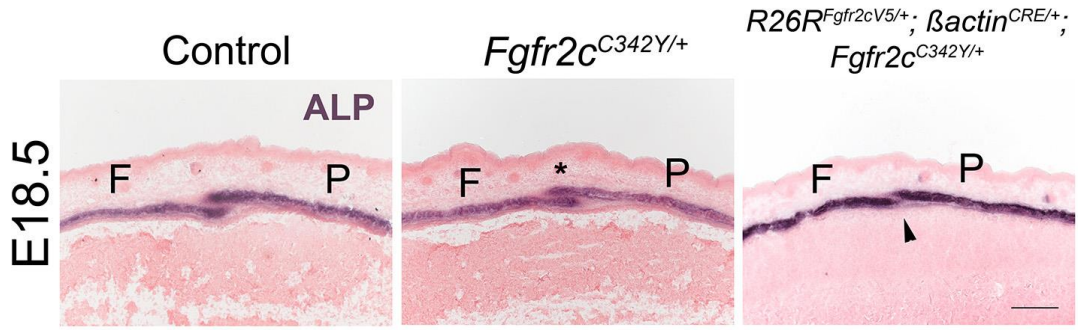

Figure 54: Attenuated osteoblast activity in *R26R*$^{Fgfr2cV5/+}$;*βactin*$^{CRE/+}$;*Fgfr2c*$^{C342Y/+}$ (n=3).

Note the dissimilar morphologies in this cohort of mutants, with undergrowth of the osteogenic front being a major characteristic (arrowhead). Asterisk indicates the overlapping region in *Fgfr2c*$^{C342Y/+}$. F: Frontal bone P: Parietal bone; ALP: Alkaline phosphatase; Scale bar: 200um.

6.3-Results: Part B

6.3.1-Overactivation of RAS-MAPK pathway with oncogenic *KRas*$^{G12D/+}$ induces severe skeletal hypoplasia with ectopic cartilage phenotype

Results from *R26R*$^{Fgfr2cV5/+}$*; βactin*$^{CRE/+}$ indicates structures derived from NCC were sensitive to FGF signalling (Chapter 2, Results Part II). Activation of FGFRs leads to downstream RAS-MAPK, PI3K-AKT and PLCγ-PKC signal transduction (Ornitz and Itoh, 2015). Oncogenic *KRas*$^{LSL-G12D/+}$ was adopted to over-activate the RAS-MAPK pathway to minimise cross talks at the level of the receptor, and to determine its role in craniofacial development. Embryos were collected and analysed at E18.5 (Figure 55). Over-activation of *KRas*$^{G12D/+}$ in the NCC lineage (*KRas*$^{G12D/+}$*; Wnt1*$^{CRE/+}$) led to brachycephaly (Figure 55 K; white arrow) with micrognathia (Figure 55 L, orange arrows; n=6/6). These *KRas*$^{G12D/+}$*; Wnt1*$^{CRE/+}$ embryos feature severe craniofacial hypoplasia with ectopic cartilage in the calvaria (Figure 55 N; Alcian blue only). Specifically, a cartilage boundary underlies the frontal bone adjacent to the coronal suture (Figure 55 M and N, ii), and bridges the suture on the ventral aspects (Figure 55 M; *). Additionally, calcified bone was absent in the NCC domain of the interparietal bone (Figure 55 M; i), while midline enlargement of sagittal and interfrontal sutures were apparent (Figure 55 M; line). A characteristic of *KRas*$^{G12D/+}$*; Wnt1*$^{CRE/+}$ embryos was the prominence of cartilage underlying the frontal bone, normally absent at this stage (Figure 55 M and N; iii). The chondrocranium of *KRas*$^{G12D/+}$*; Wnt1*$^{CRE/+}$ were also severely perturbed (Figure 55 O): Hypoplasia of the tympanic ring (Figure 55 O; bottom panel black arrow) was similar to that observed in *R26R*$^{Fgfr2cV5/+}$; *βactin*$^{CRE/+}$ despite the outer ear appearing normal. Disruptions to the palate were evident too (Figure 55 O; red box), with the palatal shelves appearing jagged and porous suggesting severe hypoplasia, in addition to the adjacent membranous bone-lamina obturans. Posterior to this, the basisphenoid and hyoid bones (Figure 55 O; bottom panel white arrow) also appearing hypoplastic, and the pterygoid plate appearance was analogous to a secondary, but smaller palatal shelf. A cleft in the maxilla was also presented anterior of the palate, owing to the lack of palatal process of the incisive bone. On the

contrary, no obvious defects were noted in *KRas*$^{G12D/+;}$ *Mesp1*$^{CRE/+}$ mouse at E18.5 (n=2) (Figure 55 F-J).

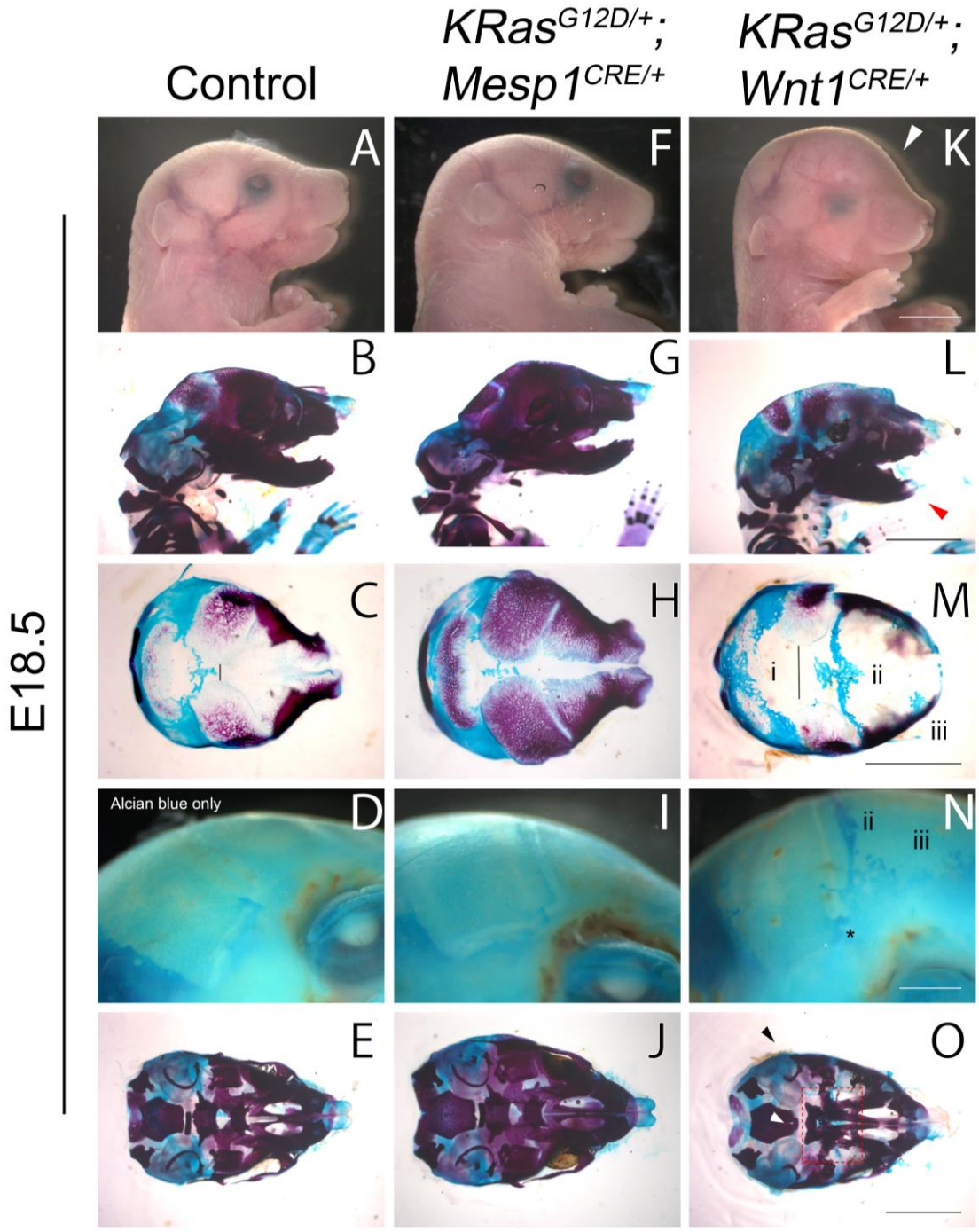

Figure 55: Severe craniofacial hypoplasia in *KRas$^{G12D/+}$; Wnt1$^{CRE/+}$* (n=6/6) at E18.5.

(A-E) Control embryos; (F-J) *KRas$^{G12D/+;}$ Mesp1$^{CRE/+}$* embryos, no apparent phenotype was seen (n=0/2) at E18.5; (K-O) *KRas$^{G12D/+;}$ Wnt1$^{CRE/+}$* embryos, brachycephaly (K, white arrow), micrognathia (L, orange arrow) were noted. The calvaria is presented with an ectopic cartilage phenotype, with expansion of cartilage in the interparietal bone (panel M, designated as 'i'), widening of the midline (line on panel M, sagittal and interfrontal sutures), a cartilage boundary lies adjacent to the edge of the frontal bone (M and N, ii), with cartilage bisecting the ventral aspects of the coronal suture (N, *), and ectopic frontal cartilage (M and N iii). The chondrocranium is also severely disrupted, with tympanic ring (panel O; black arrow) and hyoid (panel O; white arrow) hypoplasia and a series of palatal defects (see text). Scale bar: 3mm for all except 'alcian blue only' panels where it is 1mm.

6.3.2-Ectopic cartilage phenotype is also abundant in *Fgfr2c-C342Y* embryos

Membranous bone ossification does not require a cartilaginous template, with mesenchymal condensation playing a major role in calvarial osteogenesis. Previously, this lab reported the failure to form an intact coronal suture in $Fgfr2c^{C342Y/C342Y}$ embryos at E15.5, along with a fusion of the frontal and parietal bone ossification centres (Peskett et al., 2017). Owing to the excessive cartilage phenotype observed in $KRas^{G12D/+}$; $Wnt1^{CRE/+}$ embryos, there is likelihood similar phenotypic consequence occurs in *Fgfr2c-C342Y* embryos in the event of RAS-MAPK signalling misregulation. $Fgfr2c^{C342Y/+}$ and $Fgfr2c^{C342Y/C342Y}$ embryos were examined for cartilage using wholemount skeleton staining at E16.5. Upon examination of the phenotype, there was an overabundance of cartilage in both $Fgfr2c^{C342Y/+}$ (n=4) and homozygous embryos (n=3), with the latter showcasing an exacerbated phenotypic spectrum (Figure 56 A; *). Specifically, the parietal and frontal cartilage failed to retreat in both cases. Coronal sections of embryos stained with 0.01% alcian blue indicate increased thickness of cartilage underlying the calvaria in *Fgfr2c-C342Y* (Figure 56 B; arrowhead).

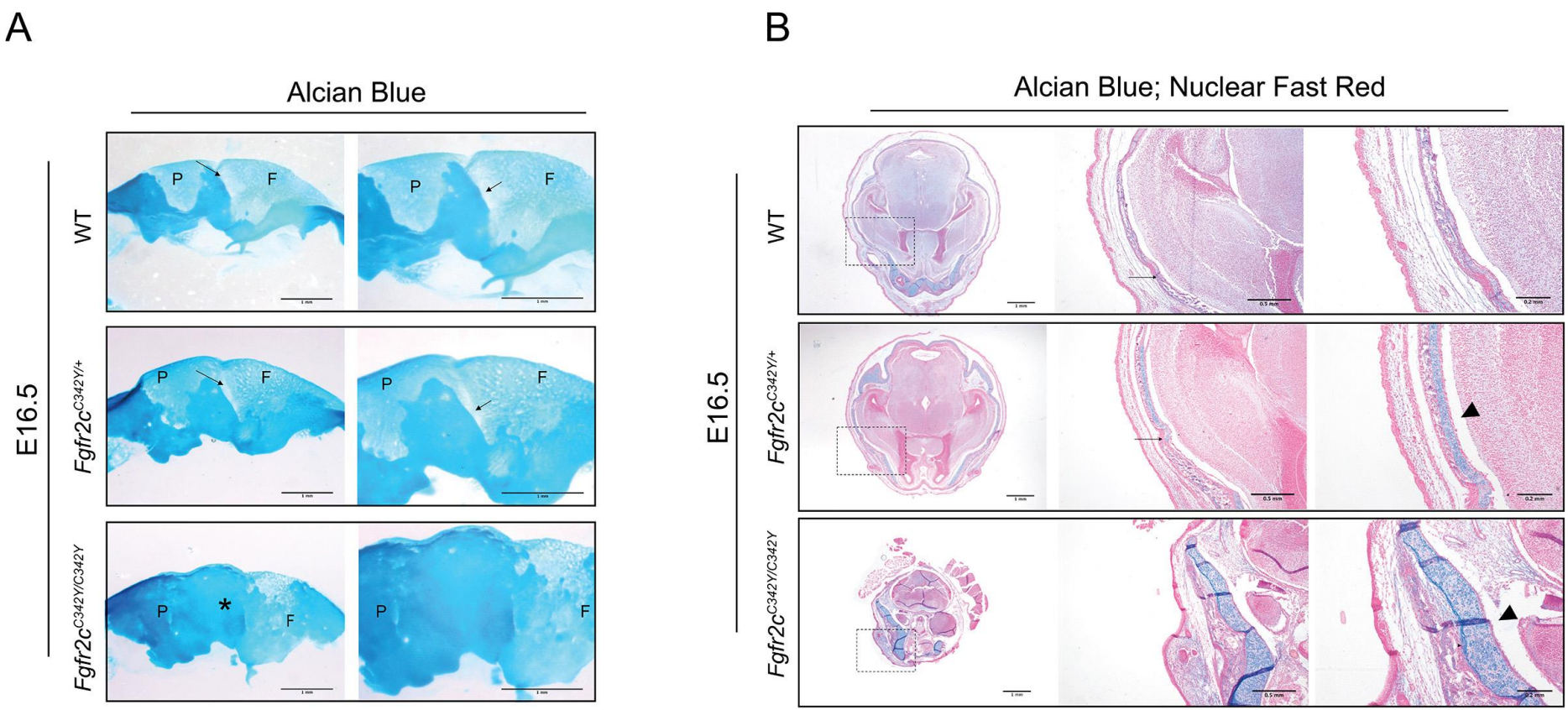

Figure 56; Expansion of calvarial cartilage in E16.5 Fgfr2c-C342Y embryos.

(A) Wholemount 0.01% alcian blue stain of the calvaria showing excess cartilage in the calvaria. Note in *Fgfr2c*$^{C342Y/C342Y}$, the suture is completely abolished (*); (B) Coronal sections of Fgfr2c-C342Y embryos showing increased thickness of calvarial cartilage (arrowheads). Dotted boxes depict magnified region of interest; Arrows mark the location of the coronal suture. P: Parietal bone, F: Frontal bone; Scale bar: 1mm, magnified panels are 0.5mm.

6.4-Discussion

6.4.1-Part A: Phenotypic considerations of *R26R$^{Fgfr2cV5/+}$;βactin$^{CRE/+}$;Fgfr2c$^{C342Y/+}$*

The paradox of FGFR2c signalling was first implicated in *Fgfr2c$^{-/-}$*, whereby removal of signalling through the IIIc isoform was sufficient to drive a phenotype similar to that of *Fgfr2c$^{C342Y/+}$* with craniosynostosis (Eswarakumar et al., 2002, Eswarakumar et al., 2004). The difference being *Fgfr2c$^{C342Y/+}$* display an early increase in cellular activity (E14.5) to that of *Fgfr2c$^{-/-}$*, whereby attenuated signalling delayed calvarial ossification resulting in a 'late onset craniosynostosis' phenotype (Eswarakumar et al., 2004, Eswarakumar et al., 2002). The consequences of premature cellular activity of *Fgfr2c$^{C342Y/+}$* were observed by E16.5 due to the sutural overgrowth in both frontal and parietal bones (Eswarakumar et al., 2004).

Augmentation of RAS-MAPK signalling is sufficient to derive a coronal synostosis phenotype in the craniofacial skeleton (Eswarakumar et al., 2004, Pfaff et al., 2016, Li et al., 2007). It is accepted that phenotypic rescue of craniofacial malformations could be achieved at the level of the receptor such as uncoupling Frs2, but complexities remain as Trk signalling activates a plethora of cascades (Eswarakumar et al., 2006, Ornitz and Itoh, 2015). Targeted knockdown of ERK was sufficient to spare the coronal suture in *Fgfr2$^{S252W/+}$*, possibly through alleviating cellular proliferation required for the early synostosis onset (Shukla et al., 2007). Ultimately, the aim is to ameliorate Crouzon phenotype through FGFR2c signalling attenuation. Despite the phenotypic similarities between *Fgfr2c$^{C342Y/+}$* and *Fgfr2c$^{-/-}$*, the downstream signalling responsible for the paradox remains elusive. This dilemma was originally reported in the palatal shelves of *Fgfr2c$^{C342Y/C342Y}$* that there was reduced RAS-MAPK output at the transcriptomic level, which led to decreased cellular proliferation and delayed shelf elevation (Snyder-Warwick et al., 2010). To compare our findings to previous studies, the coronal suture was used as a model to question this paradox.

Previous studies attempted to elucidate the paradoxical nature of FGFR2 signalling, where the perception of a GOF mutation on the receptor leads to signalling attenuation (Snyder-

Warwick et al., 2010, Pfaff et al., 2016, Bagheri-Fam et al., 2015). Specifically, two studies attempted to ameliorate phenotypes caused by the C342Y allele, by introducing the C342Y allele into the *Fgfr2c*$^{-/-}$ (Pfaff et al., 2016, Bagheri-Fam et al., 2015). Surprisingly, Pfaff et al., 2016 observed an exacerbated craniofacial spectrum of *Fgfr2c*$^{C342Y/+}$, while Bagheri-Fam et al., 2015 did not rescue gonadal sex reversal, normally caused by *Fgfr2c*$^{C342Y/C342Y}$ in compound heterozygotes (*Fgfr2c*$^{C342Y/-}$). Drawing results from this study, the question should not be restricted to the extent of downstream signalling amplitude, but as to which pathway the mutation transactivates at the level of the receptor.

This section concludes *Fgfr2c* overexpression was sufficient to delay ossification, with a successful rescue of the Wormian bone and parietal bone sparing. Furthermore, this was also reflective in the widening of the interfrontal suture similar to that observed *R26R*$^{Fgfr2cV5/+}$; *βactin*$^{CRE/+}$, owing to frontal bone reduction, and attenuated ALP activity in the suture. Interestingly, *R26R*$^{Fgfr2cV5/+}$;*βactin*$^{CRE/+}$;*Fgfr2c*$^{C342Y/+}$ spared the parietal bone, which was significantly smaller than that of *Fgfr2c*$^{C342Y/+}$. Altogether, the delayed ossification in *R26R*$^{Fgfr2cV5/+}$;*βactin*$^{CRE/+}$;*Fgfr2c*$^{C342Y/+}$ suggests the overexpression allele have delayed ectopic osteoblast differentiation, possibly through the RAS-MAPK pathway (Miraoui et al., 2009). As FGFR2 is critical for cell-renewal, one speculation for this rescue is shifting the balance from osteoblast differentiation to proliferation through 'scavenging activity' of endogenous FGF ligands by excess FGFR2c (Baddoo et al., 2003). Altogether, the delayed ossification in *R26R*$^{Fgfr2cV5/+}$;*βactin*$^{CRE/+}$;*Fgfr2c*$^{C342Y/+}$ suggests *Fgfr2c* overexpression have reduced premature osteoblast commitment normally caused by the C342Y allele (Eswarakumar et al., 2004, Peskett et al., 2017). Interestingly, the penetrance of the cleft palate phenotype increased to 100% (n=7/7) in *R26R*$^{Fgfr2cV5/+}$;*βactin*$^{CRE/+}$;*Fgfr2c*$^{C342Y/+}$ to those observed in *R26R*$^{Fgfr2cV5/+}$; *βactin*$^{CRE/+}$ (40%) in Chapter 2. This indicates that the combination of the constitutively active receptor in with *Fgfr2c* overexpression exacerbates the cleft phenotype, resembling close similarities to *Fgfr2c*^{C342Y} homozygotes (Peskett et al., 2017). However, it is also important to consider the extent of the *Fgfr2c* overexpression on the phenotype of *R26R*$^{Fgfr2cV5/+}$; *βactin*$^{CRE/+}$; *Fgfr2c*$^{C342Y/+}$. The main question is to address whether the alleles genetically interact, or those

perceived is the consequence of a combined phenotype between both alleles. For example, the tympanic ring phenotype could be the sole consequence of the *Fgfr2c* overexpression allele alone.

6.4.2-Part B: Overactive RAS-MAPK pathway potentially leads to terminal differentiation defects

Consequently, the oncogenic $KRas^{LSL\text{-}G12D/+}$ was used to examine the role of RAS-MAPK pathway in craniofacial development (Tuveson et al., 2004). The $KRas^{LSL\text{-}G12D/+}$ model minimises cross talk at the level of the receptor and overactivates the RAS-MAPK pathway. Similar to the results obtained from $R26R^{Fgfr2cV5/+}$; $\beta actin^{CRE/+}$, NCCs show greater susceptibility to changes in signalling to the mesoderm. As expected, $KRas^{G12D/+}$; $Wnt1^{CRE/+}$ yielded severe craniofacial hypoplasia, as mutant KRas increases clonogenic potentials while reducing terminal differentiation into daughter lineages (Tuveson et al., 2004, Haston et al., 2017).

It is widely accepted that FGFs are strong potentiators of ERKs and it is therefore important to characterise the roles of cascade effectors. A comprehensive review was published recently highlighting the strategies to delineate NC development using mouse models that target RAS-MAPK (and PI3K-AKT) cascade effectors (Dinsmore and Soriano, 2018). NCs are highly susceptible to ERK1 and ERK2 signalling manipulation, embryos with ERK1 deletion are viable, but knockout of the latter contributes to lethality at implantation (Saba-El-Leil et al., 2003, Mazzucchelli et al., 2002). Interestingly, ERKs are functionally redundant as embryonic lethality of ERK2 can be rescued through the introduction of the ERK1 transgene (Fremin et al., 2015). Newbern et al., 2008 determined that ERK2 acts as the dominant isoform in craniofacial development. Specifically, ERK2 knockout in the NC lineage resulted in NC defects that were associated with mandibles truncation, cleft palate, loss of tongue and cardiac outflow tract abnormalities (Newbern et al., 2008). Generally speaking, augmentation of RAS-MAPK signalling promotes NCC proliferation and differentiation is a consequence of pathway suppression (Dinsmore and Soriano, 2018). This cellular consequence is comparable to embryonic stem cells maintaining pluripotency (Yamanaka et al., 2010). In the murine palate, it is understood that proliferation of palatal mesenchyme cells are driven by activated ERK

through the exposure to FGFs in culture, and that its inhibition led to downregulation of 'stemness' genes (Vasudevan et al., 2015). In the same study, genetic ablation of *Fgfr1* (*Fgfr1*$^{-/-}$) led to ectopic osteoblast differentiation in the palatal shelves *in vivo* suggesting ERK as a negative regulator for differentiation (Vasudevan et al., 2015). Other examples were also presented in a separate conditional knockout of *Erk2* (Parada et al., 2015). Here, Parada et al., 2015 reported a compromise in terminal differentiation of osteoblasts in the developing mandibles. *Erk2*$^{-/-}$; *Wnt1*$^{CRE/+}$ embryos display a loss of osteoblast differentiation markers (*Osterix* and *Col1a1*) between E13.5-E14.5, which consequently led to micronagthia due to insufficient bone mineralisation (Parada et al., 2015). Multiple osteoblast differentiation defects were also perceived with regards to upstream (e.g. Src homology region 2 domain containing phosphatase, *Shp2*) and downstream effectors (e.g. Ribosomal S6 Kinase 2, *RSK2*) of ERK (Nakamura et al., 2009a, Nakamura et al., 2009b, Yang et al., 2004). For example, *Shp2*$^{-/-}$; *Wnt1*$^{CRE/+}$ embryos display a complete absence of NC craniofacial bones, and that *RSK2*$^{-/-}$ has delayed bone mineralisation, which implies active RAS-MAPK signalling is required for osteogenesis (Nakamura et al., 2009a, Yang et al., 2004). Furthermore, brachycephaly and delayed interfrontal suture closure are consequences of consitutively active *Shp2* caused by a knockin mutation (Q79R) in the NCC lineage (Nakamura et al., 2009b). Here, sustained ERK activation led to reduced osteoblast commitment, which could be reversed through pharmacological inhibition of ERK (Nakamura et al., 2009b). Overall, RAS-MAPK signalling is essential to maintain the correct balance of osteoblast proliferation and differentiation for normal bone formation. Genetic knockins of mutations into pathway effectors provided headway into insights to the complexity of growth factor signalling. The use of oncogenic KRas G12D presented in this section has achieved this aim for craniofacial development, and the data suggests hyperactive RAS-MAPK pathway perturbs the terminal differentiation programme that is more extreme to that of FGFR2c overexpression.

6.4.3- Emerging role of cartilage in craniosynostosis

Calvarial cartilage coincides with membranous bones during embryonic development, and the underlying anlagen gradually recedes and is absent by postnatal day 10 in the mouse

(Holmbeck et al., 1999). Ectopic cartilage is associated with craniosynostosis, albeit its role is less understood, the cartilage anlagen persist beneath the suture mesenchyme (Holmes and Basilico, 2012, Maruyama et al., 2010, Wang et al., 2005b, He and Soriano, 2017, Holmbeck et al., 1999). The striking cartilage phenotype obtained from our *KRas*$^{G12D/+}$*; Wnt1*$^{CRE/+}$ phenocopies that reported in a recent study with PDGFRα signalling misregulation (He and Soriano, 2017). He and Soriano 2017 used a mouse model that conditionally over-activates PDGFRα signalling driven under an endogenous promoter (*Pdgfr*$^{D842V/+}$), and yielded distinct cartilage phenotypes in the mesoderm and NCC lineage upon conditional activation (He and Soriano, 2017). In particular, these authors demonstrated that the cartilage is specified through the P13K-AKT pathway, and that excess chondrocytes invades the mesenchyme and transdifferentiates into osteoblasts (He and Soriano, 2017). The results yielded from the *KRas*$^{G12D/+}$*; Wnt1*$^{CRE/+}$ embryos adhere to this data, as the G12D mutation is able to mediate cross talk with the P13K-AKT pathway (Tuveson et al., 2004). Additionally, loss of PTEN-a negative regulator of P13K-AKT pathway accelerates tumorigenesis in the presence of the *KRas*$^{G12D/+}$ allele (Hill et al., 2010). PDGFR is not commonly associated with craniosynostosis however, this study and a previous report from the lab reveal *Fgfr2c*$^{C342Y/+}$ display ectopic cartilage phenotype (Peskett et al., 2017). In this study, *Fgfr2c*$^{C342Y/C342Y}$ has exacerbated cartilage. Cartilage is not usually required for calvarial development as conditional knockout of the chondrocyte marker *Sox9* does not have effects on membranous bones, raising questions about its involvement (Akiyama et al., 2002). However, several evidence have shown misregulation to FGF signalling led to ectopic chondrogenesis: It is established that long-term exposure of FGF ligand is sufficient to commit NCCs to a chondrocytic lineage, through the expression of *Sox9* (Bagheri-Fam et al., 2017, Chen et al., 2014, Sarkar et al., 2001). Similarly, forced expression of *Fgf9* in the cranial mesenchyme is sufficient to transform the calvarial mesenchyme into cartilage during embryogenesis (Govindarajan and Overbeek, 2006). In the adult mice, double knockout of *Fgfr1* and *Fgfr2* disrupts remodeling in the long bone owing to depressed chondrocyte proliferation (Karuppaiah et al., 2016).

As the underlying cartilage bridges the mesenchyme beneath the sutures under pathogenic conditions, it could be involved in stabilising the surrounding tissue. This assumption can be related to the initial phases of fracture healing as cartilage enables fissures to be bridged in the bone tissue, and Sox9+ cells residing in the periosteum plays a critical role for this regenerative process (Einhorn and Gerstenfeld, 2015, He et al., 2017). Further, chondrocyte markers such as *Col2a1* are upregulated in the mesenchyme prior to suture closure (Behr et al., 2011a). Other syndromic mouse models for craniosynostosis also display ectopic cartilage such as *Fgfr2*$^{S252W/+}$ and *Twist1*$^{+/-}$ albeit its role remains elusive, with a strikingly similar cartilage phenotype resting beneath the suture mesenchyme (Holmes et al., 2009, Behr et al., 2011a).

The role of cartilage appears to play critical roles in suture closure. This study also describes differential expression of chondrocyte markers in the embryonic suture through a transcriptomic screen (See Chapter 7). The abnormal expression of chondrocytic genes in the mesenchyme suggests ectopic bone could be generated through chondrocytes in the suture, potentially through an endochondral manner: Yang et al., 2004 demonstrated that osteoblasts could be derived from hypertrophic chondrocytes expressing *Col10a1* during endochondral ossification. Here, the authors identified osteoblast were derivatives of chondrocytes expressing *Col10a1* and in addition; these osteoblasts contributed to bone repair upon grafting into a fractured bone (Yang et al., 2014). This transition in fate contradicts the dogma that osteoblasts and chondrocytes have a fundamentally distinct lineage. In particular to Saethre-Chotzen syndrome, *Twist1* is sufficient to suppress chondrocyte gene expression. Due to the presence of *Twist1* in the suture mesenchyme, Saethre-Chotzen syndrome could be a consequence of transdifferentiation of chondrocytes into osteoblasts (Reinhold et al., 2006). Moreover, the differentiation capacity of the calvarial mesenchyme appears to be bi-potential, based on the balance between transcription factors responsible for bone and cartilage (Aberg et al., 2005). For example, a positive regulator for osteoblast differentiation- *Msx2*, suppresses expression of chondrocyte genes such as *Sox9* (Semba et al., 2000). Therefore, it would be interesting to elucidate whether there are hypertrophic chondrocytes expressed in the mesenchyme that could result in ectopic bone formation.

6.4.4-Future directions

The lack of obvious phenotype obtained in *KRas*$^{G12D/+;}$ *Mesp1*$^{CRE/+}$ could be explained by the phenotypic onset: For example, He and Soriano only observed craniosynostosis in adults of *Pdgfr*$^{GOF/+}$*; Mesp1*$^{CRE/+}$ mice (He and Soriano, 2017). Future work should therefore aim to let the *KRas*$^{G12D/+}$*; Mesp1*$^{CRE/+}$ litter down and allow them to develop the phenotype postnatally. The use of oncogenic mouse models provides a powerful tool to dissect the complexities of growth factor signalling in development. The KRas protein remains upstream of the RAS-MAPK cascade, it has potentials to crosstalk with PI3K-AKT pathway. To overcome this problem, there is an oncogenic BRaf mouse model available (*BRaf*$^{LSL\text{-}V600E/+}$) in the literature further downstream of the RAS-MAPK pathway (Dankort et al., 2007). However, the BRaf-V600E mutation is more potent than that of the KRas-G12D (Dankort et al., 2007, Tuveson et al., 2004). A cause of concern revolves around early embryonic lethality, and is advisable to select CRE lines that can bypass gastrulation defects (e.g. inducible CRE). Nonetheless, the systematic use of oncogenic mouse models allows the pathway to be isolated at multiple levels. Should there be a high correlation to that pathway, the phenotypes obtained should remain consistent across all levels of signalling. Future studies will also need to address the mechanics of cascade activation of FGFRs *in vivo*. There have been attempts in the past to elucidate this by mutating binding sites on the catalytic domains of PDGFRs in the mouse (Klinghoffer et al., 2002, Klinghoffer et al., 2001, Fantauzzo and Soriano, 2016). As generating a mouse mutant for individual binding domain is time consuming, technologies such as CRISPR-CAS9 will no doubt assist on this endeavour.

Perhaps the most striking finding from this section was the cartilage phenotypes observed in *KRas*$^{G12D/+}$*; Wnt1*$^{CRE/+}$ and *Fgfr2c*$^{C342Y/+}$. The question remains as to understanding the role of pathogenic FGFR2c signalling in chondrocyte specification. The initial approach to this problem is to determine whether there is a misexpression of chondrocytic markers between *Fgfr2c*$^{C342Y/+}$ and *R26R*$^{Fgfr2cV5/+}$*; βactin*$^{CRE/+}$. For example, this is achieved through analysis of chondrocyte markers such as *Sox9* during the initial stages of suture morphogenesis: Preliminary data in this lab shows *Sox9* is ectopically expressed beneath the suture primordia in

Fgfr2c$^{C342Y/+}$ and *Fgfr2c*$^{C342Y/C342Y}$ by E14.5 (data not shown). Similarly, primary cultures from *Fgfr2c*$^{C342Y/+}$ and *R26R*$^{Fgfr2cV5/+}$*; βactin*$^{CRE/+}$ is to be generated from the cranial mesenchyme, and compare the chondrocytic potentials of both mouse models, which could be important to explain the phenotypic differences of the coronal suture. If ectopic cartilage plays substantial roles in craniosynostosis, efforts should attempt to halt the chondrogenic progression. As a proof of concept experiment, *in vivo* ablation of cells in the chondrocytic lineage is to be targeted in the calvaria through expression of Dipheria toxin (*R26R*$^{DTA/+}$). This could be achieved through the introduction of the DTA allele into *Fgfr2c*$^{C342Y/+}$, and using a *Col2a1* CRE to target the cells (Sakagami et al., 2017). Other approaches could involve local application of beads soaked with inhibitors that halt chondrocyte proliferation, or disrupting the extracellular matrix to abrogate growth (Otsuki et al., 2010). Bone Morphogenetic Protein (BMP) signalling has been described as a co-partner to FGF signalling to regulate chondrocyte proliferation, and inhibitors of this pathway could also be explored (Retting et al., 2009). Another interesting subject discussed was the potentials of chondrocytes to fracture healing. Mechanistically, there are similarities that could be learnt between craniosynostosis and bone repair. To elucidate this, injury sites could be created in the calvaria of WT mice, and chondrocytes could be transplanted into chasms to determine its healing potential. Lastly, hypertrophic chondrocytes remain to be determined in the suture mesenchyme. This could be achieved by performing expression analysis of the suture and corresponded with appropriate protein expression *in vivo* using antibodies.

6.5-A working model for FGFR2c and syndromic craniosynostosis

Figure 57 illustrates a potential working model for FGFR2c osteogenesis and syndromic craniosynostosis. The model amalgamates all the phenotypic and biochemical data together to derive a working model, which points towards defects in regulating the balance between proliferation and differentiation. In general, RAS-MAPK signalling governs the cloning potentials of MSCs, whilst PI3K-AKT and PLCγ-PKC cascades dictate cellular commitment towards osteogenic lineage (Miraoui et al., 2009, He and Soriano, 2017, Vasudevan et al., 2015). It should be assumed under WT conditions, a status quo is maintained between these pathways and a shift in pathway activation is expected under pathological conditions.

Coronal synostosis in *Fgfr2c*$^{C342Y/+}$ is caused by hyper-proliferation and differentiation during early embryogenesis (Eswarakumar et al., 2004). This is supported by ectopic activation of pERK and ALP activity in the coronal suture in this study. However, *in vitro* evidence implies ectopic osteogenesis in mutant FGFR2 (such as FGFR2-S252W) are mechanistically different to WT-FGFR2, where cellular differentiation is caused by abnormal activation of the PLCγ-PKC cascade (Miraoui et al., 2009). In this respect, the C342Y mutation could have potentially augmented activation of both RAS-MAPK and PLCγ-PKC cascades to drive premature suture closure. FGF signalling is sufficient to drive cellular proliferation through ERK activation (Yamanaka et al., 2010, Vasudevan et al., 2015). The hypoplasia phenotype observed in *R26R*$^{Fgfr2cV5/+}$*; βactin*$^{CRE/+}$ implies insufficient osteoblast commitment for correct bone formation. This is supported by an overactive pERK readout and reduced ALP activity in the coronal suture in this study, and reaffirmed by the *KRas*$^{G12D/+}$*; Wnt1*$^{CRE/+}$ data in Figure 55 that is known to cause terminal differentiaton defects (Tuveson et al., 2004, Haston et al., 2017). Therefore, sustained ERK activation in *R26R*$^{Fgfr2cV5/+}$*; βactin*$^{CRE/+}$ resulted in a greater number of cells involved in proliferation that resulted in osteogenic delays and a patent suture. As coronal synostosis is potentially an ectopic differentiation defect in *Fgfr2c*$^{C342Y/+}$, introduction of the overexpression allele into *Fgfr2c*$^{C342Y/+}$ is likely to have delayed differentiation normally caused by the C342Y mutation by restoring proliferation.

The same model can also be used to explain craniosynostosis phenotypes observed in *Fgfr2c*$^{-/-}$ and *Fgfr2c*$^{C342Y/-}$ (Pfaff et al., 2016, Eswarakumar et al., 2002). A characteristic of *Fgfr2c*$^{-/-}$ is delayed osteogenesis and suture abolishment, which is explained by insufficient osteoblast generated for bone formation (Eswarakumar et al., 2002). A potential mechanism for coronal synostosis in the *Fgfr2c*$^{-/-}$ is linked to cellular survival. Loss of the IIIc isoform would have attenuated ERK signalling that is critical for cell renewal and furthermore, it is understood that ERK suppression is sufficient to promote cellular differentiation (Vasudevan et al., 2015). As a result, the onset of a synostosis phenotype is slower than that of the *Fgfr2c*$^{C342Y/+}$ counterpart. Finally, *Fgfr2c*$^{C342Y/-}$ has exacerbated phenotypic spectrum to that of *Fgfr2c*$^{C342Y/C342Y}$. A notable characteristic of this compound mutant is severe skeletal hypoplasia, which could be attributed to ectopic differentiation without sufficient amplification of the progenitor pool.

Therefore, using this model to explain the FGFR2c signalling paradox, it is potentially a result of altering the balance of cascade activation immediately downstream of FGFR2c. Disrupting the harmony of cascade activation would ultimately draw pronounced effects on cellular proliferation and differentiation that drive perturbed osteogenesis. As discussed previously, this model proposes the pathogenesis for coronal synostosis is mechanistically different between *Fgfr2c*$^{C342Y/+}$ and *Fgfr2c*$^{-/-}$ despite yielding the same phenotypic outcome. As these mouse models were generated by knockin technology, the phenotypic similarties are dependent on the localisation of the 'IIIc' isoform. Collectively, this study has successfully elucidated the mystery behind the signalling paradox and that it should not be judged on the signalling amplitude alone but rather, the shift in cascade activation.

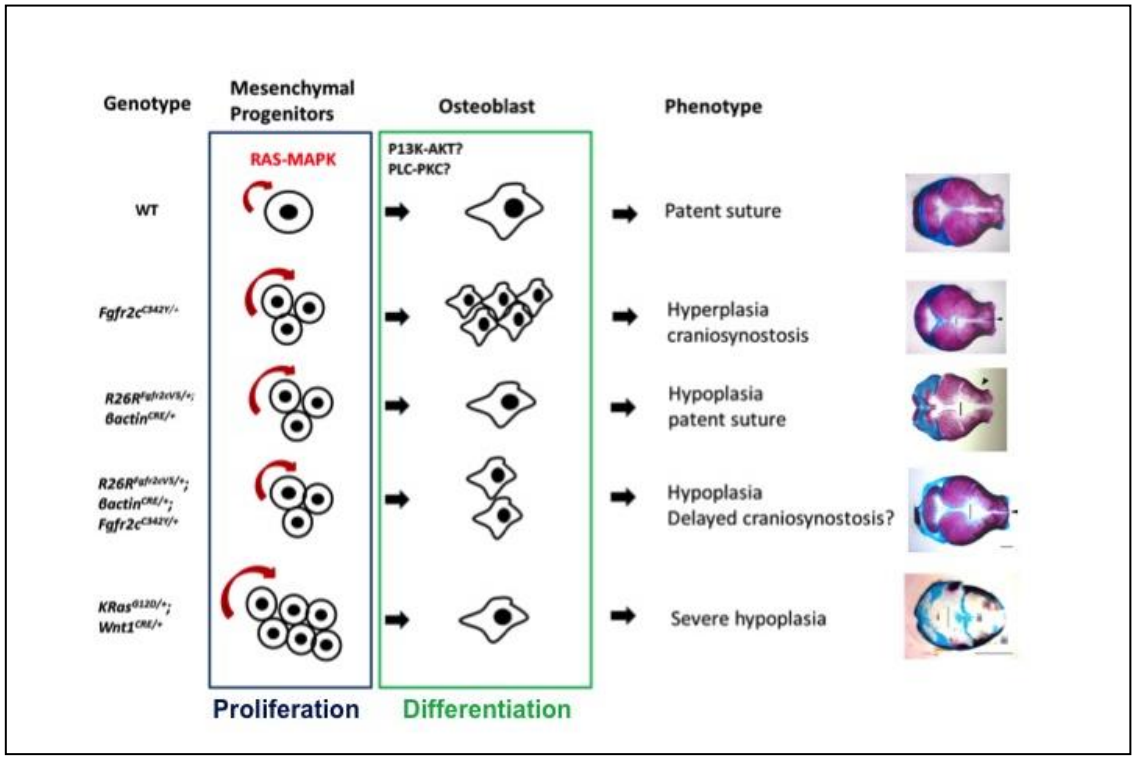

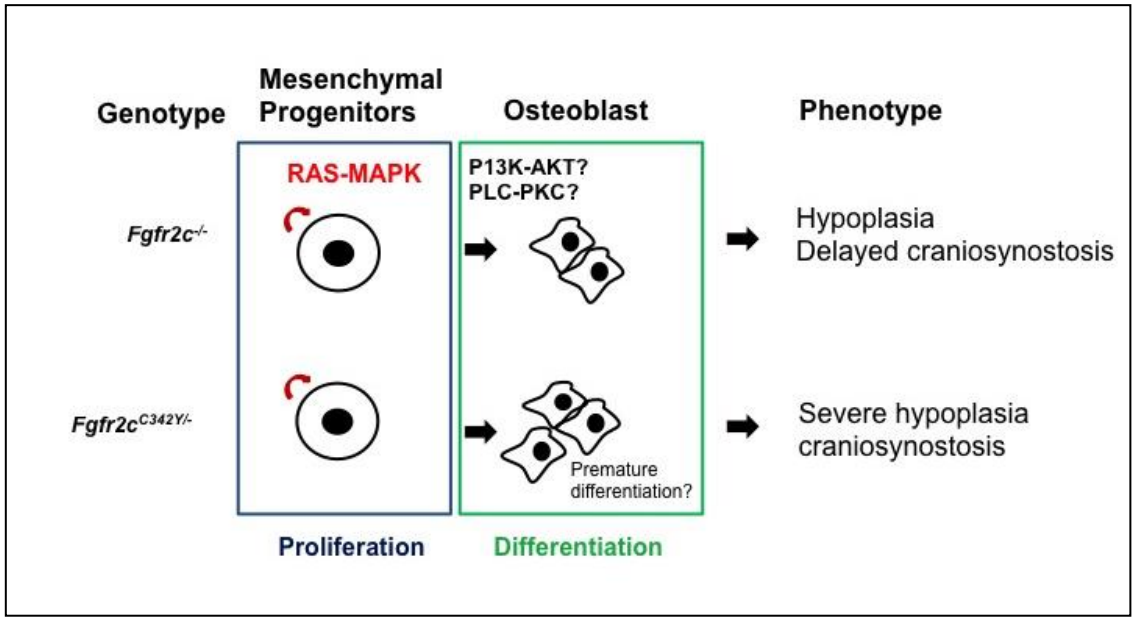

Figure 57: A working model of osteogenesis regulated by FGFR2 and craniosynostosis (Top).

Bottom: Using the same model to explain the phenotypes obtained in *Fgfr2c*$^{-/-}$ and *Fgfr2c*$^{C342Y/+}$. RAS-MAPK governs cellular proliferation (red arrows and blue box) whilst commitment is P13K-AKT/PLC-PKC pathways (Green box). Shifting this intricate balance disrupts overall integrity, and therefore yielding a series of craniofacial phenotypes associated with perturbed osteoblast differentiation.

Chapter 7

Results (Part V)

Profiling the embryonic coronal suture

7.1-Introduction

Laser captured microdissection (LCM) was chosen as a method to obtain samples from the embryonic coronal suture. This section highlights results obtained from transcriptomic profiling of the E16.5 *Fgfr2c*$^{C342Y/+}$ coronal suture, with an aim to identify genes misregulated by FGFR2c during the start of suture closure. E16.5 was chosen as the ideal embryonic stage because the morphological appearance of the coronal sutures is similar between *Fgfr2c*$^{C342Y/+}$ and WT. Only *Fgfr2c*$^{C342Y/+}$ was profiled, due to the animal as the accepted model for coronal synostosis.

7.2-Results

7.2.1-RNA was extracted from microdissected coronal sutures

To assemble samples for RNAseq, LCM was used to microdissect embryonic coronal sutures of E16.5 CD-1 WT and *Fgfr2c*$^{C342Y/+}$. E16.5 was chosen as the desired developmental stage for RNAseq owing to the morphological similarities between WT and *Fgfr2c*$^{C342Y/+}$. Figure 58 A shows the coronal suture before and after microdissection using LCM. A triplicate (n=3) of WTs and *Fgfr2c*$^{C342Y/+}$ embryos from the same litter were microdissected along the dorsal-ventral profile of the bilateral coronal suture. Roughly 50-70 sections from the same embryo were captured into the collection adhesive caps. Figure 58 B is a representative of RNA quality extracted from captured samples after Tapestation analysis. The peaks denote ribosomal subunits 18s and 28s in the electropherogram, confirming the presence of RNA.

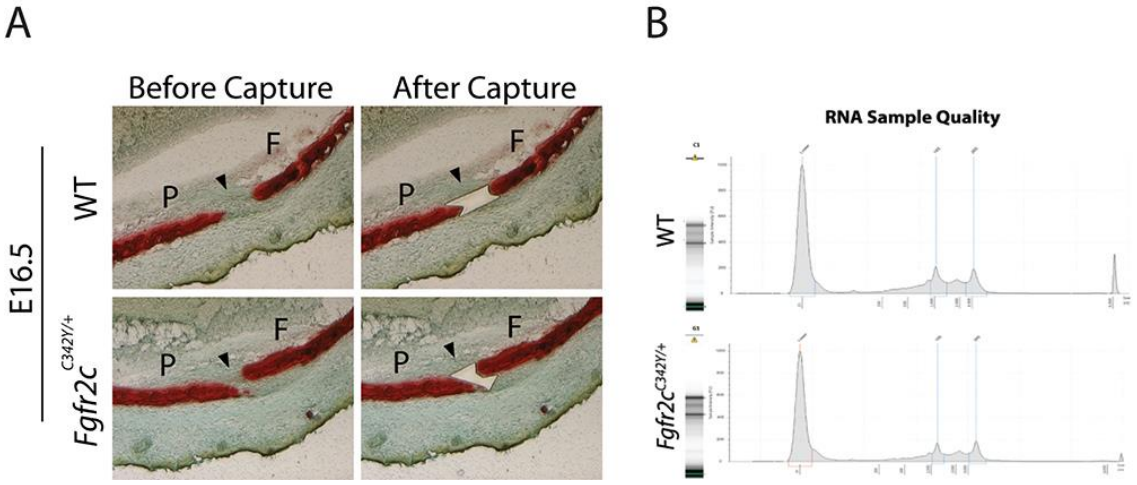

Figure 58: RNA is extracted from LCM.

(A) E16.5 coronal suture before and after capture; (B) Representative electropherogram denoting the presence of RNA. The small twin peaks denotes ribosomal subunits. F: Frontal bone, P: Parietal Bone. Arrows show the location of the coronal suture.

7.2.2-General quality of RNAseq from LCM samples

The general quality of RNAseq data was first examined on BaseSpace prior to further analysis (Figure 59). BaseSpace analysis revealed strong transcript alignment in the 3' region of the genome during the sequencing process of the captured samples (Figure 59 B). This was indicative RNA degradation and was expected for LCM.

Principal Component Analysis (PCA) plot enables the stringency between biological replicates to be examined (Figure 59 A). Should the samples display similar expression profile, samples of the same genotype should cluster in proximity to each other. In regards to *Fgfr2c*$^{C342Y/+}$ samples, they were grouped together on the PC1 axis. However, on the PC2 axis, one of the samples was dispersed from the group. The WT replicates were strongly dispersed, and no obvious cluster was identified for this genotype. However, two of the WTs were closer together along the PC1 axis (Figure 59 A). Furthermore, sequence alignment shows one of the samples-WT5 (UCLGNS1172-wt5); possess uniform coverage across the genome, indicative of a dissimilar expression profile to the rest of the samples (Figure 59 B).

An entity list designated to FGF signalling was created to determine the extent of signalling misregulation in *Fgfr2c*$^{C342Y/+}$, and to serve as an *in silico* control (Figure 60). Due to the variable nature of samples acquired by LCM, a cut off value of 1.5 fold was set to ensure subtle changes in gene expression was detected. Surprisingly, a handful of genes involved in the FGF signalling pathway were not misregulated between WT and *Fgfr2c*$^{C342Y/+}$ when the data was run against an FGF entity list (Figure 60). In addition, WT5 appears to display a higher expression level to all other samples.

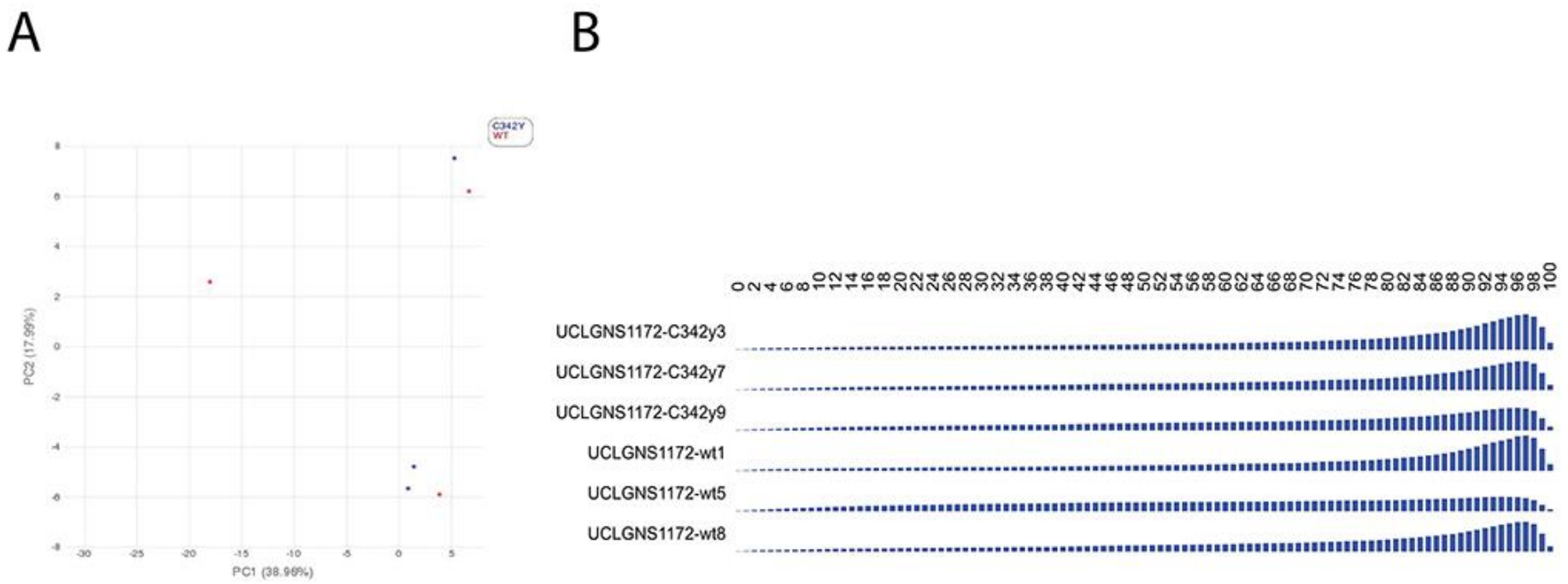

Figure 59: PCA plot and sequence alignment to reference genome of LCM captured samples.

(A) PCA plot for the sequenced LCM captured coronal sutures; (B) Alignment plot of samples processed for RNAseq. Note the 3' bias observed across the majority of samples, and the uniform alignment of 'UCLGNS1172-WT5'.

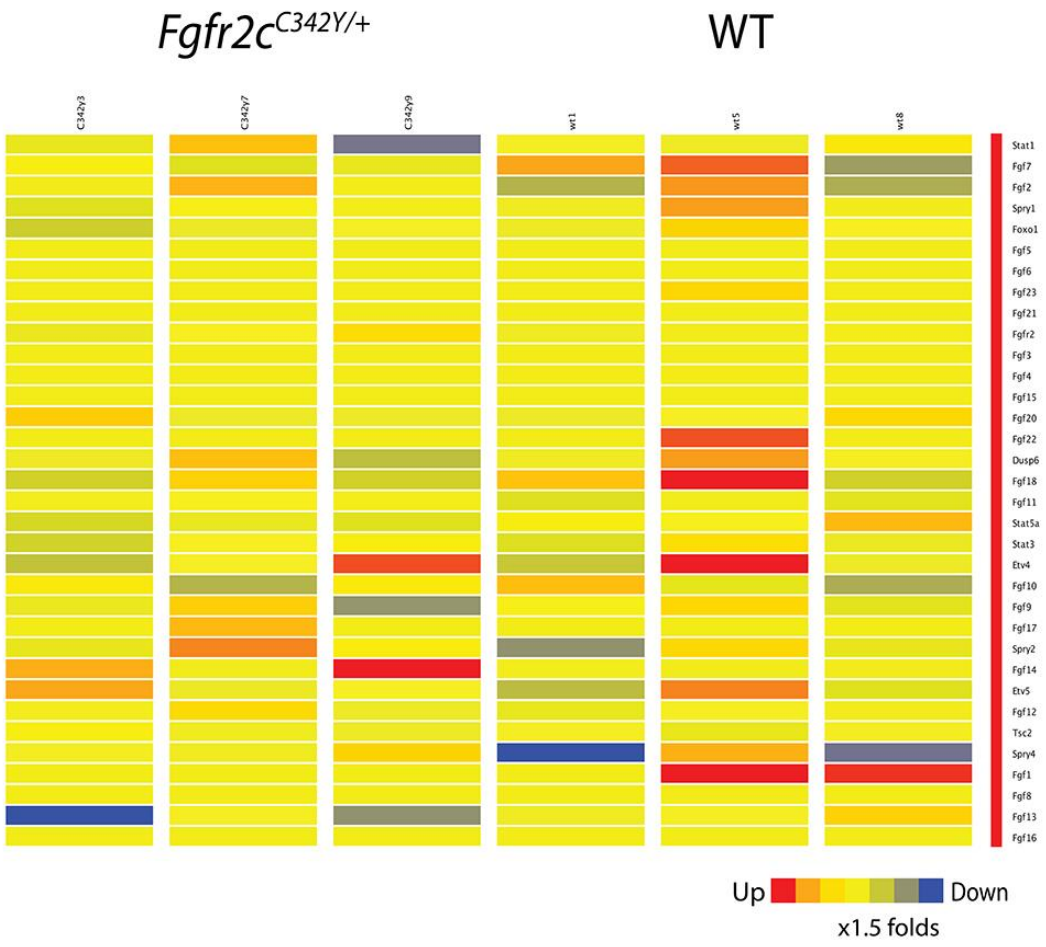

Figure 60: *In silico* control of LCM, sequenced data was run against a FGF entity list.

A majority of genes involved in the FGF signalling pathway were not misregulated. Note the increased expression of FGF genes in WT5.

7.2.3-GSEA reveals multiple molecular signatures in the embryonic suture

GSEA was used to examine the enrichment profile in the embryonic suture of *Fgfr2c*$^{C342Y/+}$ (Figure 61). GSEA reveals significant enrichment of genes associated with cell cycle, apoptosis (Enrichment score (ES): 0.27; FDR: 0.041; p=0.01) and epithelial-mesenchymal transition (EMT) (ES: 0.36; FDR: <0.001; p=0.001) in *Fgfr2c*$^{C342Y/+}$ (Figure 61 A). The enhanced enrichment for cell cycle genes were characterized by E2F target genes (ES: 0.39; FDR: 0.001; p< 0.001), Myc target genes (ES: 0.34; FDR: 0.001; p<0.001) and genes associated with G2M checkpoint (ES: 0.28; FDR; 0.001; p<0.001) Figure 61 A). Gene sets associated with growth factors signalling had attenuated enrichment in the *Fgfr2c*$^{C342Y/+}$, such as the RAS-MAPK-consisting of *KRas* signalling (UP: ES: -0.33; FDR: 0.045; p<0.001; DOWN: ES: -0.31; FDR: 0.094; p=0.013) and PI3K-AKT-mTOR signalling (ES: -0.34; FDR: 0.068; p=0.013) (Figure 61 B). Gene sets associated with myogenesis (ES:-0.30; FDR: 0.107; p=0.011) and Notch signalling (ES: -0.47; FDR: 0.039; p=0.01) were also less enriched in *Fgfr2c*$^{C342Y/+}$ (Figure 61 B). A summary of the ranked genes from GSEA can be found in Appendix 11. Altogether, GSEA reveals molecular signatures in the embryonic suture are associated with abnormal cellular activity and multiple signalling misregulations.

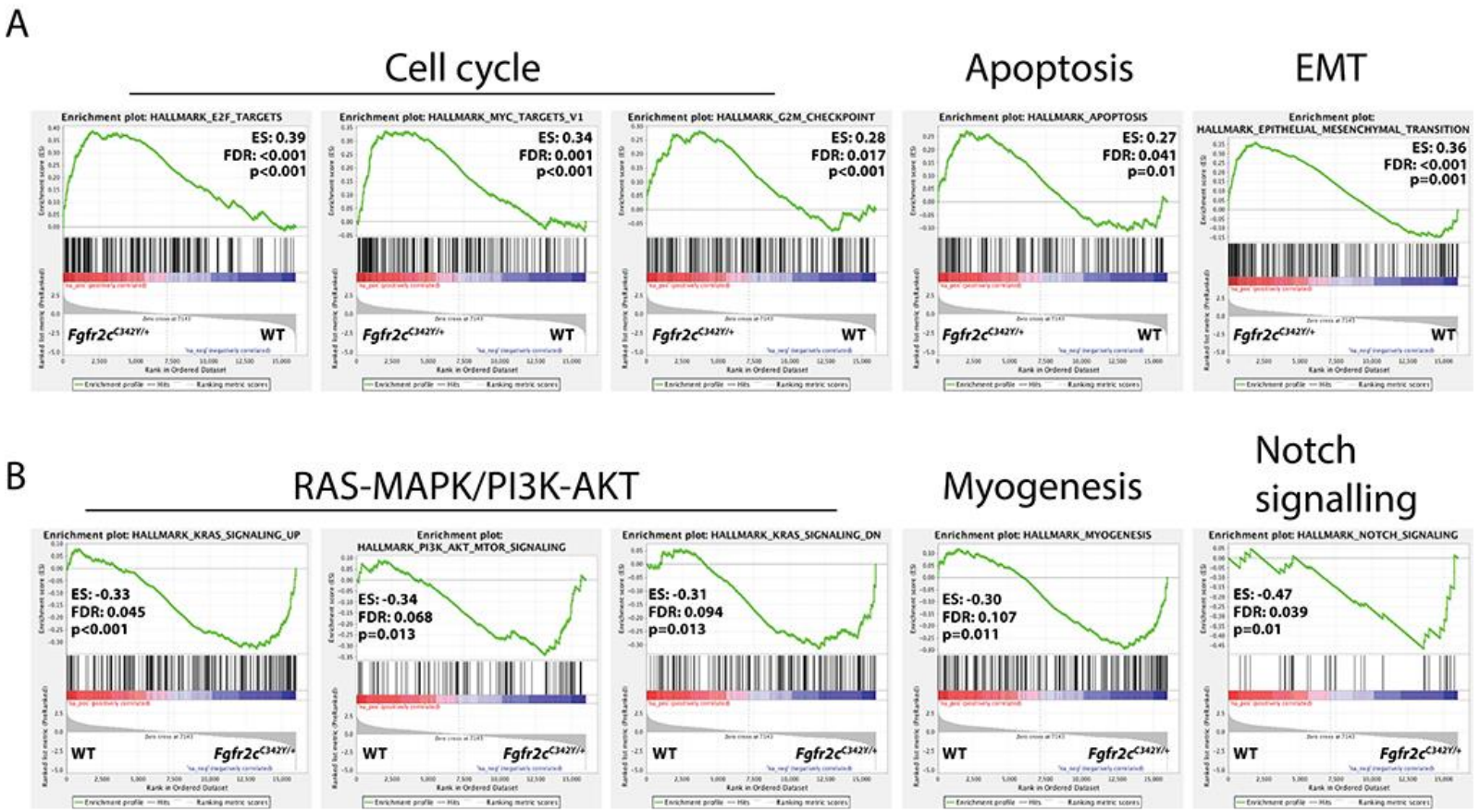

Figure 61: Enriched genes of *Fgfr2c*$^{C342Y/+}$.

(A) Indicates upregulated gene sets in *Fgfr2c*$^{C342Y/+}$ concerning cell cycle, apoptosis and EMT; (B) Indicates downregulated gene sets in *Fgfr2c*$^{C342Y/+}$ concerning RAS-MAPK/PI3K-AKT pathways, myogenesis and Notch signalling.

7.2.4-Shortlisting candidate genes for expression validation

24,421 genes were annotated throughout the screening process. Figure 62 A highlights the pipeline for shortlisting the candidates. A total of 86 genes were found to be upregulated and 325 genes downregulated more than 10-fold in mutant sutures. A further filter was to narrow the candidates, where the raw read counts must be consistent between biological replicates, and a PubMed query was performed to check its relevance to craniofacial development. Ultimately, this is to circumvent issues concerning the lack of expression uniformity between biological replicates as given by the PCA and alignment plots (Figure 59). The final shortlist consisted of 27 genes upregulated and 36 genes downregulated (Figure 62 B). Table 21 illustrates the average fold change for these genes.

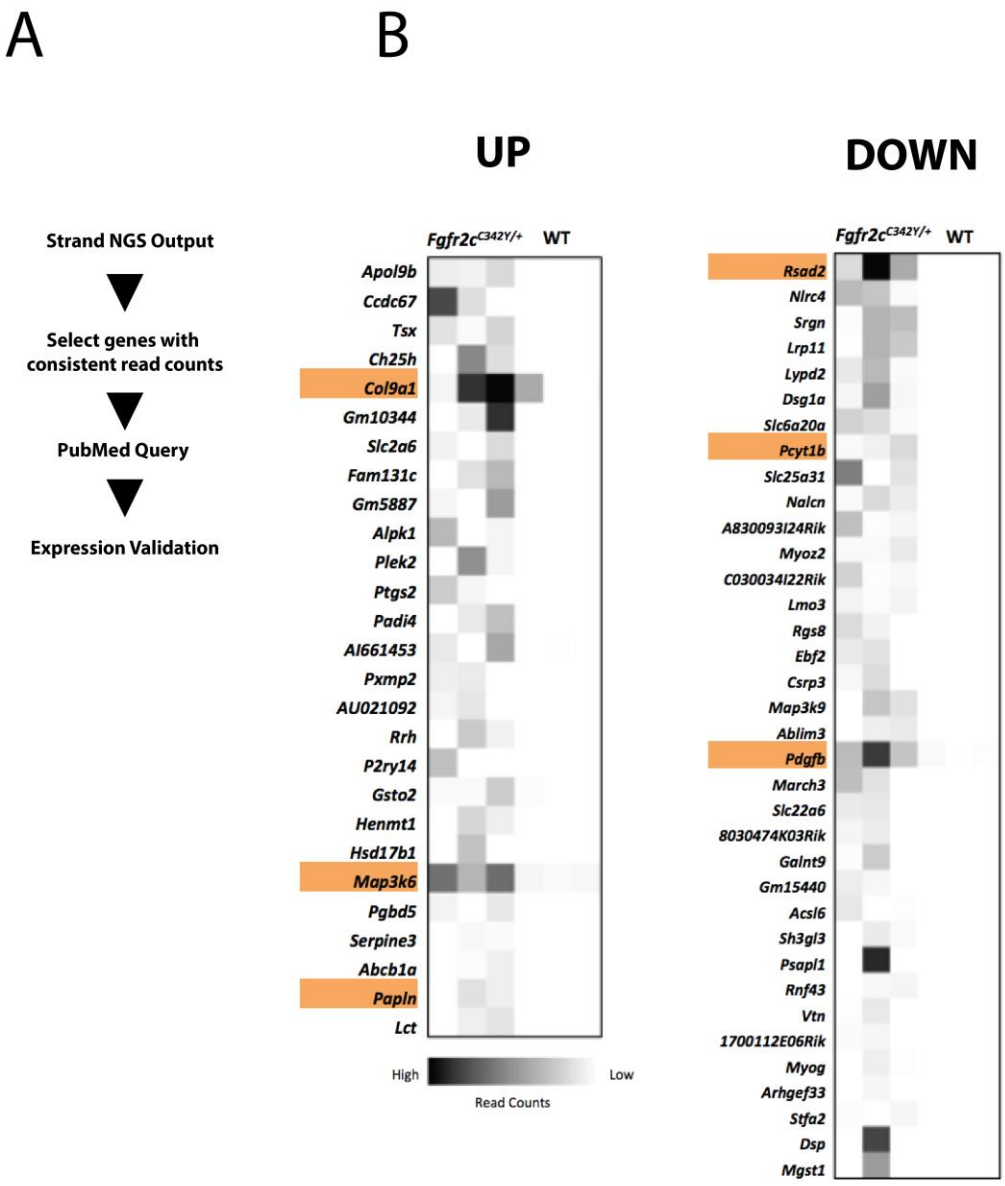

Figure 62: Pipeline for expression validation and heatmap of highly differentially expressed genes.

(A) Pipeline for expression validation; (B) Heatmaps illustrating genes that were differentially expressed by 10 folds, with consistent read counts between the biological replicates and genotypes; Genes processed for expression validation are marked in orange.

Gene Symbol	FC ([c342y] vs [wt])
Apol9b	28.819536
Ccdc67	26.348238
Tsx	25.640665
Ch25h	25.620537
Col9a1	21.75568
Gm10344	21.652868
Slc2a6	19.816038
Fam131c	16.886911
Gm5887	16.78892
Alpk1	15.403195
Plek2	14.918185
Ptgs2	14.885597
Padi4	14.739341
AI661453	13.470319
Pxmp2	13.159639
AU02109 2	12.681593
Rrh	12.209546
P2ry14	11.915451
Gsto2	11.736259
Henmt1	11.732923
Hsd17b1	11.566258
Map3k6	11.303426
Pgbd5	11.258239
Serpine3	11.111681
Abcb1a	11.089977
Papln	10.616017
Lct	10.216149

Gene Symbol	FC ([c342y] vs [wt])
Rsad2	-297.74582
Nlrc4	-100.08107
Srgn	-94.57781
Lrp11	-81.78447
Lypd2	-78.46616
Dsg1a	-76.11076
Slc6a20a	-75.41735
Pcyt1b	-58.077717
Slc25a31	-57.71174
Nalcn	-56.257942
A830093I24Rik	-49.138927
Myoz2	-39.87751
C030034I22Rik	-38.263905
Lmo3	-36.095715
Rgs8	-35.990154
Ebf2	-32.45098
Csrp3	-29.051847
Map3k9	-26.50333
Ablim3	-26.32135
Pdgfb	-26.2745
March3	-26.141647
Slc22a6	-25.984463
8030474K03Rik	-25.643427
Galnt9	-23.297153
Gm15440	-22.447887
Acsl6	-21.136223
Sh3gl3	-20.021713
Psapl1	-19.139965
Rnf43	-17.816904
Vtn	-17.70016
1700112E06Rik	-17.530369
Myog	-17.513828
Arhgef33	-16.64122
Stfa2	-15.1528015
Dsp	-13.22994
Mgst1	-12.257614

Table 21: Final shortlist of genes with at least 10 folds differential expression in *Fgfr2c*$^{C342Y/+}$.

Genes highlighted in green were processed for expression validation. The heatmap of these genes are represented in Figure 55B (Orange). Table on the left illustrates upregulated genes and downregulated on the right. FC: Fold change.

7.2.5-RT-qPCR expression validation of candidate genes

Expression validation was performed between at E12.5 controls/WT and *Fgfr2c*$^{C342Y/+}$ wholemount embryos due to the extensive experimental pipeline of LCM. *R26R*$^{Fgfr2cV5/+;}$ *βactin*$^{CRE/+}$ was also included in the analysis for comparative purposes. Table 22 illustrates the genes validated in this study.

Gene	Ensembl ID	Function	Expression
Papln	ENSG00000100767	Papilin: extracellular glycoprotein	UP
Map3k6	ENSG00000142733	Protein kinase related to RAS-MAPK signalling	UP
Col9a1	ENSG00000112280	Collagen9a1: chondrocyte marker	UP
Pcyt1b	ENSG00000102230	Choline-phosphate cytidylyltransferase B: Enzyme in metabolic pathway	DOWN
Pdgfb (Pdgfβ)	ENSG00000100311	Platelet derived growth factor beta: cell survival and proliferation	DOWN
Rsad2	ENSG00000134321	Viperin: anti-viral protein	DOWN

Table 22: Genes processed for expression validation

7.2.6-Preliminary results of RNAseq expression validation

7.2.6.1-The upregulated genes

RT-qPCR was performed for *Papln*, *Map3k6* and *Col9a1* (Figure 63). *Papln* displayed a strong difference between the mean ranks to at least a pair of genotypes as indicated by Kruskal Wallis test (p=0.031; Control: n=6; $Fgfr2c^{C342Y/+}$: n=3; $R26R^{Fgfr2cV5/+}$; $\beta actin^{CRE/+}$: n=2) (Figure 63 B). Dunn's post-hoc with Bonferroni correction was subsequently executed between the groups, and identified significant upregulation of transcript in $Fgfr2c^{C342Y/+}$ to that of $R26R^{Fgfr2cV5/+}$; $\beta actin^{CRE/+}$ (Fold change: 347, p=0.040) (Figure 63 B). No significant difference between mean ranks was identified in the subsequent groups. *Col9a1* displayed differences between the mean ranks to at least a pair of genotypes as indicated by Kruskal Wallis test (p=0.037; Control: n=6; $Fgfr2c^{C342Y/+}$: n=3; $R26R^{Fgfr2cV5/+}$; $\beta actin^{CRE/+}$: n=2) (Figure 63A). Further analysis using Dunn's post-hoc with Bonferroni correction identified significant upregulation of transcript between the control groups and $Fgfr2c^{C342Y/+}$ (Fold change: 34.4; p=0.032), no other differences were seen across genotypes. Statistical analysis was not performed for *Map3k6* over a lack of biological replicates in $Fgfr2c^{C342Y/+}$ and $R26R^{Fgfr2cV5/+}$; $\beta actin^{CRE/}$ (n=1 for both genotypes). However, $Fgfr2c^{C342Y/+}$ have increased levels of transcripts compared to controls and $R26R^{Fgfr2cV5/+}$; $\beta actin^{CRE/+}$ (Figure 63 E).

7.2.6.2-The downregulated genes

In contrast to the output of RNAseq, the downregulated genes analysed (*Pcyt1b, Pdgfb*) did not show evidence for decreased gene expression in both $Fgfr2c^{C342Y/+}$ and $R26R^{Fgfr2cV5/+}$; $\beta actin^{CRE/+}$. All of the genes analysed had augmented transcript expression (Figure 63 C and D). *Pcyt1b* display a strong trend of transcript increase between the groups, albeit close to reaching statistical significance (Kruskal Wallis: p=0.055; Control: n=5; $Fgfr2c^{C342Y/+}$: n=3; $R26R^{Fgfr2cV5/+}$; $\beta actin^{CRE/+}$: n=2) (Figure 63 C). Similarly, *Pdgfb* did not display any expression differences between the mean ranks to at least a pair of genotypes as indicated by Kruskal Wallis test (p=0.055; Control: n=6; $Fgfr2c^{C342Y/+}$: n=3; $R26R^{Fgfr2cV5/+}$; $\beta actin^{CRE/+}$: n=2), despite a strong trend for transcript upregulation (Figure 63 D). *Rsad2* was not followed up owing to high standard deviations yielded between biological replicates in the RT-qPCR plate.

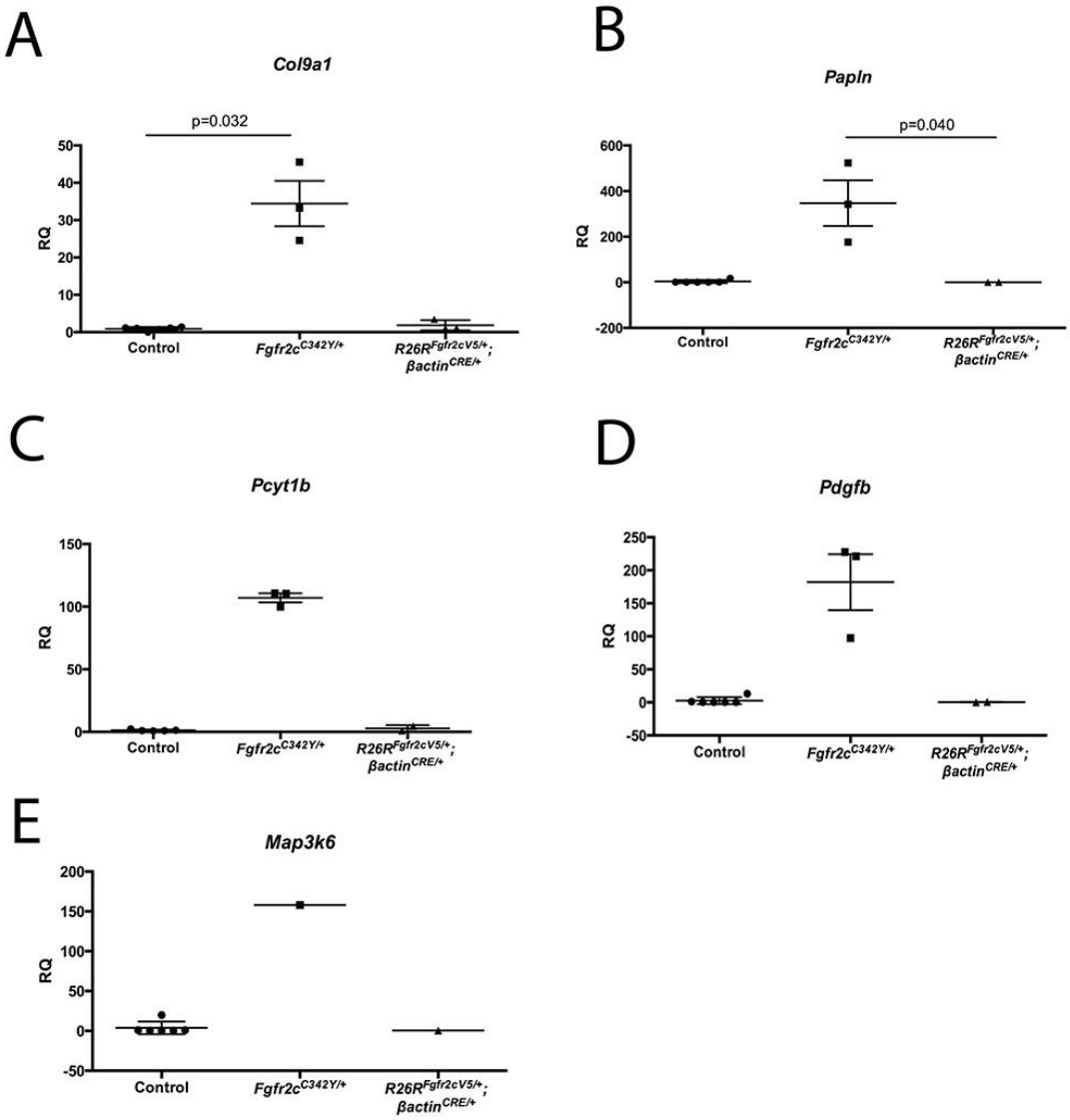

Figure 63: Expression validation of candidate genes at E12.5 embryos.

(A) *Col9a1*, (B) *Papln*, (C) *Pcyt1b*, (D) *Pdgfβ*, *Map3k6*. Statistics: Kruskal Wallis with Dunn's posthoc. Statistical analysis was not performed for *Map3k6* due to lack of biological replicates in mutant groups. *Rsad2* was not followed up for expression validation due to high standard deviation from RT-qPCR raw data (data not shown).

7.3-Discussion

Abnormal osteogenesis is characteristic to bone diseases inclusive of craniosynostosis. This experiment is the first to attempt expression profiling of the embryonic *Fgfr2c*$^{C342Y/+}$ coronal suture using samples acquired by LCM. Novel genes were identified to contribute towards the development of syndromic craniosynostosis previously unrelated to FGFR2c signalling. This mini discussion will give a brief overview of the candidate genes in addition to the experimental limitations occurred throughout this experiment.

7.3.1-Molecular events occurring in the embryonic suture

GSEA provides a snapshot of the molecular events occurring in the embryonic suture. The enrichment for genes associated with cellular activity in *Fgfr2c*$^{C342Y/+}$ is in line and expected with previous studies (Holmes and Basilico, 2012, Holmes et al., 2009, Wang et al., 2012, Eswarakumar et al., 2004). Specifically, *Fgfr2c*$^{C342Y/+}$ has an enriched signature associated with G2M checkpoint of the cell cycle, and target genes associated with the E2F and cMyc factors implicative of a dynamic suture. E2F and cMyc are downstream of RAS-MAPK and PI3K-AKT signalling and therefore, regulation of genes downstream of these transcription factors imply misregulation of these cascades (Sears and Nevins, 2002). Genes enriched for apoptosis were also upregulated in *Fgfr2c*$^{C342Y/+}$. Cellular apoptosis plays an essential role in bone resorption and is detected in the embryonic suture at E16-E17 (Rice et al., 1999). Programmed cell death allows effective calvarial remodeling to occur, and is strongly upregulated in osteoblasts within the osteogenic front and in the mesenchyme of the coronal suture (Rice et al., 1999). As the tissue extracted from LCM contains both the osteogenic front and the mesenchyme, it would have detected the apoptotic signature in *Fgfr2c*$^{C342Y/+}$. The conversion of cells from an epithelial to mesenchymal status requires a series of changes from cell-cell adhesion, polarity to migratory properties (Thiery et al., 2009). The enrichment of genes associated with EMT suggests cells in the suture mesenchyme were undergoing reprogramming and differentiation events. This is also linked to a large cohort of genes associated with the extracellular matrix (Appendix 11).

Interestingly, genes enriched for the PI3K-AKT pathway were downregulated in the *Fgfr2c*$^{C342Y/+}$. It should be noted GSEA does not account for the overall activity of the signalling pathway but rather, giving an insight into the pathways that were potentially affected. Therefore, the enrichment of KRas gene sets point towards aberrations to both the RAS-MAPK and PI3K-AKT cascades. Indeed, both pathways are linked towards craniosynostosis development (Eswarakumar et al., 2004, Pfaff et al., 2016, He and Soriano, 2017). Genes enriched for myogenesis were also downregulated in the *Fgfr2c*$^{C342Y/+}$, which could relate specifically to the suture mesenchyme: The mesenchyme is hypothesized to be a stem cell niche and is able to contribute to bone regeneration post-injury (Zhao et al., 2015). MSCs are multipotent and are sufficient to give rise to a plethora of daughter cells (Uccelli et al., 2008). The downregulated signature of myogenic genes could suggest FGFR2c signalling suppresses the myogenic programme in MSCs, and potentially promoting gene expression of the osteogenic lineage. Finally, genes associated with Notch signalling were also downregulated in *Fgfr2c*$^{C342Y/+}$, implicating FGFR2c is upstream of Notch signalling. This relationship can be referenced in somitogenesis, where FGF signalling synchronizes Notch cyclic genes through activated ERK (Dequeant and Pourquie, 2008). In particular to two of the Notch genes, *Notch3* and *Jag1* possess high enrichment scores and were strongly downregulated (Appendix 11; Notch genes). This is an interesting observation as LOF to *Jag1* is related to human Alagille syndrome and moreover, Jag1 is a binding partner to Notch3 (Yen et al., 2010, Gridley, 2010). LOF to *Jag1*, however, is insufficient to drive craniosynostosis on its own, but it is able to exacerbate coronal synostosis phenotypes such as *Twist1*$^{+/-}$ (Yen et al., 2010). Therefore, the downregulation of vital Notch genes suggests a synergistic relationship between FGFR2c signalling and suture patency.

7.3.2-Validation of selected differentially expressed genes identified by RNAseq

Upregulated genes:

7.3.2.1-*Papln* (Papilin)

Papln is an extracellular matrix glycoprotein originally identified in the *Drosophila* embryo associated with the basement membrane (Kramerova et al., 2000). The *Drosophilia* homologue *Papln* is highly conserved, with a non-catalytic N-terminal sequence resembling A Disintegrin And Metalloproteinase **(**ADAM**)** metalloproteinases. Papilin is able to inhibit ADAM activity on a non-competitive basis thanks to a conserved sequence in the N-terminal domain (Kramerova et al., 2000). Enzymes lacking this this sequence did not show any reduction of catalytic activity by Papilin. Due to its ability to modulate ADAMs, Papilin aids extracellular matrix remodelling during organogenesis. It has been reported that Papilin knockdown perturbs cell movements critical for organogenesis in both *Drosophila* and nematodes (Kramerova et al., 2000, Kawano et al., 2009). There is evidence for *Papln* involved in craniofacial development despite the link with FGFR2 signalling is not yet established: For example, *Papln* was identified to be involved in molar tooth development through a microarray screen, and is specifically expressed in ameloblasts, cells responsible for enamel deposition (Pemberton et al., 2007). However, the most interesting finding related to *Papln* is their association with A Disintegrin And Metalloproteinase with Thrombospondin Type 1 motifs (ADAMTS1) (Kramerova et al., 2000). ADAMTS1 is heavily involved in osteogenesis, and sequence alignments reveal the N-terminal domain in Papilin is specific for ADAMTS1 homolog in the mouse (Kramerova et al., 2000, Nakamura et al., 2005, Lu et al., 2009, Lind et al., 2005, Hu et al., 2012, Rehn et al., 2007, Sone et al., 2005). Overexpression of ADAMTS1 *in vivo* results in a loss of long bone density in the adult mice, strongly linking the role of metalloproteinases to bone homeostasis (Hu et al., 2012). ADAMTS1 display a peculiar pattern of expression, notably in bone nodules and growth plates of the long bones, in addition to dental pulp cells in tooth development (Lind et al., 2005, Sone et al., 2005). ADAMTS1 is secreted from osteoblasts, and promotes proteolytic processing of collagen precursors (pro-collagen type 1), versican and other matrix proteins (Lind et al., 2005, Sandy et al., 2001, Rehn et al., 2007).

The resultant products are subsequently accumulated to form the extracellular matrix composition (Rehn et al., 2007). Furthermore, ADAMTS1 is capable to alter cellular morphology which in turns alter the capacity for osteoblasts to migrate (Rehn et al., 2007). This finding is particularly relevant in cases for bone metastasis and invasive tumours, and knockdown of ADAMTS1 is sufficient to ameliorate these phenotypes (Lu et al., 2009). The extracellular matrix is also able to control cellular differentiation *in vitro* (Xiao et al., 1998). In particular, osteoblasts express integrins and collagen 1, which acts as the prime substrate to drive osteoblast gene expression (Xiao et al., 1998, Gronthos et al., 1997). Altogether, the results suggest the upregulation of *Papln* by $Fgfr2^{C342Y/+}$ negatively regulates the activity of ADAMTS1 in the ECM, to reduce bone resorption in membrous bones resulting in premature suture closure.

7.3.2.2-*Map3k6*

Map3k6 (aka Apoptosis Signalling Regulating Kinase 2-'ASK2') is an intermediate of the RAS-MAPK pathway that modulates signal transduction. It functions directly upstream of ERK and shares similar homology with its counterpart *Map3k5* (Apoptosis Signalling Regulating Kinase 1-'ASK1') (Wang et al., 1998). Both isoforms form functional dimers and play differing roles in controlling signal transduction: Both Map3k5 and Map3k6 promote the activation of tumour suppressor p38 but in the case of Map3k6, it requires Map3k5 to form a functional heterodimer. Map3k5 stabilises Map3k6 and prevents it from being processed for degradation (Takeda et al., 2007). Regulating the balance to form functional dimers therefore implies these candidates play multiple roles in regulating cellular proliferation and cell death. Despite their presence in the RAS-MAPK pathway, the link with FGFR2 signalling is not yet shown. However, the expression of Map3k6 coincides with the location of FGFR2 signalling in the skin epithelium (Petiot et al., 2003, Iriyama et al., 2009) (See Figure 49 ISH). Targeted knockout of *Map3k6 in vivo* ($Ask2^{-/-}$) increases susceptibility to papillomas due to its inability to facilitate cell death, in addition to losing protection against oxidative stress and carcinogens (Iriyama et al., 2009). The idea of FGFR2 promoting both proliferation and apoptosis is not new, and osteoblasts harbouring GOF mutations can undergo cell death (Mansukhani et al.,

2000, Rice et al., 1999). Therefore, the identification of *Map3k6* could suggest a novel molecular switch responsible for controlling cellular activity, switching between both proliferation and apoptotic fates. Altogether, the increased expression of *Map3k6* in the *Fgfr2c*$^{C342Y/+}$ points towards cell death as a mediator for suture abolishment in *Fgfr2c*$^{C342Y/+}$.

7.3.2.3-*Col9a1*

Chondrocytes express a multitude of markers throughout their maturation process. For instance, immature chondrocytes express type 2 and type 9 collagens, whilst mature chondrocytes express type 10 collagen in addition to those described in their infancy (Gomez-Picos and Eames, 2015). Collagen 9 is heterotypic, and comprises of multiple polypeptide chains in α1, α2 and α3. The α1 unit is particularly important, as it is required for the formation of all the isoforms of collagen 9 (Hagg et al., 1997). Specifically, *Col9a1* is important for the correct arrangement of the bone architecture during endochondral ossification, and is expressed prominently in hypertrophic zones of the growth plate (Dreier et al., 2008). The inability to correctly pattern the extracellular matrix by *Col9a1* has pronounced effects on chondrocyte proliferation. As a whole, the cellular consequence is disarrayed bone cytoarchitecture and loss of bone density. Ultimately, this results in the truncation of long bones (Dreier et al., 2008). On the cellular level, chondrocytes express a multitude of integrin receptors, which are specific for collagen chains (Kapyla et al., 2004). Not only were these interactions important to stabilize the extracellular matrix, it may well play roles in controlling the chondrocyte maturation program (Kapyla et al., 2004, Chen et al., 2005). Therefore, the molecular interaction between polypeptides could govern the overall process of chondrocyte differentiation, and disruption to the extracellular matrix would lead to a hypoplastic phenotype. Other phenotypes associated with *Col9a1* also display differences to cytoarchitecture, including those within the tectorial membrane of the cochlea, and multiple epiphyseal dysplasia (Asamura et al., 2005, Czarny-Ratajczak et al., 2001). In addition, *Col9a1* is essential for normal fracture healing, where the absence of *Col9a1* delays bone mineralization and healing (Opolka et al., 2007). It is well established that FGFR2 signalling is involved in chondrogenesis and drives *Sox9* expression (Sarkar et al., 2001). *Col9a1* is downstream of *Sox9*, linking it with FGFR2 signalling.

Immature chondrocytes, such as those expressing *Col2a1*, invades the suture mesenchyme under pathogenic conditions (He and Soriano, 2017). Altogether, the upregulation of *Col9a1* in *Fgfr2c*$^{C342Y/+}$ suggests increased chondrogenesis and mineralization in the coronal suture.

Downregulated genes:

7.3.2.4-*Pcyt1b*

Pcyt1b encodes for the enzyme CTP: phosphocholine cytidydyltransferase (CCT) responsible for the synthesis of phosphatidylcholine, responsible for the formation of membrane phospholipids. There are two isoforms to CCT, in CCTα and CCTβ, where the latter is a product of *Pcty1b* expression. *CCTα* is widely abundant, whilst *Pcyt1b* is mainly expressed in the brain and gonads (Karim et al., 2003). Deficiencies in phosphatidylcholine affects cellular activity *in vitro* whilst reinstatement of CCT is sufficient to restore proliferation (Karim et al., 2003). Therefore, correct formation of the plasma membrane has subsequent effect on cellular responses and in turn driving resultant phenotypes. For example, *Pcyt1α*$^{+/-}$ displays liver hypoplasia due to fewer hepatocytes, whilst *Pcyt1b*$^{-/-}$ had disrupted gonadal morphology (Jackowski et al., 2004, Wang et al., 2005a). Specifically, these *Pcyt1b*$^{-/-}$ animals had a larger lumen, reduced germinal layers owing to the degeneration of seminiferous tubes and spermatoza (Jackowski et al., 2004). FGFR2 is an established player in sex determination, providing a link between *Pcty1b* and FGF signalling (Bagheri-Fam et al., 2017, Bagheri-Fam et al., 2015). More strikingly, CCTβ and FGFR2 are both expressed testes within the seminiferous tubes (Jackowski et al., 2004, Lai et al., 2016). CCTβ is likely connected to altering the sensitivity of growth factor signalling, with specific reference to the RAS-MAPK pathway (Carter et al., 2008, Weber et al., 2003). For example, increasing exposure of Nerve Growth Factor (NGF) corresponds to the expression of *Pcyt1b* and phosphatidylcholine concentration, implying increased synthesis of phospho-membrane, whilst ERK inhibition can reverse this biochemical event (Carter et al., 2008). The molecular mechanisms dictating signalling dynamics were furthered characterised in the *Drosophila* homologue *dCCT1*, where it governs the turnover of receptors on the cell surface (Weber et al., 2003). Knockout of *dCCT1* results in increased membrane retention and cytoplasmic localisation of Epidermal Growth Factor Receptor

(EGFR). The alterations to the number of receptors on the cell surface ultimately led to disrupted cellular architecture in the eye, and terminal differentiation defects (Weber et al., 2003). Maintaining the sensitivity of signalling on the cell surface is pivotal for conveying the correct signalling interpretation for normal cellular proliferation and differentiation (Miaczynska, 2013). There has been a report of non-syndromic craniosynostosis related to the loss of *PCYT1B* in humans, with the deletion of Xp22.11 on the X chromosome (van Kogelenberg et al., 2011). The significance of cell membrane integrity appears to have substantial outcomes in monitoring signalling dyamics. Furthermore, receptors carrying the Crouzon mutation is known to have altered trafficking dynamics. In the case for FGFR2-C278F, there is an increased localisation of the receptor in the cell cytoplasm due to deficiencies in trafficking to the cell surface (Hatch et al., 2006). Overall, this implies $Fgfr2c^{C342Y/+}$ is likely to have affected receptor trafficking owing to disrupted cell membrane integrity through the indirect control of *Pcty1b*.

7.3.2.5-*Pdgfb*

Platelet derived growth factor (PDGF) signalling is prominent in embryogensis, where it is associated with cellular proliferation, survival, migration and formation of the extracellular matrix (Hoch and Soriano, 2003). Similar to FGFRs, Platelet derived growth factor receptors (PDGFR) are tyrosine receptor kinases binding to secreted PDGF ligands. Functional PDGFRs exist in three dimers αα (PDGFRα), αβ(PDGFRαβ) and ββ (PDGFRβ), for which the pairing allows differential pathways activation and ligand specificity. Similar to FGFRs, the isoforms are differentially expressed in specific tissue to promote paracrine signalling, with *PDGFRα* broadly expressed in the mesenchyme. There are four isoforms of PDGFs identified: *PDGFA*, *PDGFB, PDGFC* and *PDGFD*. All functional PDGFs are secreted homodimers, with only PDGFA and PDGFB able to form heteodimers together. These ligands have different affinities for PDGFRs, with PDGFB dimers possessing affinities to all three isoforms of PDGFRs (Hoch and Soriano, 2003).

PDGFRs are critical for skeletogenesis (Soriano, 1994, Soriano, 1997, Tallquist and Soriano, 2003). $Pdgfr\alpha^{-/-}$ embryos display multiple midline defects along the axial skeleton

likely due to somite mis-specification, and a facial cleft (Soriano, 1994, Tallquist et al., 2003). The facial cleft is due to deficiencies in NCCs populating the frontal nasal prominence, thanks to altered chemotaxis and limited proliferation capabilities (He and Soriano, 2013). In contrast, conditional deletion of *Pdgfrβ* in the NCC lineage is less severe, resulting in widening of the nasal septum and delayed palatal closure (Fantauzzo and Soriano, 2016). This redundancy may stem from the compensatory effect of the α isoform (Fantauzzo and Soriano, 2016). Both isoforms also genetically interact, as *Pdgfrβ*$^{-/-}$ in a *Pdgfrα*$^{-/-}$ background yielded extended facial clefting spectrum to the α isoform (Fantauzzo and Soriano, 2016).

Despite phenotypic spectrum yielded between both isoforms, the phenotypic consequence is largely related to the ligand specificities of the PDGF binding domains: Swapping out the catalytic domain of a PDGFR and replaced that from the other isoform (i.e α to β or β to α) resulted in largely redundant phenotypes (Klinghoffer et al., 2001). This suggests the signal transduction of PDGFRs is largely conserved, and the phenotypic consequence is minor to that of ligand specificity. It has been recently demonstrated from the same group the involvement of PDGF signalling in craniosynostosis (He and Soriano, 2017). Here, ectopic PDGFRα signalling led to expansion of the calvarial cartilage, and invasion of chondrocytes into the suture mesenchyme, which eventually trans-differentiated into osteoblasts (He et al., 2017). PDGFA is the ligand responsible for chondrocyte specification, where increasing exposure of mesenchymal cells to PDGFA promotes cartilage formation (Tallquist and Soriano, 2003). This is likely to be channelled through the PI3K-AKT pathway, a primary effector of PDGFRα (Klinghoffer et al., 2002, Fantauzzo and Soriano, 2014, He and Soriano, 2017). Taken together, PDGFRα signalling appears to be the dominant isoform in skeletogenesis and craniofacial development.

In spite of this, *Pdgfb*$^{-/-}$ displays strong phenotypic similarities to *Pdgfrβ*$^{-/-}$, suggesting the 'B' homodimer is a major binding partner to PDGFRβ (Soriano, 1994, Leveen et al., 1994). Major characteristics of signalling misregulation by the β isoform includes glomerular patterning defects and haemorrhage. One common phenotype of overactive PDGFR signalling is fibrosis reported in multiple organs, implying its role in inflammation and responses to injury

(Czochra et al., 2006, Hoyle et al., 1999, Gallini et al., 2016, Olson and Soriano, 2009). However, excessive PDGF can also stimulate proliferation in certain cell types, such as glial progenitors residing in the central nervous system (Noble et al., 1988). Overexpression of *Pdgfb* in astrocytes induces dedifferentiation into neural progenitors in gliomas (Dai et al., 2001). Similar responses were reported in osteogenesis, as MSC proliferation was less in $Pdgfr\beta^{-/-}$, but more importantly driving osteoblast differentiation (Tokunaga et al., 2008). In fact, the differentiation and mineralisation of osteoblast were in part, owed to the synergistic effects of BMPs and FGFs (Chaudhary et al., 2004). Application of PDGFB *in vitro* inhibits osteoblast differentiation, with a downregulation of osteogenic genes such as *Runx2*, *Osterix* and *osteocalcin* (Tokunaga et al., 2008). Cell therapies have been devised to take advantage of the tripartite effects of PDGFRβ, BMPs and FGFs (Chen et al., 2015b). Chen et al., 2015 demonstrated that it is possible to pre-amplify hematopoetic stem cell (HSC) population *in vitro* through the ectopic induction of *Pdgfb*, prior to delivery into an irradiated (bone marrow deficient) host animal. Here, the authors observed a substantial increase in bone density, and discussed the clinical benefits for treatment of bone diseases such as osteomalacia (Chen et al., 2015b). The downregulation of *Pdgfb* in $Fgfr2c^{C342Y/+}$ fits in line with the previous studies, implying ectopic differentiation activity in the suture mesenchyme, and that PDGF signalling acts downstream of FGFR2 to promote suture closure.

7.3.2.6-*Rsad2*

Radical SAM domain containing 2 (*Rsad2*) encodes the protein viperin. Viperin was first discovered in cells in response to human cytomegalovirus (HCMV) infection. *Rsad2* is downstream of interferon (IFN) signalling, and is responsive to IFNα, IFNβ and IFNγ (Chin and Cresswell, 2001). Upon expression of *Rsad2*, viperin is translocated to the endoplasmic reticulum, to the Golgi apparatus and finally to the cytoplasmic vacuoles-a cellular phenotype in response to cytotoxic factors (Chin and Cresswell, 2001). *Rsad2* displayed the greatest downregulation in $Fgfr2c^{C342Y/+}$, and was therefore chosen for expression validation. Despite the role of *Rsad2* in response to virus, several studies also report *Rsad2* to be downregulated in autoimmune bone diseases such as rheumatoid arthritis (He et al., 2016, Raterman et al., 2012).

This prompts the role of *Rsad2* in bone remodelling to cytokines and inflammation. Despite the link of *Rsad2* to FGFR2c signalling being elusive, the role of cytokines modulating the extracellular milieu is well described especially in the field of neurodegeneration (Blank and Prinz, 2017). IFN signalling is a major effector pathway for immune responses, and is also responsible for central nervous system homeostasis. IFNs are upregulated in astrocytes in response to neurotoxicity and is critical for microglial activation. This unique anti-inflammatory response allows microglia to secrete a series of cytokines, such as interleukins, to offer protection against neurotoxicity and degeneration. Due to their anti-inflammatory and survival properties, IFNβ has been clinically trialled to reduce relapse in multiple sclerosis patients (Chofflon, 2000). IFNs also play multiple roles in osteogenesis. For instance, IFNγ is a positive regulator for osteoblast differentiation and attenuates osteoclast activity (Croes et al., 2016, Duque et al., 2009, Takayanagi et al., 2000). Additionally, conditional knockout of IFNγ receptor (*IFNγR*$^{-/-}$) led to substantial deterioration of bone architecture (Takayanagi et al., 2000). Conversely, IFNβ augments osteoclast activity and is linked to bone resorption (Seeliger et al., 2015). The significance of IFN signalling is therefore to promote bone homeostasis and remodelling of the cytoarchitecture, and signalling misregulation has led to progressive bone diseases such as osteoporosis (Seeliger et al., 2015).

Osteoporosis has been linked to *Stat1* misexpression, a target of IFN signalling and the P13K-AKT pathway, where *Stat1* attenuates osteoblast differentiation and promotes osteoclastogenesis (Seeliger et al., 2015, Kim et al., 2003b). Specifically, Stat1 physically inhibits *Runx2* to prevent expression of osteogenic genes such as osteocalcin. IFNγ is upstream of Stat1, and is able to relieve the Stat1-Runx2 interaction to promote osteogenesis, which explains increased bone mass in *Stat1*$^{-/-}$ despite having accentuated osteoclast activity (Kim et al., 2003b). As *Rsad2*/viperin is a downstream target of IFN signalling, along with RNAseq dataset pointing towards its expression is regulated by FGFR2c, it provides a novel link between osteogenesis and inflammatory signalling. One speculation into the mode of action by viperin in osteoblast differentiation could involve the cytoskeleton (Seo et al., 2011). Despite reports of *Rsad2* expression in reponse to virus, it also promotes viral transmission between

cells (Chin and Cresswell, 2001, Seo et al., 2011). HMCVs have been hypothesised to specifically target *Rsad2* expression because of viperin's ability to disrupt adenosine triphosphate (ATP) synthesis in the mitochondria, which subsequently have adverse effects on actin stability (Seo et al., 2011). Osteoblast differentiation is dependent on the cytoskeleton, whereby stabilised actin filaments (F-actin) is required for MSCs differentiating to an osteogenic lineage (Chen et al., 2015a). Therefore, the downregulation of *Rsad2* by FGFR2c leads to the stability of the cytoskeleton, augmenting osteoblast differentiation.

7.3.3-Justifications of using LCM to screen the embryonic suture

The downstream targets of FGFR2c responsible for regulating suture patency remain relatively uncharacterized, and screening the embryonic sutures of *Fgfr2c*$^{C342Y/+}$ directly provides a useful method to identify these genes. The current transcriptomic approach involves screening human patients with syndromic craniosynostosis, where they are categorized and profiled based on their phenotype (Reardon et al., 1994, Muenke et al., 1994, Twigg et al., 2015, Twigg et al., 2004, Coussens et al., 2007). This 'shotgun' approach does not offer sufficient resolution to uncover molecular signatures inside the suture, and moreover, does not draw links between FGFR2c signalling and its targets. Furthermore, the expression of calvarial osteoblasts is different within *in vivo* and *in vitro* conditions, which makes micro-profiling analysis difficult (Zhao et al., 2015, Coussens et al., 2008). Indeed, one of the greatest challenges is to maintain stable gene expression when osteoblasts are translocated to an *in vitro* environment prior to profiling. This is related to osteoblasts reverting to a primitive state by de-differentiating into pre-osteoblasts in culture upon removal of the ECM (Owen et al., 1990, Coussens et al., 2008). An interesting study performed by Coussens et al (2008) appears to address these issues by comparing microarray profiles of human cranial sutures directly obtained from surgery and those cultured under *in vitro* conditions. By comparing the changes in expression profiles, it is possible to identify the changes in gene expression responsible for osteoblast differentiation. Despite playing a minor role in craniofacial development, one of the most intriguing observations was the ectopic upregulation of *FGFR3* more than a 100 fold (Coussens et al., 2008, Deng et al., 1996). As FGFR3 is a negative regulator of bone formation,

a speculation for this upregulation could be an attempt for osteoblasts to trigger negative feedback in response to ectopic osteoblast differentiation (Deng et al., 1996).

However, despite experimental success in humans, extracting samples accurately from mouse embryonic sutures poses a greater challenge. This challenge was addressed using LCM to access the sutures of *Fgfr2c*$^{C342Y/+}$ and profiling it. In particular to the LCM, the sutures are almost inaccessible during embryonic development due to its size. A previous microarray screen attempted in the lab involved isolating the coronal suture by cutting around the vicinity of the suture, and led to the identification of genes expressed in the periosteum (e.g. *Dlk*). Adopting FACS sorting is not possible due to the lack of markers available to the coronal suture along with the difficulty of obtaining sufficient cells to start a primary culture. Altogether, LCM was identified as a potential method to overcome these challenges, and to provide a solution for screening specificity.

7.3.4-Experimental limitations

Multiple challenges have risen throughout the LCM based gene expression analysis pipeline that has potentially compromised the quality of the experiment. Firstly the samples, since the genetic background of the mice were not uniform prior to the screening process. For example, the mice were generated on a mixed CD1 background to that of an inbred strain i.e. C57BL/6, and were also not sex matched. The latter was a decision based on the lack of phenotypic differences between males and females. Moreover, this was necessary to conform to efforts to minimize intra-litter variability by choosing littermates.

A very important technical challenge for this experiment was attempting to preserve RNA integrity. Due to the nature of extracting RNA from stained tissue sections, the RNA quality was below the average generally used for sequencing, as indicated by Tapestation analysis in Figure 58 B. Furthermore, due to low levels of starting material, it was necessary to amplify RNA prior to cDNA library synthesis which resulted in amplification of non-specific signals in the process. The consequence as such, can be seen in Figure 59 in both the PCA plot and genome alignment of the samples. Specifically, the scattered data points along the PC1 and PC2 axis gave variabilities to expression analysis (Figure 59 A). This was particularly notable

in the WT group where unique expression profiles were detected between samples, which would have skewed the overall analysis of the dataset. Furthermore, there was a strong 3' representation in the genome given by the alignment scores in Figure 59 B, implicating RNA degradation. Altogether, these factors may have skewed the overall analysis. Future experiments would aim to preserve RNA integrity by minimizing tissue processing. For instance, RNA quality could be improved if the samples were not processed for histology prior to LCM. However, histological staining was deemed critical to visualize the limits of the suture and therefore allow precise extraction of the desired tissue. This would be particularly important for an experiment profiling specific regions inside the suture such as the osteogenic front. This also implies the potentials for variability due to differential isolation from a heterogenous group of cells, including those that do not correspond to expressing *Fgfr2c. Fgfr2* expression is abundant in the osteogenic front, but this LCM experiment also incorporated a substantial amount of the mesenchyme (Johnson et al., 2000). This could further explain the lack of differential expression when the RNAseq dataset was run against the FGF signalling entity list. Owing to multiple factors giving rise to these variabilities, subsequent analysis was not determined using the 'p-value' approach, but on the overall fold change instead. To justify the analysis further, read counts must be consistent across the three biological replicates within their respective genotype. This approach has yielded success in the selection of candidate genes for expression validation, for which the results corresponds to trends reported in the previous literature.

Expression validation was attempted using different methods including RNA extracted from whole E12.5 embryos. This was partly due to the extensive pipeline required for LCM and the overall cost of the experiment. E12.5 was chosen due to the simplicity of processing the sample for RNA extraction and at a suitable stage of craniofacial morphogenesis (Deckelbaum et al., 2012). Performing expression validation at E12.5 wholemount should be proceeded with caution due to inconsistencies in spatial-temporal resolution of gene expression. A potential solution could involve RNA isolation from more precisely dissected the head mesenchyme tissues.

RT-qPCR analysis using the delta-delta CT method identified differences for the reference gene (*Rn18*) between litters (data not shown). Specifically, *Fgfr2c*$^{C342Y/+}$ possessed high Ct (Cycle threshold) values in the raw data, which ultimately led to the perception of ectopic expression of genes in question when the ratios were calculated. This false positive ('Type 1 error') can be perceived when non-parametric Kruskal Wallis test with Dunn's posthoc was performed on the analysis. Reference genes expression should not change regardless of the experimental condition and similar results were obtained when GAPDH was used against the same samples (data not shown). Therefore, the high Ct values were not due to the low input of cDNA, but endogenous expression levels between the litters. Expression validation should be processed within the same litter in the future and cDNA concentration checked within the desired benchmark across all samples.

As an alternative for RT-qPCR expression validation, the following methods could be explored. Firstly, one could attempt to cut around the vicinity of the suture at E16.5 to obtain a defined region at the correct stage. Additionally, a microneedle made from capillary tube could be inserted into the coronal suture to scrape off the mesenchyme and osteogenic fronts. Here, the extracted RNA quantity is expected to be low, and would need to be amplified if necessary prior to cDNA synthesis. Finally, RT-qPCR would give the inference on the quantity of expression; qualitative approaches would involve designing ISH probes or performing IHC on the genes in question.

7.3.5-Future Directions

7.3.5.1-Functional analysis

The immediate future requires addressing the pit-falls occurred during expression validation and to optimize the methods for quantitative and qualitative assays. In the medium term, experiments will need to confirm the candidates' relationship with FGFR2c signalling. This could be performed *in vivo, ex-vivo* or *in vitro*. The general scope revolves around the manipulation of the FGFR2c signalling pathway and examining candidate gene expression output. This could be simply achieved *in vivo* by performing IHC or ISH directly on the *Fgfr2c*$^{C342Y/+}$. *Ex vivo* or *in utero* experiments can also help achieve this aim, such as applying

FGFR2 inhibitor bead implants directly onto the embryonic suture of *Fgfr2c*$^{C342Y/+}$ and observing the candidate's response. In the long term, gene expression will need to be confirmed in the human calvaria, which could be carried out on samples procured via the Human Developmental Biology Resource (http://www.hdbr.org/). The ultimate aim of this research is to better understand the molecular events in play with a view to developing rational non-invasive compounds that can be used to minimize recurrent surgeries. Manipulating the RAS-MAPK cascade is a possibility but may prove to be highly risky owing to its potency (Shukla et al., 2007). Should a candidate gene possess significant potential as an effector of FGFR2c in relation to the development of syndromic craniosynostosis, therapeutic compounds would aim to target these candidates directly to either potentiate or attenuate their expression. Novel compounds can be tested *in vitro* prior to the translation onto *Fgfr2c*$^{C342Y/+}$ to assess the impact on suture morphogenesis. In particular, the mouse model will provide a platform for pre-clinical evaluation of the best routes of administration, safety and effectiveness of compound post surgery.

7.3.5.2-Transcriptomic experiments

'FaceBase' is a consortium available for craniofacial researchers (http://www.facebase.org). Their aim is to 'generate data in support of advancing research into craniofacial development and malformation' (www.facebase.org/about). FaceBase has a wide range of curated RNAseq datasets available online for craniofacial development. More importantly, several groups have contributed to this development by generating transcriptomic atlases of calvarial sutures, also acquired from LCM, during the time of the current study. So far, FaceBase has curated databases for the transcriptomic atlas of coronal sutures in *Fgfr2*$^{S252W/+}$ (Apert) and *Twist1*$^{+/-}$ at multiple embryonic stages. Therefore, it would be useful to cross-reference this data with that of *Fgfr2c*$^{C342Y/+}$ from this study. In particular, the data from *Fgfr2*$^{S252W/+}$ might be expected to be similar to that of *Fgfr2c*$^{C342Y/+}$ due to the mutations affecting *Fgfr2*. The aim of cross-referencing databases allows genes common to craniosynostosis to be identified, and therefore improving the chance of relevant broader acting novel therapeutic targets. As craniosynostosis is a progressive pathology, the expression profile

is expected to be dynamic and changes temporally. Further screens should involve comparing gene expression profile at multiple stages for the onset of suture morphogenesis to that of just prior to suture closure. Genes involved in craniosynostosis should be persistent throughout all the temporal times points analysed. Finally, a spatial transcriptomic atlas could also be explored through profiling landmarks within the coronal suture, such as the osteogenic front, mesenchyme and periosteum.

Chapter 8

General Discussion

And

Concluding Remarks

8.1-Overall summary and scope of research in the wider community

This doctoral research set out to investigate some of the molecular events contributing to syndromic craniosynostosis. Currently, the cellular and biochemical pathways regulated by FGFR2c during craniofacial development still remain elusive. Therefore, this lab created a conditional mouse model that overexpresses FGFR2c in order to evaluate the effect of altered expression on craniofacial development. This study first characterised the differential sensitivities to *Fgfr2c* misregulation in both NCC and mesoderm lineages. Specifically, *Fgfr2c* overexpression results in hypoplasia of the NCC derived cranial bones, suggesting NCC derivatives are affected by increased *Fgfr2c* signalling. Furthermore, *Fgfr2c* overexpression does not result in craniosynostosis. This may be secondary to ostegenic hypoplasia and/or works in concert with the attenuation of osteoblast activity in the osteogenic front. On a molecular level, it is known that lineage specific osteoblasts have differential expression profiles and altered expression *Fgfr2c* is likely to contribute to the spatio-temporal dynamics of the signalling response, potentially explaining the phenotypic consequences (Quarto et al., 2009, Quarto et al., 2010). However, tissue sensitivities towards FGFR2c signalling have not been reported *in vivo*, and questions remain as to the significance of the differences observed between the frontal and parietal osteoblasts along with their roles in bone development and suture patency. One hypothesis is that the frontal bone may be more dynamic to bone remodelling in order to accommodate the features of the skull (Moazen et al., 2015). From a clinical perspective, the osteogenic differences between both lineages have implications regarding the efficiency of bone regeneration and for selecting the correct osteoblasts for potential transplantation therapy (Doro et al., 2017). Differential sensitivities of the cranial mesenchyme demonstrated here, confirm differences in the specific embryonic lineages, particularly in response to FGF ligands during early development as recently reported for FGF8 (Schmidt et al., 2018).

One of the most striking features of *Fgfr2c* overexpression compared to the *Fgfr2c*$^{C342Y/+}$ mutant is the lack of craniosynostosis. To investigate this further, this study examined readouts of the FGF signalling pathway in the coronal suture. A key finding from this

experiment was the demonstration of pERK upregulation in both $R26R^{Fgfr2cV5/+}$; $\beta actin^{CRE/+}$ and $Fgfr2c^{C342Y/+}$. These similarities were unexpected due to the contrasting phenotypes of these sutures and the biochemical nature of receptor activation verses overexpression. Although pERK is upregulated in both $Fgfr2c^{C342Y/+}$ and $R26R^{Fgfr2cV5/+}$; $\beta actin^{CRE/+}$, only $Fgfr2c^{C342Y/+}$ sutures show increased levels of ALP. This indicated that augmentation of RAS-MAPK signalling in the suture alone was not sufficient to derive a coronal synostosis phenotype. This was further supported by amelioration of the coronal synostosis phenotype when the *Fgfr2c* overexpression allele was introduced onto the $Fgfr2c^{C342Y/+}$ background. This has pronounced implications for our understanding of the FGFR2c signalling paradox, where the complete removal or activation of FGFR2c signalling both leads to craniosynostosis (Eswarakumar et al., 2004, Eswarakumar et al., 2002). Ultimately, elucidating the paradox should involve understanding the differences between cascade activation and the events immediately occurring after receptor activation, such as receptor turnover in the presence of GOF mutations. Furthermore, little is known about the downstream consequences of individual signalling cascades in an *in vivo* context. Targeted disruption of downstream mediators should help to address the roles of individual cascades in craniofacial development. As such, this study offers experimental insights suggesting that it is possible to use cancer mouse models to understand consequences of growth factor signalling in craniofacial development. Extracellular modulators of FGF ligands (e.g. HSPGs) and negative feedback mechanisms (e.g. SPRY and DUSP6) are also crucial to FGF signalling dynamics (Ornitz and Itoh, 2015). These are currently limited in our present understanding of craniofacial development, but *in vivo* evidence already implied *Dusp6* LOF is sufficient to drive craniosynostosis (Li et al., 2007). Furthermore, overexpression of *Spry2 in vitro* preludes the expression of various osteoblast markers, which suggests low FGF signalling is required for cellular differentiation (Yang et al., 2006). This study confirmed the expression of *Spry2* and *Spry4* in the cranial bones, and therefore, understanding the relationship between FGF signalling and feedback regulators will give insights into the regulatory loops involved in maintaining suture patency.

Another interesting finding was the emerging role of cartilage in craniosynostosis, since *Fgfr2c*$^{C342Y/+}$ mice were shown to display excessive cartilage formation. Membranous bones were originally thought to form without a cartilage template (Ornitz and Marie, 2015, Akiyama et al., 2002). However, several studies have touched upon excessive cartilage in pathological conditions (Wang et al., 2005b, Peskett et al., 2017, Behr et al., 2011a, He and Soriano, 2017). Their roles are not well characterised, but similarities can be drawn between suture closure and fracture healing in endochondral bones, as chondrocytes have been witnessed to invade the damaged mesenchyme to repair the bone (He and Soriano, 2017, He et al., 2017). Therefore, lessons may be learnt from fracture healing to benefit the clinical craniofacial community.

Little is known about the downstream genes that may be misregulated as a consequence of *Fgfr2c* GOF mutation. This study therefore used the Crouzon mouse with its craniosynostosis phenotype as a model in which to monitor altered gene expression in developing sutures using RNAseq. LCM was adopted to specifically sample the embryonic coronal suture with high resolution. The long-term goal was to identify and test potential candidate genes that could in the future be targeted for therapy. This study succeeded in piloting the LCM technique and thus to generate an expression profile of the coronal suture mesenchyme. The experiment was similar to that performed elsewhere for a different mutant mouse, *Fgfr2*$^{S252W/+}$ (Brinkley et al., 2016). It will therefore, be important in the near future to cross-reference the *Fgfr2c*$^{C342Y/+}$ and *Fgfr2*$^{S252W/+}$ data in order to identify common genes affected by FGFR2 signalling.

Several other issues remain to be addressed beyond the scope of this PhD and in the general craniofacial community:

1) This project investigated the embryonic events leading towards craniosynostosis but did not look into the postnatal stages. This next stage may be especially relevant, since the craniosynostosis phenotype is progressive from late gestation and fully penetrant postnatally. Postnatal experiments with the aim of delaying or halting craniosynostosis development would be particularly relevant from a clinical perspective, and this would involve the testing of novel therapeutic compounds and surgical applications. Examples could include testing of RNA interference compounds or pharmacological agents that manipulate the FGFR2 signalling

pathway to prevent craniosynostosis in *Fgfr2c*$^{C342Y/+}$. Other means could also include investigating the optimal methods of administration. Performing these experiments *in vivo* helps to monitor for such unforeseen events as unexpected side effects that might develop over the longer term, in addition to any off target consequences. A comprehensive understanding of FGFR2 signalling is vital to developing non-invasive therapies. As an example, pharmacological interventions may not be ideal for inhibiting FGFR2-C342Y as the receptor activation is ligand independent, and efforts should aim to target intermediates or downstream target genes that contribute to craniosynostosis. Furthermore, biomechanical modelling of the calvarial bones will also be necessary to test novel surgical techniques to improve craniofacial corrections in the long term. It is therefore an important goal to translate these findings from the bench to clinical benefit, with the aim of reducing the need for recurrent surgery in patients with syndromic craniosynostosis.

2) An outstanding question remains as to the molecular events responsible for craniosynostosis in *Fgfr2c*$^{-/-}$, and whether they are similar to that of *Fgfr2c*$^{C342Y/+}$. In the short term, future work could involve performing the same experiments in this study on the *Fgfr2c*$^{-/-}$, and compare the data to that of *Fgfr2c*$^{C342Y/+}$ to determine how they differ *in vivo*. Other experiments might also aim to understand how therapeutic compounds behave in *Fgfr2c*$^{-/-}$ to that of *Fgfr2c*$^{C342Y/+}$, considering both manifest the same phenotype. In addition, transcriptomic profiling of *Fgfr2c*$^{-/-}$ could also facilitate the understanding of identifying common and/or contrasting molecular signatures, which are currently unavailable in the literature. Uncovering the molecular signatures between both these models will be crucial to generate a blueprint of FGF signalling misregulation. The outcome of this data will provide insights into novel regulatory networks and interactions required for normal FGF biology.

3) Despite the fact that *Wnt1*$^{CRE/+}$ and *Mesp1*$^{CRE/+}$ are widely used in studies of craniofacial development including calvarial bone formation (Jiang et al., 2002), these do not specifically target the suture mesenchyme. Craniosynostosis in Saethre-Chotzen syndrome, for example (*Twist1*$^{+/-}$), stems from the mesenchyme and suture abolishment is thought to be mechanistically distinct to that related to FGFR2 misregulation (Behr et al., 2011b, Zhao et al.,

2015). Therefore, obtaining suture specific CRE lines will be useful to study the mesenchyme without interference of the calvarial bones. To this end, *En1*$^{CRE/+}$ and *Gli1*$^{CRE/+}$ are CREs currently available that according to the literature specifically target the suture mesenchyme (Deckelbaum et al., 2012, Deckelbaum et al., 2005, Zhao et al., 2015). Albeit not tested, CRE lines reflective of mesenchymal markers such as *Prx1*$^{CRE/+}$ may also be explored (Logan et al., 2002). Furthermore, adopting inducible CRE lines would circumvent any postnatal lethality caused by secondary phenotypic features like cleft palate and allow for the analysis of postnatal progression of craniosynostosis.

4) Perhaps one of the foremost challenges posed is the localisation of the FGFR2 isoforms *in vivo*. The difficulty lies as a consequence of the high sequence homology of the splice variants, and understanding its spatial expression provides inference as to where to target the isoforms locally *in vivo*. Visualizing the individual splice-forms could be attempted using the following approaches:

i) Antibodies specific for FGFR2 isoforms: There are few companies that produce isoform specific antibodies against FGFR2 and most studies using isoform specific antibodies to date, have focused on protein assays (i.e. enzyme-linked immunosorbent assay; ELISA) or immunoblots (Nonogaki et al., 2016). Stringent controls must be first examined *in vitro* to establish their validity. This may be achieved using immuoblots following cellular transfection of plasmids carrying the *Fgfr2* splice form. For instance, a positive band is to be expected only in respective cellular transfection corresponding to the antibody of interest. Next, these antibodies would be assayed by IHC to determine the precise protein expression. Lineage specific controls are vital for this step. The developing limb bud serves as an excellent control as both isoforms are expected to be in the primordia (Li et al., 2007).

ii) ISH on *Fgfr2b*$^{-/-}$ and *Fgfr2c*$^{-/-}$: Whilst previous studies have attempted to perform ISH on the splice variants, the resolution has not been sufficient to derive conclusive data (Orr-Urtreger et al., 1993, Rice et al., 2000). Further inspection of the different splice variants using ISH could be performed on isoform-specific knockouts.

The overall design of the probe should cover *Fgfr2* and common to both isoforms. The aim is to locate expression patterns unique to respective isoform specific knockouts. For example, if ISH is performed in the *Fgfr2c*$^{-/-}$ developing limb bud, positive hybridization should only be expected in the epithelium but not the mesenchyme, and vice versa for *Fgfr2b*$^{-/-}$. By comparing the expression patterns unique to *Fgfr2b*$^{-/-}$ and *Fgfr2c*$^{-/-}$, the domains expressing respective isoforms can be pinpointed with accuracy and mapped in detail.

iii) Lineage tracing of FGFR2 isoforms driven under an endogenous promoter:

The use of reporter lines allow cellular behaviour to be monitored *in vivo* and has revolutionised the field of developmental biology and our understanding of both embryogenesis and organogenesis. However, there is a lack of *in vivo* evidence for lineage tracing of FGFR2 isoforms to date. The difficulty of generating a reporter line for this gene is likely due to the nature of splicing mechanism of the isoforms, making it difficult to design a targeting construct. Generating a viable construct must therefore bypass any disruption to biological function and splicing mechanism. A potential approach to transgenesis could be attempted through generation of a fusion construct (Figure 64 A and B): Here, reporters (e.g. GFP) are flanked by a nucleus tag-Histone H2B and a 2A peptide sequence (Figure 65 A). The 2A peptide sequence was originally identified in foot and mouth virus with an aim to generate the mature viral protein (Ryan et al., 1991). Upon gene expression, the 2A peptide cleaves the reporter protein from the protein of interest and generates two independent products (Figure 65 B). As the reporter protein has a histone 2B tag, it is targeted for the nucleus upon proteolytic processing (Figure 65 B). This method offers significant advantages in lineage tracing, as it corresponds to the direct readout of the endogenous promoter i.e. *Fgfr2*. Furthermore, the 2A peptide is small (approx. 25bp), which helps to minimize biological interference (Ryan et al., 1991).

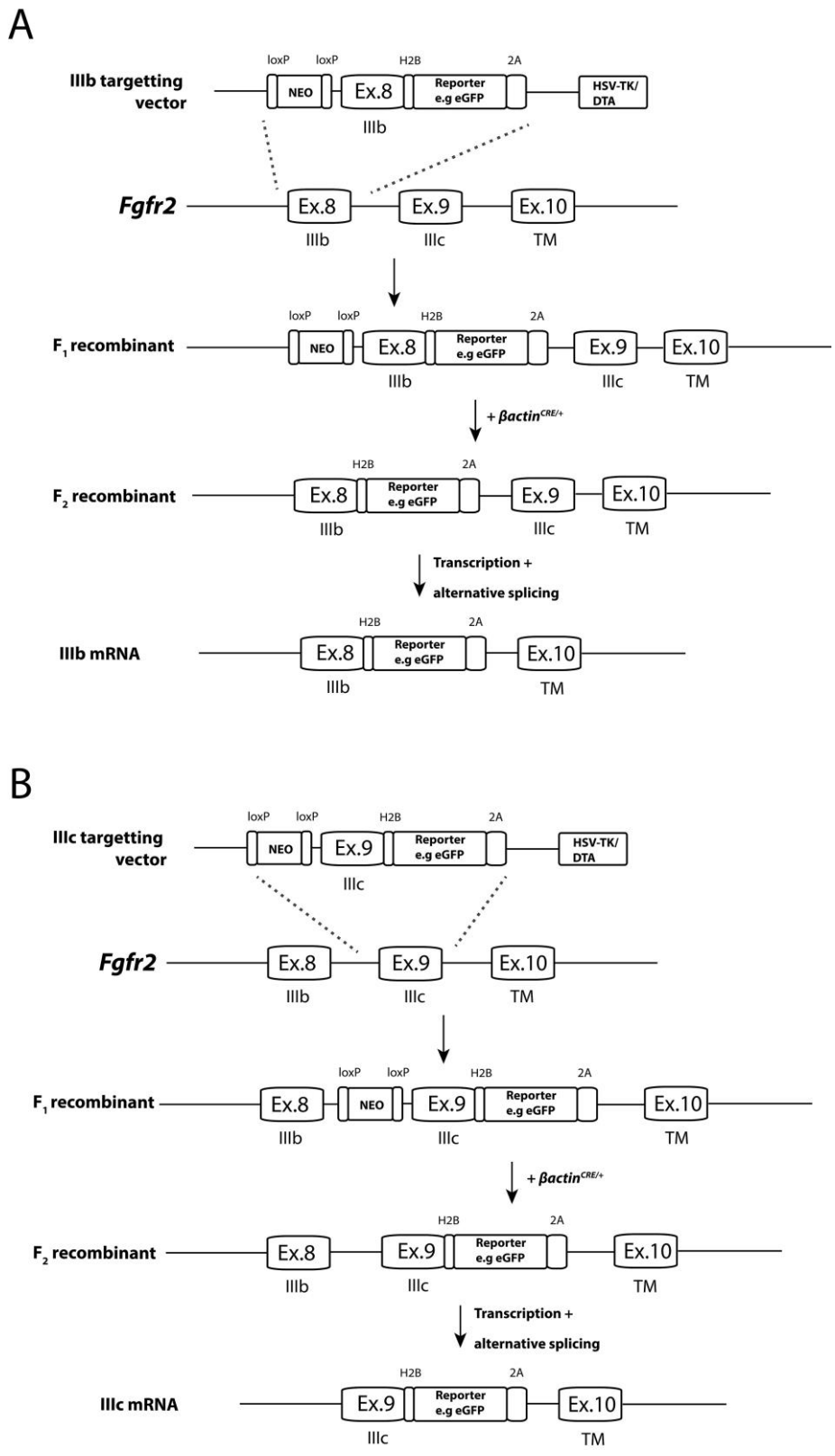

Figure 64: Potential approach to generate endogenous reporter mice for *Fgfr2b* (A) and *Fgfr2c* (B) lineage tracing.

Exon 8 or 9 is substituted with a targeting construct containing the H2B-GFP-2A construct downstream of the exon of interest. HSV-TK/DTA: Human simplex virus-thymidine kinase/Detheria toxin; IIIb: exon 8 specific for *Fgfr2b;* IIIc: exon 9 specific for *Fgfr2c*; Neo: Neomycin selection cassette.

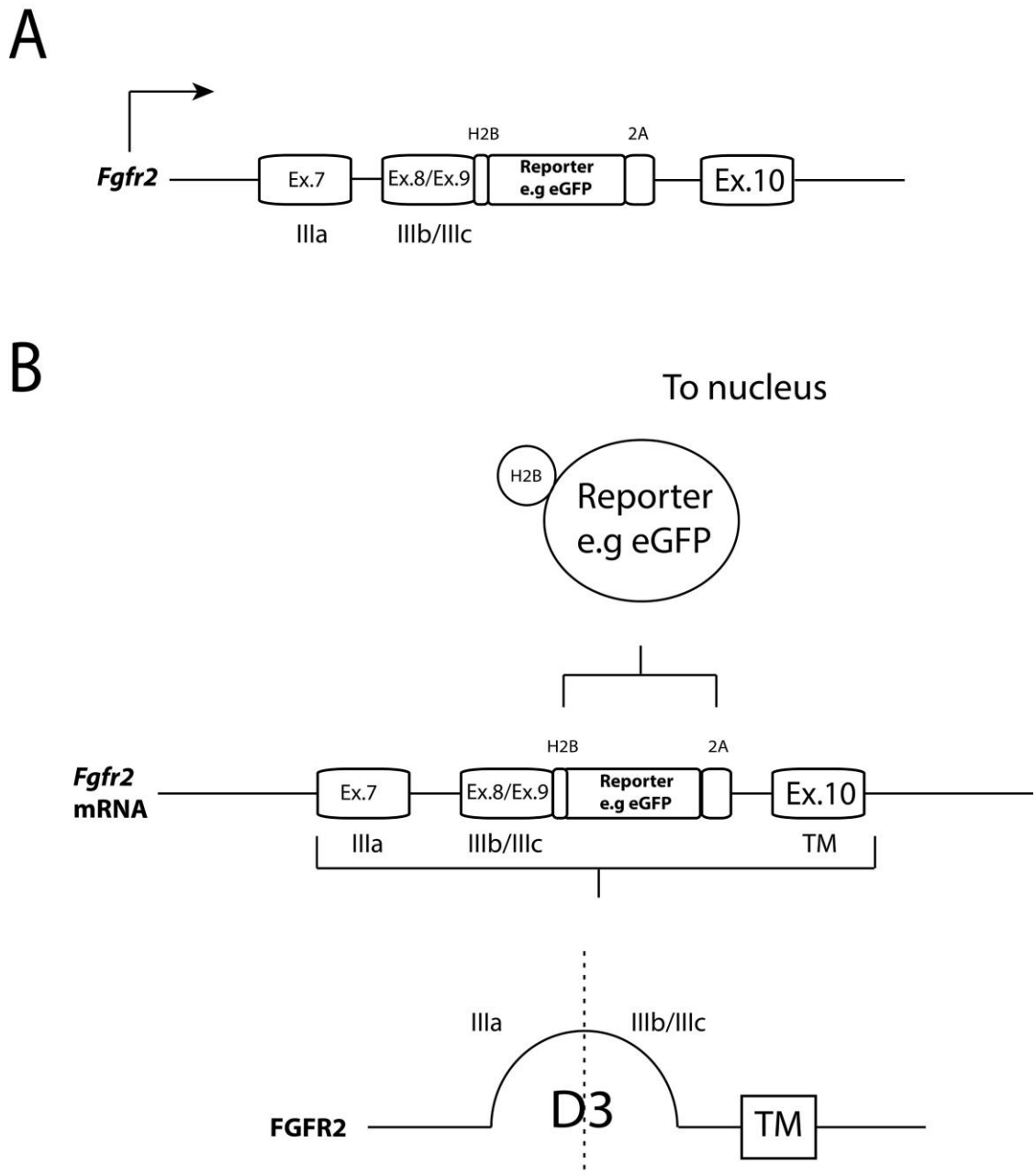

Figure 65: Expression of the H2B-eGFP-2A construct.

(A) Mature mRNA of the *Fgfr2b* or *Fgfr2c* reporter mice with H2B-GFP-H2B construct; (B) Upon transgene expression, the 2A peptide separates the reporter protein from the mature receptor (bottom; with only D3 loop illustrated). As the reporter protein is tagged with histone 2B, it is bounded for the nucleus upon proteolytic processing. TM: Transmembrane domain.

8.2-Concluding remarks

This study has demonstrated that FGFR2c overexpression yields craniofacial hypoplasia without a craniosynostosis phenotype. The most striking observation is the phenotypic variation between *R26R*$^{Fgfr2cV5/+}$*; βactin*$^{CRE/+}$ and *Fgfr2c*$^{C342Y/+}$ despite similarities in signalling dynamics. This implies that receptor overexpression and GOF mutations are mechanistically different, and require a different downstream interpretation to the WT. This is well characterised *in vitro* with preferential signal transduction, and the results in this thesis relate these findings to an *in vivo* context. Maintaining the correct balance between proliferation and differentiation is crucial for osteogenesis and suture patency, and this study has further contributed to the elucidation of the FGFR2c signalling paradox. Furthermore, this study opened up a new horizon towards the role of cartilage in syndromic craniosynostosis that is not associated with Crouzon syndrome, and identified genes that were not previously linked to FGFR2 related syndromic craniosynostosis using LCM. In conclusion, elucidating the complexity of FGFR2c signalling will improve the understanding of normal craniofacial development and its related pathologies, while providing a framework for the innovation of novel therapeutic strategies.

Publications

i) Research article:

Title

Overexpression of *Fgfr2c* causes craniofacial bone hypoplasia and ameliorates craniosynostosis in the Crouzon mouse

Authors

Kevin K.L Lee, Emma Peskett, Charlotte M. Quinn, Rosanna Aiello, Liliya Adeeva, Dale A Moulding, Philip Stanier & Erwin Pauws

Journal

Disease Models & Mechanisms (2018)

ii) Review article:

Title

Mouse models of syndromic craniosynostosis

Authors

Kevin K.L Lee, Philip Stanier & Erwin Pauws

Journal

Molecular Syndromology (2018)

© 2018. Published by The Company of Biologists Ltd | Disease Models & Mechanisms (2018) 11, dmm035311. doi:10.1242/dmm.035311

RESEARCH ARTICLE

Overexpression of *Fgfr2c* causes craniofacial bone hypoplasia and ameliorates craniosynostosis in the Crouzon mouse

Kevin K. L. Lee[1], Emma Peskett[1,2], Charlotte M. Quinn[1], Rosanna Aiello[1], Liliya Adeeva[1], Dale A. Moulding[3], Philip Stanier[2] and Erwin Pauws[1,*]

ABSTRACT

FGFR2c regulates many aspects of craniofacial and skeletal development. Mutations in the *FGFR2* gene are causative of multiple forms of syndromic craniosynostosis, including Crouzon syndrome. Paradoxically, mouse studies have shown that the activation (*Fgfr2c*^{C342Y}; a mouse model for human Crouzon syndrome), as well as the removal (*Fgfr2c*^{null}), of the FGFR2c isoform can drive suture abolishment. This study aims to address the downstream effects of pathogenic FGFR2c signalling by studying the effects of *Fgfr2c* overexpression. Conditional overexpression of *Fgfr2c* (*R26R*$^{Fgfr2c;\beta act}$) results in craniofacial hypoplasia as well as microtia and cleft palate. Contrary to *Fgfr2c*^{null} and *Fgfr2c*^{C342Y}, *Fgfr2c* overexpression is insufficient to drive onset of craniosynostosis. Examination of the MAPK/ERK pathway in the embryonic sutures of *Fgfr2c*^{C342Y} and *R26R*$^{Fgfr2c;\beta act}$ mice reveals that both mutants have increased pERK expression. The contrasting phenotypes between *Fgfr2c*^{C342Y} and *R26R*$^{Fgfr2c;\beta act}$ mice prompted us to assess the impact of the *Fgfr2c* overexpression allele on the Crouzon mouse (*Fgfr2c*^{C342Y}), in particular its effects on the coronal suture. Our results demonstrate that *Fgfr2c* overexpression is sufficient to partially rescue craniosynostosis through increased proliferation and reduced osteogenic activity in E18.5 *Fgfr2c*^{C342Y} embryos. This study demonstrates the intricate balance of FGF signalling required for correct calvarial bone and suture morphogenesis, and that increasing the expression of the wild-type FGFR2c isoform could be a way to prevent or delay craniosynostosis progression.

KEY WORDS: FGFR2, FGF, Craniosynostosis, Cleft palate, Crouzon, ERK

INTRODUCTION

Normal craniofacial development is a precisely coordinated process that involves the modelling of a framework supporting the soft tissues of the head, in particular the brain. During normal development, growth of the brain is possible because suture tissue separates the calvarial bones and allows for skull vault expansion. Craniosynostosis, a common birth defect with an incidence of 1:2500, is characterised by the loss of suture tissue followed by premature fusion of calvarial bones. This results in the restriction of brain growth and is often associated with dramatic dysmorphology of the skull and face. A significant number of craniosynostosis cases are syndromic and associated with additional skeletal phenotypic features. Many of these syndromes are caused by mutations in FGF pathway genes (Johnson and Wilkie, 2011).

FGF signalling is important for cellular proliferation, differentiation and survival. Receptor activation allows signals to be conveyed through the RAS-MAPK, P13K-AKT and PLCγ-PKC cascades via a series of protein intermediates (Ornitz and Itoh, 2015; Eswarakumar et al., 2005). FGF receptors (FGFRs) are highly conserved receptor tyrosine kinases (RTKs) located on the cell membrane with intracellular and extracellular domains. Tissue specific isoforms are produced by alternative splicing, affecting the third extracellular immunoglobulin-like loop (DIII) of FGFR1-3. The FGFR 'IIIb' and 'IIIc' isoforms differ only in the C-terminal half of DIII, which is encoded by exons 8 or 9 for the IIIb and IIIc splice forms, respectively (Eswarakumar et al., 2005; Ornitz and Itoh, 2015). Furthermore, the expression of the isoforms are tissue specific and critical for establishing paracrine reciprocal signalling loops: while the IIIb isoform is commonly expressed in epithelial cells and receives FGF ligand from the mesenchyme, the IIIc is expressed in mesenchymal cells and receives FGF ligand from the neighbouring epithelium (Orr-Urtreger et al., 1993).

Mutations affecting the *FGFR2* gene can cause a spectrum of craniofacial phenotypes commonly associated with growth dysplasia, mid-facial hypoplasia, coronal synostosis, orbit dysmorphology and cleft palate (Wilkie, 1997). Notably, synostosis of the coronal suture is a hallmark of human Crouzon and Pfeiffer syndromes (Johnson and Wilkie, 2011). Crouzon syndrome is most commonly caused by a point mutation in exon 9 of the *FGFR2* gene, is autosomal dominantly inherited and exclusively affects the IIIc isoform (Reardon et al., 1994). The substitution of a cysteine to a tyrosine residue (p.C342Y) results in the stabilisation of intermolecular disulphide bonds in the receptor extracellular domains that lead towards ligand independent receptor activation, and is often referred to as a gain-of-function (GOF) mutation (Reardon et al., 1994).

In the developing mouse cranial vault, *Fgfr2* is expressed in the osteogenic fronts of the calvarial bones, but the specific cellular localisation of the different FGFR2 isoforms remains elusive due to their high sequence homology (Johnson et al., 2000; Iseki et al., 1997). FGFR2c function is commonly associated with craniofacial and skeletal development, as genetic mutation in mouse models leads to a series of craniofacial malformations and additional skeletal dysmorphology (Lee et al., in press). Deletion of the FGFR2c isoform (*Fgfr2c*^{null}) results in skeletal hypoplasia and craniosynostosis owing

[1]Developmental Biology and Cancer Programme, UCL Great Ormond Street Institute of Child Health, 30 Guilford Street, London WC1N 1EH, UK. [2]Genetics and Genomic Medicine Programme, UCL Great Ormond Street Institute of Child Health, 30 Guilford Street, London WC1N 1EH, UK. [3]ICH GOSH Light Microscopy Core Facility, UCL Great Ormond Street Institute of Child Health, 30 Guilford Street, London WC1N 1EH, UK.

*Author for correspondence (e.pauws@ucl.ac.uk)

P.S., 0000-0001-9340-8117; E.P., 0000-0003-1751-0317

Received 4 May 2018; Accepted 19 September 2018

Appendix

Appendix 1

RNA extraction for tissue/cells	Duration
Homogenize in 1ml Trizol	Variable
Incubation at RT	5 mins
Add 0.2ml Chloroform	3 mins
Centrifuge 12,000rpm 4^{o}C	15 mins
Isolate aqueous phase and transfer to new tube *	N/A
Add 0.5ml isopropanol **	10 mins
Centrifuge 12,000rpm to pellet RNA	10 mins
Discard supernatant	N/A
Wash in 1ml 70% EtOH and vortex	N/A
Centrifuge 7,500rpm to pellet RNA	5 mins
Discard supernatant	N/A
Air dry at RT	10-20 mins
Resuspend RNA	20-100ul H_2O

*: Do not remove more than 500ul

**: Precipitate overnight at -20^{o}C if low yield

Appendix 1: Trizol extraction

Appendix 2

Cell lysis buffer	RIPA Buffer
50mM Tris Base	150mM NaCl
150mM NaCl	1% Triton X-100
1% Triton X-100	0.5% sodium deoxycholate
1mM sodium orthovanadate	0.1% SDS
25mM sodium fluoride	50mM Tris-pH 8.0
1mM protease inhibitor cocktail (MINI)	1mM protease inhibitor cocktail (MINI)

Buffers	Reagent	Weight/Volume
4x running gel buffer	1.5M Tris-Base pH8.8	90.86g
	HCl	Adjust
	H_2O	500ml
10x running buffer	Tris-Base	30.2g
	Glycine	144g
	10% SDS	100ml
	H_2O	Top up to 1000ml
10x TBS	NaCl	80g
	KCl	2g
	1M Tris HCl pH 7.5	250ml
	H_2O	Top up to 1000ml
0.1% TBST	10x TBS	100ml
	Tween-20	1ml
	H_2O	900ml

Appendix 2: Immunoblots

Appendix 3

E18.5 wholemount bone and cartilage stain	
Protocol	**Duration**
Dehydrate in 75% EtOH	overnight, 4^{o}C
0.01% Alcian Blue working solution	overnight, RT
Wash in 75% EtOH	overnight, RT
Clear in 1% KOH	Until translucent
0.01% alizarin red working solution	overnight
Wash in 1% KOH	overnight
20% Glycerol-KOH	overnight
80% Glycerol-H_2O	overnight and storage

Reagent	**Stock**	**Ratio**
	Alcian blue	0.01%
	Acetic acid	20%
Alcian blue working solution	75% EtOH	80%
	Alizarin red	0.01%
Alizarin red working solution	KOH	1%

Appendix 3: Wholemount bone and cartilage stain

Appendix 4

Reagent	Stock	Volume/Weight
NTMT	100mM NaCl (5M stock)	1ml
	100mM Tris Base pH9.5 (1M stock)	5ml
	50mM $MgCl_2$ (2M stock)	1.25ml
	1% Tween	0.5ml
	H_2O	Top up to 50ml
NBT/BCIP-NTMT solution	4-nitroblue tetrazolium chloride (NBT): 4.5ul/ml	22.5ul
	5-bromo-4-chloro-3-indoyl-phosphate (BCIP): 3.5ul/ml	17.5ul
	NTMT	Top up to 5ml
1% Nuclear Fast Red	Nuclear fast red	5g
	H_2O	500ml

ALP assay (frozen sections)	
Protocol	**Duration**
Thaw frozen sections	Variable
Fix in 4% PFA	8mins
Wash in 1x TBS	2x 5mins
Permeabilise in 0.1% TBST	5mins
Wash in NTMT	2x 5mins
Develop in NBT/BCIP-NTMT	Variable
Wash in 1xTBS	5mins
Counterstain in 1% nuclear fast red	5mins
Wash in H_2O	5mins
Mount in Mowiol	

Appendix 4: ALP assay

Appendix 5

Linearisation	**Volume**		***In vitro* Transcription**	**Volume**
pDNA	10ug		linearised pDNA	1ug
Enzyme buffer	20ul		DIG labelling mix	2ul
Restriction Enzyme	3ul		Transcription buffer	2ul
BSA	2ul		RNAse inhibitor	0.5ul
			RNA polymerase	2ul
H_2O	Up to 200ul		H_2O (Sigma)	Up to 20ul

Appendix 5: Plasmid linearization and *in vitro* transcription

Appendix 6

Reagent	Stock	Volume/Weight	Notes
	Diethylpyrocarbonate (DEPC)	1ml	
DEPC-H_2O	H_2O	1000ml	Autoclave
	10x PBS (autoclaved)	10ml	
DEPC-PBS	DEPC-H_2O	990ml	
	NaCl	146.1g	
5M NaCl	H_2O	500ml	Autoclave
	$MgCl_2.6H_2O$	203.3g	
2M $MgCl_2$	H_2O	500ml	Autoclave
	NaCl	87.7g	
	Sodium Citrate Tribasic Dihydrate	44.1g	
	Adjust to pH4.5 with HCl	Variable	
20x SSC pH4.5	H_2O	Top up to 500ml	Autoclave
	Sodium dodecyl sulphate	50g	
10% SDS	H_2O	500ml	
	Tris Base	121.14g	
	adjust to pH9.5 with HCl	Variable	
1M Tris Base pH9.5	H_2O	Top up to 1000ml	Autoclave
	Tris HCl	157.6g	
	adjust to pH7.5 with HCl	Variable	
1M Tris HCl pH9.5	H_2O	Top up to 1000ml	Autoclave
	NaCl	80g	
	KCl	2g	
	1M Tris HCl pH 7.5	250ml	
10x TBS	H_2O	Top up to 1000ml	Autoclave
	MeOH	make 25%, 50%, 75%	
DEPC-MeOH	DEPC- H_2O	Up to 500ml	
MeOH	100% MeOH	500ml	

Appendix 6: WMISH

Stocks	Reagents	Volume/Weight	Notes
	Tween-20	1ml	
0.1% PTW	DEPC-PBS	1000ml	
4% Paraformaldehyde (PFA)	PFA powder	20g	Dissolve in 65ºC water bath
	DEPC-PBS	500ml	
	50% Formamide	25ml	
	5x SSC pH4.5 (20x stock)	12.5ml	
	50ug/ml yeast tRNA (10mg/ml stock)	250ul	
	1% SDS (10% stock)	5ml	
	50ug/ml heparin (25mg/ml stock)	100ul	
Hybridisation Mix	DEPC-H_2O	Top up to 50ml	Store in -20ºC
	50% Formamide	25ml	
	5x SSC (20% stock)	12.5ml	
	1% SDS (10% Stock)	5ml	
Solution 1	DEPC-H_2O	Top up to 50ml	
	50% Formamide	25ml	
	2x SSC	5ml	
	1% SDS	5ml	
Solution 2	DEPC-H2O	Top up to 50ml	
	TBS (10x stock)	50ml	
	Tween-20	5ml	
1% TBST	DEPC-H_2O	Top up to 500ml	
	100mM NaCl (5M stock)	1ml	
	100mM Tris Base pH9.5 (1M stock)	5ml	
	50mM MgCl2 (2M stock)	1.25ml	
	1% Tween	0.5ml	
NTMT	H_2O	Top up to 50ml	
	4-nitroblue tetrazolium chloride (NBT): 4.5ul/ml	22.5ul	
	5-bromo-4-chloro-3-indoyl-phosphate (BCIP): 3.5ul/ml	17.5ul	
Developing solution	NTMT	Top up to 5ml	
Proteinase K solution	Proteinase K	10ug/ml	
	0.1% PTW	10ml	
	0.2% Glutaraldehyde (20% stock)	80ul	
Post fix	4% PFA	10ml	

Wholemount ISH Protocol	Duration
Embryo preparation	
Fix in 4% PFA	Overnight
Wash in PTW	2x 5 mins
25% MeOH	until embryos sink
50% MeOH	until embryos sink
75% MeOH	until embryos sink
Proceed or store in -20oC indefinitely	
Hybridisation	
6% H_2O_2-MeOH	1 hour
75% MeOH	until embryos sink
50% MeOH	until embryos sink
25% MeOH	until embryos sink
0.1% PTW	3x 5mins
Incubate in Proteinase K solution	20 mins
0.1% PTW	2x rinse
Post fix	20mins
0.1% PTW	3x 5mins
1ml hybridisation mix at 70^{o}C	2 hours
Proceed or store in -20^{o}C indefinitely	
Add ISH probe to 1ug/ml of hybridisation mix	Overnight, 65/70^{o}C
Post-hybridisation wash and antibody	
Remove hybridisation mix (probes can be reused 5x)	N/A
Wash in solution 1 in hybridisation temperature	Rinse
Wash in solution 1 in hybridisation temperature	1 hour
Wash in solution 2 in hybridisation temperature	1 hour
0.1% TBST	3x 5mins
Block in 10% sheep serum-TBST	1 hour
Anti-DIG antibody (1:2000) in 1% sheep serum-TBST	4^{o}C, overnight
Post antibody wash and development	
1% TBST	5x 10mins
NTMT	2x 10mins
Substrate reaction (NBT-BCIP in NTMT)	Until developed
NTMT	3x 5mins
PBT	3x 5mins
Fix in 4% PFA	For storage

Appendix 7

Reagent	Stock	Volume/Weight	Notes
	Diethylpyrocarbonate (DEPC)	1ml	
DEPC-H_2O	H_2O	1000ml	Autoclave
	10x PBS (autoclaved)	10ml	
DEPC-PBS	DEPC-H_2O	990ml	
	NaCl	146.1g	
5M NaCl	H_2O	500ml	Autoclave
	$MgCl_2.6H_2O$	203.3g	
2M $MgCl_2$	H_2O	500ml	Autoclave
	NaCl	87.7g	
	Sodium Citrate Tribasic Dihydrate	44.1g	
	adjust to pH 7.0 with HCl	Variable	
20x SSC pH 7.0	H_2O	Top up to 500ml	Autoclave
	Tris Base	121.14g	
	adjust to pH9.5 with HCl	Variable	
1M Tris Base pH9.5	H_2O	Top up to 1000ml	Autoclave
	Tris HCl	157.6g	
	adjust to pH7.5 with HCl	Variable	
1M Tris HCl pH7.5	H_2O	Top up to 1000ml	Autoclave
	Tris Base	121.14g	
	adjust to pH8.5 with HCl	Variable	
1M Tris Base pH8.5	H_2O	Top up to 1000ml	Autoclave
	PVA powder	50g	
10% Polyvinyl alcohol	H_2O	500ml	65ºC water bath
Graded DEPC-EtOH	EtOH	25%, 50%, 70%	
	DEPC- H_2O	Up to 500 ml	
EtOH	100% EtOH	500ml	

Appendix 7: Section ISH

Reagent	Stock	Volume/Weight/Conc.	Notes
	Formamide	25ml	
	5M NaCl	3ml	
	1M Tris-Base pH 8.5	1ml	
	0.5M EDTA pH 8.0	0.5ml	
	1ml Denhart's solution	1ml Denhart's solution	
	Dextran sulphate	5g	
Hybridisation solution	DEPC- H_2O	Top up to 50ml	Store in -20ºC
	Hybridisation solution	120ul/slide	
	Rnase inhibitor	1ul/ml	
Working hybridisation mix	Yeast tRNA	0.5mg/ml	
	Formamide	350ml	
Formamide wash	20x SSC	70ml	
	20x SSC	100ml	
2x SSC	H_2O	900ml	
	20x SSC	10ml	
0.2x SSC	H_2O	990ml	Warm to 65ºC
20ug/ml Proteinase K solution	10mg/ml Proteinase K	800ul	
	DEPC-PBS	400ml	
	1M Tris-HCl pH 7.6	100ml	
	5M NaCl	30ml	
Buffer 1	H_2O	870ml	
	HISS	10%	
Blocking solution	Buffer 1	Up to 500ml	
	Anti-DIG antibody	1.2000	
	HISS	1%	
Antibody solution	Buffer 1	Vol. depends on slides	
	1M Tris-Base pH9.5	200ml	
	5M NaCl	40ml	
	2M $MgCl_2$	50ml	
2x Buffer 2	H_2O	710ml	
	2x Buffer 2	500ml	
Buffer 2	H_2O	500ml	
	2x Buffer 2	7.5ml	
	10% PVA	7.5ml	
	NBT	67.5ul	
Developing solution	BCIP	52.5ul	

Section ISH Protocol	Duration	Notes
Pre-hybridisation		
Histoclear	2x 10 mins	Paraffin start
100% EtOH	2x 2mins	
75% EtOH	2 mins	
50% EtOH	2 mins	
25% EtOH	2 mins	
PBS	2 mins	Cryo start
Fix in 4% PFA	20 mins	
PBS	2x 2mins	
Proteinase K solution	8 mins	
4% PFA	5 mins	
PBS	2 mins	
Triethanolamine solution drizzle 1ml acetic anhydride	10 mins	On stirrer
PBS	2x 2 mins	
25% EtOH	2 mins	
50% EtOH	2 mins	
75% EtOH	2 mins	
100% EtOH	2x 2 mins	
Air dry slides on bench	Until dry	
Hybridisation		
Hybridisation at 300ng probe and 120ul hybridisation solution per slide. Coverslip slides and lay flat. Transfer into humidified chamber with a wet tissue soaked in 1:1 ratio of formamide and 2x SSC		
Hybridise overnight at 65ºC		
Post hybridisation washes (in 65ºC water bath)		Warm up SSC and formamide solution beforehand
2x SSC	20mins	Allows coverslip to fall off
Formamide solution	2x 20 mins	
2x SSC	2x 20mins	
0.2x SSC	2x 20mins	Allow to cool after last wash
Antibody detection		
Buffer 1	2 mins	
Blocking solution	1 hour	
Antibody solution	Overnight, 4ºC	500ul/slide in humidified chamber.
Post-antibody washes and development		
Buffer 1	3x 5 mins	
Buffer 2	2x 5 mins	
Developing solution	Until developed	500ul/slide in humidified chamber. Incubate 4ºC for overnight
Running tap water	10 mins	
PBS	2 mins	
Mount in mowiol	-	

Appendix 8

Stock	Reagent	Volume/Weight	Notes
Blocking Buffer (BB):	0.1% Tx-100	250ul	
	0.15% Glycine	375mg	
	2mg/ml BSA	500mg	
	PBS	250ml	
0.1% PBST	Triton X-100	1ml	
	PBS	1000ml	
0.1% Sudan black	Sudan black	50mg	Quench background. Filter and wrap in foil
	70% EtOH	50ml	
Blocking solution	BB	Volume is slide dependent	
	10% HISS		
Antibody solution	BB	Volume and antibody concentration are slide dependent. HISS may vary depending on background.	
	10%/1% HISS		
	Primary antibody		
Antigen retrieval solution, sodium citrate pH6.5	Sodium citrate	2.94g	
	HCl	Adjust to pH6.5	
	0.05% Tween-20	500ul	
	H_2O	Top up to 1000ml	

HISS: Heat Inactivated Sheep Serum

BSA: Bovine Serum Albumin

Appendix 8: Frozen section IHC

	Cryosection IHC Protocol	**Duration**
Day 1	Thaw sections in humidified chamber	Variable
	Fix in 4% PFA	10mins
	PBS	5mins
	(Optional) Antigen retrieval	110^{o}C, 2mins
	0.1% PBST	3x 5mins
	Block: BB and 10% HISS	1 hour
	Primaries in BB, 10% or 1% HISS	Overnight
Day 2	0.1% PBST	3x 5mins
	Secondaries in 10% HISS	1 hour
	0.1% PBST	3x 5mins
	1.500 Streptavidin 555 amplification in BB and 1% HISS	1 hour
	(Optional) Sudan Black 0.1% Sudan Black-70% EtOH 0.02% PBST	 5mins 3x 5mins
	PBS	5mins
	DAPI (1.10,000) in PBS	2mins
	PBS	2x 5mins
	Mount in Mowiol/Hydromount	N/A

Appendix 9

	Paraffin IHC Protocol	Duration
Day 1	Dewax: Histolear	2x 10mins
	100% EtOH	5mins
	70% EtOH	5mins
	50% EtOH	5mins
	25% EtOH	5mins
	Running Tap water	5mins
	Antigen Retrieval (appropriate buffer)	110ºC, 2mins
	0.1% PBST	3x 5mins
	Block: BB and 10% HISS	1 hour
	Primaries in BB and 10% or 1% HISS	Overnight
Day 2	0.1% PBST	3x 5mins
	Appropriate secondaries in 10% HISS	1 hour
	*0.1% PBST	3x 5mins
	(Optional) 1.500 Streptavidin 555 amplification in BB and 1% HISS	*1 hour*
	(Optional) 0.1% Sudan Black	*5mins*
	0.02% PBST	*3x 5mins*
	*PBS	5mins
	DAPI (1:10,000) in PBS	2mins
	PBS	2x 5mins
	Mount in Mowiol/Hydromount	N/A

*Proceed to PBS washes if amplification is not required.
Working reagents can be found in Appendix.8

Appendix 9: Paraffin sections IHC

Appendix 10

Prenatal Calvarial Osteoblast cultures. HSR Mar 2011

DAY 1: Osteoblast digestion

1. Collect embryos
    - This protocol works between E15.5 and E18.5
    - This protocol works on individual embryos at E18.5 (I haven't tried it any younger)
2. Remove embryos from uterus, and dissect into sterile PBS. Keep cold
3. Decapitate, cut the skull cap off just above the eyes, remove the skin, and brain

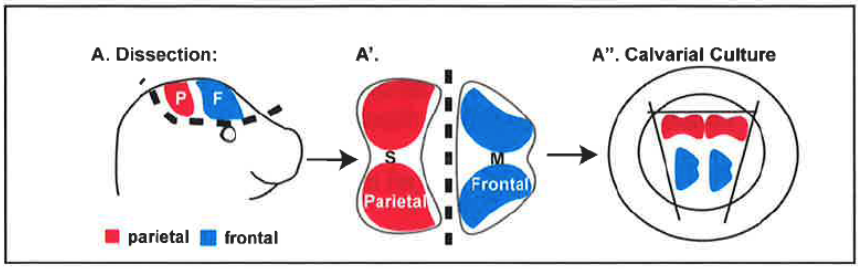

4. Dissect out frontal and parietal bones following the sutures
    - Parietal - between the lamboid and coronal suture
    - Frontal – between nasal and coronal suture.
    - On the endocranial side remove the dura and the nasal cavity cartilages and/or the ala temporalis cartilages.
    - Rip and tear at the bones
    - At E15.5 I pooled 4-5 embryos; At E18.5 I pooled 3 embryos
    - Place pooled bones in Falcon round bottomed 15X75mm snap top tubes with ~ 500 ul of PBS on ice
5. For the rest of the steps I do them on the bench with a P1000 using filtered tips.
6. Remove the PBS and replace with 750 ul 0.5% Trypsin in HBSS (Hanks Balanced Salt Solution). Incubate at 37 C in shaking waterbath (150 RPM) for 10 min.
    - Make collagenase (2mg/ml in HBSS) I use 750 ul/digestion per pool
    - Make Dispase (2 mg/ml in HBSS) I use 750 ul/digestion per pool
    - Filter sterilize with syringe 0.22 um Filter
7. Remove trypsin, replace with HBSS
8. Remove HBSS and replace with Dispase 750 ul
    - 20 mins, 37 C 150 RPMs
    - you will plate out the Dispase and collagenase digests-set up cell collections tubes-eppendorf tubes with 750 ul FBS
9. Remove Dispase, put into FBS tubes
10. Replace with 2 mg/ml collagenase 30 min, shaking 150 RPM, 37 C
11. Remove collagenase into FBS tubes
12. Repeat 10 and 11 twice.
13. Spin FBS samples at 1000 RPM 5 min

In TC room:

14. Aspirate most of the supernatant and replace with 0.75 – 1 ml osteoblast differentiation media- resuspend tiny pellet
15. plate into 6-well dishes already with 1 ml media
16. Culture overnight to 2 days in 37 C with 5% CO2.

Appendix 10: Protocol for generating prenatal calvarial osteoblast cultures.

Adapted from Daniel Doro Pereira (Dept. of Craniofacial Development & Stem Cell Biology, King's College London).

Appendix 11

GENE SYMBOL				
E2F	Myc_targets_V1	G2M Checkpoint	EMT	Apoptosis
PLK1	*RPS2*	*PLK1*	*COL6A2*	*RHOT2*
TUBG1	*FBL*	*AURKB*	*ACTA2*	*TIMP1*
AURKB	*POLD2*	*BIRC5*	*MATN2*	*APP*
BIRC5	*CCT2*	*TPX2*	*TIMP1*	*TNFRSF12A*
CCP110	*RPL18*	*PLK4*	*ELN*	*BGN*
PLK4	*PSMB3*	*UPF1*	*FERMT2*	*CCND2*
CCNE1	*RPS3*	*CDK1*	*PDLIM4*	*TSPO*
POLD2	*NAP1L1*	*BCL3*	*TNFRSF12A*	*CREBBP*
CDK1	*SNRPG*	*PML*	*MGP*	*BTG2*
BUB1B	*RPS10*	*UBE2C*	*BGN*	*RARA*
DNMT1	*NHP2*	*EFNA5*	*GEM*	*TAP1*
ING3	*PSMA7*	*ATF5*	*FMOD*	*EBP*
NCAPD2	*SRM*	*KPNA2*	*LOXL1*	*LMNA*
CDCA8	*RPL14*	*SMC1A*	*LGALS1*	*ROCK1*
NAP1L1	*KPNA2*	*SNRPD1*	*COL5A1*	*IFNGR1*
MLH1	*CAD*	*RAD54L*	*ANPEP*	*BCL2L2*
RNASEH2A	*RPS5*	*H2AFX*	*PMEPA1*	*TIMP3*
KPNA2	*SNRPD1*	*RAD23B*	*VIM*	*SMAD7*
CSE1L	*SET*	*CHEK1*	*GPC1*	*TGFB2*
SMC1A	*NME1*	*KIF23*	*COL6A3*	*PPP3R1*
RRM2	*SNRPA*	*PRIM2*	*ITGB5*	*CD44*
RPA1	*RAD23B*	*BARD1*	*MYL9*	*TIMP2*
H2AFX	*NPM1*	*CDC27*	*COL12A1*	*IRF1*
CDCA3	*GNB2L1*	*CDKN1B*	*COL7A1*	*CDKN1B*
MTHFD2	*RFC4*	*TOP2A*	*COL4A2*	*TOP2A*
NME1	*RPL6*	*SMC4*	*LRP1*	*CASP6*
CBX5	*HSP90AB1*	*CDC25A*	*FLNA*	*TNF*
DEK	*PTGES3*	*CCND1*	*MAGEE1*	*CCND1*
CHEK1	*DEK*	*GINS2*	*PLOD3*	*SOD1*
PRIM2	*LDHA*	*NUSAP1*	*COL16A1*	*IGF2R*
BARD1	*CANX*	*UBE2S*	*MEST*	*PSEN1*
UBE2T	*PSMD7*	*CUL5*	*FBLN1*	*DAP*
MCM7	*RPL22*	*INCENP*	*SNAI2*	*IER3*
NAA38	*CCT5*	*KIF22*	*COL4A1*	
PSIP1	*XPOT*	*MKI67*	*EMP3*	
DCTPP1	*MCM7*	*HSPA8*	*POSTN*	
CDKN1B	*SF3B3*	*E2F1*	*ITGA5*	
TOP2A	*UBE2L3*	*SYNCRIP*	*TIMP3*	
CENPM	*SNRPD2*	*H2AFV*	*COL8A2*	
SMC4	*EIF2S2*	*PAFAH1B1*	*COL5A2*	
CDC25A	*ABCE1*	*E2F4*	*CD44*	
LIG1	*PSMD3*	*CCNB2*	*TNC*	
UBE2S	*LSM7*	*SETD8*	*PLOD1*	
KIF22	*PGK1*	*PRC1*	*MCM7*	
MKI67	*SYNCRIP*	*MCM6*	*COL3A1*	
SPC24	*EIF1AX*	*HMGA1*	*LRRC15*	
SYNCRIP	*MCM4*	*RASAL2*	*TPM4*	
MCM4	*HSPE1*	*CDC25B*	*LAMC1*	
DCK	*EEF1B2*	*KIF15*	*TGFBI*	
ASF1B	*PHB*	*FBXO5*	*LOXL2*	
		HMMR	*PFN2*	
		HIF1A	*THY1*	
		TNPO2	*THBS2*	
		CDC20	*SERPINE1*	
		UCK2	*IGFBP2*	
		NUP50	*TPM2*	
		XPO1		
		HUS1		
		PRMT5		
		CKS2		
		ESPL1		
		NUMA1		
		PURA		

Appendix 11: Enriched gene sets in *Fgfr2c*$^{C342Y/+}$

GENE SYMBOL				
KRas signalling UP	**KRas signalling DOWN**	**PI3K-AKT mTOR**	**Myogenesis**	**Notch signalling**
LCP1	*RSAD2*	*TRIB3*	*ACTC1*	*NOTCH3*
DOCK2	*ACTC1*	*UBE2N*	*ACTN2*	*JAG1*
SLMO2	*CKM*	*ADCY2*	*APOD*	*CUL1*
HDAC9	*CCDC132*	*MAPKAP1*	*CKM*	*ARRB1*
APOD	*RYR1*	*TIAM1*	*RYR1*	*LFNG*
CBX8	*TFAP2B*	*MYD88*	*MYLPF*	*WNT2*
SATB1	*ADCK3*	*MAPK8*	*TNNI2*	*DTX2*
CROT	*KRT1*	*MKNK1*	*ATP6AP1*	*DLL1*
CSF2RA	*SEPP1*	*PPP1CA*	*PFKM*	*TCF7L2*
MMP9	*SGK1*	*ACTR3*	*MYL1*	*FZD5*
GLRX	*LFNG*	*RPS6KA1*	*CLU*	
TNFRSF1B	*YPEL1*	*MAPK10*	*TNNT3*	
F13A1	*SLC16A7*	*MAP2K6*	*GPX3*	
ANGPTL4	*MSH5*	*GSK3B*	*APLNR*	
SPP1	*STAG3*	*SLA*	*TNNI1*	
LY96	*COL2A1*	*CXCR4*	*GABARAPL2*	
LAPTM5	*THNSL2*	*TRAF2*	*SOD3*	
PLVAP	*FAM46C*	*PRKCB*	*ACTA1*	
ITGA2	*SPHK2*	*RIT1*	*CKB*	
BPGM	*MTHFR*	*IL2RG*	*LDB3*	
TFPI	*FGGY*	*ITPR2*	*ITGA7*	
PRDM1	*LYPD3*	*RALB*	*DMD*	
PRKG2	*ZFP112*	*TBK1*	*MYH3*	
G0S2	*YBX2*	*RPTOR*	*SYNGR2*	
BTC	*RGS11*	*GNA14*	*CSRP3*	
CFH	*CHST2*	*SFN*	*TNNC2*	
TMEM176B	*CYP39A1*	*AKT1*	*MYH8*	
ALDH1A2	*EGF*	*VAV3*	*CKMT2*	
CXCR4	*GPRC5C*	*RIPK1*	*RB1*	
GUCY1A3	*SOX10*	*EIF4E*	*LAMA2*	
ITGB2	*SLC38A3*	*TNFRSF1A*	*PYGM*	
MAP7	*ITIH3*		*RIT1*	
IL2RG	*SNCB*		*SLN*	
RABGAP1L	*SHOX2*		*ADCY9*	
GPNMB	*SNN*		*DMPK*	
AKAP12	*RYR2*		*NAV2*	
ID2	*PTGFR*		*PPP1R3C*	
CFB	*KCNMB1*		*IGFBP7*	
AVL9	*OXT*		*DTNA*	
TSPAN1	*NRIP2*		*EIF4A2*	
FLT4	*ATP6V1B1*		*SH2B1*	
FUCA1	*CAPN9*		*COX7A1*	
CFHR2	*KLK7*		*SPEG*	
WNT7A	*NOS1*		*COX6A2*	
MYCN	*TNNI3*		*MYOG*	
PECAM1			*BAG1*	
			TNNC1	
			FST	
			MYLK	
			CAMK2B	
			SPHK1	
			MEF2A	

Appendix 11: Enriched genes for *Fgfr2c*$^{C342Y/+}$

References

ABERG, T., RICE, R., RICE, D., THESLEFF, I. & WALTIMO-SIREN, J. 2005. Chondrogenic potential of mouse calvarial mesenchyme. *J Histochem Cytochem,* 53**,** 653-63.

AKIYAMA, H., CHABOISSIER, M.-C., MARTIN, J. F., SCHEDL, A. & DE CROMBRUGGHE, B. 2002. The transcription factor Sox9 has essential roles in successive steps of the chondrocyte differentiation pathway and is required for expression of Sox5 and Sox6. *Genes & Development,* 16**,** 2813-2828.

ARMAN, E., HAFFNER-KRAUSZ, R., CHEN, Y., HEATH, J. K. & LONAI, P. 1998. Targeted disruption of fibroblast growth factor (FGF) receptor 2 suggests a role for FGF signaling in pregastrulation mammalian development. *Proc Natl Acad Sci U S A,* 95**,** 5082-7.

ARMAN, E., HAFFNER-KRAUSZ, R., GORIVODSKY, M. & LONAI, P. 1999. Fgfr2 is required for limb outgrowth and lung-branching morphogenesis. *Proc Natl Acad Sci U S A,* 96**,** 11895-9.

ASAMURA, K., ABE, S., IMAMURA, Y., ASZODI, A., SUZUKI, N., HASHIMOTO, S., TAKUMI, Y., HAYASHI, T., FASSLER, R., NAKAMURA, Y. & USAMI, S. 2005. Type IX collagen is crucial for normal hearing. *Neuroscience,* 132**,** 493-500.

AUNE, C. N., CHATTERJEE, B., ZHAO, X. Q., FRANCIS, R., BRACERO, L., YU, Q., ROSENTHAL, J., LEATHERBURY, L. & LO, C. W. 2008. Mouse model of heterotaxy with single ventricle spectrum of cardiac anomalies. *Pediatr Res,* 63**,** 9-14.

BADDOO, M., HILL, K., WILKINSON, R., GAUPP, D., HUGHES, C., KOPEN, G. C. & PHINNEY, D. G. 2003. Characterization of mesenchymal stem cells isolated from murine bone marrow by negative selection. *J Cell Biochem,* 89**,** 1235-49.

BAGHERI-FAM, S., BIRD, A. D., ZHAO, L., RYAN, J. M., YONG, M., WILHELM, D., KOOPMAN, P., ESWARAKUMAR, V. P. & HARLEY, V. R. 2017. Testis Determination Requires a Specific FGFR2 Isoform to Repress FOXL2. *Endocrinology,* 158**,** 3832-3843.

BAGHERI-FAM, S., ONO, M., LI, L., ZHAO, L., RYAN, J., LAI, R., KATSURA, Y., ROSSELLO, F. J., KOOPMAN, P., SCHERER, G., BARTSCH, O., ESWARAKUMAR, J. V. P. & HARLEY, V. R. 2015. FGFR2 mutation in 46,XY sex reversal with craniosynostosis. *Human Molecular Genetics,* 24**,** 6699-6710.

BANDYOPADHYAY, A., TSUJI, K., COX, K., HARFE, B. D., ROSEN, V. & TABIN, C. J. 2006. Genetic analysis of the roles of BMP2, BMP4, and BMP7 in limb patterning and skeletogenesis. *PLoS Genet,* 2**,** e216.

BANNISTER, A. J. & KOUZARIDES, T. 2011. Regulation of chromatin by histone modifications. *Cell Res,* 21**,** 381-95.

BARAK, H., HUH, S.-H., CHEN, S., JEANPIERRE, C., MARTINOVIC, J., PARISOT, M., BOLE-FEYSOT, C., NITSCHKÉ, P., SALOMON, R., ANTIGNAC, C., ORNITZ, DAVID M. & KOPAN, R. 2012. FGF9 and FGF20 Maintain the Stemness of Nephron Progenitors in Mice and Man. *Developmental Cell,* 22**,** 1191-1207.

BARNA, M. & NISWANDER, L. 2007. Visualization of cartilage formation: insight into cellular properties of skeletal progenitors and chondrodysplasia syndromes. *Dev Cell,* 12**,** 931-41.

BEHR, B., LONGAKER, M. & QUARTO, N. 2011a. Craniosynostosis of Coronal Suture in Twist1+/− Mice Occurs Through Endochondral Ossification Recapitulating the Physiological Closure of Posterior Frontal Suture. *Frontiers in Physiology,* 2.

BEHR, B., LONGAKER, M. T. & QUARTO, N. 2011b. Craniosynostosis of coronal suture in twist1 mice occurs through endochondral ossification recapitulating the physiological closure of posterior frontal suture. *Front Physiol,* 2**,** 37.

BEHR, B., PANETTA, N. J., LONGAKER, M. T. & QUARTO, N. 2010. Different endogenous threshold levels of Fibroblast Growth Factor-ligands determine the healing potential of frontal and parietal bones. *Bone,* 47**,** 281-94.

BEIER, F., ALI, Z., MOK, D., TAYLOR, A. C., LEASK, T., ALBANESE, C., PESTELL, R. G. & LUVALLE, P. 2001. TGFbeta and PTHrP control chondrocyte proliferation by activating cyclin D1 expression. *Mol Biol Cell,* 12**,** 3852-63.

BEIER, F., LEASK, T. A., HAQUE, S., CHOW, C., TAYLOR, A. C., LEE, R. J., PESTELL, R. G., BALLOCK, R. T. & LUVALLE, P. 1999. Cell cycle genes in chondrocyte proliferation and differentiation. *Matrix Biol,* 18**,** 109-20.

BELLOT, F., CRUMLEY, G., KAPLOW, J. M., SCHLESSINGER, J., JAYE, M. & DIONNE, C. A. 1991. Ligand-induced transphosphorylation between different FGF receptors. *EMBO J,* 10**,** 2849-54.

BELLUS, G. A., HEFFERON, T. W., ORTIZ DE LUNA, R. I., HECHT, J. T., HORTON, W. A., MACHADO, M., KAITILA, I., MCINTOSH, I. & FRANCOMANO, C. A. 1995. Achondroplasia is defined by recurrent G380R mutations of FGFR3. *Am J Hum Genet,* 56**,** 368-73.

BENAZET, J. D., PIGNATTI, E., NUGENT, A., UNAL, E., LAURENT, F. & ZELLER, R. 2012. Smad4 is required to induce digit ray primordia and to initiate the aggregation and differentiation of chondrogenic progenitors in mouse limb buds. *Development,* 139**,** 4250-60.

BI, W., DENG, J. M., ZHANG, Z., BEHRINGER, R. R. & DE CROMBRUGGHE, B. 1999. Sox9 is required for cartilage formation. *Nat Genet,* 22**,** 85-9.

BIALEK, P., KERN, B., YANG, X., SCHROCK, M., SOSIC, D., HONG, N., WU, H., YU, K., ORNITZ, D. M., OLSON, E. N., JUSTICE, M. J. & KARSENTY, G. 2004. A twist code determines the onset of osteoblast differentiation. *Dev Cell,* 6**,** 423-35.

BILDSOE, H., LOEBEL, D. A., JONES, V. J., HOR, A. C., BRAITHWAITE, A. W., CHEN, Y. T., BEHRINGER, R. R. & TAM, P. P. 2013. The mesenchymal architecture of the cranial mesoderm of mouse embryos is disrupted by the loss of Twist1 function. *Dev Biol,* 374**,** 295-307.

BLANK, T. & PRINZ, M. 2017. Type I interferon pathway in CNS homeostasis and neurological disorders. *Glia,* 65**,** 1397-1406.

BOURGEOIS, P., BOLCATO-BELLEMIN, A. L., DANSE, J. M., BLOCH-ZUPAN, A., YOSHIBA, K., STOETZEL, C. & PERRIN-SCHMITT, F. 1998. The variable expressivity and incomplete penetrance of the twist-null heterozygous mouse phenotype resemble those of human Saethre-Chotzen syndrome. *Hum Mol Genet,* 7**,** 945-57.

BREWER, J. R., MOLOTKOV, A., MAZOT, P., HOCH, R. V. & SORIANO, P. 2015. Fgfr1 regulates development through the combinatorial use of signaling proteins. *Genes Dev,* 29**,** 1863-74.

BRINKLEY, J. F., FISHER, S., HARRIS, M. P., HOLMES, G., HOOPER, J. E., JABS, E. W., JONES, K. L., KESSELMAN, C., KLEIN, O. D., MAAS, R. L., MARAZITA, M. L., SELLERI, L., SPRITZ, R. A., VAN BAKEL, H., VISEL, A., WILLIAMS, T. J., WYSOCKA, J., FACEBASE, C. & CHAI, Y. 2016. The FaceBase Consortium: a comprehensive resource for craniofacial researchers. *Development,* 143**,** 2677-88.

BURGERS, T. A., HOFFMANN, M. F., COLLINS, C. J., ZAHATNANSKY, J., ALVARADO, M. A., MORRIS, M. R., SIETSEMA, D. L., MASON, J. J., JONES, C. B., PLOEG, H. L. & WILLIAMS, B. O. 2013. Mice lacking pten in osteoblasts have improved intramembranous and late endochondral fracture healing. *PLoS One,* 8**,** e63857.

BUSH, J. O. & JIANG, R. 2012. Palatogenesis: morphogenetic and molecular mechanisms of secondary palate development. *Development,* 139**,** 231-43.

BYUN, M. R., KIM, A. R., HWANG, J. H., KIM, K. M., HWANG, E. S. & HONG, J. H. 2014. FGF2 stimulates osteogenic differentiation through ERK induced TAZ expression. *Bone,* 58**,** 72-80.

CARLTON, M. B., COLLEDGE, W. H. & EVANS, M. J. 1998. Crouzon-like craniofacial dysmorphology in the mouse is caused by an insertional mutation at the Fgf3/Fgf4 locus. *Dev Dyn,* 212**,** 242-9.

CARMIGNAC, V., THEVENON, J., ADES, L., CALLEWAERT, B., JULIA, S., THAUVIN-ROBINET, C., GUENEAU, L., COURCET, J. B., LOPEZ, E., HOLMAN, K., RENARD, M., PLAUCHU, H., PLESSIS, G., DE BACKER, J., CHILD, A., ARNO, G., DUPLOMB, L., CALLIER, P., ARAL, B., VABRES, P., GIGOT, N., ARBUSTINI, E., GRASSO, M., ROBINSON, P. N., GOIZET, C., BAUMANN, C., DI ROCCO, M., SANCHEZ DEL POZO, J., HUET, F., JONDEAU, G., COLLOD-BEROUD, G., BEROUD, C., AMIEL, J., CORMIER-DAIRE, V., RIVIERE, J. B., BOILEAU, C., DE

PAEPE, A. & FAIVRE, L. 2012. In-frame mutations in exon 1 of SKI cause dominant Shprintzen-Goldberg syndrome. *Am J Hum Genet,* 91**,** 950-7.
CARTA, L., PEREIRA, L., ARTEAGA-SOLIS, E., LEE-ARTEAGA, S. Y., LENART, B., STARCHER, B., MERKEL, C. A., SUKOYAN, M., KERKIS, A., HAZEKI, N., KEENE, D. R., SAKAI, L. Y. & RAMIREZ, F. 2006. Fibrillins 1 and 2 perform partially overlapping functions during aortic development. *J Biol Chem,* 281**,** 8016-23.
CARTER, J. M., DEMIZIEUX, L., CAMPENOT, R. B., VANCE, D. E. & VANCE, J. E. 2008. Phosphatidylcholine biosynthesis via CTP:phosphocholine cytidylyltransferase 2 facilitates neurite outgrowth and branching. *J Biol Chem,* 283**,** 202-12.
CARVER, E. A., ORAM, K. F. & GRIDLEY, T. 2002. Craniosynostosis in Twist heterozygous mice: a model for Saethre-Chotzen syndrome. *Anat Rec,* 268**,** 90-2.
CHAI, Y., JIANG, X., ITO, Y., BRINGAS, P., HAN, J., ROWITCH, D. H., SORIANO, P., MCMAHON, A. P. & SUCOV, H. M. 2000. Fate of the mammalian cranial neural crest during tooth and mandibular morphogenesis. *Development,* 127**,** 1671.
CHAN, S. S., SHI, X., TOYAMA, A., ARPKE, R. W., DANDAPAT, A., IACOVINO, M., KANG, J., LE, G., HAGEN, H. R., GARRY, D. J. & KYBA, M. 2013. Mesp1 patterns mesoderm into cardiac, hematopoietic, or skeletal myogenic progenitors in a context-dependent manner. *Cell Stem Cell,* 12**,** 587-601.
CHAUDHARY, L. R., HOFMEISTER, A. M. & HRUSKA, K. A. 2004. Differential growth factor control of bone formation through osteoprogenitor differentiation. *Bone,* 34**,** 402-11.
CHEN, F. H., THOMAS, A. O., HECHT, J. T., GOLDRING, M. B. & LAWLER, J. 2005. Cartilage oligomeric matrix protein/thrombospondin 5 supports chondrocyte attachment through interaction with integrins. *J Biol Chem,* 280**,** 32655-61.
CHEN, L., ADAR, R., YANG, X., MONSONEGO, E. O., LI, C., HAUSCHKA, P. V., YAYON, A. & DENG, C. X. 1999. Gly369Cys mutation in mouse FGFR3 causes achondroplasia by affecting both chondrogenesis and osteogenesis. *J Clin Invest,* 104**,** 1517-25.
CHEN, L., LI, C., QIAO, W., XU, X. & DENG, C. 2001. A Ser(365)-->Cys mutation of fibroblast growth factor receptor 3 in mouse downregulates Ihh/PTHrP signals and causes severe achondroplasia. *Hum Mol Genet,* 10**,** 457-65.
CHEN, L., LI, D., LI, C., ENGEL, A. & DENG, C. X. 2003. A Ser252Trp [corrected] substitution in mouse fibroblast growth factor receptor 2 (Fgfr2) results in craniosynostosis. *Bone,* 33**,** 169-78.
CHEN, L., SHI, K., FRARY, C. E., DITZEL, N., HU, H., QIU, W. & KASSEM, M. 2015a. Inhibiting actin depolymerization enhances osteoblast differentiation and bone formation in human stromal stem cells. *Stem Cell Res,* 15**,** 281-9.
CHEN, W., BAYLINK, D. J., BRIER-JONES, J., NEISES, A., KIROYAN, J. B., RUNDLE, C. H., LAU, K. H. & ZHANG, X. B. 2015b. PDGFB-based stem cell gene therapy increases bone strength in the mouse. *Proc Natl Acad Sci U S A,* 112**,** E3893-900.
CHEN, Z., HUANG, J., LIU, Y., DATTILO, L. K., HUH, S. H., ORNITZ, D. & BEEBE, D. C. 2014. FGF signaling activates a Sox9-Sox10 pathway for the formation and branching morphogenesis of mouse ocular glands. *Development,* 141**,** 2691-701.
CHEN, Z. F. & BEHRINGER, R. R. 1995. twist is required in head mesenchyme for cranial neural tube morphogenesis. *Genes Dev,* 9**,** 686-99.
CHIN, K. C. & CRESSWELL, P. 2001. Viperin (cig5), an IFN-inducible antiviral protein directly induced by human cytomegalovirus. *Proc Natl Acad Sci U S A,* 98**,** 15125-30.
CHOFFLON, M. 2000. Recombinant human interferon beta in relapsing-remitting multiple sclerosis: a review of the major clinical trials. *Eur J Neurol,* 7**,** 369-80.
CHOI, S.-C., KIM, S.-J., CHOI, J.-H., PARK, C.-Y., SHIM, W.-J. & LIM, D.-S. 2008. Fibroblast Growth Factor-2 and -4 Promote the Proliferation of Bone Marrow Mesenchymal Stem Cells by the Activation of the PI3K-Akt and ERK1/2 Signaling Pathways. *Stem Cells and Development,* 17**,** 725-736.
CHOTTEAU-LELIEVRE, A., DOLLE, P., PERONNE, V., COUTTE, L., DE LAUNOIT, Y. & DESBIENS, X. 2001. Expression patterns of the Ets transcription factors from the PEA3 group during early stages of mouse development. *Mech Dev,* 108**,** 191-5.

COHEN, M. M. & KRELBORG, S. 1992. Birth prevalence studies of the Crouzon syndrome: comparison of direct and indirect methods. *Clinical Genetics,* 41**,** 12-15.

COLEMAN, S. J., CHIONI, A. M., GHALLAB, M., ANDERSON, R. K., LEMOINE, N. R., KOCHER, H. M. & GROSE, R. P. 2014. Nuclear translocation of FGFR1 and FGF2 in pancreatic stellate cells facilitates pancreatic cancer cell invasion. *EMBO Mol Med,* 6**,** 467-81.

COLNOT, C., LU, C., HU, D. & HELMS, J. A. 2004. Distinguishing the contributions of the perichondrium, cartilage, and vascular endothelium to skeletal development. *Dev Biol,* 269**,** 55-69.

COLVIN, J. S., BOHNE, B. A., HARDING, G. W., MCEWEN, D. G. & ORNITZ, D. M. 1996. Skeletal overgrowth and deafness in mice lacking fibroblast growth factor receptor 3. *Nat Genet,* 12**,** 390-7.

COLVIN, J. S., GREEN, R. P., SCHMAHL, J., CAPEL, B. & ORNITZ, D. M. 2001a. Male-to-female sex reversal in mice lacking fibroblast growth factor 9. *Cell,* 104**,** 875-89.

COLVIN, J. S., WHITE, A. C., PRATT, S. J. & ORNITZ, D. M. 2001b. Lung hypoplasia and neonatal death in Fgf9-null mice identify this gene as an essential regulator of lung mesenchyme. *Development,* 128**,** 2095-106.

CONNERNEY, J., ANDREEVA, V., LESHEM, Y., MERCADO, M. A., DOWELL, K., YANG, X., LINDNER, V., FRIESEL, R. E. & SPICER, D. B. 2008. Twist1 homodimers enhance FGF responsiveness of the cranial sutures and promote suture closure. *Dev Biol,* 318**,** 323-34.

CORREA, D., HESSE, E., SERIWATANACHAI, D., KIVIRANTA, R., SAITO, H., YAMANA, K., NEFF, L., ATFI, A., COILLARD, L., SITARA, D., MAEDA, Y., WARMING, S., JENKINS, N. A., COPELAND, N. G., HORNE, W. C., LANSKE, B. & BARON, R. 2010. Zfp521 is a target gene and key effector of parathyroid hormone-related peptide signaling in growth plate chondrocytes. *Dev Cell,* 19**,** 533-46.

COUSSENS, A. K., HUGHES, I. P., WILKINSON, C. R., MORRIS, C. P., ANDERSON, P. J., POWELL, B. C. & VAN DAAL, A. 2008. Identification of genes differentially expressed by prematurely fused human sutures using a novel in vivo – in vitro approach. *Differentiation,* 76**,** 531-545.

COUSSENS, A. K., WILKINSON, C. R., HUGHES, I. P., MORRIS, C. P., VAN DAAL, A., ANDERSON, P. J. & POWELL, B. C. 2007. Unravelling the molecular control of calvarial suture fusion in children with craniosynostosis. *BMC Genomics,* 8**,** 458.

CROES, M., ONER, F. C., VAN NEERVEN, D., SABIR, E., KRUYT, M. C., BLOKHUIS, T. J., DHERT, W. J. & ALBLAS, J. 2016. Proinflammatory T cells and IL-17 stimulate osteoblast differentiation. *Bone,* 84**,** 262-70.

CZARNY-RATAJCZAK, M., LOHINIVA, J., ROGALA, P., KOZLOWSKI, K., PERALA, M., CARTER, L., SPECTOR, T. D., KOLODZIEJ, L., SEPPANEN, U., GLAZAR, R., KROLEWSKI, J., LATOS-BIELENSKA, A. & ALA-KOKKO, L. 2001. A mutation in COL9A1 causes multiple epiphyseal dysplasia: further evidence for locus heterogeneity. *Am J Hum Genet,* 69**,** 969-80.

CZOCHRA, P., KLOPCIC, B., MEYER, E., HERKEL, J., GARCIA-LAZARO, J. F., THIERINGER, F., SCHIRMACHER, P., BIESTERFELD, S., GALLE, P. R., LOHSE, A. W. & KANZLER, S. 2006. Liver fibrosis induced by hepatic overexpression of PDGF-B in transgenic mice. *J Hepatol,* 45**,** 419-28.

DAI, C., CELESTINO, J. C., OKADA, Y., LOUIS, D. N., FULLER, G. N. & HOLLAND, E. C. 2001. PDGF autocrine stimulation dedifferentiates cultured astrocytes and induces oligodendrogliomas and oligoastrocytomas from neural progenitors and astrocytes in vivo. *Genes Dev,* 15**,** 1913-25.

DANKORT, D., FILENOVA, E., COLLADO, M., SERRANO, M., JONES, K. & MCMAHON, M. 2007. A new mouse model to explore the initiation, progression, and therapy of BRAFV600E-induced lung tumors. *Genes Dev,* 21**,** 379-84.

DAY, T. F., GUO, X., GARRETT-BEAL, L. & YANG, Y. 2005. Wnt/beta-catenin signaling in mesenchymal progenitors controls osteoblast and chondrocyte differentiation during vertebrate skeletogenesis. *Dev Cell,* 8**,** 739-50.

DE CROMBRUGGHE, B., LEFEBVRE, V. & NAKASHIMA, K. 2001. Regulatory mechanisms in the pathways of cartilage and bone formation. *Curr Opin Cell Biol,* 13**,** 721-7.

DE MOERLOOZE, L., SPENCER-DENE, B., REVEST, J., HAJIHOSSEINI, M., ROSEWELL, I. & DICKSON, C. 2000. An important role for the IIIb isoform of fibroblast growth factor receptor 2 (FGFR2) in mesenchymal-epithelial signalling during mouse organogenesis. *Development,* 127**,** 483.

DECKELBAUM, R. A., HOLMES, G., ZHAO, Z., TONG, C., BASILICO, C. & LOOMIS, C. A. 2012. Regulation of cranial morphogenesis and cell fate at the neural crest-mesoderm boundary by engrailed 1. *Development,* 139**,** 1346-1358.

DECKELBAUM, R. A., MAJITHIA, A., BOOKER, T., HENDERSON, J. E. & LOOMIS, C. A. 2005. The homeoprotein engrailed 1 has pleiotropic functions in calvarial intramembranous bone formation and remodeling. *Development,* 133**,** 63.

DEL PICCOLO, N., SARABIPOUR, S. & HRISTOVA, K. 2017. A New Method to Study Heterodimerization of Membrane Proteins and Its Application to Fibroblast Growth Factor Receptors. *J Biol Chem,* 292**,** 1288-1301.

DELEZOIDE, A. L., BENOIST-LASSELIN, C., LEGEAI-MALLET, L., LE MERRER, M., MUNNICH, A., VEKEMANS, M. & BONAVENTURE, J. 1998. Spatio-temporal expression of FGFR 1, 2 and 3 genes during human embryo-fetal ossification. *Mech Dev,* 77**,** 19-30.

DENG, C., WYNSHAW-BORIS, A., ZHOU, F., KUO, A. & LEDER, P. 1996. Fibroblast growth factor receptor 3 is a negative regulator of bone growth. *Cell,* 84**,** 911-21.

DENG, C. X., WYNSHAW-BORIS, A., SHEN, M. M., DAUGHERTY, C., ORNITZ, D. M. & LEDER, P. 1994. Murine FGFR-1 is required for early postimplantation growth and axial organization. *Genes Dev,* 8**,** 3045-57.

DEQUEANT, M. L. & POURQUIE, O. 2008. Segmental patterning of the vertebrate embryonic axis. *Nat Rev Genet,* 9**,** 370-82.

DERDERIAN, C. & SEAWARD, J. 2012. Syndromic craniosynostosis. *Semin Plast Surg,* 26**,** 64-75.

DERYNCK, R. & ZHANG, Y. E. 2003. Smad-dependent and Smad-independent pathways in TGF-beta family signalling. *Nature,* 425**,** 577-84.

DIETZ, H. C., CUTTING, G. R., PYERITZ, R. E., MASLEN, C. L., SAKAI, L. Y., CORSON, G. M., PUFFENBERGER, E. G., HAMOSH, A., NANTHAKUMAR, E. J., CURRISTIN, S. M. & ET AL. 1991. Marfan syndrome caused by a recurrent de novo missense mutation in the fibrillin gene. *Nature,* 352**,** 337-9.

DINSMORE, C. J. & SORIANO, P. 2018. MAPK and PI3K signaling: At the crossroads of neural crest development. *Dev Biol*.

DORO, D. H., GRIGORIADIS, A. E. & LIU, K. J. 2017. Calvarial Suture-Derived Stem Cells and Their Contribution to Cranial Bone Repair. *Frontiers in Physiology,* 8**,** 956.

DOYLE, A. J., DOYLE, J. J., BESSLING, S. L., MARAGH, S., LINDSAY, M. E., SCHEPERS, D., GILLIS, E., MORTIER, G., HOMFRAY, T., SAULS, K., NORRIS, R. A., HUSO, N. D., LEAHY, D., MOHR, D. W., CAULFIELD, M. J., SCOTT, A. F., DESTREE, A., HENNEKAM, R. C., ARN, P. H., CURRY, C. J., VAN LAER, L., MCCALLION, A. S., LOEYS, B. L. & DIETZ, H. C. 2012. Mutations in the TGF-beta repressor SKI cause Shprintzen-Goldberg syndrome with aortic aneurysm. *Nat Genet,* 44**,** 1249-54.

DREIER, R., OPOLKA, A., GRIFKA, J., BRUCKNER, P. & GRASSEL, S. 2008. Collagen IX-deficiency seriously compromises growth cartilage development in mice. *Matrix Biol,* 27**,** 319-29.

DUCY, P. & KARSENTY, G. 2000. The family of bone morphogenetic proteins. *Kidney Int,* 57**,** 2207-14.

DUQUE, G., HUANG, D. C., MACORITTO, M., RIVAS, D., YANG, X. F., STE-MARIE, L. G. & KREMER, R. 2009. Autocrine regulation of interferon gamma in mesenchymal stem cells plays a role in early osteoblastogenesis. *Stem Cells,* 27**,** 550-8.

DY, P., WANG, W., BHATTARAM, P., WANG, Q., WANG, L., BALLOCK, R. T. & LEFEBVRE, V. 2012. Sox9 directs hypertrophic maturation and blocks osteoblast differentiation of growth plate chondrocytes. *Dev Cell,* 22**,** 597-609.

EGGENSCHWILER, J. T., BULGAKOV, O. V., QIN, J., LI, T. & ANDERSON, K. V. 2006. Mouse Rab23 regulates hedgehog signaling from smoothened to Gli proteins. *Dev Biol,* 290**,** 1-12.

EGGENSCHWILER, J. T., ESPINOZA, E. & ANDERSON, K. V. 2001. Rab23 is an essential negative regulator of the mouse Sonic hedgehog signalling pathway. *Nature,* 412**,** 194-8.

EINHORN, T. A. & GERSTENFELD, L. C. 2015. Fracture healing: mechanisms and interventions. *Nat Rev Rheumatol,* 11**,** 45-54.

EL GHOUZZI, V., LE MERRER, M., PERRIN-SCHMITT, F., LAJEUNIE, E., BENIT, P., RENIER, D., BOURGEOIS, P., BOLCATO-BELLEMIN, A. L., MUNNICH, A. & BONAVENTURE, J. 1997. Mutations of the TWIST gene in the Saethre-Chotzen syndrome. *Nat Genet,* 15**,** 42-6.

ELMS, P., SIGGERS, P., NAPPER, D., GREENFIELD, A. & ARKELL, R. 2003. Zic2 is required for neural crest formation and hindbrain patterning during mouse development. *Dev Biol,* 264**,** 391-406.

ESWARAKUMAR, V. P., HOROWITZ, M. C., LOCKLIN, R., MORRISS-KAY, G. M. & LONAI, P. 2004. A gain-of-function mutation of Fgfr2c demonstrates the roles of this receptor variant in osteogenesis. *Proceedings of the National Academy of Sciences of the United States of America,* 101**,** 12555-12560.

ESWARAKUMAR, V. P., LAX, I. & SCHLESSINGER, J. 2005. Cellular signaling by fibroblast growth factor receptors. *Cytokine & Growth Factor Reviews,* 16**,** 139-149.

ESWARAKUMAR, V. P., MONSONEGO-ORNAN, E., PINES, M., ANTONOPOULOU, I., MORRISS-KAY, G. M. & LONAI, P. 2002. The IIIc alternative of Fgfr2 is a positive regulator of bone formation. *Development,* 129**,** 3783-3793.

ESWARAKUMAR, V. P., ÖZCAN, F., LEW, E. D., BAE, J. H., TOMÉ, F., BOOTH, C. J., ADAMS, D. J., LAX, I. & SCHLESSINGER, J. 2006. Attenuation of signaling pathways stimulated by pathologically activated FGF-receptor 2 mutants prevents craniosynostosis. *Proceedings of the National Academy of Sciences,* 103**,** 18603-18608.

ESWARAKUMAR, V. P. & SCHLESSINGER, J. 2007. Skeletal overgrowth is mediated by deficiency in a specific isoform of fibroblast growth factor receptor 3. *Proc Natl Acad Sci U S A,* 104**,** 3937-42.

FAKHRY, A., RATISOONTORN, C., VEDHACHALAM, C., SALHAB, I., KOYAMA, E., LEBOY, P., PACIFICI, M., KIRSCHNER, R. E. & NAH, H. D. 2005. Effects of FGF-2/-9 in calvarial bone cell cultures: differentiation stage-dependent mitogenic effect, inverse regulation of BMP-2 and noggin, and enhancement of osteogenic potential. *Bone,* 36**,** 254-66.

FANTAUZZO, K. A. & SORIANO, P. 2014. PI3K-mediated PDGFRalpha signaling regulates survival and proliferation in skeletal development through p53-dependent intracellular pathways. *Genes Dev,* 28**,** 1005-17.

FANTAUZZO, K. A. & SORIANO, P. 2016. PDGFRbeta regulates craniofacial development through homodimers and functional heterodimers with PDGFRalpha. *Genes Dev,* 30**,** 2443-2458.

FEI, Y., XIAO, L., DOETSCHMAN, T., COFFIN, D. J. & HURLEY, M. M. 2011. Fibroblast growth factor 2 stimulation of osteoblast differentiation and bone formation is mediated by modulation of the Wnt signaling pathway. *J Biol Chem,* 286**,** 40575-83.

FIRNBERG, N. & NEUBUSER, A. 2002. FGF signaling regulates expression of Tbx2, Erm, Pea3, and Pax3 in the early nasal region. *Dev Biol,* 247**,** 237-50.

FOSTER, J. W., DOMINGUEZ-STEGLICH, M. A., GUIOLI, S., KWOK, C., WELLER, P. A., STEVANOVIC, M., WEISSENBACH, J., MANSOUR, S., YOUNG, I. D., GOODFELLOW, P. N. & ET AL. 1994. Campomelic dysplasia and autosomal sex reversal caused by mutations in an SRY-related gene. *Nature,* 372**,** 525-30.

FRANCAVILLA, C., RIGBOLT, K. T., EMDAL, K. B., CARRARO, G., VERNET, E., BEKKER-JENSEN, D. B., STREICHER, W., WIKSTROM, M., SUNDSTROM, M., BELLUSCI, S., CAVALLARO, U., BLAGOEV, B. & OLSEN, J. V. 2013. Functional proteomics defines the molecular switch underlying FGF receptor trafficking and cellular outputs. *Mol Cell,* 51**,** 707-22.

FREEM, L. J., ESCOT, S., TANNAHILL, D., DRUCKENBROD, N. R., THAPAR, N. & BURNS, A. J. 2010. The intrinsic innervation of the lung is derived from neural crest cells as shown by optical projection tomography in Wnt1-Cre;YFP reporter mice. *J Anat,* 217**,** 651-64.

FREMIN, C., SABA-EL-LEIL, M. K., LEVESQUE, K., ANG, S. L. & MELOCHE, S. 2015. Functional Redundancy of ERK1 and ERK2 MAP Kinases during Development. *Cell Rep,* 12**,** 913-21.

GALLINI, R., LINDBLOM, P., BONDJERS, C., BETSHOLTZ, C. & ANDRAE, J. 2016. PDGF-A and PDGF-B induces cardiac fibrosis in transgenic mice. *Exp Cell Res,* 349**,** 282-290.

GALLO, E. M., LOCH, D. C., HABASHI, J. P., CALDERON, J. F., CHEN, Y., BEDJA, D., VAN ERP, C., GERBER, E. E., PARKER, S. J., SAULS, K., JUDGE, D. P., COOKE, S. K., LINDSAY, M. E., ROUF, R., MYERS, L., AP RHYS, C. M., KENT, K. C., NORRIS, R. A., HUSO, D. L. & DIETZ, H. C. 2014. Angiotensin II-dependent TGF-beta signaling contributes to Loeys-Dietz syndrome vascular pathogenesis. *J Clin Invest,* 124**,** 448-60.

GOMEZ-PICOS, P. & EAMES, B. F. 2015. On the evolutionary relationship between chondrocytes and osteoblasts. *Front Genet,* 6**,** 297.

GOPALAKRISHNAN, S., COMAI, G., SAMBASIVAN, R., FRANCOU, A., KELLY, R. G. & TAJBAKHSH, S. 2015. A Cranial Mesoderm Origin for Esophagus Striated Muscles. *Dev Cell,* 34**,** 694-704.

GOVINDARAJAN, V. & OVERBEEK, P. A. 2006. FGF9 can induce endochondral ossification in cranial mesenchyme. *BMC Dev Biol,* 6**,** 7.

GRAHAM, A., BEGBIE, J. & MCGONNELL, I. 2004. Significance of the cranial neural crest. *Developmental Dynamics,* 229**,** 5-13.

GRIDLEY, T. 2010. Notch signaling in the vasculature. *Curr Top Dev Biol,* 92**,** 277-309.

GRONTHOS, S., STEWART, K., GRAVES, S. E., HAY, S. & SIMMONS, P. J. 1997. Integrin expression and function on human osteoblast-like cells. *J Bone Miner Res,* 12**,** 1189-97.

GUENOU, H., KAABECHE, K., DUFOUR, C., MIRAOUI, H. & MARIE, P. J. 2006. Down-regulation of ubiquitin ligase Cbl induced by twist haploinsufficiency in Saethre-Chotzen syndrome results in increased PI3K/Akt signaling and osteoblast proliferation. *Am J Pathol,* 169**,** 1303-11.

GUENOU, H., KAABECHE, K., MEE, S. L. & MARIE, P. J. 2005. A role for fibroblast growth factor receptor-2 in the altered osteoblast phenotype induced by Twist haploinsufficiency in the Saethre-Chotzen syndrome. *Hum Mol Genet,* 14**,** 1429-39.

GUNTUR, A. R., REINHOLD, M. I., CUELLAR, J., JR. & NASKI, M. C. 2011. Conditional ablation of Pten in osteoprogenitors stimulates FGF signaling. *Development,* 138**,** 1433-44.

HADARI, Y. R., GOTOH, N., KOUHARA, H., LAX, I. & SCHLESSINGER, J. 2001. Critical role for the docking-protein FRS2α in FGF receptor-mediated signal transduction pathways. *Proceedings of the National Academy of Sciences,* 98**,** 8578-8583.

HAGG, R., HEDBOM, E., MOLLERS, U., ASZODI, A., FASSLER, R. & BRUCKNER, P. 1997. Absence of the alpha1(IX) chain leads to a functional knock-out of the entire collagen IX protein in mice. *J Biol Chem,* 272**,** 20650-4.

HAJIHOSSEINI, M. K. & HEATH, J. K. 2002. Expression patterns of fibroblast growth factors-18 and -20 in mouse embryos is suggestive of novel roles in calvarial and limb development. *Mechanisms of Development,* 113**,** 79-83.

HAJIHOSSEINI, M. K., WILSON, S., DE MOERLOOZE, L. & DICKSON, C. 2001. A splicing switch and gain-of-function mutation in FgfR2-IIIc hemizygotes causes Apert/Pfeiffer-syndrome-like phenotypes. *Proc Natl Acad Sci U S A,* 98**,** 3855-60.

HANAFUSA, H., TORII, S., YASUNAGA, T. & NISHIDA, E. 2002. Sprouty1 and Sprouty2 provide a control mechanism for the Ras/MAPK signalling pathway. *Nat Cell Biol,* 4**,** 850-8.

HARADA, M., MURAKAMI, H., OKAWA, A., OKIMOTO, N., HIRAOKA, S., NAKAHARA, T., AKASAKA, R., SHIRAISHI, Y.-I., FUTATSUGI, N., MIZUTANI-KOSEKI, Y., KUROIWA, A., SHIROUZU, M., YOKOYAMA, S., TAIJI, M., ISEKI,

S., ORNITZ, D. M. & KOSEKI, H. 2009. FGF9 monomer-dimer equilibrium regulates extracellular matrix affinity and tissue diffusion. *Nat Genet,* 41**,** 289-298.

HARRIS, J. A., CORSI, M., QUARTAROLI, M., ARBAN, R. & BENTIVOGLIO, M. 1996. Upregulation of spinal glutamate receptors in chronic pain. *Neuroscience,* 74**,** 7-12.

HASTON, S., POZZI, S., CARRENO, G., MANSHAEI, S., PANOUSOPOULOS, L., GONZALEZ-MELJEM, J. M., APPS, J. R., VIRASAMI, A., THAVARAJ, S., GUTTERIDGE, A., FORSHEW, T., MARAIS, R., BRANDNER, S., JACQUES, T. S., ANDONIADOU, C. L. & MARTINEZ-BARBERA, J. P. 2017. MAPK pathway control of stem cell proliferation and differentiation in the embryonic pituitary provides insights into the pathogenesis of papillary craniopharyngioma. *Development,* 144**,** 2141-2152.

HATCH, N. E., HUDSON, M., SETO, M. L., CUNNINGHAM, M. L. & BOTHWELL, M. 2006. Intracellular Retention, Degradation, and Signaling of Glycosylation-deficient FGFR2 and Craniosynostosis Syndrome-associated FGFR2C278F. *Journal of Biological Chemistry,* 281**,** 27292-27305.

HE, F. & SORIANO, P. 2013. A critical role for PDGFRalpha signaling in medial nasal process development. *PLoS Genet,* 9**,** e1003851.

HE, F. & SORIANO, P. 2017. Dysregulated PDGFRalpha signaling alters coronal suture morphogenesis and leads to craniosynostosis through endochondral ossification. *Development,* 144**,** 4026-4036.

HE, P., ZHANG, Z., LIAO, W., XU, D., FU, M. & KANG, Y. 2016. Screening of gene signatures for rheumatoid arthritis and osteoarthritis based on bioinformatics analysis. *Mol Med Rep,* 14**,** 1587-93.

HE, X., BOUGIOUKLI, S., ORTEGA, B., AREVALO, E., LIEBERMAN, J. R. & MCMAHON, A. P. 2017. Sox9 positive periosteal cells in fracture repair of the adult mammalian long bone. *Bone,* 103**,** 12-19.

HILL, R., CALVOPINA, J. H., KIM, C., WANG, Y., DAWSON, D. W., DONAHUE, T. R., DRY, S. & WU, H. 2010. PTEN loss accelerates KrasG12D-induced pancreatic cancer development. *Cancer Res,* 70**,** 7114-24.

HIRAKAWA, K., HIROTA, S., IKEDA, T., YAMAGUCHI, A., TAKEMURA, T., NAGOSHI, J., YOSHIKI, S., SUDA, T., KITAMURA, Y. & NOMURA, S. 1994. Localization of the mRNA for bone matrix proteins during fracture healing as determined by in situ hybridization. *Journal of Bone and Mineral Research,* 9**,** 1551-1557.

HOCH, R. V. & SORIANO, P. 2003. Roles of PDGF in animal development. *Development,* 130**,** 4769-84.

HOLMBECK, K., BIANCO, P., CATERINA, J., YAMADA, S., KROMER, M., KUZNETSOV, S. A., MANKANI, M., GEHRON ROBEY, P., POOLE, A. R., PIDOUX, I., WARD, J. M. & BIRKEDAL-HANSEN, H. 1999. MT1-MMP-Deficient Mice Develop Dwarfism, Osteopenia, Arthritis, and Connective Tissue Disease due to Inadequate Collagen Turnover. *Cell,* 99**,** 81-92.

HOLMES, G. & BASILICO, C. 2012. Mesodermal expression of Fgfr2S252W is necessary and sufficient to induce craniosynostosis in a mouse model of Apert syndrome. *Developmental Biology,* 368**,** 283-293.

HOLMES, G., ROTHSCHILD, G., ROY, U. B., DENG, C.-X., MANSUKHANI, A. & BASILICO, C. 2009. Early onset of craniosynostosis in an Apert mouse model reveals critical features of this pathology. *Developmental Biology,* 328**,** 273-284.

HOWARD, T. D., PAZNEKAS WA FAU - GREEN, E. D., GREEN ED FAU - CHIANG, L. C., CHIANG LC FAU - MA, N., MA N FAU - ORTIZ DE LUNA, R. I., ORTIZ DE LUNA RI FAU - GARCIA DELGADO, C., GARCIA DELGADO C FAU - GONZALEZ-RAMOS, M., GONZALEZ-RAMOS M FAU - KLINE, A. D., KLINE AD FAU - JABS, E. W. & JABS, E. W. 1997. Mutations in TWIST, a basic helix-loop-helix transcription factor, in Saethre-Chotzen syndrome. *Nat Genet.,* 15**,** 36-41.

HOYLE, G. W., LI, J., FINKELSTEIN, J. B., EISENBERG, T., LIU, J.-Y., LASKY, J. A., ATHAS, G., MORRIS, G. F. & BRODY, A. R. 1999. Emphysematous Lesions, Inflammation, and Fibrosis in the Lungs of Transgenic Mice Overexpressing Platelet-Derived Growth Factor. *The American Journal of Pathology,* 154**,** 1763-1775.

HU, L., JONSSON, K. B., ANDERSEN, H., EDENRO, A., BOHLOOLY, Y. M., MELHUS, H. & LIND, T. 2012. Over-expression of Adamts1 in mice alters bone mineral density. *J Bone Miner Metab,* 30**,** 304-11.

HUI, C. C. & JOYNER, A. L. 1993. A mouse model of greig cephalopolysyndactyly syndrome: the extra-toesJ mutation contains an intragenic deletion of the Gli3 gene. *Nat Genet,* 3**,** 241-6.

IATROPOULOS, M. J. & WILLIAMS, G. M. 1996. Proliferation markers. *Exp Toxicol Pathol,* 48**,** 175-81.

INAGAKI, T., CHOI, M., MOSCHETTA, A., PENG, L., CUMMINS, C. L., MCDONALD, J. G., LUO, G., JONES, S. A., GOODWIN, B., RICHARDSON, J. A., GERARD, R. D., REPA, J. J., MANGELSDORF, D. J. & KLIEWER, S. A. 2005. Fibroblast growth factor 15 functions as an enterohepatic signal to regulate bile acid homeostasis. *Cell Metabolism,* 2**,** 217-225.

IONESCU, A., KOZHEMYAKINA, E., NICOLAE, C., KAESTNER, K. H., OLSEN, B. R. & LASSAR, A. B. 2012. FoxA family members are crucial regulators of the hypertrophic chondrocyte differentiation program. *Dev Cell,* 22**,** 927-39.

IRIYAMA, T., TAKEDA, K., NAKAMURA, H., MORIMOTO, Y., KUROIWA, T., MIZUKAMI, J., UMEDA, T., NOGUCHI, T., NAGURO, I., NISHITOH, H., SAEGUSA, K., TOBIUME, K., HOMMA, T., SHIMADA, Y., TSUDA, H., AIKO, S., IMOTO, I., INAZAWA, J., CHIDA, K., KAMEI, Y., KOZUMA, S., TAKETANI, Y., MATSUZAWA, A. & ICHIJO, H. 2009. ASK1 and ASK2 differentially regulate the counteracting roles of apoptosis and inflammation in tumorigenesis. *EMBO J,* 28**,** 843-53.

ISEKI, S., WILKIE, A. O., HEATH, J. K., ISHIMARU, T., ETO, K. & MORRISS-KAY, G. M. 1997. Fgfr2 and osteopontin domains in the developing skull vault are mutually exclusive and can be altered by locally applied FGF2. *Development,* 124**,** 3375-3384.

ISEKI, S., WILKIE, A. O. & MORRISS-KAY, G. M. 1999. Fgfr1 and Fgfr2 have distinct differentiation- and proliferation-related roles in the developing mouse skull vault. *Development,* 126**,** 5611-5620.

ISHII, M., MERRILL, A. E., CHAN, Y. S., GITELMAN, I., RICE, D. P., SUCOV, H. M. & MAXSON, R. E., JR. 2003. Msx2 and Twist cooperatively control the development of the neural crest-derived skeletogenic mesenchyme of the murine skull vault. *Development,* 130**,** 6131-42.

IWASAKI, M., LE, A. X. & HELMS, J. A. 1997. Expression of indian hedgehog, bone morphogenetic protein 6 and gli during skeletal morphogenesis. *Mech Dev,* 69**,** 197-202.

IWATA, T., CHEN, L., LI, C., OVCHINNIKOV, D. A., BEHRINGER, R. R., FRANCOMANO, C. A. & DENG, C. X. 2000. A neonatal lethal mutation in FGFR3 uncouples proliferation and differentiation of growth plate chondrocytes in embryos. *Hum Mol Genet,* 9**,** 1603-13.

JABS, E. W., MÜLLER, U., LI, X., MA, L., LUO, W., HAWORTH, I. S., KLISAK, I., SPARKES, R., WARMAN, M. L., MULLIKEN, J. B., SNEAD, M. L. & MAXSON, R. 1993. A mutation in the homeodomain of the human MSX2 gene in a family affected with autosomal dominant craniosynostosis. *Cell,* 75**,** 443-450.

JACKOWSKI, S., REHG, J. E., ZHANG, Y. M., WANG, J., MILLER, K., JACKSON, P. & KARIM, M. A. 2004. Disruption of CCTbeta2 expression leads to gonadal dysfunction. *Mol Cell Biol,* 24**,** 4720-33.

JACOB, A. L., SMITH, C., PARTANEN, J. & ORNITZ, D. M. 2006. Fibroblast growth factor receptor 1 signaling in the osteo-chondrogenic cell lineage regulates sequential steps of osteoblast maturation. *Dev Biol,* 296**,** 315-28.

JAMES, A. W., SHEN, J., ZHANG, X., ASATRIAN, G., GOYAL, R., KWAK, J. H., JIANG, L., BENGS, B., CULIAT, C. T., TURNER, A. S., SEIM III, H. B., WU, B. M., LYONS, K., ADAMS, J. S., TING, K. & SOO, C. 2015. NELL-1 in the treatment of osteoporotic bone loss. *Nat Commun,* 6**,** 7362.

JENKINS, D., SEELOW, D., JEHEE, F. S., PERLYN, C. A., ALONSO, L. G., BUENO, D. F., DONNAI, D., JOSIFOVA, D., MATHIJSSEN, I. M., MORTON, J. E., ORSTAVIK, K. H., SWEENEY, E., WALL, S. A., MARSH, J. L., NURNBERG, P., PASSOS-BUENO,

M. R. & WILKIE, A. O. 2007. RAB23 mutations in Carpenter syndrome imply an unexpected role for hedgehog signaling in cranial-suture development and obesity. *Am J Hum Genet,* 80**,** 1162-70.

JIANG, X., ISEKI, S., MAXSON, R. E., SUCOV, H. M. & MORRISS-KAY, G. M. 2002. Tissue Origins and Interactions in the Mammalian Skull Vault. *Developmental Biology,* 241**,** 106-116.

JIANG, X., ROWITCH, D. H., SORIANO, P., MCMAHON, A. P. & SUCOV, H. M. 2000. Fate of the mammalian cardiac neural crest. *Development,* 127**,** 1607.

JOHNSON, D., ISEKI, S., WILKIE, A. O. M. & MORRISS-KAY, G. M. 2000. Expression patterns of Twist and Fgfr1, -2 and -3 in the developing mouse coronal suture suggest a key role for Twist in suture initiation and biogenesis. *Mechanisms of Development,* 91**,** 341-345.

JOHNSON, D. & WILKIE, A. O. 2011. Craniosynostosis. *Eur J Hum Genet,* 19**,** 369-76.

JOHNSON, D. R. 1967. Extra-toes: a new mutant gene causing multiple abnormalities in the mouse. *Journal of Embryology and Experimental Morphology,* 17**,** 543.

JUDGE, D. P., BIERY, N. J., KEENE, D. R., GEUBTNER, J., MYERS, L., HUSO, D. L., SAKAI, L. Y. & DIETZ, H. C. 2004. Evidence for a critical contribution of haploinsufficiency in the complex pathogenesis of Marfan syndrome. *J Clin Invest,* 114**,** 172-81.

JUDGE, D. P. & DIETZ, H. C. 2005. Marfan's syndrome. *Lancet,* 366**,** 1965-76.

KAABECHE, K., LEMONNIER, J., LE MEE, S., CAVERZASIO, J. & MARIE, P. J. 2004. Cbl-mediated degradation of Lyn and Fyn induced by constitutive fibroblast growth factor receptor-2 activation supports osteoblast differentiation. *J Biol Chem,* 279**,** 36259-67.

KAPYLA, J., JAALINOJA, J., TULLA, M., YLOSTALO, J., NISSINEN, L., VIITASALO, T., VEHVILAINEN, P., MARJOMAKI, V., NYKVIST, P., SAAMANEN, A. M., FARNDALE, R. W., BIRK, D. E., ALA-KOKKO, L. & HEINO, J. 2004. The fibril-associated collagen IX provides a novel mechanism for cell adhesion to cartilaginous matrix. *J Biol Chem,* 279**,** 51677-87.

KARIM, M., JACKSON, P. & JACKOWSKI, S. 2003. Gene structure, expression and identification of a new CTP:phosphocholine cytidylyltransferase beta isoform. *Biochim Biophys Acta,* 1633**,** 1-12.

KARUPPAIAH, K., YU, K., LIM, J., CHEN, J., SMITH, C., LONG, F. & ORNITZ, D. M. 2016. FGF signaling in the osteoprogenitor lineage non-autonomously regulates postnatal chondrocyte proliferation and skeletal growth. *Development,* 143**,** 1811-22.

KAWANO, T., ZHENG, H., MERZ, D. C., KOHARA, Y., TAMAI, K. K., NISHIWAKI, K. & CULOTTI, J. G. 2009. C. elegans mig-6 encodes papilin isoforms that affect distinct aspects of DTC migration, and interacts genetically with mig-17 and collagen IV. *Development,* 136**,** 1433-42.

KIECKER, C. & LUMSDEN, A. 2005. Compartments and their boundaries in vertebrate brain development. *Nat Rev Neurosci,* 6**,** 553-564.

KIM, H. J., KIM, J. H., BAE, S. C., CHOI, J. Y., KIM, H. J. & RYOO, H. M. 2003a. The protein kinase C pathway plays a central role in the fibroblast growth factor-stimulated expression and transactivation activity of Runx2. *J Biol Chem,* 278**,** 319-26.

KIM, H. J., RICE, D. P., KETTUNEN, P. J. & THESLEFF, I. 1998. FGF-, BMP- and Shh-mediated signalling pathways in the regulation of cranial suture morphogenesis and calvarial bone development. *Development,* 125**,** 1241-51.

KIM, I. S., OTTO, F., ZABEL, B. & MUNDLOS, S. 1999. Regulation of chondrocyte differentiation by Cbfa1. *Mech Dev,* 80**,** 159-70.

KIM, S., KOGA, T., ISOBE, M., KERN, B. E., YOKOCHI, T., CHIN, Y. E., KARSENTY, G., TANIGUCHI, T. & TAKAYANAGI, H. 2003b. Stat1 functions as a cytoplasmic attenuator of Runx2 in the transcriptional program of osteoblast differentiation. *Genes Dev,* 17**,** 1979-91.

KISSEBERTH, W. C., BRETTINGEN, N. T., LOHSE, J. K. & SANDGREN, E. P. 1999. Ubiquitous expression of marker transgenes in mice and rats. *Dev Biol,* 214**,** 128-38.

KIYOZUMI, D., SUGIMOTO, N. & SEKIGUCHI, K. 2006. Breakdown of the reciprocal stabilization of QBRICK/Frem1, Fras1, and Frem2 at the basement membrane provokes Fraser syndrome-like defects. *Proc Natl Acad Sci U S A,* 103**,** 11981-6.

KLINGHOFFER, R. A., HAMILTON, T. G., HOCH, R. & SORIANO, P. 2002. An allelic series at the PDGFalphaR locus indicates unequal contributions of distinct signaling pathways during development. *Dev Cell,* 2**,** 103-13.

KLINGHOFFER, R. A., MUETING-NELSEN, P. F., FAERMAN, A., SHANI, M. & SORIANO, P. 2001. The two PDGF receptors maintain conserved signaling in vivo despite divergent embryological functions. *Mol Cell,* 7**,** 343-54.

KOBAYASHI, T., SOEGIARTO, D. W., YANG, Y., LANSKE, B., SCHIPANI, E., MCMAHON, A. P. & KRONENBERG, H. M. 2005. Indian hedgehog stimulates periarticular chondrocyte differentiation to regulate growth plate length independently of PTHrP. *J Clin Invest,* 115**,** 1734-42.

KOMORI, T., YAGI, H., NOMURA, S., YAMAGUCHI, A., SASAKI, K., DEGUCHI, K., SHIMIZU, Y., BRONSON, R. T., GAO, Y. H., INADA, M., SATO, M., OKAMOTO, R., KITAMURA, Y., YOSHIKI, S. & KISHIMOTO, T. 1997. Targeted Disruption of Cbfa1 Results in a Complete Lack of Bone Formation owing to Maturational Arrest of Osteoblasts. *Cell,* 89**,** 755-764.

KOZHEMYAKINA, E., LASSAR, A. B. & ZELZER, E. 2015. A pathway to bone: signaling molecules and transcription factors involved in chondrocyte development and maturation. *Development,* 142**,** 817-31.

KOZIEL, L., WUELLING, M., SCHNEIDER, S. & VORTKAMP, A. 2005. Gli3 acts as a repressor downstream of Ihh in regulating two distinct steps of chondrocyte differentiation. *Development,* 132**,** 5249-60.

KRAMEROVA, I. A., KAWAGUCHI, N., FESSLER, L. I., NELSON, R. E., CHEN, Y., KRAMEROV, A. A., KUSCHE-GULLBERG, M., KRAMER, J. M., ACKLEY, B. D., SIERON, A. L., PROCKOP, D. J. & FESSLER, J. H. 2000. Papilin in development; a pericellular protein with a homology to the ADAMTS metalloproteinases. *Development,* 127**,** 5475-85.

KURO-O, M. 2008. Endocrine FGFs and Klothos: emerging concepts. *Trends Endocrinol Metab,* 19**,** 239-45.

LABONNE, C. & BRONNER-FRASER, M. 1998. Neural crest induction in Xenopus: evidence for a two-signal model. *Development,* 125**,** 2403-2414.

LAI, M. S., WANG, C. Y., YANG, S. H., WU, C. C., SUN, H. S., TSAI, S. J., CHUANG, J. I., CHEN, Y. C. & HUANG, B. M. 2016. The expression profiles of fibroblast growth factor 9 and its receptors in developing mice testes. *Organogenesis,* 12**,** 61-77.

LEE, D. W., HAM, K. W., KWON, S. M., LEW, D. H. & CHO, E. J. 2012. Dual midfacial distraction osteogenesis for Crouzon syndrome: long-term follow-up study for relapse and growth. *J Oral Maxillofac Surg,* 70**,** e242-51.

LEE, Y. C., SONG, I. W., PAI, Y. J., CHEN, S. D. & CHEN, Y. T. 2017. Knock-in human FGFR3 achondroplasia mutation as a mouse model for human skeletal dysplasia. *Sci Rep,* 7**,** 43220.

LEFEBVRE, V., BEHRINGER, R. R. & DE CROMBRUGGHE, B. 2001. L-Sox5, Sox6 and Sox9 control essential steps of the chondrocyte differentiation pathway. *Osteoarthritis Cartilage,* 9 Suppl A**,** S69-75.

LESCROART, F., KELLY, R. G., LE GARREC, J. F., NICOLAS, J. F., MEILHAC, S. M. & BUCKINGHAM, M. 2010. Clonal analysis reveals common lineage relationships between head muscles and second heart field derivatives in the mouse embryo. *Development,* 137**,** 3269-79.

LEVEEN, P., PEKNY, M., GEBRE-MEDHIN, S., SWOLIN, B., LARSSON, E. & BETSHOLTZ, C. 1994. Mice deficient for PDGF B show renal, cardiovascular, and hematological abnormalities. *Genes Dev,* 8**,** 1875-87.

LI, C., CHEN, L., IWATA, T., KITAGAWA, M., FU, X.-Y. & DENG, C.-X. 1999. A Lys644Glu Substitution in Fibroblast Growth Factor Receptor 3 (FGFR3) Causes Dwarfism in Mice by Activation of STATs and Ink4 Cell Cycle Inhibitors. *Human Molecular Genetics,* 8**,** 35-44.

LI, C., SCOTT, D. A., HATCH, E., TIAN, X. & MANSOUR, S. L. 2007. Dusp6 (Mkp3) is a negative feedback regulator of FGF-stimulated ERK signaling during mouse development. *Development,* 134**,** 167-176.

LI, C., XU, X., NELSON, D. K., WILLIAMS, T., KUEHN, M. R. & DENG, C.-X. 2005. FGFR1 function at the earliest stages of mouse limb development plays an indispensable role in subsequent autopod morphogenesis. *Development,* 132**,** 4755.

LI, S., QUARTO, N. & LONGAKER, M. T. 2010. Activation of FGF signaling mediates proliferative and osteogenic differences between neural crest derived frontal and mesoderm parietal derived bone. *PLoS One,* 5**,** e14033.

LI, S. W., PROCKOP, D. J., HELMINEN, H., FÄSSLER, R., LAPVETELÄINEN, T., KIRALY, K., PELTARRI, A., AROKOSKI, J., LUI, H. & ARITA, M. 1995. Transgenic mice with targeted inactivation of the Col2 alpha 1 gene for collagen II develop a skeleton with membranous and periosteal bone but no endochondral bone. *Genes & Development,* 9**,** 2821-2830.

LIM, J., TU, X., CHOI, K., AKIYAMA, H., MISHINA, Y. & LONG, F. 2015. BMP–Smad4 signaling is required for precartilaginous mesenchymal condensation independent of Sox9 in the mouse. *Developmental Biology,* 400**,** 132-138.

LIN, X. 2004. Functions of heparan sulfate proteoglycans in cell signaling during development. *Development,* 131**,** 6009-21.

LIND, T., MCKIE, N., WENDEL, M., RACEY, S. N. & BIRCH, M. A. 2005. The hyalectan degrading ADAMTS-1 enzyme is expressed by osteoblasts and up-regulated at regions of new bone formation. *Bone,* 36**,** 408-17.

LIU, J., NAM, H. K., WANG, E. & HATCH, N. E. 2013. Further analysis of the Crouzon mouse: effects of the FGFR2(C342Y) mutation are cranial bone-dependent. *Calcif Tissue Int,* 92**,** 451-66.

LIU, Y. H., KUNDU, R., WU, L., LUO, W., IGNELZI, M. A., SNEAD, M. L. & MAXSON, R. E. 1995. Premature suture closure and ectopic cranial bone in mice expressing Msx2 transgenes in the developing skull. *Proceedings of the National Academy of Sciences of the United States of America,* 92**,** 6137-6141.

LIU, Z., XU, J., COLVIN, J. S. & ORNITZ, D. M. 2002. Coordination of chondrogenesis and osteogenesis by fibroblast growth factor 18. *Genes Dev,* 16**,** 859-69.

LOEBEL, D. A., HOR, A. C., BILDSOE, H., JONES, V., CHEN, Y. T., BEHRINGER, R. R. & TAM, P. P. 2012. Regionalized Twist1 activity in the forelimb bud drives the morphogenesis of the proximal and preaxial skeleton. *Dev Biol,* 362**,** 132-40.

LOEYS, B. L., CHEN, J., NEPTUNE, E. R., JUDGE, D. P., PODOWSKI, M., HOLM, T., MEYERS, J., LEITCH, C. C., KATSANIS, N., SHARIFI, N., XU, F. L., MYERS, L. A., SPEVAK, P. J., CAMERON, D. E., DE BACKER, J., HELLEMANS, J., CHEN, Y., DAVIS, E. C., WEBB, C. L., KRESS, W., COUCKE, P., RIFKIN, D. B., DE PAEPE, A. M. & DIETZ, H. C. 2005. A syndrome of altered cardiovascular, craniofacial, neurocognitive and skeletal development caused by mutations in TGFBR1 or TGFBR2. *Nat Genet,* 37**,** 275-81.

LOGAN, C. Y. & NUSSE, R. 2004. The Wnt signaling pathway in development and disease. *Annu Rev Cell Dev Biol,* 20**,** 781-810.

LOGAN, M., MARTIN, J. F., NAGY, A., LOBE, C., OLSON, E. N. & TABIN, C. J. 2002. Expression of Cre Recombinase in the developing mouse limb bud driven by a Prxl enhancer. *Genesis,* 33**,** 77-80.

LONG, F. 2012. Building strong bones: molecular regulation of the osteoblast lineage. *Nat Rev Mol Cell Biol,* 13**,** 27-38.

LONG, F., ZHANG, X. M., KARP, S., YANG, Y. & MCMAHON, A. P. 2001. Genetic manipulation of hedgehog signaling in the endochondral skeleton reveals a direct role in the regulation of chondrocyte proliferation. *Development,* 128**,** 5099-108.

LU, X., WANG, Q., HU, G., VAN POZNAK, C., FLEISHER, M., REISS, M., MASSAGUE, J. & KANG, Y. 2009. ADAMTS1 and MMP1 proteolytically engage EGF-like ligands in an osteolytic signaling cascade for bone metastasis. *Genes Dev,* 23**,** 1882-94.

LUMSDEN, A., SPRAWSON, N. & GRAHAM, A. 1991. Segmental origin and migration of neural crest cells in the hindbrain region of the chick embryo. *Development,* 113**,** 1281-1291.

MA, L., GOLDEN, S., WU, L. & MAXSON, R. 1996. The molecular basis of Boston-type craniosynostosis: the Pro148-->His mutation in the N-terminal arm of the MSX2 homeodomain stabilizes DNA binding without altering nucleotide sequence preferences. *Hum Mol Genet,* 5**,** 1915-20.

MACCARRICK, G., BLACK, J. H., 3RD, BOWDIN, S., EL-HAMAMSY, I., FRISCHMEYER-GUERRERIO, P. A., GUERRERIO, A. L., SPONSELLER, P. D., LOEYS, B. & DIETZ, H. C., 3RD 2014. Loeys-Dietz syndrome: a primer for diagnosis and management. *Genet Med,* 16**,** 576-87.

MAENO, T., MORIISHI, T., YOSHIDA, C. A., KOMORI, H., KANATANI, N., IZUMI, S., TAKAOKA, K. & KOMORI, T. 2011. Early onset of Runx2 expression caused craniosynostosis, ectopic bone formation, and limb defects. *Bone,* 49**,** 673-82.

MAESTRO, R., DEI TOS, A. P., HAMAMORI, Y., KRASNOKUTSKY, S., SARTORELLI, V., KEDES, L., DOGLIONI, C., BEACH, D. H. & HANNON, G. J. 1999. Twist is a potential oncogene that inhibits apoptosis. *Genes Dev,* 13**,** 2207-17.

MAHER, P. A. 1996. Nuclear Translocation of fibroblast growth factor (FGF) receptors in response to FGF-2. *J Cell Biol,* 134**,** 529-36.

MAI, S., WEI, K., FLENNIKEN, A., ADAMSON, S. L., ROSSANT, J., AUBIN, J. E. & GONG, S. G. 2010. The missense mutation W290R in Fgfr2 causes developmental defects from aberrant IIIb and IIIc signaling. *Dev Dyn,* 239**,** 1888-900.

MAK, K. K., KRONENBERG, H. M., CHUANG, P. T., MACKEM, S. & YANG, Y. 2008. Indian hedgehog signals independently of PTHrP to promote chondrocyte hypertrophy. *Development,* 135**,** 1947-56.

MAKARENKOVA, H. P., HOFFMAN, M. P., BEENKEN, A., ELISEENKOVA, A. V., MEECH, R., TSAU, C., PATEL, V. N., LANG, R. A. & MOHAMMADI, M. 2009. Differential interactions of FGFs with heparan sulfate control gradient formation and branching morphogenesis. *Sci Signal,* 2**,** ra55.

MALAVAL, L., MODROWSKI, D., GUPTA, A. K. & AUBIN, J. E. 1994. Cellular expression of bone-related proteins during in vitro osteogenesis in rat bone marrow stromal cell cultures. *Journal of Cellular Physiology,* 158**,** 555-572.

MANSOUR, S. L., LI, C. & URNESS, L. D. 2013. Genetic rescue of Muenke syndrome model hearing loss reveals prolonged FGF-dependent plasticity in cochlear supporting cell fates. *Genes Dev,* 27**,** 2320-31.

MANSOUR, S. L., TWIGG, S. R., FREELAND, R. M., WALL, S. A., LI, C. & WILKIE, A. O. 2009. Hearing loss in a mouse model of Muenke syndrome. *Hum Mol Genet,* 18**,** 43-50.

MANSUKHANI, A., BELLOSTA, P., SAHNI, M. & BASILICO, C. 2000. Signaling by Fibroblast Growth Factors (Fgf) and Fibroblast Growth Factor Receptor 2 (Fgfr2)–Activating Mutations Blocks Mineralization and Induces Apoptosis in Osteoblasts. *The Journal of Cell Biology,* 149**,** 1297-1308.

MAO, X., FUJIWARA, Y. & ORKIN, S. H. 1999. Improved reporter strain for monitoring Cre recombinase-mediated DNA excisions in mice. *Proc Natl Acad Sci U S A,* 96**,** 5037-42.

MARIE, P. J. 2012. Fibroblast growth factor signaling controlling bone formation: an update. *Gene,* 498**,** 1-4.

MARTIN, L., KACI, N., ESTIBALS, V., GOUDIN, N., GARFA-TRAORE, M., BENOIST-LASSELIN, C., DAMBROISE, E. & LEGEAI-MALLET, L. 2018. Constitutively-active FGFR3 disrupts primary cilium length and IFT20 trafficking in various chondrocyte models of achondroplasia. *Hum Mol Genet,* 27**,** 1-13.

MARUYAMA, T., JEONG, J., SHEU, T. J. & HSU, W. 2016. Stem cells of the suture mesenchyme in craniofacial bone development, repair and regeneration. *Nat Commun,* 7**,** 10526.

MARUYAMA, T., MIRANDO, A. J., DENG, C. X. & HSU, W. 2010. The balance of WNT and FGF signaling influences mesenchymal stem cell fate during skeletal development. *Sci Signal,* 3**,** ra40.

MASSARI, M. E. & MURRE, C. 2000. Helix-loop-helix proteins: regulators of transcription in eucaryotic organisms. *Mol Cell Biol,* 20**,** 429-40.

MAY, M., MOSTO, J., VAZQUEZ, P. M., GONZALEZ, P., ROJAS, P., GASS, H., LANARI, C. & MOLINOLO, A. A. 2016. Nuclear staining of fgfr-2/stat-5 and runx-2 in mucinous breast cancer. *Exp Mol Pathol,* 100**,** 39-44.

MAYOR, R., GUERRERO, N. & MARTÍNEZ, C. 1997. Role of FGF andNogginin Neural Crest Induction. *Developmental Biology,* 189**,** 1-12.

MAZZUCCHELLI, C., VANTAGGIATO, C., CIAMEI, A., FASANO, S., PAKHOTIN, P., KREZEL, W., WELZL, H., WOLFER, D. P., PAGES, G., VALVERDE, O., MAROWSKY, A., PORRAZZO, A., ORBAN, P. C., MALDONADO, R., EHRENGRUBER, M. U., CESTARI, V., LIPP, H. P., CHAPMAN, P. F., POUYSSEGUR, J. & BRAMBILLA, R. 2002. Knockout of ERK1 MAP kinase enhances synaptic plasticity in the striatum and facilitates striatal-mediated learning and memory. *Neuron,* 34**,** 807-20.

MCBRATNEY-OWEN, B., ISEKI, S., BAMFORTH, S. D., OLSEN, B. R. & MORRISS-KAY, G. M. 2008. Development and tissue origins of the mammalian cranial base. *Developmental Biology,* 322**,** 121-132.

MERRILL, A. E., BOCHUKOVA, E. G., BRUGGER, S. M., ISHII, M., PILZ, D. T., WALL, S. A., LYONS, K. M., WILKIE, A. O. M. & MAXSON, J. R. E. 2006. Cell mixing at a neural crest-mesoderm boundary and deficient ephrin-Eph signaling in the pathogenesis of craniosynostosis. *Human Molecular Genetics,* 15**,** 1319-1328.

MEYERS, G. A., ORLOW, S. J., MUNRO, I. R., PRZYLEPA, K. A. & JABS, E. W. 1995. Fibroblast growth factor receptor 3 (FGFR3) transmembrane mutation in Crouzon syndrome with acanthosis nigricans. *Nat Genet,* 11**,** 462-4.

MIACZYNSKA, M. 2013. Effects of membrane trafficking on signaling by receptor tyrosine kinases. *Cold Spring Harb Perspect Biol,* 5**,** a009035.

MIN, H., DANILENKO, D. M., SCULLY, S. A., BOLON, B., RING, B. D., TARPLEY, J. E., DEROSE, M. & SIMONET, W. S. 1998. Fgf-10 is required for both limb and lung development and exhibits striking functional similarity to Drosophila branchless. *Genes & Development,* 12**,** 3156-3161.

MIRAOUI, H., OUDINA, K., PETITE, H., TANIMOTO, Y., MORIYAMA, K. & MARIE, P. J. 2009. Fibroblast Growth Factor Receptor 2 Promotes Osteogenic Differentiation in Mesenchymal Cells via ERK1/2 and Protein Kinase C Signaling. *Journal of Biological Chemistry,* 284**,** 4897-4904.

MIRAOUI, H., RINGE, J., HAUPL, T. & MARIE, P. J. 2010a. Increased EFG- and PDGFalpha-receptor signaling by mutant FGF-receptor 2 contributes to osteoblast dysfunction in Apert craniosynostosis. *Hum Mol Genet,* 19**,** 1678-89.

MIRAOUI, H., SEVERE, N., VAUDIN, P., PAGÈS, J.-C. & MARIE, P. J. 2010b. Molecular silencing of Twist1 enhances osteogenic differentiation of murine mesenchymal stem cells: Implication of FGFR2 signaling. *Journal of Cellular Biochemistry,* 110**,** 1147-1154.

MOAZEN, M., PESKETT, E., BABBS, C., PAUWS, E. & FAGAN, M. J. 2015. Mechanical Properties of Calvarial Bones in a Mouse Model for Craniosynostosis. *PLoS ONE,* 10**,** e0125757.

MOENNING, A., JAGER, R., EGERT, A., KRESS, W., WARDELMANN, E. & SCHORLE, H. 2009. Sustained platelet-derived growth factor receptor alpha signaling in osteoblasts results in craniosynostosis by overactivating the phospholipase C-gamma pathway. *Mol Cell Biol,* 29**,** 881-91.

MOLOTKOV, A., MAZOT, P., BREWER, J. R., CINALLI, R. M. & SORIANO, P. 2017. Distinct Requirements for FGFR1 and FGFR2 in Primitive Endoderm Development and Exit from Pluripotency. *Dev Cell,* 41**,** 511-526 e4.

MONSONEGO-ORNAN, E., ADAR, R., FEFERMAN, T., SEGEV, O. & YAYON, A. 2000. The transmembrane mutation G380R in fibroblast growth factor receptor 3 uncouples ligand-mediated receptor activation from down-regulation. *Mol Cell Biol,* 20**,** 516-22.

MONTERO, A., OKADA, Y., TOMITA, M., ITO, M., TSURUKAMI, H., NAKAMURA, T., DOETSCHMAN, T., COFFIN, J. D. & HURLEY, M. M. 2000. Disruption of the fibroblast growth factor-2 gene results in decreased bone mass and bone formation. *J Clin Invest,* 105**,** 1085-93.

MUENKE, M., GRIPP KW FAU - MCDONALD-MCGINN, D. M., MCDONALD-MCGINN DM FAU - GAUDENZ, K., GAUDENZ K FAU - WHITAKER, L. A., WHITAKER LA FAU - BARTLETT, S. P., BARTLETT SP FAU - MARKOWITZ, R. I., MARKOWITZ RI FAU - ROBIN, N. H., ROBIN NH FAU - NWOKORO, N.,

NWOKORO N FAU - MULVIHILL, J. J., MULVIHILL JJ FAU - LOSKEN, H. W., LOSKEN HW FAU - MULLIKEN, J. B., MULLIKEN JB FAU - GUTTMACHER, A. E., GUTTMACHER AE FAU - WILROY, R. S., WILROY RS FAU - CLARKE, L. A., CLARKE LA FAU - HOLLWAY, G., HOLLWAY G FAU - ADES, L. C., ADES LC FAU - HAAN, E. A., HAAN EA FAU - MULLEY, J. C., MULLEY JC FAU - COHEN, M. M., JR., COHEN MM JR FAU - BELLUS, G. A., BELLUS GA FAU - FRANCOMANO, C. A., FRANCOMANO CA FAU - MOLONEY, D. M., MOLONEY DM FAU - WALL, S. A., WALL SA FAU - WILKIE, A. O., WILKIE, A. O. & ET AL. 1997. A unique point mutation in the fibroblast growth factor receptor 3 gene (FGFR3) defines a new craniosynostosis syndrome. *Am J Hum Genet.* , 60**,** 555-564.

MUENKE, M., SCHELL U FAU - HEHR, A., HEHR A FAU - ROBIN, N. H., ROBIN NH FAU - LOSKEN, H. W., LOSKEN HW FAU - SCHINZEL, A., SCHINZEL A FAU - PULLEYN, L. J., PULLEYN LJ FAU - RUTLAND, P., RUTLAND P FAU - REARDON, W., REARDON W FAU - MALCOLM, S., MALCOLM, S. & ET AL. 1994. A common mutation in the fibroblast growth factor receptor 1 gene in Pfeiffer syndrome. *Nat Genet.,* 8**,** 269-274.

MURAKAMI, S., BALMES, G., MCKINNEY, S., ZHANG, Z., GIVOL, D. & DE CROMBRUGGHE, B. 2004. Constitutive activation of MEK1 in chondrocytes causes Stat1-independent achondroplasia-like dwarfism and rescues the Fgfr3-deficient mouse phenotype. *Genes Dev,* 18**,** 290-305.

MURRAY, S. A. & GRIDLEY, T. 2006. Snail family genes are required for left-right asymmetry determination, but not neural crest formation, in mice. *Proc Natl Acad Sci U S A,* 103**,** 10300-4.

MUZUMDAR, M. D., TASIC, B., MIYAMICHI, K., LI, L. & LUO, L. 2007. A global double-fluorescent Cre reporter mouse. *Genesis,* 45**,** 593-605.

MYERS, J. M., MARTINS, G. G., OSTROWSKI, J. & STACHOWIAK, M. K. 2003. Nuclear trafficking of FGFR1: a role for the transmembrane domain. *J Cell Biochem,* 88**,** 1273-91.

NAKAMURA, M., SONE, S., TAKAHASHI, I., MIZOGUCHI, I., ECHIGO, S. & SASANO, Y. 2005. Expression of versican and ADAMTS1, 4, and 5 during bone development in the rat mandible and hind limb. *J Histochem Cytochem,* 53**,** 1553-62.

NAKAMURA, T., GULICK, J., COLBERT, M. C. & ROBBINS, J. 2009a. Protein tyrosine phosphatase activity in the neural crest is essential for normal heart and skull development. *Proc Natl Acad Sci U S A,* 106**,** 11270-5.

NAKAMURA, T., GULICK, J., PRATT, R. & ROBBINS, J. 2009b. Noonan syndrome is associated with enhanced pERK activity, the repression of which can prevent craniofacial malformations. *Proc Natl Acad Sci U S A,* 106**,** 15436-41.

NAKASHIMA, K., ZHOU, X., KUNKEL, G., ZHANG, Z., DENG, J. M., BEHRINGER, R. R. & DE CROMBRUGGHE, B. 2002. The Novel Zinc Finger-Containing Transcription Factor Osterix Is Required for Osteoblast Differentiation and Bone Formation. *Cell,* 108**,** 17-29.

NEWBERN, J., ZHONG, J., WICKRAMASINGHE, R. S., LI, X., WU, Y., SAMUELS, I., CHEROSKY, N., KARLO, J. C., O'LOUGHLIN, B., WIKENHEISER, J., GARGESHA, M., DOUGHMAN, Y. Q., CHARRON, J., GINTY, D. D., WATANABE, M., SAITTA, S. C., SNIDER, W. D. & LANDRETH, G. E. 2008. Mouse and human phenotypes indicate a critical conserved role for ERK2 signaling in neural crest development. *Proc Natl Acad Sci U S A,* 105**,** 17115-20.

NG, C. M., CHENG, A., MYERS, L. A., MARTINEZ-MURILLO, F., JIE, C., BEDJA, D., GABRIELSON, K. L., HAUSLADEN, J. M., MECHAM, R. P., JUDGE, D. P. & DIETZ, H. C. 2004. TGF-beta-dependent pathogenesis of mitral valve prolapse in a mouse model of Marfan syndrome. *J Clin Invest,* 114**,** 1586-92.

NIK, A. M., JOHANSSON, J. A., GHIAMI, M., REYAHI, A. & CARLSSON, P. 2016. Foxf2 is required for secondary palate development and Tgfbeta signaling in palatal shelf mesenchyme. *Dev Biol,* 415**,** 14-23.

NOBLE, M., MURRAY, K., STROOBANT, P., WATERFIELD, M. D. & RIDDLE, P. 1988. Platelet-derived growth factor promotes division and motility and inhibits premature

differentiation of the oligodendrocyte/type-2 astrocyte progenitor cell. *Nature,* 333**,** 560-2.

NONOGAKI, K., KAJI, T., YAMAZAKI, T. & MURAKAMI, M. 2016. Treatment with FGFR2-IIIc monoclonal antibody suppresses weight gain and adiposity in KKA(y) mice. *Nutr Diabetes,* 6**,** e233.

NYABI, O., NAESSENS, M., HAIGH, K., GEMBARSKA, A., GOOSSENS, S., MAETENS, M., DE CLERCQ, S., DROGAT, B., HAENEBALCKE, L., BARTUNKOVA, S., DE VOS, I., DE CRAENE, B., KARIMI, M., BERX, G., NAGY, A., HILSON, P., MARINE, J. C. & HAIGH, J. J. 2009. Efficient mouse transgenesis using Gateway-compatible ROSA26 locus targeting vectors and F1 hybrid ES cells. *Nucleic Acids Res,* 37**,** e55.

OHBAYASHI, N., SHIBAYAMA, M., KUROTAKI, Y., IMANISHI, M., FUJIMORI, T., ITOH, N. & TAKADA, S. 2002. FGF18 is required for normal cell proliferation and differentiation during osteogenesis and chondrogenesis. *Genes Dev,* 16**,** 870-9.

OKADA, T., OKUMURA, Y., MOTOYAMA, J. & OGAWA, M. 2008. FGF8 signaling patterns the telencephalic midline by regulating putative key factors of midline development. *Dev Biol,* 320**,** 92-101.

OLSEN, S. K., GARBI, M., ZAMPIERI, N., ELISEENKOVA, A. V., ORNITZ, D. M., GOLDFARB, M. & MOHAMMADI, M. 2003. Fibroblast Growth Factor (FGF) Homologous Factors Share Structural but Not Functional Homology with FGFs. *Journal of Biological Chemistry,* 278**,** 34226-34236.

OLSON, L. E. & SORIANO, P. 2009. Increased PDGFRalpha activation disrupts connective tissue development and drives systemic fibrosis. *Dev Cell,* 16**,** 303-13.

OPOLKA, A., RATZINGER, S., SCHUBERT, T., SPIEGEL, H. U., GRIFKA, J., BRUCKNER, P., PROBST, A. & GRASSEL, S. 2007. Collagen IX is indispensable for timely maturation of cartilage during fracture repair in mice. *Matrix Biol,* 26**,** 85-95.

ORNITZ, D. M. & ITOH, N. 2015. The Fibroblast Growth Factor signaling pathway. *Wiley Interdisciplinary Reviews: Developmental Biology,* 4**,** 215-266.

ORNITZ, D. M. & MARIE, P. J. 2015. Fibroblast growth factor signaling in skeletal development and disease. *Genes Dev,* 29**,** 1463-86.

ORR-URTREGER, A., BEDFORD, M. T., BURAKOVA, T., ARMAN, E., ZIMMER, Y., YAYON, A., GIVOL, D. & LONAI, P. 1993. Developmental Localization of the Splicing Alternatives of Fibroblast Growth Factor Receptor-2 (FGFR2). *Developmental Biology,* 158**,** 475-486.

OTSUKI, S., HANSON, S. R., MIYAKI, S., GROGAN, S. P., KINOSHITA, M., ASAHARA, H., WONG, C. H. & LOTZ, M. K. 2010. Extracellular sulfatases support cartilage homeostasis by regulating BMP and FGF signaling pathways. *Proc Natl Acad Sci U S A,* 107**,** 10202-7.

OWEN, T. A., ARONOW, M., SHALHOUB, V., BARONE, L. M., WILMING, L., TASSINARI, M. S., KENNEDY, M. B., POCKWINSE, S., LIAN, J. B. & STEIN, G. S. 1990. Progressive development of the rat osteoblast phenotype in vitro: reciprocal relationships in expression of genes associated with osteoblast proliferation and differentiation during formation of the bone extracellular matrix. *J Cell Physiol,* 143**,** 420-30.

PANNIER, S., COULOIGNER, V., MESSADDEQ, N., ELMALEH-BERGES, M., MUNNICH, A., ROMAND, R. & LEGEAI-MALLET, L. 2009. Activating Fgfr3 Y367C mutation causes hearing loss and inner ear defect in a mouse model of chondrodysplasia. *Biochim Biophys Acta,* 1792**,** 140-7.

PAPADAKI, C., ALEXIOU, M., CECENA, G., VERYKOKAKIS, M., BILITOU, A., CROSS, J. C., OSHIMA, R. G. & MAVROTHALASSITIS, G. 2007. Transcriptional repressor erf determines extraembryonic ectoderm differentiation. *Mol Cell Biol,* 27**,** 5201-13.

PARADA, C., HAN, D., GRIMALDI, A., SARRION, P., PARK, S. S., PELIKAN, R., SANCHEZ-LARA, P. A. & CHAI, Y. 2015. Disruption of the ERK/MAPK pathway in neural crest cells as a potential cause of Pierre Robin sequence. *Development,* 142**,** 3734-45.

PARK, D. H. & YOON, S. H. 2012. Craniofacial malformation treatment: craniosynostosis and positional plagiocephaly. *J Korean Med Assoc.,* 55**,** 878-886.

PARK, W. J., MEYERS, G. A., LI, X., THEDA, C., DAY, D., ORLOW, S. J., JONES, M. C. & JABS, E. W. 1995. Novel FGFR2 mutations in Crouzon and Jackson-Weiss syndromes show allelic heterogeneity and phenotypic variability. *Hum Mol Genet,* 4**,** 1229-33.

PARK, W. J., YOU, S. H., CHOI, H. A., CHU, Y. J. & KIM, G. J. 2015. Over-expression of recombinant proteins with N-terminal His-tag via subcellular uneven distribution in Escherichia coli. *Acta Biochim Biophys Sin (Shanghai),* 47**,** 661.

PARTANEN, J., SCHWARTZ, L. & ROSSANT, J. 1998. Opposite phenotypes of hypomorphic and Y766 phosphorylation site mutations reveal a function for Fgfr1 in anteroposterior patterning of mouse embryos. *Genes Dev,* 12**,** 2332-44.

PEMBERTON, T. J., LI, F. Y., OKA, S., MENDOZA-FANDINO, G. A., HSU, Y. H., BRINGAS, P., JR., CHAI, Y., SNEAD, M. L., MEHRIAN-SHAI, R. & PATEL, P. I. 2007. Identification of novel genes expressed during mouse tooth development by microarray gene expression analysis. *Dev Dyn,* 236**,** 2245-57.

PEREIRA, L., LEE, S. Y., GAYRAUD, B., ANDRIKOPOULOS, K., SHAPIRO, S. D., BUNTON, T., BIERY, N. J., DIETZ, H. C., SAKAI, L. Y. & RAMIREZ, F. 1999. Pathogenetic sequence for aneurysm revealed in mice underexpressing fibrillin-1. *Proc Natl Acad Sci U S A,* 96**,** 3819-23.

PERLYN, C. A., MORRISS-KAY, G., DARVANN, T., TENENBAUM, M. & ORNITZ, D. M. 2006. A model for the pharmacological treatment of crouzon syndrome. *Neurosurgery,* 59**,** 210-5; discussion 210-5.

PESKETT, E., KUMAR, S., BAIRD, W., JAISWAL, J., LI, M., PATEL, P., BRITTO, J. A. & PAUWS, E. 2017. Analysis of the Fgfr2C342Y mouse model shows condensation defects due to misregulation of Sox9 expression in prechondrocytic mesenchyme. *Biol Open,* 6**,** 223-231.

PETIOT, A., CONTI, F. J., GROSE, R., REVEST, J. M., HODIVALA-DILKE, K. M. & DICKSON, C. 2003. A crucial role for Fgfr2-IIIb signalling in epidermal development and hair follicle patterning. *Development,* 130**,** 5493-501.

PFAFF, M. J., XUE, K., LI, L., HOROWITZ, M. C., STEINBACHER, D. M. & ESWARAKUMAR, J. V. P. 2016. FGFR2c-mediated ERK–MAPK activity regulates coronal suture development. *Developmental Biology,* 415**,** 242-250.

PIRVOLA, U., SPENCER-DENE, B., XING-QUN, L., KETTUNEN, P., THESLEFF, I., FRITZSCH, B., DICKSON, C. & YLIKOSKI, J. 2000. FGF/FGFR-2(IIIb) signaling is essential for inner ear morphogenesis. *J Neurosci,* 20**,** 6125-34.

PITTELOUD, N., ACIERNO, J. S., MEYSING, A., ELISEENKOVA, A. V., MA, J., IBRAHIMI, O. A., METZGER, D. L., HAYES, F. J., DWYER, A. A., HUGHES, V. A., YIALAMAS, M., HALL, J. E., GRANT, E., MOHAMMADI, M. & CROWLEY, W. F. 2006. Mutations in fibroblast growth factor receptor 1 cause both Kallmann syndrome and normosmic idiopathic hypogonadotropic hypogonadism. *Proceedings of the National Academy of Sciences,* 103**,** 6281-6286.

PRATILAS, C. A., TAYLOR, B. S., YE, Q., VIALE, A., SANDER, C., SOLIT, D. B. & ROSEN, N. 2009. (V600E)BRAF is associated with disabled feedback inhibition of RAF-MEK signaling and elevated transcriptional output of the pathway. *Proc Natl Acad Sci U S A,* 106**,** 4519-24.

PUSAPATI, G. V., KONG, J. H., PATEL, B. B., KRISHNAN, A., SAGNER, A., KINNEBREW, M., BRISCOE, J., ARAVIND, L. & ROHATGI, R. 2018. CRISPR Screens Uncover Genes that Regulate Target Cell Sensitivity to the Morphogen Sonic Hedgehog. *Dev Cell,* 44**,** 113-129 e8.

QIN, Q., XU, Y., HE, T., QIN, C. & XU, J. 2012. Normal and disease-related biological functions of Twist1 and underlying molecular mechanisms. *Cell Res,* 22**,** 90-106.

QUARTO, N., BEHR, B., LI, S. & LONGAKER, M. T. 2009. Differential FGF ligands and FGF receptors expression pattern in frontal and parietal calvarial bones. *Cells Tissues Organs,* 190**,** 158-69.

QUARTO, N., WAN, D. C., KWAN, M. D., PANETTA, N. J., LI, S. & LONGAKER, M. T. 2010. Origin matters: differences in embryonic tissue origin and Wnt signaling determine the osteogenic potential and healing capacity of frontal and parietal calvarial bones. *J Bone Miner Res,* 25**,** 1680-94.

RATERMAN, H. G., VOSSLAMBER, S., DE RIDDER, S., NURMOHAMED, M. T., LEMS, W. F., BOERS, M., VAN DE WIEL, M., DIJKMANS, B. A., VERWEIJ, C. L. & VOSKUYL, A. E. 2012. The interferon type I signature towards prediction of non-response to rituximab in rheumatoid arthritis patients. *Arthritis Res Ther,* 14**,** R95.

RAUCCI, A., BELLOSTA, P., GRASSI, R., BASILICO, C. & MANSUKHANI, A. 2008. Osteoblast proliferation or differentiation is regulated by relative strengths of opposing signaling pathways. *Journal of Cellular Physiology,* 215**,** 442-451.

REARDON, W., WINTER RM FAU - RUTLAND, P., RUTLAND P FAU - PULLEYN, L. J., PULLEYN LJ FAU - JONES, B. M., JONES BM FAU - MALCOLM, S. & MALCOLM, S. 1994. Mutations in the fibroblast growth factor receptor 2 gene cause Crouzon syndrome. *Nat Genet.,* 8**,** 98-103.

REHN, A. P., BIRCH, M. A., KARLSTROM, E., WENDEL, M. & LIND, T. 2007. ADAMTS-1 increases the three-dimensional growth of osteoblasts through type I collagen processing. *Bone,* 41**,** 231-8.

REILLY, J. F. & MAHER, P. A. 2001. Importin beta-mediated nuclear import of fibroblast growth factor receptor: role in cell proliferation. *J Cell Biol,* 152**,** 1307-12.

REILLY, J. F., MIZUKOSHI, E. & MAHER, P. A. 2004. Ligand dependent and independent internalization and nuclear translocation of fibroblast growth factor (FGF) receptor 1. *DNA Cell Biol,* 23**,** 538-48.

REINHOLD, M. I., KAPADIA, R. M., LIAO, Z. & NASKI, M. C. 2006. The Wnt-inducible transcription factor Twist1 inhibits chondrogenesis. *J Biol Chem,* 281**,** 1381-8.

RETTING, K. N., SONG, B., YOON, B. S. & LYONS, K. M. 2009. BMP canonical Smad signaling through Smad1 and Smad5 is required for endochondral bone formation. *Development,* 136**,** 1093-104.

REVEST, J.-M., SPENCER-DENE, B., KERR, K., DE MOERLOOZE, L., ROSEWELL, I. & DICKSON, C. 2001. Fibroblast Growth Factor Receptor 2-IIIb Acts Upstream of Shh and Fgf4 and Is Required for Limb Bud Maintenance but Not for the Induction of Fgf8, Fgf10, Msx1, or Bmp4. *Developmental Biology,* 231**,** 47-62.

RICE, D. P., ABERG, T., CHAN, Y., TANG, Z., KETTUNEN, P. J., PAKARINEN, L., MAXSON, R. E. & THESLEFF, I. 2000. Integration of FGF and TWIST in calvarial bone and suture development. *Development,* 127**,** 1845-55.

RICE, D. P., CONNOR, E. C., VELTMAAT, J. M., LANA-ELOLA, E., VEISTINEN, L., TANIMOTO, Y., BELLUSCI, S. & RICE, R. 2010. Gli3Xt-J/Xt-J mice exhibit lambdoid suture craniosynostosis which results from altered osteoprogenitor proliferation and differentiation. *Hum Mol Genet,* 19**,** 3457-67.

RICE, D. P., KIM, H. J. & THESLEFF, I. 1999. Apoptosis in murine calvarial bone and suture development. *Eur J Oral Sci,* 107**,** 265-75.

RICE, R., SPENCER-DENE, B., CONNOR, E. C., GRITLI-LINDE, A., MCMAHON, A. P., DICKSON, C., THESLEFF, I. & RICE, D. P. 2004. Disruption of Fgf10/Fgfr2b-coordinated epithelial-mesenchymal interactions causes cleft palate. *J Clin Invest,* 113**,** 1692-700.

ROHMANN, E., BRUNNER, H. G., KAYSERILI, H., UYGUNER, O., NURNBERG, G., LEW, E. D., DOBBIE, A., ESWARAKUMAR, V. P., UZUMCU, A., ULUBIL-EMEROGLU, M., LEROY, J. G., LI, Y., BECKER, C., LEHNERDT, K., CREMERS, C. W., YUKSEL-APAK, M., NURNBERG, P., KUBISCH, C., SCHLESSINGER, J., VAN BOKHOVEN, H. & WOLLNIK, B. 2006. Mutations in different components of FGF signaling in LADD syndrome. *Nat Genet,* 38**,** 414-7.

ROUSSEAU, F., BONAVENTURE, J., LEGEAI-MALLET, L., PELET, A., ROZET, J. M., MAROTEAUX, P., LE MERRER, M. & MUNNICH, A. 1994. Mutations in the gene encoding fibroblast growth factor receptor-3 in achondroplasia. *Nature,* 371**,** 252-4.

ROYBAL, P. G., WU, N. L., SUN, J., TING, M.-C., SCHAFER, C. A. & MAXSON, R. E. 2010. Inactivation of Msx1 and Msx2 in neural crest reveals an unexpected role in suppressing heterotopic bone formation in the head. *Developmental Biology,* 343**,** 28-39.

RYAN, M. D., KING, A. M. & THOMAS, G. P. 1991. Cleavage of foot-and-mouth disease virus polyprotein is mediated by residues located within a 19 amino acid sequence. *J Gen Virol,* 72 (Pt 11)**,** 2727-32.

SABA-EL-LEIL, M. K., VELLA, F. D., VERNAY, B., VOISIN, L., CHEN, L., LABRECQUE, N., ANG, S. L. & MELOCHE, S. 2003. An essential function of the mitogen-activated protein kinase Erk2 in mouse trophoblast development. *EMBO Rep,* 4**,** 964-8.

SAGA, Y., KITAJIMA, S. & MIYAGAWA-TOMITA, S. 2000. Mesp1 expression is the earliest sign of cardiovascular development. *Trends Cardiovasc Med,* 10**,** 345-52.

SAGA, Y., MIYAGAWA-TOMITA, S., TAKAGI, A., KITAJIMA, S., MIYAZAKI, J. & INOUE, T. 1999. MesP1 is expressed in the heart precursor cells and required for the formation of a single heart tube. *Development,* 126**,** 3437-47.

SAHNI, M., AMBROSETTI, D. C., MANSUKHANI, A., GERTNER, R., LEVY, D. & BASILICO, C. 1999. FGF signaling inhibits chondrocyte proliferation and regulates bone development through the STAT-1 pathway. *Genes Dev,* 13**,** 1361-6.

SAKAGAMI, N., ONO, W. & ONO, N. 2017. Diverse contribution of Col2a1-expressing cells to the craniofacial skeletal cell lineages. *Orthod Craniofac Res,* 20 Suppl 1**,** 44-49.

SAKAI, K. & MIYAZAKI, J. 1997. A transgenic mouse line that retains Cre recombinase activity in mature oocytes irrespective of the cre transgene transmission. *Biochem Biophys Res Commun,* 237**,** 318-24.

SANDILANDS, E., AKBARZADEH, S., VECCHIONE, A., MCEWAN, D. G., FRAME, M. C. & HEATH, J. K. 2007. Src kinase modulates the activation, transport and signalling dynamics of fibroblast growth factor receptors. *EMBO Rep,* 8**,** 1162-9.

SANDY, J. D., WESTLING, J., KENAGY, R. D., IRUELA-ARISPE, M. L., VERSCHAREN, C., RODRIGUEZ-MAZANEQUE, J. C., ZIMMERMANN, D. R., LEMIRE, J. M., FISCHER, J. W., WIGHT, T. N. & CLOWES, A. W. 2001. Versican V1 proteolysis in human aorta in vivo occurs at the Glu441-Ala442 bond, a site that is cleaved by recombinant ADAMTS-1 and ADAMTS-4. *J Biol Chem,* 276**,** 13372-8.

SARKAR, S., PETIOT, A., COPP, A., FERRETTI, P. & THOROGOOD, P. 2001. FGF2 promotes skeletogenic differentiation of cranial neural crest cells. *Development,* 128**,** 2143-2152.

SASAKI, A., TAKETOMI, T., KATO, R., SAEKI, K., NONAMI, A., SASAKI, M., KURIYAMA, M., SAITO, N., SHIBUYA, M. & YOSHIMURA, A. 2003. Mammalian Sprouty4 suppresses Ras-independent ERK activation by binding to Raf1. *Nat Cell Biol,* 5**,** 427-32.

SATO, T., SASAI, N. & SASAI, Y. 2005. Neural crest determination by co-activation of Pax3 and Zic1 genes in Xenopus ectoderm. *Development,* 132**,** 2355-2363.

SCHMIDT, L., TAIYAB, A., MELVIN, V. S., JONES, K. L. & WILLIAMS, T. 2018. Increased FGF8 signaling promotes chondrogenic rather than osteogenic development in the embryonic skull. *Disease Models & Mechanisms,* 11.

SCHNEIDER, R. A. 1999. Neural Crest Can Form Cartilages Normally Derived from Mesoderm during Development of the Avian Head Skeleton. *Developmental Biology,* 208**,** 441-455.

SCHWARTZBERG, P. L. 1998. The many faces of Src: multiple functions of a prototypical tyrosine kinase. *Oncogene,* 17**,** 1463-8.

SEARS, R. C. & NEVINS, J. R. 2002. Signaling networks that link cell proliferation and cell fate. *J Biol Chem,* 277**,** 11617-20.

SEELIGER, C., SCHYSCHKA, L., KRONBACH, Z., WOTTGE, A., VAN GRIENSVEN, M., WILDEMANN, B. & VESTER, H. 2015. Signaling pathway STAT1 is strongly activated by IFN-beta in the pathogenesis of osteoporosis. *Eur J Med Res,* 20**,** 1.

SEGEV, O., CHUMAKOV, I., NEVO, Z., GIVOL, D., MADAR-SHAPIRO, L., SHEININ, Y., WEINREB, M. & YAYON, A. 2000. Restrained chondrocyte proliferation and maturation with abnormal growth plate vascularization and ossification in human FGFR-3(G380R) transgenic mice. *Hum Mol Genet,* 9**,** 249-58.

SEKINE, K., OHUCHI, H., FUJIWARA, M., YAMASAKI, M., YOSHIZAWA, T., SATO, T., YAGISHITA, N., MATSUI, D., KOGA, Y., ITOH, N. & KATO, S. 1999. Fgf10 is essential for limb and lung formation. *Nat Genet,* 21**,** 138-41.

SEMBA, I., NONAKA, K., TAKAHASHI, I., TAKAHASHI, K., DASHNER, R., SHUM, L., NUCKOLLS, G. H. & SLAVKIN, H. C. 2000. Positionally-dependent chondrogenesis induced by BMP4 is co-regulated by Sox9 and Msx2. *Dev Dyn,* 217**,** 401-14.

SENARATH-YAPA, K., LI, S., MEYER, N. P., LONGAKER, M. T. & QUARTO, N. 2013. Integration of multiple signaling pathways determines differences in the osteogenic potential and tissue regeneration of neural crest-derived and mesoderm-derived calvarial bones. *Int J Mol Sci,* 14**,** 5978-97.

SEO, J. Y., YANEVA, R., HINSON, E. R. & CRESSWELL, P. 2011. Human cytomegalovirus directly induces the antiviral protein viperin to enhance infectivity. *Science,* 332**,** 1093-7.

SERBEDZIJA, G. N., BRONNER-FRASER, M. & FRASER, S. E. 1992. Vital dye analysis of cranial neural crest cell migration in the mouse embryo. *Development,* 116**,** 297-307.

SETTLE, S. H., ROUNTREE, R. B., SINHA, A., THACKER, A., HIGGINS, K. & KINGSLEY, D. M. 2003. Multiple joint and skeletal patterning defects caused by single and double mutations in the mouse Gdf6 and Gdf5 genes. *Developmental Biology,* 254**,** 116-130.

SHAMS, I., ROHMANN, E., ESWARAKUMAR, V. P., LEW, E. D., YUZAWA, S., WOLLNIK, B., SCHLESSINGER, J. & LAX, I. 2007. Lacrimo-auriculo-dento-digital syndrome is caused by reduced activity of the fibroblast growth factor 10 (FGF10)-FGF receptor 2 signaling pathway. *Mol Cell Biol,* 27**,** 6903-12.

SHARMA, V. P., FENWICK, A. L., BROCKOP, M. S., MCGOWAN, S. J., GOOS, J. A., HOOGEBOOM, A. J., BRADY, A. F., JEELANI, N. O., LYNCH, S. A., MULLIKEN, J. B., MURRAY, D. J., PHIPPS, J. M., SWEENEY, E., TOMKINS, S. E., WILSON, L. C., BENNETT, S., CORNALL, R. J., BROXHOLME, J., KANAPIN, A., WHOLE-GENOME SEQUENCES, C., JOHNSON, D., WALL, S. A., VAN DER SPEK, P. J., MATHIJSSEN, I. M., MAXSON, R. E., TWIGG, S. R. & WILKIE, A. O. 2013. Mutations in TCF12, encoding a basic helix-loop-helix partner of TWIST1, are a frequent cause of coronal craniosynostosis. *Nat Genet,* 45**,** 304-7.

SHIANG, R., THOMPSON, L. M., ZHU, Y. Z., CHURCH, D. M., FIELDER, T. J., BOCIAN, M., WINOKUR, S. T. & WASMUTH, J. J. 1994. Mutations in the transmembrane domain of FGFR3 cause the most common genetic form of dwarfism, achondroplasia. *Cell,* 78**,** 335-42.

SHUKLA, V., COUMOUL, X., WANG, R.-H., KIM, H.-S. & DENG, C.-X. 2007. RNA interference and inhibition of MEK-ERK signaling prevent abnormal skeletal phenotypes in a mouse model of craniosynostosis. *Nat Genet,* 39**,** 1145-1150.

SMITS, P., DY, P., MITRA, S. & LEFEBVRE, V. 2004. Sox5 and Sox6 are needed to develop and maintain source, columnar, and hypertrophic chondrocytes in the cartilage growth plate. *J Cell Biol,* 164**,** 747-58.

SMITS, P., LI, P., MANDEL, J., ZHANG, Z., DENG, J. M., BEHRINGER, R. R., DE CROMBRUGGHE, B. & LEFEBVRE, V. 2001. The transcription factors L-Sox5 and Sox6 are essential for cartilage formation. *Dev Cell,* 1**,** 277-90.

SMYTH, I., DU, X., TAYLOR, M. S., JUSTICE, M. J., BEUTLER, B. & JACKSON, I. J. 2004. The extracellular matrix gene Frem1 is essential for the normal adhesion of the embryonic epidermis. *Proc Natl Acad Sci U S A,* 101**,** 13560-5.

SNYDER-WARWICK, A. K., PERLYN, C. A., PAN, J., YU, K., ZHANG, L. & ORNITZ, D. M. 2010. Analysis of a gain-of-function FGFR2 Crouzon mutation provides evidence of loss of function activity in the etiology of cleft palate. *Proceedings of the National Academy of Sciences,* 107**,** 2515-2520.

SONE, S., NAKAMURA, M., MARUYA, Y., TAKAHASHI, I., MIZOGUCHI, I., MAYANAGI, H. & SASANO, Y. 2005. Expression of versican and ADAMTS during rat tooth eruption. *J Mol Histol,* 36**,** 281-8.

SOOD, S., ELDADAH, Z. A., KRAUSE, W. L., MCINTOSH, I. & DIETZ, H. C. 1996. Mutation in fibrillin-1 and the Marfanoid-craniosynostosis (Shprintzen-Goldberg) syndrome. *Nat Genet,* 12**,** 209-11.

SORIANO, P. 1994. Abnormal kidney development and hematological disorders in PDGF beta-receptor mutant mice. *Genes Dev,* 8**,** 1888-96.

SORIANO, P. 1997. The PDGF alpha receptor is required for neural crest cell development and for normal patterning of the somites. *Development,* 124**,** 2691-700.

SORIANO, P. 1999. Generalized lacZ expression with the ROSA26 Cre reporter strain. *Nat Genet,* 21**,** 70-1.

SOSIC, D., RICHARDSON, J. A., YU, K., ORNITZ, D. M. & OLSON, E. N. 2003. Twist regulates cytokine gene expression through a negative feedback loop that represses NF-kappaB activity. *Cell,* 112**,** 169-80.

STANIER, P. & PAUWS, E. 2012. Development of the lip and palate: FGF signalling. *Front Oral Biol,* 16**,** 71-80.

SUZUKI, H., SUDA, N., SHIGA, M., KOBAYASHI, Y., NAKAMURA, M., ISEKI, S. & MORIYAMA, K. 2012. Apert syndrome mutant FGFR2 and its soluble form reciprocally alter osteogenesis of primary calvarial osteoblasts. *J Cell Physiol,* 227**,** 3267-77.

TABLER, JACQUELINE M., BARRELL, WILLIAM B., SZABO-ROGERS, HEATHER L., HEALY, C., YEUNG, Y., PERDIGUERO, ELISA G., SCHULZ, C., YANNAKOUDAKIS, BASIL Z., MESBAHI, A., WLODARCZYK, B., GEISSMANN, F., FINNELL, RICHARD H., WALLINGFORD, JOHN B. & LIU, KAREN J. 2013. Fuz Mutant Mice Reveal Shared Mechanisms between Ciliopathies and FGF-Related Syndromes. *Developmental Cell,* 25**,** 623-635.

TABLER, J. M., RICE, C. P., LIU, K. J. & WALLINGFORD, J. B. 2016. A novel ciliopathic skull defect arising from excess neural crest. *Developmental Biology,* 417**,** 4-10.

TAKARADA, T., NAKAZATO, R., TSUCHIKANE, A., FUJIKAWA, K., IEZAKI, T., YONEDA, Y. & HINOI, E. 2016. Genetic analysis of Runx2 function during intramembranous ossification. *Development,* 143**,** 211.

TAKAYANAGI, H., OGASAWARA, K., HIDA, S., CHIBA, T., MURATA, S., SATO, K., TAKAOKA, A., YOKOCHI, T., ODA, H., TANAKA, K., NAKAMURA, K. & TANIGUCHI, T. 2000. T-cell-mediated regulation of osteoclastogenesis by signalling cross-talk between RANKL and IFN-gamma. *Nature,* 408**,** 600-5.

TAKEDA, K., SHIMOZONO, R., NOGUCHI, T., UMEDA, T., MORIMOTO, Y., NAGURO, I., TOBIUME, K., SAITOH, M., MATSUZAWA, A. & ICHIJO, H. 2007. Apoptosis signal-regulating kinase (ASK) 2 functions as a mitogen-activated protein kinase kinase kinase in a heteromeric complex with ASK1. *J Biol Chem,* 282**,** 7522-31.

TALLQUIST, M. D., FRENCH, W. J. & SORIANO, P. 2003. Additive effects of PDGF receptor beta signaling pathways in vascular smooth muscle cell development. *PLoS Biol,* 1**,** E52.

TALLQUIST, M. D. & SORIANO, P. 2003. Cell autonomous requirement for PDGFRalpha in populations of cranial and cardiac neural crest cells. *Development,* 130**,** 507-18.

TAVORMINA, P. L., SHIANG, R., THOMPSON, L. M., ZHU, Y. Z., WILKIN, D. J., LACHMAN, R. S., WILCOX, W. R., RIMOIN, D. L., COHN, D. H. & WASMUTH, J. J. 1995. Thanatophoric dysplasia (types I and II) caused by distinct mutations in fibroblast growth factor receptor 3. *Nat Genet,* 9**,** 321-8.

TCHORZ, J. S., SUPLY, T., KSIAZEK, I., GIACHINO, C., CLOETTA, D., DANZER, C. P., DOLL, T., ISKEN, A., LEMAISTRE, M., TAYLOR, V., BETTLER, B., KINZEL, B. & MUELLER, M. 2012. A modified RMCE-compatible Rosa26 locus for the expression of transgenes from exogenous promoters. *PLoS One,* 7**,** e30011.

TEVEN, C. M., FARINA, E. M., RIVAS, J. & REID, R. R. 2014. Fibroblast growth factor (FGF) signaling in development and skeletal diseases. *Genes Dis,* 1**,** 199-213.

THIERY, J. P., ACLOQUE, H., HUANG, R. Y. & NIETO, M. A. 2009. Epithelial-mesenchymal transitions in development and disease. *Cell,* 139**,** 871-90.

TING, K., VASTARDIS, H., MULLIKEN, J. B., SOO, C., TIEU, A., DO, H., KWONG, E., BERTOLAMI, C. N., KAWAMOTO, H., KURODA, S. & LONGAKER, M. T. 1999. Human NELL-1 expressed in unilateral coronal synostosis. *J Bone Miner Res,* 14**,** 80-9.

TING, M. C., WU, N. L., ROYBAL, P. G., SUN, J., LIU, L., YEN, Y. & MAXSON, R. E., JR. 2009. EphA4 as an effector of Twist1 in the guidance of osteogenic precursor cells during calvarial bone growth and in craniosynostosis. *Development,* 136**,** 855-64.

TOKUNAGA, A., OYA, T., ISHII, Y., MOTOMURA, H., NAKAMURA, C., ISHIZAWA, S., FUJIMORI, T., NABESHIMA, Y., UMEZAWA, A., KANAMORI, M., KIMURA, T. & SASAHARA, M. 2008. PDGF receptor beta is a potent regulator of mesenchymal stromal cell function. *J Bone Miner Res,* 23**,** 1519-28.

TRAN, H., BRUNET, A., GRIFFITH, E. C. & GREENBERG, M. E. 2003. The many forks in FOXO's road. *Sci STKE,* 2003**,** RE5.

TUVESON, D. A., SHAW, A. T., WILLIS, N. A., SILVER, D. P., JACKSON, E. L., CHANG, S., MERCER, K. L., GROCHOW, R., HOCK, H., CROWLEY, D., HINGORANI, S. R., ZAKS, T., KING, C., JACOBETZ, M. A., WANG, L., BRONSON, R. T., ORKIN, S. H., DEPINHO, R. A. & JACKS, T. 2004. Endogenous oncogenic K-rasG12D stimulates proliferation and widespread neoplastic and developmental defects. *Cancer Cell,* 5**,** 375-387.

TWIGG, S. R., HEALY, C., BABBS, C., SHARPE, J. A., WOOD, W. G., SHARPE, P. T., MORRISS-KAY, G. M. & WILKIE, A. O. 2009. Skeletal analysis of the Fgfr3(P244R) mouse, a genetic model for the Muenke craniosynostosis syndrome. *Dev Dyn,* 238**,** 331-42.

TWIGG, S. R., LLOYD, D., JENKINS, D., ELCIOGLU, N. E., COOPER, C. D., AL-SANNAA, N., ANNAGUR, A., GILLESSEN-KAESBACH, G., HUNING, I., KNIGHT, S. J., GOODSHIP, J. A., KEAVNEY, B. D., BEALES, P. L., GILEADI, O., MCGOWAN, S. J. & WILKIE, A. O. 2012. Mutations in multidomain protein MEGF8 identify a Carpenter syndrome subtype associated with defective lateralization. *Am J Hum Genet,* 91**,** 897-905.

TWIGG, S. R., VORGIA, E., MCGOWAN, S. J., PERAKI, I., FENWICK, A. L., SHARMA, V. P., ALLEGRA, M., ZARAGKOULIAS, A., SADIGHI AKHA, E., KNIGHT, S. J., LORD, H., LESTER, T., IZATT, L., LAMPE, A. K., MOHAMMED, S. N., STEWART, F. J., VERLOES, A., WILSON, L. C., HEALY, C., SHARPE, P. T., HAMMOND, P., HUGHES, J., TAYLOR, S., JOHNSON, D., WALL, S. A., MAVROTHALASSITIS, G. & WILKIE, A. O. 2013. Reduced dosage of ERF causes complex craniosynostosis in humans and mice and links ERK1/2 signaling to regulation of osteogenesis. *Nat Genet,* 45**,** 308-13.

TWIGG, S. R. & WILKIE, A. O. 1999. Characterisation of the human snail (SNAI1) gene and exclusion as a major disease gene in craniosynostosis. *Hum Genet,* 105**,** 320-6.

TWIGG, STEPHEN R. F., FORECKI, J., GOOS, JACQUELINE A. C., RICHARDSON, IVY C. A., HOOGEBOOM, A. JEANNETTE M., VAN DEN OUWELAND, ANS M. W., SWAGEMAKERS, SIGRID M. A., LEQUIN, MAARTEN H., VAN ANTWERP, D., MCGOWAN, SIMON J., WESTBURY, I., MILLER, KERRY A., WALL, STEVEN A., VAN DER SPEK, PETER J., MATHIJSSEN, IRENE M. J., PAUWS, E., MERZDORF, CHRISTA S. & WILKIE, ANDREW O. M. 2015. Gain-of-Function Mutations in ZIC1 Are Associated with Coronal Craniosynostosis and Learning Disability. *The American Journal of Human Genetics,* 97**,** 378-388.

TWIGG, S. R. F., KAN, R., BABBS, C., BOCHUKOVA, E. G., ROBERTSON, S. P., WALL, S. A., MORRISS-KAY, G. M. & WILKIE, A. O. M. 2004. Mutations of ephrin-B1 (EFNB1), a marker of tissue boundary formation, cause craniofrontonasal syndrome. *Proceedings of the National Academy of Sciences of the United States of America,* 101**,** 8652-8657.

UCCELLI, A., MORETTA, L. & PISTOIA, V. 2008. Mesenchymal stem cells in health and disease. *Nat Rev Immunol,* 8**,** 726-36.

UENO, H., GUNN, M., DELL, K., TSENG, A., JR. & WILLIAMS, L. 1992. A truncated form of fibroblast growth factor receptor 1 inhibits signal transduction by multiple types of fibroblast growth factor receptor. *J Biol Chem,* 267**,** 1470-6.

URNESS, L. D., BLEYL, S. B., WRIGHT, T. J., MOON, A. M. & MANSOUR, S. L. 2011. Redundant and dosage sensitive requirements for Fgf3 and Fgf10 in cardiovascular development. *Developmental Biology,* 356**,** 383-397.

VALTA, M. P., HENTUNEN, T., QU, Q., VALVE, E. M., HARJULA, A., SEPPANEN, J. A., VAANANEN, H. K. & HARKONEN, P. L. 2006. Regulation of osteoblast differentiation: a novel function for fibroblast growth factor 8. *Endocrinology,* 147**,** 2171-82.

VAN KOGELENBERG, M., LERONE, M., DE TONI, T., DIVIZIA, M. T., DE BROUWER, A. P., VELTMAN, J. A., VAN BOKHOVEN, H. & ROBERTSON, S. P. 2011. A novel Xp22.11 deletion causing a syndrome of craniosynostosis and periventricular nodular heterotopia. *Am J Med Genet A,* 155A**,** 3144-7.

VASUDEVAN, H. N., MAZOT, P., HE, F. & SORIANO, P. 2015. Receptor tyrosine kinases modulate distinct transcriptional programs by differential usage of intracellular pathways. *Elife*, 4.

VEGA, R. B., MATSUDA, K., OH, J., BARBOSA, A. C., YANG, X., MEADOWS, E., MCANALLY, J., POMAJZL, C., SHELTON, J. M., RICHARDSON, J. A., KARSENTY, G. & OLSON, E. N. 2004. Histone deacetylase 4 controls chondrocyte hypertrophy during skeletogenesis. *Cell*, 119**,** 555-66.

VERBEECK, C., DENG, Q., DEJESUS-HERNANDEZ, M., TAYLOR, G., CEBALLOS-DIAZ, C., KOCERHA, J., GOLDE, T., DAS, P., RADEMAKERS, R., DICKSON, D. W. & KUKAR, T. 2012. Expression of Fused in sarcoma mutations in mice recapitulates the neuropathology of FUS proteinopathies and provides insight into disease pathogenesis. *Mol Neurodegener*, 7**,** 53.

VERHEYDEN, J. M., LEWANDOSKI, M., DENG, C., HARFE, B. D. & SUN, X. 2005. Conditional inactivation of Fgfr1 in mouse defines its role in limb bud establishment, outgrowth and digit patterning. *Development*, 132**,** 4235.

VISSERS, L. E., COX, T. C., MAGA, A. M., SHORT, K. M., WIRADJAJA, F., JANSSEN, I. M., JEHEE, F., BERTOLA, D., LIU, J., YAGNIK, G., SEKIGUCHI, K., KIYOZUMI, D., VAN BOKHOVEN, H., MARCELIS, C., CUNNINGHAM, M. L., ANDERSON, P. J., BOYADJIEV, S. A., PASSOS-BUENO, M. R., VELTMAN, J. A., SMYTH, I., BUCKLEY, M. F. & ROSCIOLI, T. 2011. Heterozygous mutations of FREM1 are associated with an increased risk of isolated metopic craniosynostosis in humans and mice. *PLoS Genet*, 7**,** e1002278.

VORTKAMP, A., LEE, K., LANSKE, B., SEGRE, G. V., KRONENBERG, H. M. & TABIN, C. J. 1996. Regulation of rate of cartilage differentiation by Indian hedgehog and PTH-related protein. *Science*, 273**,** 613-22.

WANG, E., NAM, H. K., LIU, J. & HATCH, N. E. 2015. The effects of tissue-non-specific alkaline phosphatase gene therapy on craniosynostosis and craniofacial morphology in the FGFR2C342Y/+ mouse model of Crouzon craniosynostosis. *Orthod Craniofac Res*, 18 Suppl 1**,** 196-206.

WANG, L., MAGDALENO, S., TABAS, I. & JACKOWSKI, S. 2005a. Early embryonic lethality in mice with targeted deletion of the CTP:phosphocholine cytidylyltransferase alpha gene (Pcyt1a). *Mol Cell Biol*, 25**,** 3357-63.

WANG, X. S., DIENER, K., TAN, T. H. & YAO, Z. 1998. MAPKKK6, a novel mitogen-activated protein kinase kinase kinase, that associates with MAPKKK5. *Biochem Biophys Res Commun*, 253**,** 33-7.

WANG, Y., SPATZ, M. K., KANNAN, K., HAYK, H., AVIVI, A., GORIVODSKY, M., PINES, M., YAYON, A., LONAI, P. & GIVOL, D. 1999. A mouse model for achondroplasia produced by targeting fibroblast growth factor receptor 3. *Proc Natl Acad Sci U S A*, 96**,** 4455-60.

WANG, Y., SUN, M., UHLHORN, V. L., ZHOU, X., PETER, I., MARTINEZ-ABADIAS, N., HILL, C. A., PERCIVAL, C. J., RICHTSMEIER, J. T., HUSO, D. L. & JABS, E. W. 2010. Activation of p38 MAPK pathway in the skull abnormalities of Apert syndrome Fgfr2(+P253R) mice. *BMC Dev Biol*, 10**,** 22.

WANG, Y., XIAO, R., YANG, F., KARIM, B. O., IACOVELLI, A. J., CAI, J., LERNER, C. P., RICHTSMEIER, J. T., LESZL, J. M., HILL, C. A., YU, K., ORNITZ, D. M., ELISSEEFF, J., HUSO, D. L. & JABS, E. W. 2005b. Abnormalities in cartilage and bone development in the Apert syndrome FGFR2+/S252W mouse. *Development*, 132**,** 3537-3548.

WANG, Y., ZHOU, X., OBEROI, K., PHELPS, R., COUWENHOVEN, R., SUN, M., REZZA, A., HOLMES, G., PERCIVAL, C. J., FRIEDENTHAL, J., KREJCI, P., RICHTSMEIER, J. T., HUSO, D. L., RENDL, M. & JABS, E. W. 2012. p38 Inhibition ameliorates skin and skull abnormalities in Fgfr2 Beare-Stevenson mice. *J Clin Invest*, 122**,** 2153-64.

WARZECHA, C. C., JIANG, P., AMIRIKIAN, K., DITTMAR, K. A., LU, H., SHEN, S., GUO, W., XING, Y. & CARSTENS, R. P. 2010. An ESRP-regulated splicing programme is abrogated during the epithelial-mesenchymal transition. *EMBO J*, 29**,** 3286-300.

WEBER, U., EROGLU, C. & MLODZIK, M. 2003. Phospholipid membrane composition affects EGF receptor and Notch signaling through effects on endocytosis during Drosophila development. *Dev Cell,* 5**,** 559-70.

WILKIE, A. O. & MORRISS-KAY, G. M. 2001. Genetics of craniofacial development and malformation. *Nat Rev Genet,* 2**,** 458-68.

WILKIE, A. O., TANG, Z., ELANKO, N., WALSH, S., TWIGG, S. R., HURST, J. A., WALL, S. A., CHRZANOWSKA, K. H. & MAXSON, R. E., JR. 2000. Functional haploinsufficiency of the human homeobox gene MSX2 causes defects in skull ossification. *Nat Genet,* 24**,** 387-90.

WILKIE, A. O. M. 2005. Bad bones, absent smell, selfish testes: The pleiotropic consequences of human FGF receptor mutations. *Cytokine & Growth Factor Reviews,* 16**,** 187-203.

WRIGHT, T. J. & MANSOUR, S. L. 2003. Fgf3 and Fgf10 are required for mouse otic placode induction. *Development,* 130**,** 3379-3390.

WU, Q. F., YANG, L., LI, S., WANG, Q., YUAN, X. B., GAO, X., BAO, L. & ZHANG, X. 2012. Fibroblast growth factor 13 is a microtubule-stabilizing protein regulating neuronal polarization and migration. *Cell,* 149**,** 1549-64.

WU, X.-L., GU, M.-M., HUANG, L., LIU, X.-S., ZHANG, H.-X., DING, X.-Y., XU, J.-Q., CUI, B., WANG, L., LU, S.-Y., CHEN, X.-Y., ZHANG, H.-G., HUANG, W., YUAN, W.-T., YANG, J.-M., GU, Q., FEI, J., CHEN, Z., YUAN, Z.-M. & WANG, Z.-G. 2009. Multiple Synostoses Syndrome Is Due to a Missense Mutation in Exon 2 of FGF9 Gene. *The American Journal of Human Genetics,* 85**,** 53-63.

XIAO, G., JIANG, D., THOMAS, P., BENSON, M. D., GUAN, K., KARSENTY, G. & FRANCESCHI, R. T. 2000. MAPK pathways activate and phosphorylate the osteoblast-specific transcription factor, Cbfa1. *J Biol Chem,* 275**,** 4453-9.

XIAO, G., WANG, D., BENSON, M. D., KARSENTY, G. & FRANCESCHI, R. T. 1998. Role of the alpha2-integrin in osteoblast-specific gene expression and activation of the Osf2 transcription factor. *J Biol Chem,* 273**,** 32988-94.

XU, X., WEINSTEIN, M., LI, C., NASKI, M., COHEN, R. I., ORNITZ, D. M., LEDER, P. & DENG, C. 1998. Fibroblast growth factor receptor 2 (FGFR2)-mediated reciprocal regulation loop between FGF8 and FGF10 is essential for limb induction. *Development,* 125**,** 753-65.

YAMAGUCHI, T. P., HARPAL, K., HENKEMEYER, M. & ROSSANT, J. 1994. fgfr-1 is required for embryonic growth and mesodermal patterning during mouse gastrulation. *Genes Dev,* 8**,** 3032-44.

YAMANAKA, Y., LANNER, F. & ROSSANT, J. 2010. FGF signal-dependent segregation of primitive endoderm and epiblast in the mouse blastocyst. *Development,* 137**,** 715-24.

YANG, L., TSANG, K. Y., TANG, H. C., CHAN, D. & CHEAH, K. S. 2014. Hypertrophic chondrocytes can become osteoblasts and osteocytes in endochondral bone formation. *Proc Natl Acad Sci U S A,* 111**,** 12097-102.

YANG, X., MATSUDA, K., BIALEK, P., JACQUOT, S., MASUOKA, H. C., SCHINKE, T., LI, L., BRANCORSINI, S., SASSONE-CORSI, P., TOWNES, T. M., HANAUER, A. & KARSENTY, G. 2004. ATF4 is a substrate of RSK2 and an essential regulator of osteoblast biology; implication for Coffin-Lowry Syndrome. *Cell,* 117**,** 387-98.

YANG, X., WEBSTER, J. B., KOVALENKO, D., NADEAU, R. J., ZUBANOVA, O., CHEN, P.-Y. & FRIESEL, R. 2006. Sprouty Genes Are Expressed in Osteoblasts and Inhibit Fibroblast Growth Factor-Mediated Osteoblast Responses. *Calcified Tissue International,* 78**,** 233-240.

YEN, H.-Y., TING, M.-C. & MAXSON, R. E. 2010. Jagged1 functions downstream of Twist1 in the specification of the coronal suture and the formation of a boundary between osteogenic and non-osteogenic cells. *Developmental Biology,* 347**,** 258-270.

YEUNG TSANG, K., WA TSANG, S., CHAN, D. & CHEAH, K. S. 2014. The chondrocytic journey in endochondral bone growth and skeletal dysplasia. *Birth Defects Res C Embryo Today,* 102**,** 52-73.

YOSHIDA, T., VIVATBUTSIRI, P., MORRISS-KAY, G., SAGA, Y. & ISEKI, S. 2008. Cell lineage in mammalian craniofacial mesenchyme. *Mechanisms of Development,* 125**,** 797-808.

YOUSFI, M., LASMOLES, F., KERN, B. & MARIE, P. J. 2002. TWIST inactivation reduces CBFA1/RUNX2 expression and DNA binding to the osteocalcin promoter in osteoblasts. *Biochemical and Biophysical Research Communications,* 297**,** 641-644.

YOUSFI, M., LASMOLES, F., LOMRI, A., DELANNOY, P. & MARIE, P. J. 2001. Increased bone formation and decreased osteocalcin expression induced by reduced Twist dosage in Saethre-Chotzen syndrome. *The Journal of Clinical Investigation,* 107**,** 1153-1161.

YU, H. M., JERCHOW, B., SHEU, T. J., LIU, B., COSTANTINI, F., PUZAS, J. E., BIRCHMEIER, W. & HSU, W. 2005. The role of Axin2 in calvarial morphogenesis and craniosynostosis. *Development,* 132**,** 1995-2005.

YU, K., XU, J., LIU, Z., SOSIC, D., SHAO, J., OLSON, E. N., TOWLER, D. A. & ORNITZ, D. M. 2003. Conditional inactivation of FGF receptor 2 reveals an essential role for FGF signaling in the regulation of osteoblast function and bone growth. *Development,* 130**,** 3063-74.

ZHANG, X., IBRAHIMI, O. A., OLSEN, S. K., UMEMORI, H., MOHAMMADI, M. & ORNITZ, D. M. 2006. Receptor Specificity of the Fibroblast Growth Factor Family: THE COMPLETE MAMMALIAN FGF FAMILY. *Journal of Biological Chemistry,* 281**,** 15694-15700.

ZHANG, X., KURODA, S. I., CARPENTER, D., NISHIMURA, I., SOO, C., MOATS, R., IIDA, K., WISNER, E., HU, F.-Y., MIAO, S., BEANES, S., DANG, C., VASTARDIS, H., LONGAKER, M., TANIZAWA, K., KANAYAMA, N., SAITO, N. & TING, K. 2002. Craniosynostosis in transgenic mice overexpressing Nell-1. *Journal of Clinical Investigation,* 110**,** 861-870.

ZHANG, Z., ALPERT, D., FRANCIS, R., CHATTERJEE, B., YU, Q., TANSEY, T., SABOL, S. L., CUI, C., BAI, Y., KORIABINE, M., YOSHINAGA, Y., CHENG, J. F., CHEN, F., MARTIN, J., SCHACKWITZ, W., GUNN, T. M., KRAMER, K. L., DE JONG, P. J., PENNACCHIO, L. A. & LO, C. W. 2009. Massively parallel sequencing identifies the gene Megf8 with ENU-induced mutation causing heterotaxy. *Proc Natl Acad Sci U S A,* 106**,** 3219-24.

ZHAO, H., FENG, J., HO, T.-V., GRIMES, W., URATA, M. & CHAI, Y. 2015. The suture provides a niche for mesenchymal stem cells of craniofacial bones. *Nat Cell Biol,* 17**,** 386-396.

ZHOU, G., LEFEBVRE, V., ZHANG, Z., EBERSPAECHER, H. & DE CROMBRUGGHE, B. 1998. Three high mobility group-like sequences within a 48-base pair enhancer of the Col2a1 gene are required for cartilage-specific expression in vivo. *J Biol Chem,* 273**,** 14989-97.

ZHOU, G., ZHENG, Q., ENGIN, F., MUNIVEZ, E., CHEN, Y., SEBALD, E., KRAKOW, D. & LEE, B. 2006. Dominance of SOX9 function over RUNX2 during skeletogenesis. *Proc Natl Acad Sci U S A,* 103**,** 19004-9.

ZHOU, L., YAO, L. T., LIANG, Z. Y., ZHOU, W. X., YOU, L., SHAO, Q. Q., HUANG, S., GUO, J. C. & ZHAO, Y. P. 2015a. Nuclear translocation of fibroblast growth factor receptor 3 and its significance in pancreatic cancer. *Int J Clin Exp Pathol,* 8**,** 14640-8.

ZHOU, S., XIE, Y., TANG, J., HUANG, J., HUANG, Q., XU, W., WANG, Z., LUO, F., WANG, Q., CHEN, H., DU, X., SHEN, Y., CHEN, D. & CHEN, L. 2015b. FGFR3 Deficiency Causes Multiple Chondroma-like Lesions by Upregulating Hedgehog Signaling. *PLoS Genet,* 11**,** e1005214.

ZHOU, Y.-X., XU, X., CHEN, L., LI, C., BRODIE, S. G. & DENG, C.-X. 2000. A Pro250Arg substitution in mouse Fgfr1 causes increased expression of Cbfa1 and premature fusion of calvarial sutures. *Human Molecular Genetics,* 9**,** 2001-2008.